UNIVERSITÉ DE STRASBOURG

ÉCOLE DOCTORALE DES SCIENCES ET DE LA SANTÉ

INSERM U1113 :

Interface de Recherche Fondamentale et Appliquée en Cancérologie (IRFAC)

THÈSE présentée par :

Jana MOURTADA

soutenue le : **19 Décembre 2023**

pour obtenir le grade de : **Docteur de l'université de Strasbourg**

Discipline/ Spécialité :

Sciences de la vie et de la santé- Aspects moléculaires et cellulaires de la biologie

Mécanismes d'activation de la réponse immunitaire par ΔNp63 dans les cancers des voies aérodigestives supérieures HPV-positifs

THÈSE dirigée par :

Dr. JUNG Alain	HDR, Centre de lutte contre le cancer, Université de Strasbourg
Dr. TRAVE Gilles	DR, CNRS UMR 7104, Université de Strasbourg

RAPPORTEURS :

Pr. BADOUAL Cécile	HDR, PU-PH, Hôpital Européen Georges Pompidou
Dr. BOURDON Jean-Christophe	HDR, MCU-PH, University of Dundee

---

EXAMINATEURS :

Dr. DEBACK Claire	HDR, MCU-PH, INSERM U996-Université Paris Saclay
Dr. MUELLER Christopher	DR, CNRS UPR 3572, Université de Strasbourg

Ce travail a été financé par la Ligue Nationale Contre le Cancer

REMERCIEMENTS

Tout d'abord, je souhaite exprimer mes sincères remerciements à Cécile BADOUAL, Claire DEBACK, Jean-Christophe BOURDON et Christopher MUELLER pour avoir accepté de faire partie de mon jury de thèse. Leur précieuse contribution à la lecture de mon manuscrit est très appréciée.

Je remercie la Ligue Contre le Cancer pour avoir financé ma thèse.

Je tiens à exprimer ma gratitude envers Jean-Noël FREUND, directeur précédent de l'Unité Inserm U1113, pour m'avoir offert l'opportunité de réaliser ma thèse au sein de cette unité.

Je souhaite également remercier Christian GAIDDON et Georg MELLITZER pour leur soutien et leur collaboration.

J'aimerais remercier particulièrement mon directeur de thèse, Alain JUNG, pour m'avoir permis de concrétiser ce projet qui me revêtait une grande importance et qui me tenait à cœur. J'ai entamé ce travail de recherche lors de mon stage de Master 2, et malgré la situation handicapante du covid-19 qui m'a empêché de poursuivre mon travail et d'avoir le bagage nécessaire en expérimentations scientifiques, j'ai pu, grâce à son soutien obtenir un financement de la Ligue contre le cancer et poursuivre mon travail en thèse. Malgré les difficultés que je ressentais au début de ma thèse dû au manque d'expérience nécessaire pour commencer une telle étape, tu étais présent, et je t'en suis reconnaissante. Merci Alain d'avoir consacré du temps à prodiguer des conseils, à apporter un soutien moral et à répondre à mes questions à tout moment. Ton accompagnement m'a permis de gagner en confiance au fil des années et de me sentir la détentrice de ce projet auquel je m'y suis vraiment attachée. Je tiens à te remercier pour ton implication, tes encouragements à tout moment, et surtout pour ta précieuse contribution à la rédaction de mon manuscrit qui est le fruit de ce beau travail de 3 ans. Merci pour tout, et surtout merci d'avoir été un modèle d'humanité et de gentillesse. Grâce à toi, je me sens prête à avancer sereinement dans ce domaine.

Je voudrais également remercier mon co-directeur Gilles TRAVE, pour son soutien, sa présence et ses conseils qui mon permis d'avancer sans aucune hésitation.

Merci à Christelle LONY, qui m'a encadré et soutenu durant mon stage, qui m'a transféré son attachement à ce projet sur lequel elle a réalisé également sa thèse. Merci pour ses encouragements et ses réponses à tous moments à mes questions.

Cyril, mon partenaire de bureau, le babouche à ma Dora, milles merci pour la personne que tu es. Merci pour ton aide, que ce soit au niveau expérimentale ou informatique (oui tu es un expert en informatique comme je te le disais souvent). Tu as été pour moi, tout d'abord un encadrant ensuite un collègue et enfin un ami très cher avec qui j'ai pu partager des moments précieux de fou rire, de migraine, de fatigue, de discussions profondes et pleins de conseils. Grâce à toi et à ta passion pour les oiseaux j'ai appris pleins de chose et j'ai découvert un nouveau monde. Merci pour ta gentillesse et pour la personne adorable que tu es, et merci pour les délicieuses pâtisseries que tu m'as fait découvrir.

Véro, aucun mot suffira pour te remercier. Tu étais d'un soutien énorme que ce soit au niveau professionnel ou personnel. Merci d'être la maman de labo qui n'hésitait pas à fournir de nombreux conseils. Merci pour nos longues discussions et pour nos séances de culture générale, d'histoire et de géographie. J'ai de la chance d'avoir été dans le bureau des bisounours avec Cyril et toi. Au fil des années, j'ai pu découvrir de nombreuses expressions françaises avec vous. Ces années de thèse n'auraient pas été identiques sans ta présence et sans les boites de chocolats… Je te souhaite une bonne continuation dans le domaine que tu as toujours adoré, très chère.

Merci à Murielle MASSON, avec qui je n'ai pu partager le même bureau que pendant quelques mois. Merci mumu pour ta gentillesse, tes conseils et pour la bonne personne que tu es.

Je remercie Erwan PENCREAC'H pour ses conseils, et surtout pour les merveilleuses pâtisseries dont il nous a régalés.

J'aimerais remercier Isabelle GROSS pour son aide et tous ses conseils constructifs.

Merci à Aurélie qui nous a formé à l'expérimentation animale et surtout merci pour sa bonne humeur et son rire contagieux.

Je tiens à remercier Léonor pour son aide et son efficacité dans les démarches administratives.

Merci Christophe d'avoir été un bon collègue.

Pascal, merci pour ta bonne humeur et pour les moments agréables que nous avons partagés en déjeunant ensemble.

Je remercie les doctorants qui étaient très proche de moi tout au long de ma thèse.

Merci Amandine pour ton précieux soutien, ta rigueur et tes conseils. Grâce à toi j'ai appris beaucoup de choses durant mes années de thèse. En plus, tu étais un exemple de détermination, de rigueur et d'engagement envers ton travail, allant au-delà des attentes. Tu as voulu faire ton post-doc au Canada, et te voilà sur le point de commencer un nouveau chapitre de ta vie. Et surtout merci pour les soirées que nous avons passé chez toi à papoter sans ennuis. Je te souhaite une très bonne continuation et beaucoup de succès pour la suite de ta carrière.

Merci Justine pour ton aide, ta simplicité et ta bonne humeur. Merci pour les moments que nous avons partagés, que ce soit au sein du labo ou en dehors. J'espère que tu trouveras ton bonheur dans la suite de ta carrière, mais surtout, n'oublie pas de saouler tes nouveaux collègues avec ton minuteur qui sonne sans fin ;)

Mingyi, merci pour ta gentillesse et pour les discussions que nous avons eues sur tout et rien, grâce à toi j'ai découvert un peu la culture chinoise et certains mots (très compliqués à prononcer…). Merci aussi d'avoir pris le soin de relire ma thèse.

Xué, I appreciate your kindness and warm-hearted personality. It was a delightful experience getting to know you. I wish you nothing but the best as you continue your journey.

Masha, mon amie libanaise, je n'oublierai pas nos longues discussions et nos pauses de midi. Merci pour les moments qu'on a passés ensemble et d'avoir été proche de moi.

Un merci à notre corbeau, Mathieu Vogt. Grâce à toi, on ne s’ennuyait pas trop au labo ;)

David, tu incarnes les qualités d'humilité, de gentillesse et de bienveillance. Je te remercie pour les précieux moments passés au labo.

Yasmine, quelle belle rencontre ! Je regrette de t'avoir connue seulement pendant quelques mois lors de ton stage de Master. J'ai eu le plaisir de te guider au sein du laboratoire. Des personnes comme toi sont rares. J'admire ta bienveillance, l'égard que tu portes aux personnes qui t'entourent, ta gentillesse et ton intelligence. Merci pour nos longues discussions (entre les temps d’incubation) et pour ton soutien. Tu arrivais toujours à choisir les bons mots pour me remotiver.

Finalement, je tiens à conclure avec les doctorants, en adressant mes sincères remerciements aux inséparables, Sevda et Chloé. Je vous remercie profondément pour votre assistance précieuse, votre aide et surtout pour vos précieuses relectures. Grâce à vous j’ai beaucoup appris, partagé des moments de découragement et de joie. Merci pour toutes les sorties que nous avons organisées ensemble. Ceux sont des précieux moments que je n’oublierai pas. Continuez à être les personnes pétillantes que vous êtes ! Je vous souhaite une bonne fin de thèse, même si les circonstances n’ont pas toujours été faciles, je suis convaincu que vous avez tout ce qu’il faut pour réussir.

Je tiens à exprimer ma sincère gratitude envers ma famille pour leur soutien inestimable tout au long de ma thèse.

Papa, Maman, c'est grâce à votre soutien inconditionnel que j'en suis arrivé là aujourd'hui. Depuis le début de mes études, vous avez été mes piliers, toujours à l'écoute, me motivant et me donnant la force d'aller en avant. Votre présence et vos encouragements m'ont permis de poursuivre ce chemin jusqu'au bout. Merci de m'avoir apporté votre aide et réconfort, particulièrement dans les moments les plus difficiles. Merci papa pour m'avoir épaulé, me donné la force et le support nécessaire. À toi, maman, un grand merci pour ton soutien émotionnel et pour toutes les

délicieuses gourmandises que tu préparais pour moi en prévision de mes longues journées à l'étranger.

Mon petit frère, ma grande sœur, merci d'avoir été à mes côtés et de m'avoir donné tant d'amour. Vos petits et grands câlins ont toujours été une source de réconfort et de force pour moi.

Zeina, ma très chère cousine, merci pour tes conseils et ton avis dans la préparation des figures de ma thèse. Merci de m'avoir soutenu, écouté et motivé.

Un petit merci à mon chat (Daisy) qui restait à mes côtés tout au long de ma rédaction et qui cherchait toujours à être câliné.

Enfin, j'aimerais remercier sincèrement mon chéri, mon fiancé, qui était toujours à mes côtés, que ce soit à distance au cours de ma thèse ou près de moi pendant mes longues journées de rédactions. Merci de m'avoir épaulé, soutenu, motivé et de ne pas avoir cessé de me donner beaucoup d'amour. Tu as été ma source de motivation inestimable, me redonnant le moral lorsque j'en avais besoin. Merci d'avoir supporté mes longues dépressions à distance et de m'avoir donné toute la force et la confiance nécessaire. Une relation à distance n'était pas la chose la plus facile, que dire lorsqu'il y a une thèse à passer en même temps ? Voilà un défi que nous avons relevé ensemble. Sans toi je n'aurais pas été en mesure de prendre des pauses pour me ressourcer de mes longues journées fatigantes. Merci pour tout.

إلى عائلتي، هذه الرسالة تُقدَم لكم من القلب…

Table des matières

Table des illustrations

Abréviations

ADN: Acide Désoxribonucléique

ADULT: AcroDermato-Ungual-Lacrimal-Tooth

AEC: Ankyloblepharon-Ectodermal Defects Cleft Lip/Palate

ARN: Acide Ribonucléique

ANGPT1: Angiopoietin 1

APC: Adenomatous Polyposis Coli

AT: Atypical

ATF6: Activation transcription factor 6

BA: Basal

BAX: Bcl-2-associated X protein

BC: Breast Cancer

BPH: Benign Prostatic Hyperplasia

Brd4: Bromodomain-containing protein 4

CAFs: Cancer Associated Fibroblasts

Casp1: Caspase-1

CCL: C-C motif chemokine ligand

CD: Cluster of Differentiation

CDKN1A: Cyclin-dependent kinase inhibitor 1A

CDSN: Corneodesmosin

CK1α: Casein kinase 1 alpha

CKAP4: Cytoskeleton-Associated Protein 4

CL: Classical

CL/P: Cleft Lip/Palate

CLDN1: Claudin 1

ChIP: Chromatin Immunoprecipitation

CLIMP-63: Cytoskeleton-linking membrane protein 63

CTLA4: Cytotoxic T Lymphocyte-Associated protein 4

CNS: Central Nervous System

CRD: Cystein Rich Domain

Ct: Cycle Threshold
CXCL: C-X-C chemokine Ligand

DAMPs: Damage-Associated Molecular Patterns
DC: Dendritic cells
DKK : Dickkopf protein
rDKK3 ou rhDKK3: Recombinant (human) protein DKK-3
DMEM: Dulbecco's Modified Eagle Medium
DMSO: Dimethyl sulfoxide

E: Early
EGFR: Epidermal Growth Factor Receptor
E6AP: E6-associated protein
EBV: Epstein-Barr virus
EMT: Epithelial–mesenchymal transition
EEC: Ectrodactylie
ERGIC-63: ER-Golgi intermediate compartment-63
ER: Endoplasmic Reticulum
ERK: Extracellular signal-Regulated Kinase

FDA: Food and Drug Administration

GADD45: Growth Arrest and DNA Damage-inducible proteins
GBP: Guanylate binding protein
GJB4: Gap junction protein beta 4
GO: Gene Ontology
GSK3β: Glycogen synthase kinase-3β
GZMK: Granzyme K

HAP: Hydrocarbures Aromatiques Polycycliques
HEK: Human Embryonic Kidney
HER3: Human epidermal growth factor receptor 3

HGF: Hepatocyte Growth Factor
HLA-DRA: Human Leukocyte Antigen -DR isotype
HNSCC: Head and Neck Squamous Cell Carcinomas
HPV: Human Papillomavirus
HRP: Horseradish peroxidase
Hsp70: Heat shock protein 7
HUVEC: Human Umbilical Vein Endothelial Cells

IARC: International Agency for Research on Cancer
ICH: Intracerebral Hemorrhage
ICOS: Inducible costimulator
IFN: Interferon
IGFBP-3: Insulin-like growth factor binding protein 3
IGFR: Insulin-like growth factor Receptor
IgG : Immunoglobulin G
IL : Interleukines
IMS : Inflammé/Mésenchymateux
IRF: Interferon regulatory factor

JNK: Jun N-terminal kinase

Kb: Kilobase
KRAS: Kirsten rat sarcoma virus
Krm: Kremen
KRT: Keratin

L: Late
LAD1: Leukocyte adhesion deficiency type 1
LCR: Ligase Chain Receptor
LMS: Limb-mammary syndrome
LB: Lymphocyte B

LEF: Lymphoid Enhancer Factor
LiCL: Chlorure de Lithium
LT: Lymphocyte T
LRP5/6: Low-density lipoprotein receptor-related protein

MEK: Mitogen-activated protein kinase
MCP counter: Microenvironment Cell Population-counter
MHC: Major Histocompatibility Complex
M1: pro-inflammatory macrophages
M2: anti-inflammatory macrophages
MMP7: Matrix Metalloproteinase-7
MS: Mésenchymal
miRNA: micro-ARN
mTOR: Mechanistic Target Of Rapamycin kinase

NFATC: Nuclear factor of activated T cells
NF-κB: Nuclear factor-kappa B
NK: Natural Killer
NLRP1: NLR Family Pyrin Domain Containing 1
NSCLC: Non-Small Cell Lung Cancer

OD : Oligomerization Domain
OMS : Organisation Mondiale de la Santé
ORF: Open Reading Frame
ORL: Otorhinolaryngology
OS: Overall Survival

PAMPs: Pathogen-associated Molecular Pattern
PC: prostate Cancer
PCR: Polymerase Chain reaction
PCP: Planar cell polarity
PDA: Pancreatic Ductal Adenocarcinomas
PD-1: Programmed cell Death 1

PDL1: Programmed cell Death 1 Ligand 1

PFA : Paraformaldehyde

PMA : Phorbol 12-myristate 13-acetate

PI3K: Phosphoinositide 3-kinases

P53: Tumor protein 53

P63: Tumor protein 63

P73: Tumor protein 73

RE: Response Element

Rb: Retinoblastoma protein

RECIST: Response evaluation criteria in solid tumors

REIC: Reduced expression in immortalized cells

RHS: Rapp-Hodgkin Sydrom

RPLP0: Ribosomal Protein Long P0

SAM: Sterile-α-motif

SCC: Squamous Cell Carcinoma

SCS: Single cell sequencing

SE: Super Enhancer

SHFM: Split Hand Foot Malformation

sh: short hairpin

STRING: Search Tool for the Retrieval of Interacting Genes/Proteins

TAD: Transactivation domain

TARC: Thymus and activating-regulated chemokine

TCF: T-cell factor

TCGA: The Cancer Genome Atlas

TCR: T cell receptor

TGF: Transforming growth factor

THP-1: Tohoku Hospital Pediatrics-1

TID: Inhibitory transactivation domain

TIMP: Metallopeptidase Inhibitor

TME: Tumor Microenvironment

TNBC: Triple Negative Breast Cancer

TNFRSF11B: Tumour necrosis factor receptor superfamily member 11B

TNM : Tumour, Node, Metastasis.

TSM : Taux d'incidence standardisés au niveau mondial

Treg : Lymphocyte T régulateurs

TrCP : Transducin repeats-containing proteins

URR: Upstream Regulatory Region

VADS : Voies Aérodigestives Supérieurs

VEGF: Vascular Endothelial Growth Factor

Wnt: Wingless/Integrated

ZNF385B: Zinc Finger Protein 385B

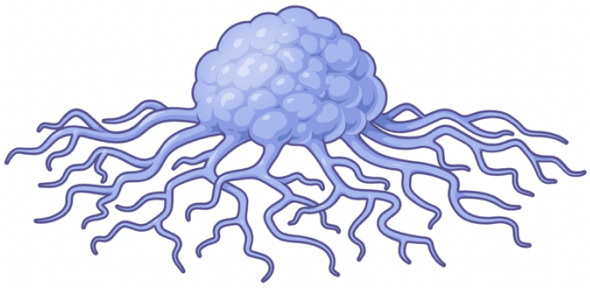

INTRODUCTION

I. Les papillomavirus humains (HPV)

1. Structure et caractéristiques

Les papillomavirus humains (HPV) sont des petits virus non enveloppés de 50 à 60 nm de diamètre, appartenant à la famille des Papillomaviridés. Ils possèdent un génome circulaire d'ADN double brin (dsDNA) d'environ 8000 paires de bases protégées par une capside icosaédrique formée de 72 capsomères. Aujourd'hui, plus de 200 HPV ont été identifiés et classés en cinq genres, à savoir alpha (α), bêta (β), gamma (γ), mu (μ) et nu (ν) (Doorbar, 2005; Doorbar *et al.*, 2015). Les HPV du genre β ont un tropisme pour les épithéliums squameux et sont transmis par contact cutané, alors que les HPV du genre α ont plutôt un tropisme pour les épithéliums muqueux et sont sexuellement transmissibles. De manière importante, le genre α comporte des HPV dits de bas risque oncogène (par exemple les types viraux HPV 6 et 11) à l'origine de lésions bénignes (verrues, condylomes) et des HPV dits de haut risque oncogène (HR-HPV ; par exemple les types viraux HPV 16 et 18), qui provoquent des lésions cancéreuses au niveau de la sphère ano-génitale (col de l'utérus, canal anal) et au niveau de l'oropharynx.

De nombreuses études biologiques et épidémiologiques menées au cours des quarante dernières années ont clairement mis en évidence la nature oncogène des types α des HR-HPV. En effet, leur génome comprend trois régions fonctionnelles : (i) la région précoce ou early (E) qui code des protéines régulatrices, à savoir E1, E2, E4, E5, E6 et E7 (Zheng and Baker, 2006; Doorbar *et al.*, 2015), (ii) la région tardive ou late (L) qui code pour les protéines structurelles de la capside virale L1 et L2, et (iii) la région longue de contrôle (LCR) ou région de régulation en amont (URR) qui contient une région régulatrice importante pour la réplication et la transcription virale **(Figure 1)**. Les génomes des HPV contiennent 6 à 8 cadres de lecture ouverts (ORF) qui sont exprimés sous forme de transcriptions polycistroniques, puis sont soumis à un épissage alternatif pour produire des produits géniques individuels (Graham, 2017). E6 et E7 constituent les principales oncoprotéines virales des HR-HPV muqueux, capables d'altérer la régulation d'événements cellulaires fondamentaux tels que le cycle cellulaire, l'apoptose et la réparation de l'ADN. Ils induisent la prolifération des couches basales et parabasales de l'épithélium. Par conséquent, ces oncoprotéines

facilitent l'accumulation des dommages à l'ADN et une progression maligne à travers l'interaction et l'inactivation de plusieurs protéines cellulaires, y compris les produits de plusieurs gènes suppresseurs de tumeur.

A

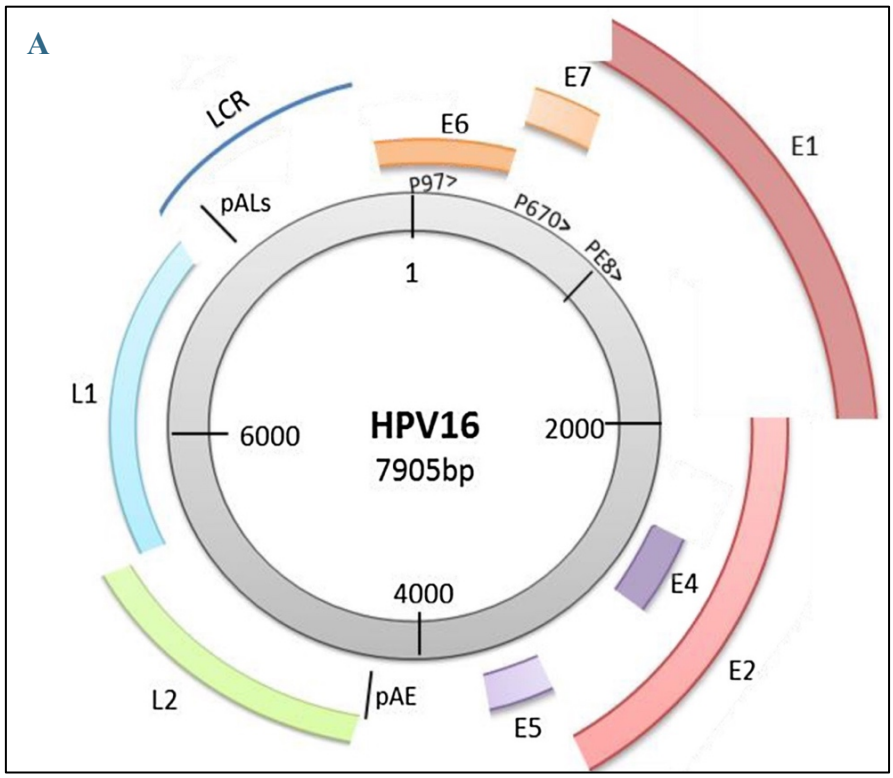

B

Protéine	Fonction
L1	Protéine de la capside majeure.
L2	Protéine de la capside mineure.
E1	Facteur de transcription, activité hélicase. Assure la réplication de l'ADN épisomal.
E2	Facteur de transcription. Régule le nombre de copies virales.
E4	Facilite la libération des virions.
E5	Stimule la prolifération cellulaire et empêche la différenciation. Régule à la baisse l'expression du CMH de classe I à la surface des cellules.
E6	Dérégule le contrôle du cycle cellulaire par inactivation/dégradation de p53. Induit une transformation maligne avec E7.
E7	Maintient les cellules activent dans le cycle cellulaire à travers l'inactivation de Rb. Induit une transformation maligne seul ou avec E6.

Figure 1- Génome du HPV-16 et fonction des protéines virales codées.

(A) Diagramme schématique du génome du HPV16 (Adapté de Graham *et al. 2017*) ;

(B) Principales fonctions des gènes précoces et tardifs du virus HPV (Adapté de Riemer *et al. 2010*)

2. Cycle de réplication virale

Les HPV pénètrent les cellules basales de l'épithélium cutané ou muqueux suite à une microlésion. Par ailleurs, l'infection initiale peut survenir dans la couche cellulaire unique de l'épithélium cervical, entre l'ectocervix et l'endocervix (Herfs *et al.*, 2012), avant de se propager vers l'épithélium pluristratifié. A l'heure actuelle, le processus d'entrée du virus n'est cependant pas entièrement compris. Pour la plupart des HPV étudiés, la protéine capsidique L1 se lie aux protéoglycanes à héparane sulfate sur la lame basale ou la surface cellulaire de l'épithélium basal, et pénètre dans la cellule par micro-pinocytose (Sapp and Bienkowska-Haba, 2009). Les récepteurs d'entrée des HPV ne sont pas tous identifiés, mais pourraient impliquer plusieurs protéines, notamment le récepteur du facteur de croissance épidermique (EGFR), les intégrines, les microdomaines membranaires enrichis en tétraspanine, les laminines et l'hétérotétramère d'annexine-A2 (Raff *et al.*, 2013). A l'issue de cette étape, les virions pénètrent à l'intérieur de la cellule hôte et se déplacent dans le cytoplasme depuis les endosomes jusqu'au réseau trans-Golgi et atteignent le noyau environ 24 heures après la première fixation. Des preuves récentes suggèrent que le génome viral entre dans le noyau suite à la rupture de la membrane pendant la mitose (DiGiuseppe *et al.*, 2016).

A l'intérieur du noyau, une amplification initiale du génome viral de 50 à 100 copies se produit grâce à l'expression des protéines de réplication virale E1 et E2 (Ozbun, 2002). La protéine E2 inhibe l'expression des protéines E6 et E7 dans les kératinocytes de la couche basale. L'intégration du génome viral dans le génome de l'hôte entraine la rupture de l'ORF de la protéine E2, diminuant son expression et favorisant l'expression des protéines E6 et E7 dans les couches basales de l'épithélium. De plus, l'augmentation de l'expression d'E6 et E7 dans les couches basales et parabasale stimule la mitose des kératinocytes, et donc l'amplification du génome viral en détournant la machinerie cellulaire de réplication de l'ADN. Lors de la division des cellules infectées, des protéines de liaison à E2, telles que Brd4, peuvent attacher des épisomes viraux à la chromatine cellulaire pour permettre une ségrégation équitable des génomes viraux dans les cellules épithéliales filles (Wu and Chiang, 2007). Celles-ci peuvent alors rester dans la couche basale ou devenir des cellules amplificatrices

de transit qui commencent à se déplacer vers les couches épithéliales supra basales (Doorbar, 2005).

Enfin, la formation de virions s'établit dans les couches supérieures du tissu infecté et ceci grâce à l'expression des protéines structurales L1 et L2 formant la capside et permettant l'empaquetage des copies néo-synthétisées du génome viral **(Figure 2)**. Finalement, les virions sont relargués dans le milieu extracellulaire à l'occasion de la desquamation et de la lyse naturelle des kératinocytes (Graham, 2017).

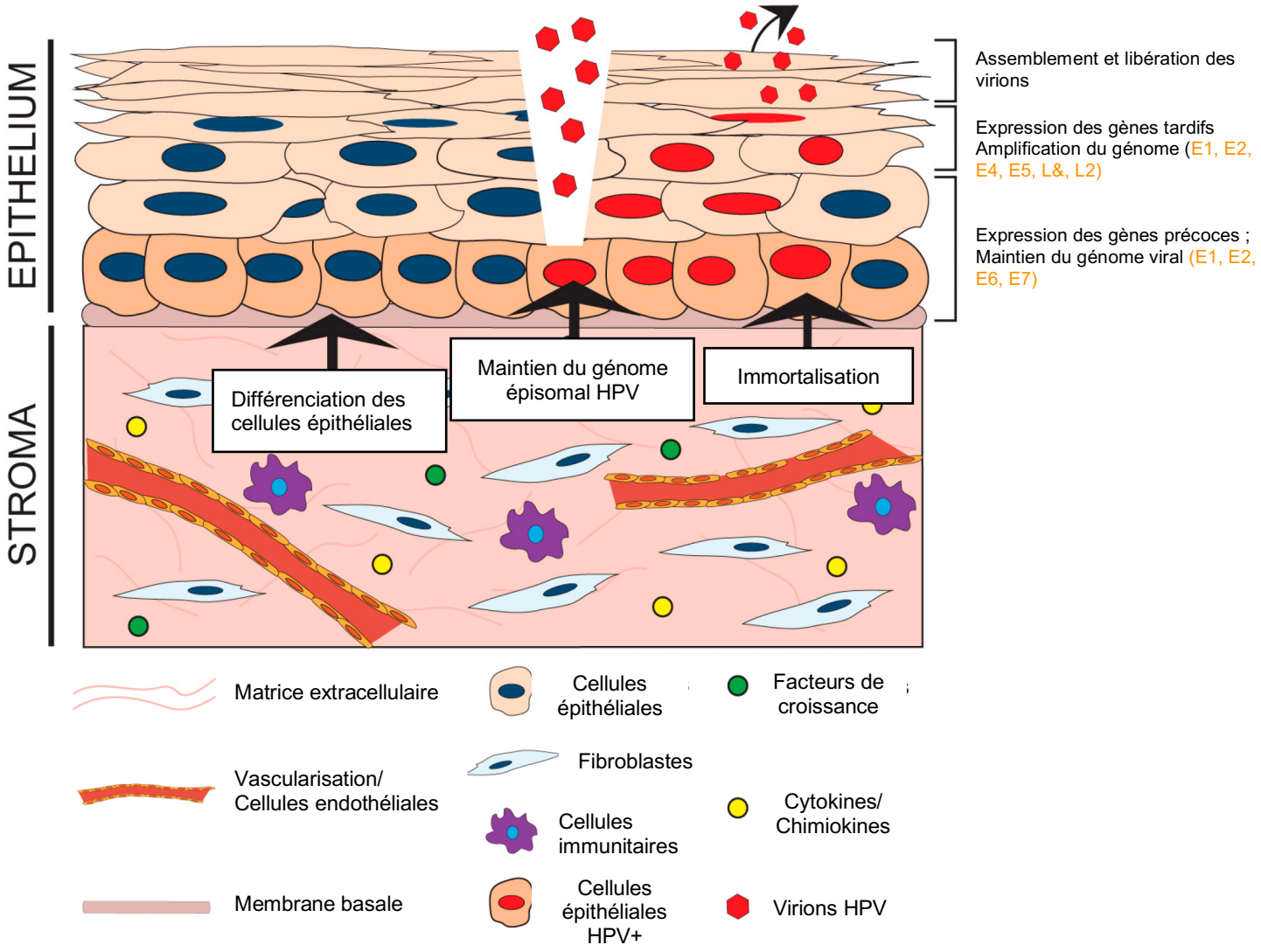

Figure 2 - Représentation schématique de l'épithélium stratifié, du stroma sous-jacent et du cycle de vie du virus HPV (Adapté par Spurgeon et al. 2017)

Les cellules basales, adjacentes à la membrane basale et au stroma sous-jacent, sont représentées en brun foncé. Les virions du HPV infectent les cellules basales de l'épithélium stratifié, probablement à travers une rupture ou une blessure dans la couche épithéliale. Le cycle de vie du virus progresse tout au long de l'épithélium et est lié à la différenciation, se terminant par la production de la progéniture virale et sa libération à partir des cellules totalement différenciées. Des étiquettes indiquant la régulation spatiotemporelle des évènements clés du cycle de vie du HPV sont montrées à droite de l'épithélium stratifié.

3. Comment l'intégration du génome HPV favorise-t-elle l'oncogenèse ?

L'infection par HPV constitue un facteur de risque majeur dans le développement de tumeurs malignes à divers sites anatomiques (zur Hausen, 2002; Ganti *et al.*, 2015). En effet, le génome viral d'HPV est souvent retrouvés intégrés dans le génome de l'hôte dans des lésions pré-malignes ainsi que dans différents types de cancers ano-génitaux et oropharyngés (Parfenov *et al.*, 2014), et presque tous les évènements d'intégration qui ont été étudiés en détail jusqu'à présent sont liés à l'oncogenèse par ce virus. L'intégration entraine généralement la perte de l'ORF codant E2, ce qui provoque une dérégulation de l'expression des oncogènes viraux E6 et E7, favorisant ainsi la prolifération cellulaire, la suppression des points de contrôle du cycle cellulaire et une instabilité génétique progressive. Cela confère donc aux cellules un avantage de croissance sélectif et favorise la progression oncogène (Jeon, Allen-Hoffmann and Lambert, 1995). Ainsi, une des caractéristiques des cancers induits par HPV est l'expression continue des oncoprotéines virales E6 et E7 (Smotkin and Wettstein, 1986; Androphy *et al.*, 1987).

En effet, E6 induit la dégradation du suppresseur de tumeurs p53, qui joue un rôle fondamental dans la prévention de l'établissement d'un cancer (Zilfou and Lowe, 2009) provoquant ainsi une instabilité chromosomique et conduisant à la carcinogénèse (Thomas and Laimins, 1998). L'évènement clé de la dégradation de p53 induite par E6 est la formation d'un complexe ternaire contenant E6, l'ubiquitine E3 ligase E6-associated (E6AP) et p53 **(Figure 3A)**. Dans le genre alpha, seuls les types de HPV à haut risque sont capables d'induire la dégradation de p53 (Scheffner *et al.*, 1992; Werness, no date).

L'oncoprotéine E7 quant-à-elle contient au niveau de son extrémité N-terminale le motif LXCXE qui permet sa liaison avec le produit du gène suppresseur de tumeurs rétinoblastome (pRb) et ses protéines associées p107 et p130. Dans les cellules infectées par les HR-HPV, l'interaction entre E7 et pRb1 entraîne la dégradation du suppresseur de tumeurs via la voie du protéasome (Dyson *et al.*, 1989; Roman and Munger, 2013), avec pour conséquence l'activation du facteur de transcription E2F et

la perturbation de la prolifération cellulaire de manière indépendante des stimuli externes **(Figure 3B)**.

Pour conclure, il existe une forte corrélation entre l'infection par HPV et la carcinogénèse. Actuellement, l'incidence croissante de l'infection par HPV est devenue un facteur de risque majeur pour les cancers des voies aérodigestives supérieures (VADS). Ces cancers se distinguent nettement de ceux qui ne sont pas liés à cette infection et présentent des caractéristiques distinctes. Prendre en considération le statut HPV pourrait ainsi ouvrir la voie à une médecine plus personnalisée et mieux adaptée.

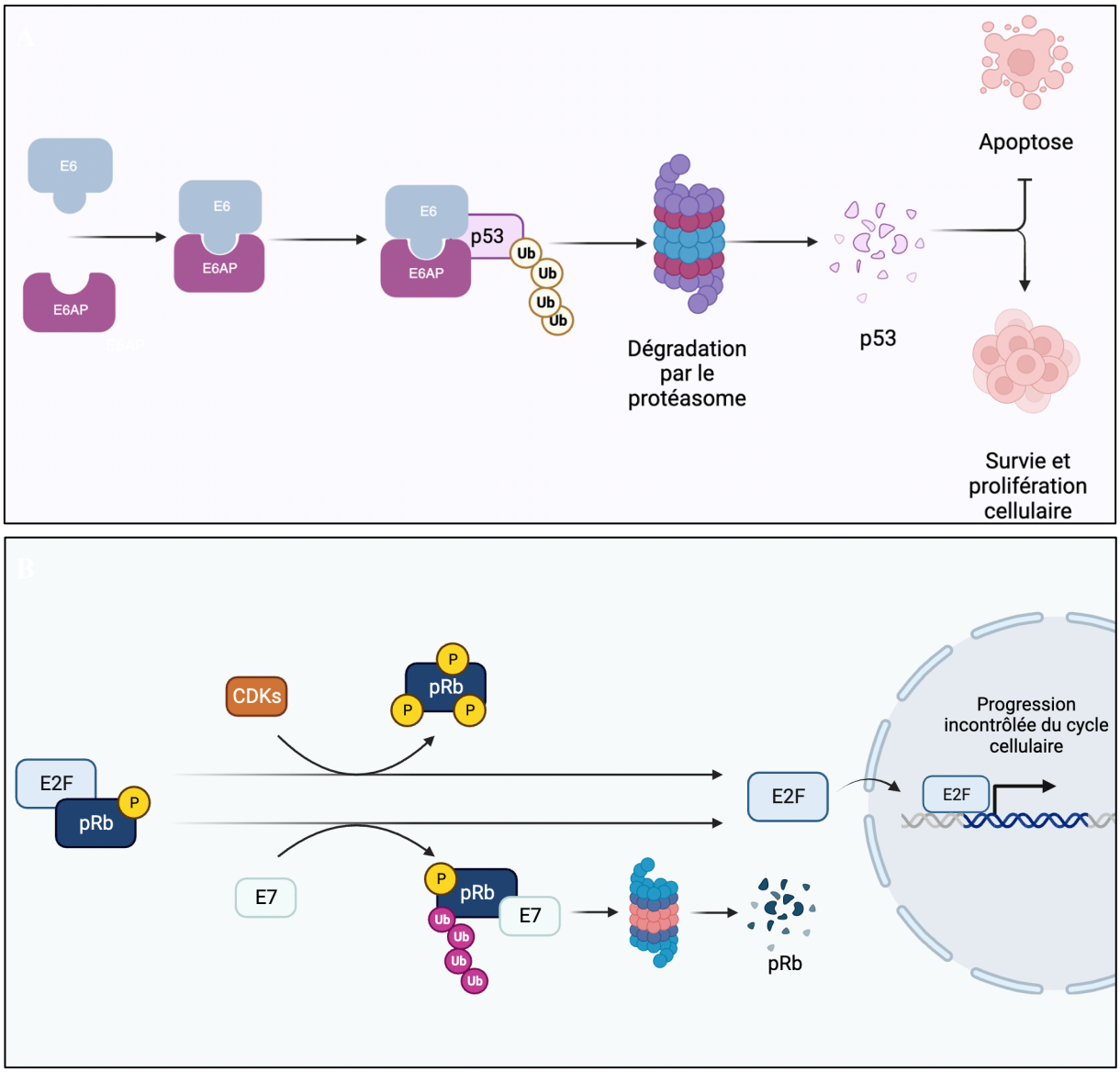

Figure 3- Les oncoprotéines virales E6 et E7 dégradent p53 et pRb, respectivement.

(A) Dégradation de p53 induite par E6 par le biais de la formation d'un complexe ternaire. La liaison d'E6 à p53 induit son ubiquitinylation et sa dégradation médiée par le protéasome, via l'ubiquitine E3 ligase E6-associated protein (E6AP). **(B)** La dégradation de pRb et la surexpression des CDKs contribuent à la surexpression d'E2F et à la progression incontrôlée du cycle cellulaire dans les cancers. Alors que l'hypophosphorylation de pRb empêche les effets d'E2F et rend les cellules quiescentes, l'association de certains complexes cycline/CDK provoque sa phosphorylation et sa libération d'E2F. La liaison d'E7 provoque également la libération d'E2F par ubiquitinylation et la dégradation médiée par le protéasome de pRb. (Adapté de Galati et al. 2022) ; Crée avec BioRender.com

II. Les cancers des voies aérodigestives supérieures

1. Généralités

Les cancers des voies aérodigestives supérieures (VADS) affectent la région anatomique située dans la partie haute des voies digestives et respiratoires. D'un point de vue histologique, plus de 90% des cancers des VADS sont des carcinomes épidermoïdes qui touchent spécifiquement l'épithélium muqueux de la cavité buccale, du pharynx et du larynx (Johnson *et al.*, 2020) **(Figure 4)**.

Ces cancers occupent la sixième place parmi les cancers les plus fréquents à l'échelle mondiale. Leur incidence annuelle est élevée que ce soit pour la cavité orale, le larynx, le nasopharynx, l'oropharynx ou l'hypopharynx avec des chiffres qui s'élèvent à plus de 830 000 cas dans le monde et entrainant plus de 450 000 décès en 2018 (Bray *et al.*, 2018). Ainsi, les taux d'incidence standardisés au niveau mondial (TSM) s'élèvent à 18,3 cas pour 100 000 personnes-années chez les hommes et à 5,8 cas pour 100 000 personnes-années chez les femmes, avec un rapport hommes/femmes de 3,2. Selon les données de GLOBOCAN, cette incidence continue de croître et devrait augmenter de 30% d'ici 2030, ce qui équivaut à environ 1,08 million de nouveaux cas par an (Ferlay *et al.*, 2015).

Parmi les pays d'Europe occidentale, la France demeure le pays avec les taux d'incidence les plus élevés des cancers des VADS (Ferlay *et al.*, 2018)**.** Or, la prévalence des cancers des VADS chez les hommes en France a diminué de 26,7% (passant de 17 474 nouveaux cas en 1990 à 12 808 en 2018) alors que celle des femmes a augmenté de 116% au cours de la même période (passant de 1 869 nouveaux cas en 1980 à 4 044 en 2018). Ces cancers sont de mauvais pronostic : en France, le taux de survie à 5 ans est de 40 à 50%, et varie de 28% pour l'hypopharynx à 57% pour le larynx, montrant des taux de survie extrêmement faibles et ne présentant aucune amélioration significative au cours des 20 dernières années (Cowppli-Bony A *et al.*, 2016). Ainsi, les taux de mortalité standardisés sont respectivement de 4,9 pour 100 000 personnes-années chez les hommes et de 1,2 pour 100 000 personnes-années chez les femmes, avec un rapport hommes/femmes de 4,1 **(Figure 5)**.

En 2018, l'âge médian au moment du diagnostic était de 62 ans pour les hommes et de 64 ans pour les femmes, tandis que l'âge médian au décès était de 65 ans pour les hommes et de 69 ans pour les femmes (Defossez G et al., 2019).

De manière générale, le pronostic des patients atteints de cancer des VADS dépend du stade tumoral au moment du diagnostic. Le stade de la tumeur selon la classification internationale TNM dépend de la taille de la tumeur (T), la présence de ganglions envahis (N) et la présence de métastases à distance (M). Ainsi, le classement se fait par examen clinique, imagerie, cytologie des ganglions lymphatiques et histopathologie définitive après chirurgie (Leemans, Braakhuis and Brakenhoff, 2011). Une étude réalisée sur une population française en 2017 montre que 70,9% des cas ont été diagnostiqués en raison de symptôme graves et concernaient des tumeurs à des stades tardifs (stade III-IV) (Guizard *et al.*, 2017).

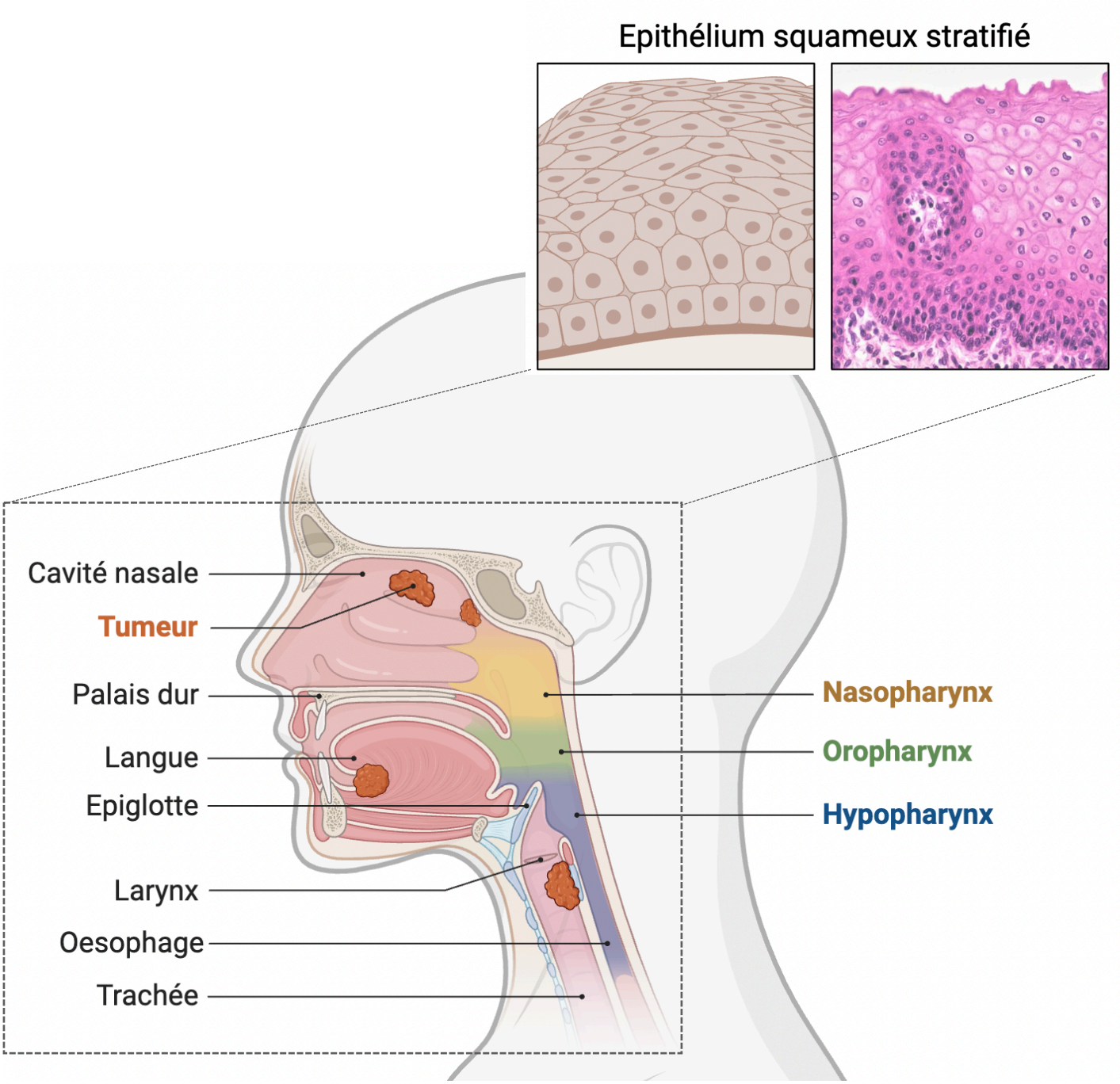

Figure 4- Principaux sites anatomiques du carcinome épidermoïde des cancers des VADS.

L'encart montre les caractéristiques histologiques typiques du carcinome épidermoïde que l'on peut observer dans les cancers des VADS ; Crée avec *BioRender.com*

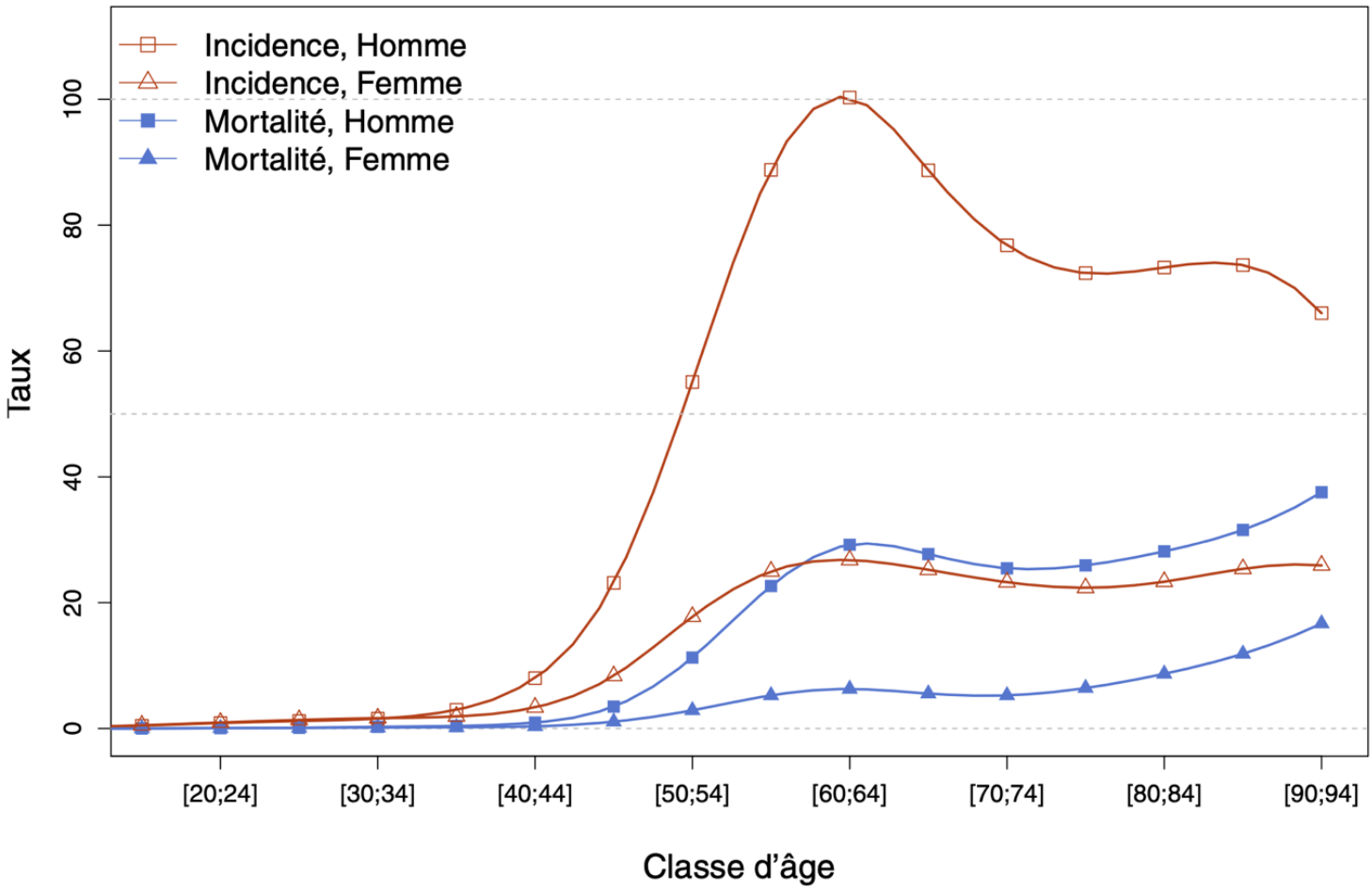

Figure 5- Taux d'incidence et de mortalité des cancers des VADS selon la classe d'âge en France en 2018 (courbe transversale de l'âge) (Cowppli-Bony A *et al*., 2016).

2. Traitements

Le choix de l'approche thérapeutique pour chaque patient est déterminé en fonction du site anatomique de la tumeur, du stade TNM, de la différenciation histologique de la tumeur ainsi que des considérations fonctionnelles et des préférences du patient. Ainsi, les principales modalités de traitement pour les cancers des VADS comprennent la chirurgie, la radiothérapie, la chimiothérapie systémique et plus récemment, la thérapie ciblée et l'immunothérapie. Cependant, le taux de survie globale dans le monde ne dépasse pas 50%, 5 ans après traitement, notamment à cause d'un diagnostic tardif ou de résistances innées et acquises.

a. Chirurgie, radiothérapie et chimiothérapie

Pour les patients atteints d'un cancer primaire sans atteinte ganglionnaire, ou avec une atteinte d'un seul ganglion, des taux de guérison de 80% peuvent être obtenus grâce à une intervention monomodale, que ce soit par chirurgie [cela inclut souvent une lymphadénectomie régionale (Gillison *et al.*, 2014)] ou par radiothérapie (Lee *et al.*, 2018). De manière générale, la chirurgie est couramment utilisée pour les cancers de la cavité buccale et consiste à retirer la tumeur ainsi qu'une marge de tissu sain l'entourant et les ganglions lymphatiques avoisinants, tandis que la radiothérapie peut être plus fréquemment utilisée pour les cancers du pharynx et du larynx (Lyhne *et al.*, 2015) et repose sur l'irradiation et la destruction des cellules cancéreuses. En revanche, le traitement standard pour les tumeurs des VADS de stade plus avancé (tumeur de taille importante avec métastases ganglionnaires et/ou à distance, dites localement avancées) est multimodal, et associe la chirurgie, la radiothérapie et une chimiothérapie concomitante à base de cisplatine (chimiothérapie de référence dans les cancers des VADS) et ceci indépendamment du statut HPV. Ajoutons que la radiothérapie ainsi que la chimiothérapie sont des modalités thérapeutiques génotoxiques induisant des cassures doubles brins de l'ADN. En effet, le cisplatine est un complexe à base de platine qui forme des adduits covalents cisplatine- ADN, ce qui induit une variation de la conformation et des cassures de l'ADN au moment de la réplication, provoquant par ce biais la mort cellulaire.

De manière intéressante, des méta-analyses ont démontré que l'administration concomitante de chimiothérapie et de radiothérapie réduit le risque de récurrence locorégionale ainsi que le risque de décès des patients atteints de cancer des VADS (Pignon *et al.*, 2009).

b. Thérapie ciblée

En plus de ces stratégies thérapeutiques conventionnelles, une thérapie ciblée pour traiter les tumeurs en rechute locale et/ou métastatique est utilisée. Celle-ci repose sur l'utilisation du cetuximab associé à de la radio- ou chimiothérapie (cisplatine). Le cetuximab est un anticorps monoclonal dirigé contre l'Epidermal Growth Factor Receptor (EGFR), un récepteur à tyrosine kinase. Il se lie au domaine extracellulaire de l'EGFR, bloque la liaison ligand-récepteur et favorise l'internalisation de ce récepteur conduisant à une régulation négative de l'EGFR à la surface des cellules (Lo Nigro *et al.*, 2017). Cependant, celui-ci n'améliore que marginalement la situation des patients quand il est associé à une chimiothérapie à base de cisplatine, avec une augmentation de la médiane de survie de trois mois uniquement (Vermorken *et al.*, 2008). Ainsi, il n'existe pas à ce jour de thérapie véritablement efficace pour traiter un cancer des VADS à un stade localement avancé, d'où la nécessité de mettre à jour les mécanismes moléculaires associés à la carcinogénèse et la réponse aux traitements pour aboutir à un traitement adapté.

c. L'immunothérapie

Les immunothérapies sont développées pour réactiver l'activité du système immunitaire afin d'éliminer les cellules cancéreuses (Farkona, Diamandis and Blasutig, 2016). Certaines immunothérapies exploitent des mécanismes naturels de régulation de la réponse immunitaire, comme les points de contrôle immunitaire. Par exemple, la liaison de la protéine PD-1, exprimée par les lymphocytes T, à la protéine PD-L1, souvent exprimée par les cellules tumorales, entraîne la suppression des réponses immunitaires des lymphocytes T et constitue un mécanisme d'évasion immunitaire de la tumeur. Les inhibiteurs des points de contrôle immunitaire anti-PD-1/PD-L1 peuvent

ainsi bloquer cette signalisation suppressive et renforcer l'activité immunitaire contre le cancer (Ferris, 2015; Gong *et al.*, 2018). D'autre part, le récepteur CTLA-4 exprimé par les lymphocytes T, se lie avec forte affinité au récepteur B7 de la cellule dendritique ce qui entraîne un rétrocontrôle négatif au niveau de l'activation lymphocytaire, contrôlant ainsi la réponse immunitaire. Par conséquent, les inhibiteurs des points de contrôle immunitaire constituent une classe d'immunothérapies largement efficace qui agissent en bloquant les voies inhibitrices de régulation immunitaire, permettant ainsi de réactiver les réponses immunitaires anti-tumorales. Ainsi l'efficacité clinique récente des anticorps monoclonaux (moAbs) approuvés par la FDA (Food and Drug Administration) des États-Unis ciblant les points de contrôle immunitaire, notamment l'anti-CTLA-4 et l'anti-PD-1, offre de nouvelles perspectives pour le bénéfice des patients, à mesure que des données cliniques positives émergent (Ferris, 2015) **(Tableau 1)**.

Dans les cancers des VADS, certaines études ont montré une association entre les lymphocytes T régulateurs suppressifs (Tregs) et la progression tumorale. Les Tregs sécrètent des cytokines suppressives telles que le TGF-β et l'IL-10, expriment la protéine 4 associée aux lymphocytes T cytotoxiques (CTLA-4) et sont corrélés avec la progression tumorale (Kammertoens, Schüler and Blankenstein, 2005). Par conséquent, l'utilisation clinique des inhibiteurs de contrôle immunitaire comme les anti-CTLA4 et les anti-PD-1 a récemment été validée en tant que traitements de tumeurs métastatiques et/ou récurrentes dans les cancers des VADS (Ferris *et al.*, 2016; Burtness *et al.*, 2019) et présentent un potentiel thérapeutique chez ces patients. Cependant, une étude réalisée par Badoual *et al.* sur des tumeurs primaires de carcinomes épidermoïdes des VADS montre une association positive entre les Treg (CD4+ Foxp3+) et un meilleur contrôle locorégional de la tumeur (Badoual *et al.*, 2006). De plus, d'autres études ont montré qu'une infiltration plus élevée de cellules Treg Foxp3+ dans les compartiments intraépithélial et stromal était associée à une meilleure survie globale (Punt *et al.*, 2016). Ainsi, plusieurs facteurs influencent le lien entre la présence des cellules Tregs et l'évolution clinique de la tumeur. Il a été observé que la fréquence des Tregs augmente au fur et à mesure que la tumeur progresse, et leur élimination est efficace pour éradiquer une tumeur établie, uniquement si elle n'est pas réalisée pendant la phase initiale de la réponse immunitaire anti-tumorale (Yu *et al.*, 2005).

Finalement, cela met en lumière la complexité et les subtilités du microenvironnement immunitaire tumoral et son implication dans le pronostic du patient, mettant en évidence l'ampleur du travail qui reste à accomplir afin de pouvoir attribuer un traitement adapté à chaque patient.

Drogue (compagnie)	Cible	Classe IgG	Phase de développement des cancers des VADS	Références
MoAbs ciblant un antigène tumoral				
- Cetuximab (Bristol-Myers Squibb, Eli Lilly)	Antagoniste de l'EGFR	IgG1	Phase III et IV	(Cripps *et al.*, 2010)
- Panitumumab (Amgen)	Antagoniste de l'EGFR	IgG2	Phase II et III	(Foon *et al.*, 2004)
- AV-203 (Aveo)	Antagoniste de HER3	IgG1	Phase I (monothérapie ; combinaison du cetuximab)	(Liao *et al.*, 2021)
- Cixutumumab (Eli Lilly)	Antagoniste de l'IGFR	IgG1	Phase 0-II (monothérapie néoadjuvante ; combinaison du cetuximab)	(McKian and Haluska, 2009)
MoAbs ciblant des cytokines				
- Bevacizumab (Genentech)	Anticorps neutralisant anti-VEGF	IgG1	Phase III (chimiothérapie à base de platine ±)	(Garcia *et al.*, 2020)
- Ficlatuzumab (Aveo)	Anticorps neutralisant anti-HGF	IgG1	Phase I (combinaison du cetuximab ; combinaison du cisplatine plus radiation)	(Bauman *et al.*, 2020)
MoAbs ciblant les récepteurs TNF				
- MEDI0562 (Astra-Zeneca/Medimmune)	Agoniste de l'OX40	IgG2	Phase IB	(Glisson *et al.*, 2020)
- Urelumab (Bristol-Myers Squibb)	Agoniste de CD137	IgG4	Phase I	(Srivastava *et al.*, 2017)
- Utomilumab PF-05082566 (Pfizer)	Agoniste de CD137	IgG2	Phase I	(Hamid *et al.*, 2022)
MoAbs ciblant les points de contrôle immunitaires				
- Ipilimumab (Bristol-Myers Squibb)	CTLA4	IgG1	Phase I (combinaison du cetuximab plus radiation)	(Ferris *et al.*, 2022)
- Tremelimumab (AZ/Medimmune)	CTLA4	IgG2	Phase I	(Keam, 2023)
- Durvalumab (MEDI4736, AZ/Medimmune)	PD-L1	IgG1	Phase II	(Moutafi *et al.*, 2023)
- Pembrolizumab (MK-3475, Merck)	PD-1	IgG4	Phase I	(Burtness *et al.*, 2019)
- Nivolumab (Bristol-Myers Squibb/ONO)	PD-1	IgG4	Phase III	(Janjigian et al., 2021)
Abréviations : Abs, antibodies; EGFR, epidermal growth factor receptor; HER, human epidermal growth factor receptor; IGFR, insulin-like growth factor receptor; IgG, immunoglobulin G; moAbs, monoclonal antibodies; PD-1, programmed death-1; PD-L1, programmed death-1 ligand; VEGF, vascular endothelial growth factor.				

Table 1- Anticorps monoclonaux en étude dans les cancers des VADS

Adapté de Journal of Clinical Oncology (Ferris et al. 2015)

3. Facteurs de risque

Les études épidémiologiques ont révélé divers facteurs de risque pour les cancers épidermoïdes des VADS, tels que classifiés par l'Agence Internationale de Recherche sur le Cancer (IARC) de l'Organisation Mondiale de la Santé (OMS) (de Villiers *et al.*, 2004). Ces facteurs de risque comprennent la consommation de tabac, d'alcool, l'exposition à des polluants environnementaux et l'infection par des agents viraux, à savoir le papillomavirus humain (HPV) et l'Epstein-Barr virus (EBV). Il est important de noter que la consommation de tabac et d'alcool constitue le facteur de risque le plus répandu géographiquement et que la consommation excessive de ces deux substances simultanément augmente de 35 fois le risque de développer un cancer des VADS (Blot *et al.*, 1988).

Le tabac contient plus de 5 000 substances chimiques, dont de nombreuses sont connues pour être cancérigènes. Les deux principales substances responsables de ces effets cancérigènes sont les hydrocarbures aromatiques polycycliques (HAP) et les nitrosamines qui subissent des processus métaboliques qui peuvent les rendre toxiques, en formant notamment des adduits covalents à l'ADN (Hecht, 1999). Ainsi, si ces lésions ne subissent pas une réparation correcte, elles peuvent entrainer des mutations et d'autres altérations génétiques contribuant ainsi au développement du cancer lié au tabac (Johnson *et al.*, 2020). La consommation excessive d'alcool constitue un autre facteur risque clé dans le développement d'un cancer des VADS en agissant en synergie avec l'utilisation du tabac pour favoriser la carcinogénèse (Talamini *et al.*, 2002). En effet, l'alcool pourrait agir en tant que solvant pour les agents cancérigènes, augmentant ainsi l'exposition des cellules épithéliales à ces substances (Pai and Westra, 2009). De plus, l'alcool est métabolisé en acétaldéhyde, connu pour former des adduits à l'ADN (Brooks and Theruvathu, 2005).

Par ailleurs, l'exposition à des polluants de l'air cancérogènes, qu'il s'agisse de substances chimiques organiques ou inorganiques, ainsi que de particules en suspension représente un facteur de risque accru, surtout dans les pays ou régions en développement où la pollution atmosphérique s'aggrave, tels que l'Inde et la Chine (Mishra and Meherotra, 2014; Wong, Ng and Lui, 2014). D'autres facteurs de risque

incluent le vieillissement, une mauvaise hygiène buccale et des régimes alimentaires pauvres en légumes (Guha *et al.*, 2007; Freedman *et al.*, 2008).

En ce qui concerne les agents infectieux, une infection persistante par HPV et EBV constitue des facteurs de risque connus pour les cancers des VADS et se développent respectivement dans l'oropharynx et le nasopharynx (Hennessey, Westra and Califano, 2009; Tsang *et al.*, 2020). De manière globale, le rapport homme/femme pour l'incidence des cancers des VADS positifs pour HPV (HPV+) varie de 3 à 6 (Viens *et al.*, 2016), ce qui s'explique par des taux plus élevés d'infection oropharyngées persistante par HPV chez les hommes malgré la prévalence similaire de l'infection au niveau ano-génital chez les hommes et les femmes (Gillison *et al.*, 2012, 2015; Chaturvedi *et al.*, 2015). En effet, l'infection par HPV à l'origine d'un cancer des VADS est principalement transmise par les relations sexuelles bucco-génitales, et son incidence continue d'augmenter, notamment dans les populations qui ne sont pas vaccinées contre ce virus avant une première exposition (Gillison, Chaturvedi and Lowy, 2008; Rowhani-Rahbar *et al.*, 2009). Par ailleurs, le comportement sexuel [tels que le nombre de partenaires sexuels, le type de rapport (bucco-génital, bucco-anal, ano-génital) ainsi que l'âge du 1er rapport] constitue un facteur de risque significatif pour la détection du virus HPV et peut être associé à l'augmentation des cancers des VADS HPV induits. Ceci a été souligné par Smith *et al.* lors d'une étude réalisée sur une cohorte de 193 patients atteints d'un cancer de la cavité buccale ou de l'oropharynx. Le statut HPV a été détecté dans les tissus cancéreux et les cellules exfoliées de la cavité buccale et de l'oropharynx chez 20% des patients. En effet, le statut HPV+ concernait les patients qui avaient en moyenne un nombre plus élevé de partenaires sexuels par rapport au groupe ayant un statut HPV- (19 contre 13 partenaires ; $p<0,02$) et a été observé plus fréquemment chez les patients plus jeunes ($\leq$ 55 ans). De plus, leur étude montre que l'âge moyen au moment du premier contact bucco-génital était significativement plus précoce chez les personnes âgées de moins de 55 ans par rapport à celles de plus de 55 ans (20 ans contre 27 ans, $p<0,006$; tous types histologiques confondus) (Smith *et al.*, 2004).

Bien que les cancers des VADS varient considérablement en fonction de leur origine, qu'elle soit virale (HPV+) ou liée au tabac, et que la thérapie intensive soit plus difficile

pour les patients âgés, il n'existe malheureusement pas de différences absolues dans la prise en charge des patients (Johnson *et al.*, 2020).

4. Classification moléculaire des cancers des VADS

Les carcinomes épidermoïdes des VADS forment un ensemble hétérogène de tumeurs malignes. En effet, les facteurs pronostiques reconnus reposent sur des caractéristiques cliniques et biologiques, comprenant principalement le stade de la tumeur, le site de la tumeur, l'état général du patient, les comorbidités, les antécédents de tabagisme et le statut du virus HPV (Grégoire *et al.*, 2010). En clinique, la majorité des décisions thérapeutiques sont couramment basées sur le stade clinique, qui repose sur le statut ganglionnaire et la taille de la tumeur (Chung *et al.*, 2004). Cependant, les patients regroupés selon ces paramètres présentent toujours des différences dans leur comportement clinique et leur réponse à la thérapie (Carvalho *et al.*, 2005; Denaro *et al.*, 2014).

Les analyses de l'expression génique se sont avérées être un outil utile pour la classification des tumeurs solides humaines provenant d'un seul site (Perou *et al.*, 2000; Garber *et al.*, 2001) ou de sites différents (Ramaswamy *et al.*, 2001). Ces études ont généralement subdivisé les tumeurs en groupes relativement homogènes en fonction de leurs schémas d'expression génique et ont montré que ces regroupements pouvaient prédire les résultats cliniques (Alizadeh *et al.*, 2000; Sørlie *et al.*, 2001). De plus, le statut des métastases ganglionnaires peut être parfois prédit à partir des profils d'expression génique des tumeurs primaires (Huang *et al.*, 2003), ce qui pourrait limiter à de nombreux patients des dissections ganglionnaires inutiles. Ainsi, et afin de détecter les profils d'expression de gènes et les évènements génomiques sous-jacents présents dans les cancers des VADS, plusieurs études génomiques à haut débit ont été réalisées aboutissant à la description de 3 à 6 sous-groupes avec des profils d'expressions de gènes différents.

En 2004, une étude a été réalisée sur des puces à ADN afin d'analyser les profils d'expression génique de 60 tumeurs du carcinome épidermoïde des VADS et a pu mettre en évidence des sous-types distincts de tumeurs des VADS présentant

différents résultats cliniques. Ces tumeurs étaient ainsi classées en 4 sous-groupes moléculaires : le sous-groupe 1 (G1) caractérisé par une activation de la voie EGFR reflétant un mauvais pronostic, le sous-groupe 2 (G2) qui montre une importante signature mésenchymateuse, le sous-groupe 3 (G3) présentant un profil proche à celui d'un épithélium normal, et finalement le sous-groupe 4 (G4) caractérisé par un profil d'expression d'enzymes antioxidantes induites suite à une exposition à la fumée de cigarette (Chung *et al.*, 2004).

Plus tard, Walter *et al.* ont effectué une classification hiérarchique de manière non supervisée en utilisant des techniques bien établie et objectives. En se basant sur les caractéristiques biologiques des gènes exprimés dans chaque sous-type, 4 nouveaux sous-types ont été définis comme suit : basal (BA), mésenchymal (MS), atypique (AT) et classique (CL). Le sous-type BA est caractérisé par une expression élevée de gènes associés à la matrice extracellulaire, au facteur de croissance TGFα et au récepteur EGFR ainsi qu'au facteur de transcription p63. Le sous-type MS présente quant à lui une expression des marqueurs de la transition épithélio-mésenchymateuse (EMT), alors que le sous-type AT présente une signature moléculaire relative à la présence d'HPV. Enfin le sous-type CL montre une surexpression de gènes associés au métabolisme xénobiotique dû à l'exposition au tabac. De plus, il n'y a pas de corrélation entre chaque sous-type moléculaire et l'âge, le genre, la race, la consommation d'alcool et la taille de la tumeur (Walter *et al.*, 2013).

En revanche, une analyse non supervisée utilisant une approche inter-cohorte et inter-plateforme regroupant un total de 938 patients, décrit 5 sous-types différents. Dans cette classification, on retrouve 2 sous-groupes biologiquement distincts et dépendant du statut HPV. Les tumeurs HPV- se répartissent en 3 sous-groupes : BA, CL-nonHPV et inflammé/mésenchymateux (IMS)-nonHPV. D'autre part, les tumeurs HPV+ se répartissent en deux sous-groupes : CL-HPV+ et IMS-HPV+.

Les sous-types inflammés/mésenchymateux (IMS-HPV et IMS-nonHPV) présentent un enrichissement en gènes du système immunitaire (*CD8*, *ICOS*, *LAG3* et *HLA-DRA*) relatifs à l'infiltration des lymphocytes T CD8+. Aux gènes de la réponse immunitaire s'ajoutent des marqueurs des cellules mésenchymateuses (*VIM*) et une sous-expression des marqueurs de cellules épithéliales (*P- cadhérine*, *KRT1* et *KRT9*) suggérant une signature de la transition épithélio-mésenchymateuse associée au

risque de métastase. Les sous-types classique (CL-nonHPV et CL-HPV) se caractérisent par un enrichissement de gènes impliqués dans le cycle cellulaire et le métabolisme xénobiotique. De manière frappante, le sous-groupe IMS-HPV+ présente un meilleur pronostic que le sous-groupe CL-HPV+ (Keck *et al.*, 2015). Il convient de souligner que l'efficacité de l'inhibition des points de contrôle immunitaire a récemment été démontrée dans le cancer des VADS grâce à l'utilisation de thérapies anti-PD-1, et l'expression de PD-L1 est associée à un phénotype inflammatoire qui est en accord avec les sous-types inflammés/mésenchymateux (Saloura *et al.*, 2014).

En revanche, grâce à une approche de séquençage single-cell (SCS), les chercheurs proposent que le sous-type mésenchymal décrit précédemment dans la littérature ne soit pas un sous-groupe à part entière, mais qu'il soit artéfactuellement mis en évidence par les études sur des tumeurs entières uniquement en raison d'infiltrats importants du microenvironnement par des fibroblastes, responsables de cette identité moléculaire. De plus, des analyses bio-informatiques montrent que le profil d'expression était indiscernable pour les sous-types basaux et mésenchymateux formant une seule cohorte « maligne-basale » (Qi *et al.*, 2019). Bien que les études SCS aient apporté de nombreuses données et hypothèses en cancérologie, elles ont également mis en évidence la complexité et les nuances de l'écosystème tumoral et souligné le travail important restant à accomplir.

En résumé, l'ensemble des données de la littérature met en lumière l'hétérogénéité moléculaire et pronostique des tumeurs HPV+ et offre un aperçu de la biologie des tumeurs des VADS HPV+/-, avec des implications translationnelles majeures pour le développement de biomarqueurs et la personnalisation des soins aux patients atteints de ce type de cancer.

Ainsi, près de 5 ans après la publication la plus récente de la classification moléculaire des cancers des VADS, aucune des connaissances acquises n'a été transférée au lit du patient et n'a permis d'améliorer leur prise en charge. Le seul facteur à l'origine de l'hétérogénéité des cancers des VADS, dont il est aujourd'hui clairement reconnu qu'il impacte la réponse aux traitements et le pronostic, est l'infection par HPV, sans pour autant que cela ne se traduise par une adaptation du traitement proposé aux patients. Par conséquent, il est impératif de mettre en place une classification plus robuste et applicable en clinique pour une meilleure pris en charge des patients.

5. Hétérogénéité tumorale des cancers de l'oropharynx HPV+

Malgré une légère baisse globale de l'incidence de certains cancers des VADS, l'incidence du carcinome épidermoïde de l'oropharynx a considérablement augmenté, en particulier dans les pays développés (Mehanna *et al.*, 2010). Dans les années 1970, une relation de cause à effet entre l'infection par HPV et les tumeurs du col de l'utérus, principalement des carcinomes épidermoïdes, a été mise en évidence (Spence *et al.*, 2016). En 1983, des études d'immunohistochimie ont mis en évidence la présence d'antigènes du virus HPV dans certaines sous-catégories de carcinomes oropharyngés (Syrjänen *et al.*, 1983). Ces données ont été renforcées ultérieurement par Gillison *et al.* en 2000, démontrant un lien étroit entre l'infection au à un sous-ensemble de cancers des VADS. Les cancers de l'oropharynx HPV+ en particulier forment une entité distincte sur le plan moléculaire et pathologique, directement liée à l'infection par les HPV (Gillison *et al.*, 2000). Aujourd'hui, l'infection par HPV est de plus en plus courante en tant que facteur de risque pour les cancers des VADS. Elle est associée à la plupart des cancers de l'oropharynx (>70%) et à une petite minorité des cancers sur d'autres sites anatomiques de la tête et du cou (Stein *et al.*, 2015). La plupart de ces cancers se développent à partir de cryptes profondes dans les amygdales palatines et linguales ; HPV16 étant le type viral causatif principal (Michaud *et al.*, 2014). Les cancers des VADS HPV+ présentent des différences distinctes par rapport aux cancers des VADS HPV-, en particulier concernant l'expression génique ainsi que les profils mutationnels et immunitaires, soulignant la biologie unique de ce type de cancer [**(Tableau 2)** (Martín-Hernán *et al.*, 2013)]. Les cancers de l'oropharynx positifs au virus HPV touchent généralement des patients plus jeunes (âgés de moins de 55 ans) et ceux-ci ont tendance à consommer moins d'alcool et de tabac. En France, ceci a été démontré grâce à une étude rétrospective réalisée sur une cohorte de 523 patients indiquant que HPV est présent dans 47% des cas de carcinomes de l'oropharynx, en sachant que les sites anatomiques les plus fréquemment touchés dans cette étude étaient les amygdales (58,9%) et la base de la langue (13,7%) pour l'oropharynx. De plus, environ 95% des cas positifs au HPV étaient infectés par un seul type de HPV. Ainsi, le HPV16 était le type le plus prévalent et a été trouvé dans 89,7% des carcinomes oropharyngés (St Guily *et al.*, 2011).

De plus, il existe une forte corrélation entre la présence du génome viral et le degré de différenciation de la tumeur, car les tumeurs HPV+ ont souvent une histologie peu ou

non différenciée. Il est également important de noter que les patients atteints de tumeurs de l'oropharynx HPV+ ont généralement un meilleur pronostic et une meilleure survie par rapport aux patients atteints de tumeurs HPV-.

En 2010, cette corrélation a été établie au moyen d'une analyse rétrospective basée sur les données d'un essai clinique (NCT00047008) impliquant des patients ayant bénéficié soit d'une radiothérapie en fractionnement accéléré ou d'une radiothérapie en fractionnement standard, en combinaison avec une chimiothérapie à base de cisplatine. L'analyse de ces données visait à évaluer la relation entre le statut HPV de la tumeur et la survie des patients atteints de carcinome épidermoïde de l'oropharynx de stade III ou IV. Les résultats ont montré que le taux de survie global à trois ans était de 82,4% pour les patients HPV+, tandis qu'il était de 57,1% pour les patients dont les tumeurs étaient HPV- (Ang *et al.*, 2010a). Cela peut s'expliquer en partie par la sensibilité accrue des cellules HPV+ à la chimiothérapie et à la radiothérapie (Nagel *et al.*, 2013; Liu *et al.*, 2018).

De plus, une analyse prospective qui évaluait l'association entre le statut HPV des tumeurs et la réponse au traitement ainsi que la survie de 96 patients atteints d'un cancer des VADS (de l'oropharynx ou du larynx) à un stade tardif montrait une meilleure réponse des patients HPV+ vs HPV- après chimiothérapie d'induction (82% vs 55%) et après un traitement par chimioradiothérapie (84% vs 57%). De manière intéressante, les patients positifs au HPV avaient une meilleure survie globale (95% vs 62%, 2 ans après traitement), et après ajustement en fonction de l'âge, du stade de la tumeur et de l'état de performance, présentaient des risques plus faibles de progression et de décès, toutes causes confondues, que ceux ayant des tumeurs négatives au HPV (Fakhry *et al.*, 2008).

En considérant le statut HPV comme un facteur de stratification, il pourrait donc être envisagé de distinguer ce sous-groupe de patients et de leur proposer une thérapie adaptée (Jung *et al.*, 2010). Ainsi, les protocoles de radiothérapie actuels, y compris la radio-chimiothérapie, peuvent entraîner un traitement des patients atteints de cancer induit par les HPV associé à des toxicités importantes. Des schémas thérapeutiques moins agressifs pourraient donc offrir une efficacité similaire tout en réduisant la toxicité et en améliorant la qualité de vie des patients. De nombreux essais cliniques visent actuellement à explorer des approches de désescalade thérapeutique telles que : la réduction de la dose de médicament associée à la radiothérapie, la réduction

de la dose de radiothérapie (dans le cadre de la chimioradiothérapie concomitante, après une chimiothérapie d'induction, ou en situation postopératoire) et enfin la réduction des volumes ciblés par la radiothérapie (Lahmamssi *et al.*, 2020). Cependant, la désescalade thérapeutique pour les cancers localisés et avancés induits par les HPV, bien que conceptuellement intéressante et prometteuse dans des essais de phase II, n'a pas encore atteint un niveau de preuve suffisant pour être recommandée en pratique clinique courante. Ainsi, les résultats des essais cliniques de phase III ont clairement démontré que l'utilisation de la radiothérapie associée au cetuximab dans le but de réduire la toxicité sévère de la chimiothérapie se traduit par une légère mais significative diminution de la survie globale par rapport à l'utilisation de la radiothérapie associée au cisplatine. En outre, il a été observé que les risques de progression du cancer, de décès et de défaillance locorégionale étaient plus élevés avec le cetuximab (Gillison *et al.*, 2019)(Mehanna *et al.*, 2019). Par conséquent, jusqu'à présent, le standard thérapeutique pour les patients atteints d'un carcinome oropharyngé demeure l'utilisation concomitante du cisplatine avec la radiothérapie. En conclusion, il est essentiel de souligner l'importance des essais cliniques de phase III avant de modifier les pratiques cliniques dans le but d'assurer une meilleure prise en charge des patients.

Il existe des différences dans le microenvironnement tumoral entre les cancers de l'oropharynx HPV+ et HPV-. Des études ont montré que les tumeurs HPV+ se caractérisent par une expression plus élevée de gènes impliqués dans la réponse immunitaire, et une infiltration plus fréquente et abondante de lymphocytes T CD8 cytotoxiques reflétant une réponse adaptative (Thurlow *et al.*, 2010; Jung *et al.*, 2013). Bien que cette infiltration immunitaire soit corrélée à un meilleur pronostic des patients (Badoual *et al.*, 2006), il convient de noter que cette réponse peut ne pas être optimale d'un point de vue fonctionnel vu que ces lymphocytes T produisent peu d'interféron γ (IFN-γ) et leur activité cytotoxique anti-tumorale peut être limitée (Heusinkveld *et al.*, 2011).

De plus, une étude sur des tumeurs de l'oropharynx a été réalisée par Jung *et al.* en 2013 et révèle des niveaux plus élevés de gènes liés à la réponse immunitaire et une infiltration importante de lymphocytes T CD8+ cytotoxiques dans le stroma des carcinomes épidermoïdes oropharyngés liés au HPV par rapport aux tumeurs HPV-,

et ceci a été corrélé à une survie prolongée (Jung *et al.*, 2013). Il serait donc intéressant d'évaluer si l'infiltration immunitaire du microenvironnement peut servir de biomarqueur pour prédire la réponse tumorale au traitement, en particulier à l'immunothérapie visant à stimuler la réponse immunitaire, afin de réduire les effets secondaires induits par la radiothérapie et la chimiothérapie.

Finalement, d'un point de vue moléculaire, ce meilleur pronostic peut être attribué au fait que les mutations affectant le gène suppresseur de tumeur *TP53* sont rares dans les tumeurs oropharyngées HPV+ et qu'elles présentent moins d'anomalies génétiques que les tumeurs HPV- (Westra *et al.*, 2008; Stransky *et al.*, 2011). Enfin, de nombreuses études ont montré une amplification de *P63*, un membre de la famille de *TP53*, dans 80% des tumeurs de l'oropharynx HPV+, pouvant ainsi intervenir en tant que facteur de bon pronostic dans ces tumeurs HPV+.

	HPV-positive	HPV-négative
Âge	Patients plus jeunes (30-50)	Patients plus âgés (50-70)
Facteurs de risque	Sexe oral, la multiplicité des partenaires, antécédents d'ITS (Infections sexuellement transmissibles)	Des antécédents de consommation excessive de tabac et/ou d'alcool
Incidence	Croissante	Décroissante
Localisation	Base de la langue, amygdales	Muqueuse buccale
Histologie	Peu ou non différenciée - basaloïde	Clairement différenciée-Kératinisé
Stade lors du dépistage	T3-4 ; N2-3	Variable
Biomarqueurs	P16-surexprimé ; inactivation de P16 et de pRb	Perte du P16 ; mutation sur les gènes *TP53* et *RB1* ; cyclin-D1, EGFR et survivine surexprimés
Mutation chromosomique	Moins fréquente	Fréquente
Pronostic	Favorable, sensibilité accrue suite à la radiothérapie et la chimiothérapie	Défavorable
Second cancer primitif	Rare	Fréquent
Taux de survie à cinq ans	60%-90%	20%-70%

Table 2- Les différences entre les cancers de l'oropharynx HPV+ et HPV-

Adapté de Oral Medicine and Pathology (Martín-Hernán *et al.*, 2013)

III. P63 : un membre de la famille p53

1. Généralités sur la famille p53

Le gène humain *TP53* (Chr.17p13.1) mesure environ 20 kb, contient 11 exons et code pour la protéine suppresseur de tumeurs p53, également connue sous le nom de « gardien du génome » (Lane, 1992). La protéine p53 est un facteur de transcription capable d'intégrer de nombreux signaux qui contrôlent la prolifération ou la mort cellulaire (Vogelstein, Lane and Levine, 2000) et cela à travers la régulation de l'expression de gènes cibles impliqués dans l'arrêt du cycle cellulaire (*CDKN1A*), la réparation de l'ADN (*GADD45*) ou la mort cellulaire par apoptose (*BAX, NOXA...*). p53 n'est pas seulement capable d'agir en tant que facteur de transcription, mais il est également impliqué dans des réponses indépendantes de la transcription, telles que l'apoptose (Vousden and Prives, 2009). *TP53* est le gène le plus fréquemment muté dans les cancers humains (Freed-Pastor and Prives, 2012), avec plus de la moitié de toutes les tumeurs présentant des mutations à ce locus (Vogelstein, Lane and Levine, 2000; Petitjean *et al.*, 2007).

Le gène *TP53* est également le membre fondateur d'une famille complexe comprenant deux autres membres appelés *TP63* et *TP73*, qui codent respectivement pour les facteurs de transcription p63 et p73 **(Figure 6).** Les membres de la famille p53 sont activés par divers types de stress cellulaire, y compris les dommages à l'ADN et les oncogènes. Ces derniers présentent avec p53 des homologies de séquence dans leurs principaux domaines fonctionnels. Ces domaines comprennent, les domaines N-terminaux de transactivation (TAD1 et TAD2) qui sont des sites de liaisons pour les régulateurs positifs ou négatifs de la transcription des gènes (Lin, Teresky and Levine, 1995) ; Le domaine de liaison à l'ADN (DBD), qui se lie aux éléments de réponse des gènes cibles (Melino, 2003) et est principalement affecté par des mutations ponctuelles de type faux sens dans les cancers humains (Harris, 1993; Chan *et al.*, 2004) et finalement le domaine d'oligomérisation (OD) qui permet la tétramérisation de la protéine et est sujet à des épissages et à des modifications post-traductionnelles. Il a été démontré qu'il influence également la liaison à l'ADN et l'activité transcriptionnelle des membres de la famille p53 (Sauer *et al.*, 2008) (Kaghad *et al.*, 1997; Yang *et al.*, 1998).

La complexité de cette famille est liée à l'existence d'une multitude d'isoformes générées par épissages et promoteurs alternatifs. Deux type majeurs d'isoformes résultent de la transcription à partir de promoteurs alternatifs : les isoformes « TA » présentant un domaine de transactivation N-terminal, et les isoformes « ΔN » dépourvues du domaine de transactivation. De plus, un épissage alternatif au niveau de la région 3', aboutit à plusieurs isoformes variant dans la région C-terminale (Ct) de la protéine, nommées α, β, γ, δ, ε, ζ et η. Certains variants Ct de p63 et p73 présentent un domaine inhibiteur de transactivation supplémentaire (TID) ou un domaine de motif alpha stérile (SAM) impliqué dans les interactions protéiques **(Figure 6)** (Kunst *et al.*, 2016).

Cependant, contrairement aux souris déficientes en p53, les animaux dépourvus de p73 et p63 ne développent pas de tumeurs spontanées, mais présentent des défauts dans le développement neuronal (Yang *et al.*, 2000; Pozniak *et al.*, 2002) et épidermique (Mills *et al.*, 1999; Yang *et al.*, 1999), respectivement. Ces phénotypes murins déficients sur le plan génétique se reflètent dans les maladies humaines. Ainsi, alors que p53 est muté dans environ 50 % des cancers humains et fonctionnellement inactivé dans 20 % supplémentaires, les mutations de p73 et p63 dans le cancer humain sont plutôt rares (Cai *et al.*, 2022). Cependant, plusieurs mutations dans le gène *TP63* humain sont associées à des syndromes épidermiques génétiques, et la surexpression de *TP73* est suffisante pour déclencher la différenciation neuronale *in vitro* (De Laurenzi *et al.*, 2000).

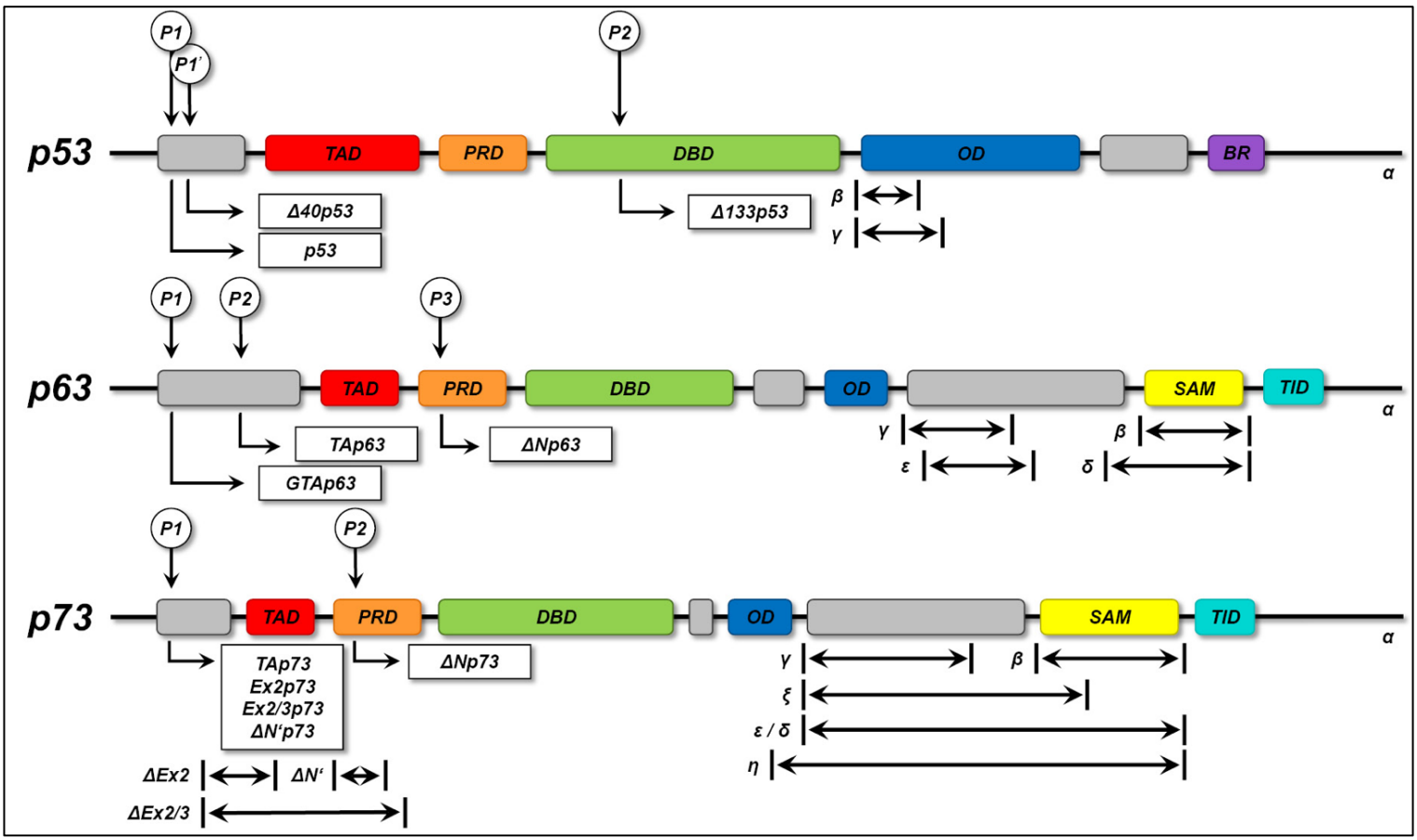

Figure 6- Structure des différentes isoformes des membres de la famille p53 (Adapté de Kunst et al. 2016)

L'architecture des gènes de la famille humaine p53 se compose de quatre composants communs à toutes les isoformes de p53, ainsi qu'à celles de p63 et p73 : un domaine d'activation de la transcription (TAD), un domaine de reconnaissance riche en proline (PRD), un domaine de liaison à l'ADN (DBD) et un domaine d'oligomérisation (OD). Dans des isoformes spécifiques de p63 et p73, il existe un domaine inhibiteur de la transactivation (TID) ou un domaine à motif alpha stérile (SAM) supplémentaire. Un domaine de base (BR) ne se trouve que dans les isoformes de p53. En utilisant de multiples promoteurs (P1, P1', P2, P3) et l'épissage alternatif, les gènes de la famille p53 produisent une diversité d'isoformes.

2. P63

a. Structure et fonctions

Le gène humain *TP63* est situé sur le chromosome 3q27 et est composé de 15 exons s'étendant sur plus de 25 kb (McKeon, 2004). *TP63* possède deux promoteurs différents : le premier promoteur régule la transcription de TAp63, tandis que le second promoteur déclenche l'activation transcriptionnelle des isoformes ΔNp63. Par conséquent, la protéine p63 est exprimée sous la forme de deux isoformes, en fonction des différents domaines. Les formes TA comprennent le TAD, tandis que les isoformes ΔN ne le possède pas (Mangiulli *et al.*, 2009). Ayant une structure similaire à p53, p63 est capable de reconnaître et de se lier au domaine d'activation de la transcription (TAD) des éléments de réponse de p53, et d'initier la transcription de différents gènes. Ainsi, p63 remplace une partie des fonctions de p53, telles que l'arrêt du cycle cellulaire et l'activation de l'apoptose (Osada *et al.*, 2005).

Il est néanmoins généralement admis que les deux isoformes de p63 ont des fonctions différentes. Certains chercheurs estiment que l'isoforme TAp63 possède une région d'activation transcriptionnelle N-terminale plus longue et similaire à celle de p53, ce qui lui permet d'activer incontestablement les gènes cibles de p53, d'inhiber le cycle cellulaire et d'induire l'apoptose, ce qui entraîne des effets biologiques similaires à ceux de p53 et lui confère un rôle de suppresseur de tumeur (Vakonaki *et al.*, 2012; Yao and Chen, 2012; Nekulova *et al.*, 2013). En revanche, certaines études proposent que l'absence du domaine de transactivation des isoformes ΔNp63 leur confère une activité de dominant négatif des protéines TAp63 et p53, ce qui entraîne des résultats opposés en ce qui concerne l'arrêt du cycle cellulaire et l'apoptose liés à p53 (Missero and Antonini, 2014; Osterburg and Dötsch, 2022). Par contre, d'autres études montrent que ΔNp63 est une protéine tronquée de la majeure partie du domaine de transactivation, mais présente toujours 26 acides aminés à l'extrémité N-terminale (TAD2) où la fonction de transactivation a été conservée et peut donc transactiver des gènes cibles qui lui sont spécifiques (Ying *et al.*, 2005).

Des études ont montré que p63 joue un rôle important dans le développement épidermique embryonnaire et dans la prolifération et la différenciation des kératinocytes épidermiques, où elle régule directement l'expression de nombreux

gènes cibles impliqués dans la prolifération cellulaire, la différenciation et l'adhérence (Carroll *et al.*, 2006; Truong *et al.*, 2006). L'épiderme est un épithélium stratifié multicouche qui constitue une barrière physique pour l'organisme, le protégeant ainsi des agents pathogènes et de la déshydratation. L'épiderme est continuellement régénéré par des kératinocytes en voie de différenciation terminale qui migrent de la couche basale interne (compartiment prolifératif) vers la couche cornée externe (compartiment de différenciation terminale) ; ce processus est appelé cornification. Le rôle de p63 dans le développement de l'épiderme a été prouvé dans divers modèles animaux ainsi que dans les maladies humaines associées à des mutations de p63. Par exemple, la suppression complète de p63 chez les souris entraîne l'absence de l'épiderme et des appendices cutanés associés, ainsi que des défauts dans d'autres tissus épithéliaux associés (Yang *et al.*, 1998, 1999; Mills *et al.*, 1999).

ΔNp63α est l'isoforme prédominante au niveau de la couche basale de l'épithélium stratifié de la peau ainsi qu'au niveau des VADS. Ainsi, ΔNp63α est exprimé de façon prédominante au niveau des cellules moins différenciées et cette expression diminue voire disparaît au niveau des cellules au stade terminal de leur différenciation (Nylander *et al.*, 2002) **(Figure 7)**. La délétion complète de p63 (à la fois les formes TA et ΔNp63), ainsi que la délétion spécifique de ΔNp63, par knock-out chez la souris entraîne la formation de membres tronqués, des défauts cranio-faciaux et une perte des glandes salivaires, des follicules pileux et des dents (Lin-Shiao *et al.*, 2019). Des défauts de développement et de morphologie dans l'épithélium pavimenteux et l'épiderme sont également observés aboutissant à l'absence de peau provoquant ainsi une déshydratation et la mort après naissance. Ainsi, il a été démontré que l'expression ΔNp63α dirigée par la kératine 5 chez les souris p63-/-, restaure partiellement la couche basale épidermique et l'expression des kératines 5 et 14, mais pas des marqueurs de la couche épidermique supérieure tels que la kératine 1 ou la loricrine (Candi *et al.*, 2006). De manière similaire, dans un modèle distinct, l'induction de ΔNp63α ou ΔNp63β par le promoteur de kératine 5 dans un contexte p63-null restaure partiellement l'intégrité épithéliale, la stratification et l'expression des marqueurs de différenciation, conduisant à la conclusion que ΔNp63α ou ΔNp63β sont impliqués dans la stratification épithéliale (Romano *et al.*, 2009). De plus, en accord avec le rôle de ΔNp63α dans la régulation du développement épidermique et de

l'engagement, l'élimination spécifique de l'isoforme ΔNp63α a en grande partie reproduit le phénotype des souris p63-null originales, suggérant que, d'un point de vue fonctionnel, ce rôle est essentiellement assuré par ΔNp63 (Romano *et al.*, 2012) .

En outre, un degré plus élevé de formation épidermique structurée et de différenciation a été observé chez les souris exprimant à la fois TAp63α et ΔNp63α avec l'expression des kératines 1, 5, 14 et de la loricrine, par rapport à la reconstitution avec une seule isoforme (Candi *et al.*, 2006). Dans l'ensemble, ces résultats suggèrent qu'un équilibre finement ajusté des isoformes est nécessaire pour une stratification épidermique complète.

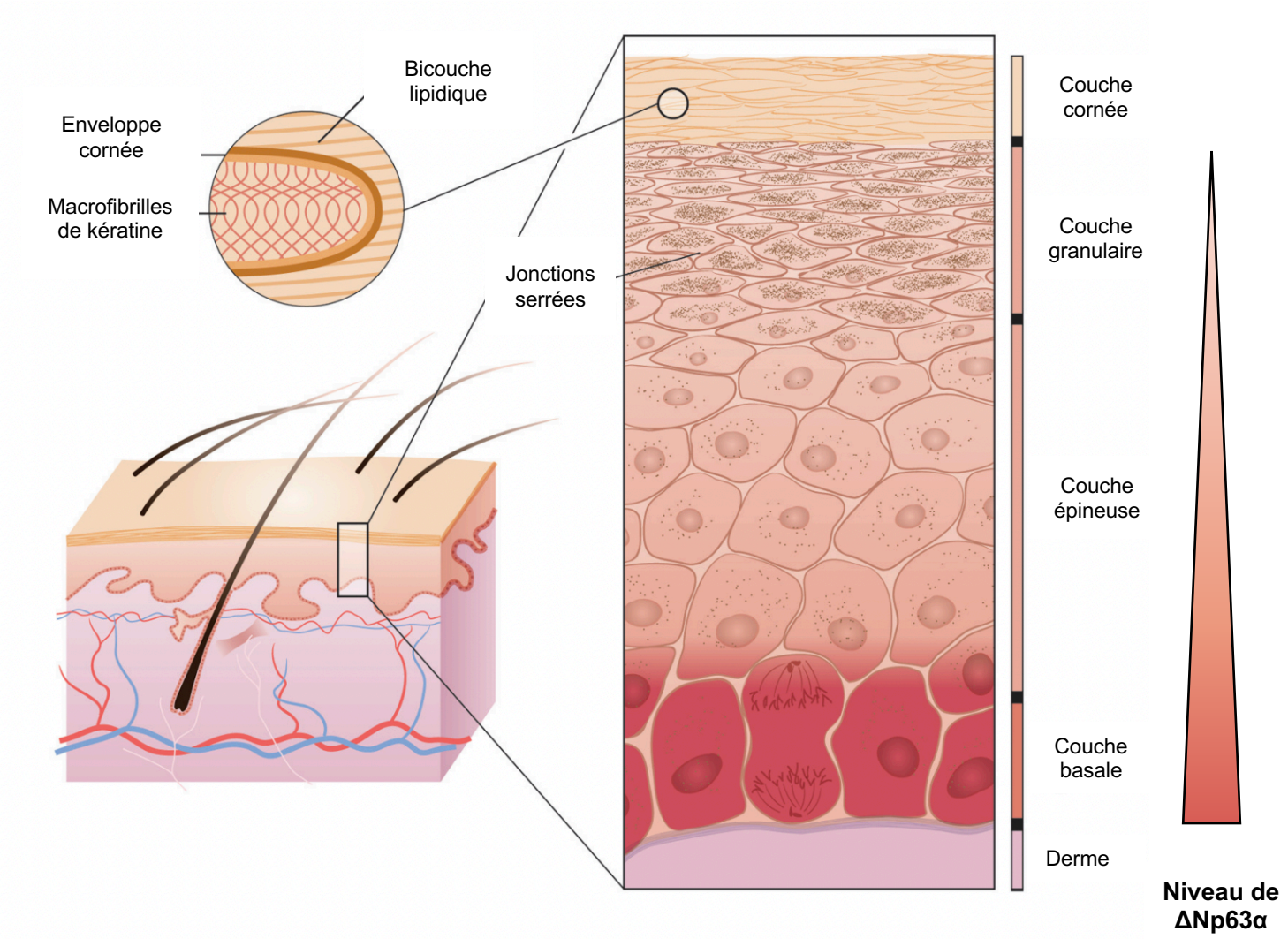

Figure 7- Diagramme schématique des étapes de la différenciation épidermique, aboutissant à une barrière de perméabilité.

ΔNp63α régule des processus biologiques intrinsèques et extrinsèques impliqués dans la morphogenèse épidermique normale et l'homéostasie. Les kératinocytes épidermiques suivent un programme linéaire de différenciation, passant des cellules basales mitotiques aux cellules épineuses transcriptionnellement actives, puis aux cellules granulaires sans noyau, pour finalement donner naissance à des squames différenciées dans la couche cornée (Adapté de Segre A *et al.* 2006).

b. Syndromes associés

Chez les humains, les mutations hétérozygotes autosomiques dominantes dans le gène *TP63* provoquent plusieurs troubles du développement, dont beaucoup se manifestent par des anomalies cutanées (Duijf, van Bokhoven and Brunner, 2003; Rinne, Brunner and van Bokhoven, 2007). Ainsi, ces mutations donnent lieu à cinq syndromes et deux conditions cliniques non syndromiques.

Les syndromes associés aux mutations de *TP63* comprennent :

- Le syndrome de l'ectrodactylie, de la dysplasie ectodermique et de la fente labiale/palatine (**EEC**) et qui est principalement associé à des mutations dans le domaine de liaison à l'ADN (DBD) (Celli *et al.*, 1999)
- Le syndrome d'anomalies des membres et des mammaires (**LMS**) et qui résulte de mutations dans le DBD, le domaine motif-α-stérile (SAM) et le domaine inhibiteur de transactivation (TID) (Van Bokhoven *et al.*, 2001)
- Le syndrome de l'ankyloblépharon-défauts-ectodermiques-fente labiale/palatine (**AEC**) qui est caractérisé par des mutations principalement dans le domaine SAM, et rarement dans le TID et le DBD (McGrath, 2001)
- Le syndrome de Rapp-Hodgkin (**RHS**), qui se caractérise par une dysplasie ectodermique anhydrotique et une fente labiopalatine, et qui est associé à des mutations dans le DBD, le domaine SAM et le domaine TID (Bougeard *et al.*, 2003)
- Le syndrome acro-dermato-unguéale-lacrymal-dentaire (**ADULT**) qui est principalement lié à des mutations dans le DBD, avec 6 mutations identifiées à ce niveau (Propping *et al.*, 2000)

Ces maladies présentent une combinaison de défauts dans différents tissus avec trois caractéristiques majeures : l'ectrodactylie (malformations de la main/du pied fendues, SHFM), les fentes orofaciales (CL/P) et la dysplasie ectodermique, comprenant des défauts de la peau, des dents, des ongles, des cheveux et diverses glandes exocrines (Celli *et al.*, 1999; Leoyklang, Siriwan and Shotelersuk, 2006; Rinne *et al.*, 2006) **(Figure 8).**

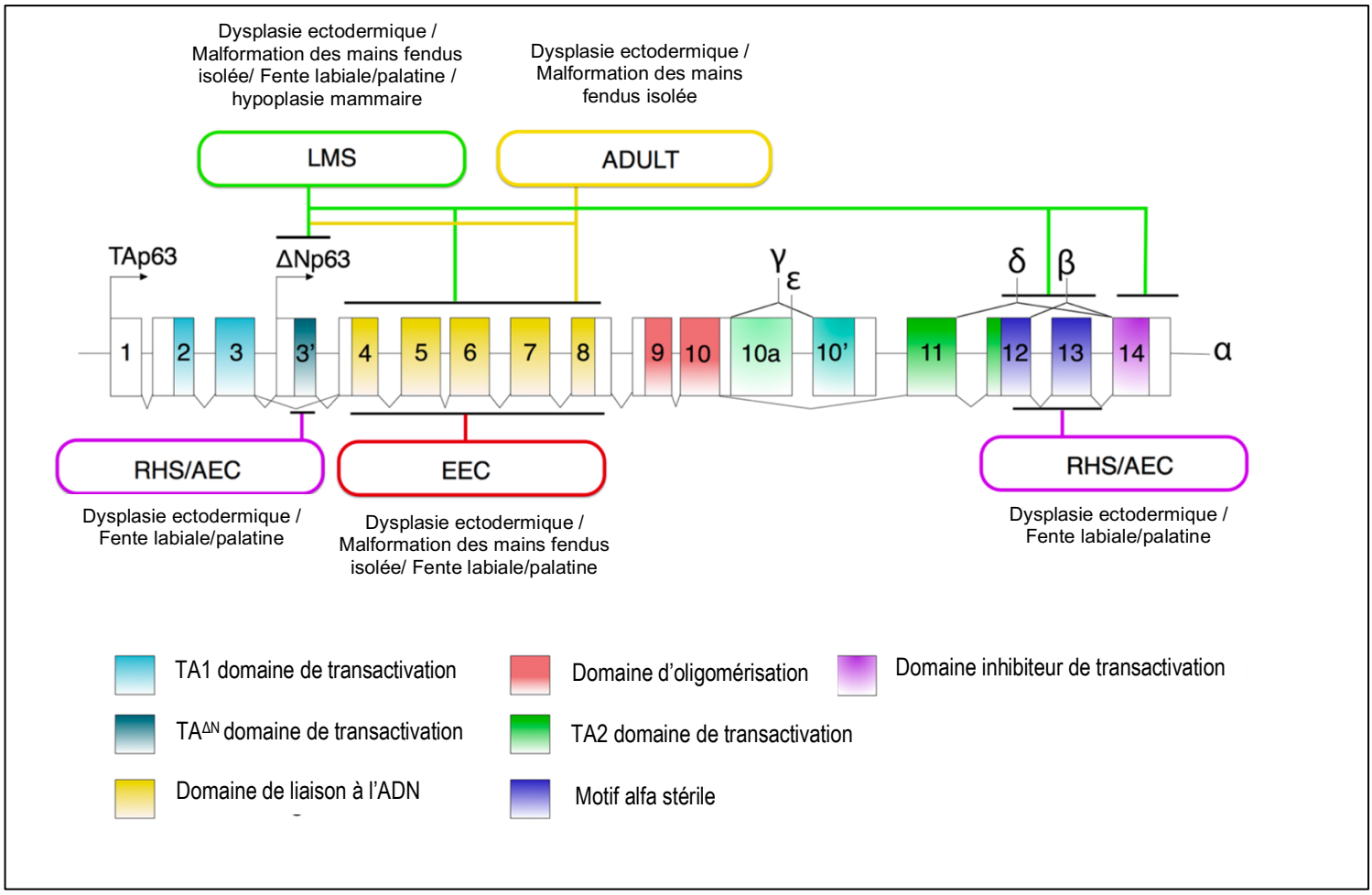

Figure 8- Structure génique et protéique de p63 et mutations impliquées dans les syndromes de développement avec des phénotypes épidermiques (dysplasie ectodermique) - (Adapté de Soares and Zhou ,2018)

Deux promoteurs conduisant aux isoformes N-terminales TA et ΔN sont indiqués par des flèches. Les exons et les domaines protéiques sont numérotés et codés par couleur comme indiqué. Les syndromes de dysplasie ectodermique associés à des mutations de la p63 sont marqués dans des rectangles à bords arrondis, et les emplacements de leurs mutations fréquentes sont indiqués par des lignes noires. Les principaux phénotypes liés aux syndromes sont indiqués près des rectangles.

En raison du phénotype épidermique frappant des modèles murins de suppression de p63 et des maladies humaines associées à des mutations de ce gène, le rôle moléculaire et cellulaire de p63 dans les kératinocytes épidermiques a été largement étudié. Il a été démontré que ΔNp63α est important à la fois dans la prolifération et la différenciation de modèles de kératinocytes humains *in vitro* (Truong *et al.*, 2006; Truong and Khavari, 2007). Une autre étude montre qu'une expression plus élevée de p63 (toutes isoformes incluses) est trouvée dans les cellules plus prolifératives, telles que les holoclones qui représentent les cellules souches épidermiques humaines (Pellegrini *et al.*, 2001), ce qui indique que la protéine p63 (sachant que l'isoforme prédominante est ΔNp63α) est importante pour la prolifération des kératinocytes. Ainsi, de nombreuses études ont utilisé des approches de knock-down par siARN pour étudier le rôle des différentes isoformes de p63 dans la prolifération et la différenciation. Le knock-down de ΔNp63 dans les kératinocytes primaires humains entraîne une hypoplasie, une hypoprolifération, un arrêt du cycle cellulaire (Truong *et al.*, 2006) et des anomalies de l'adhérence cellulaire (Carroll *et al.*, 2006). De plus, la régulation à la baisse de ΔNp63 empêche les cellules de se différencier et de se stratifier à la fois dans les modèles de différenciation des kératinocytes en 2D et 3D. Bien que la prolifération et la différenciation soient liées, p63 semble avoir des rôles indépendants dans les deux processus. Cela a été confirmé par une étude où le knock-down de p63 (toutes isoformes incluses) a provoqué à la fois une hypoplasie et des défauts de différenciation, et le knock-down concomitant de p53 ne peut sauver que la carence en hypoplasie, mais pas les défauts de différenciation (Truong *et al.*, 2006).

Au niveau moléculaire, le knock-down de p63 induit des gènes qui contrôlent l'arrêt du cycle cellulaire, tels que *CDKN1A* (codant pour p21) (Westfall *et al.*, 2003; Truong *et al.*, 2006; LeBoeuf *et al.*, 2010), et des gènes qui régulent négativement la prolifération cellulaire, tels que *JunB*. En même temps, le knock-down de ΔNp63α régule à la baisse des gènes qui peuvent réguler positivement la prolifération cellulaire, tels que *Fos* et *c-Jun* (Della Gatta *et al.*, 2008), et des gènes importants pour la différenciation épidermique, tels que *Perp* et *KRT14* (codant pour K14) (Ihrie *et al.*, 2005; Romano, Birkaya and Sinha, 2007). De manière cohérente, de nombreux gènes impliqués dans la prolifération cellulaire, le contrôle du cycle cellulaire et la différenciation des kératinocytes ont été montrés comme des gènes cibles directs de p63 (Kouwenhoven, van Bokhoven and Zhou, 2015).

3. Le double rôle de p63 dans le cancer

Des mutations au niveau du gène p63 provoquent des anomalies épidermiques caractérisées par une dysplasie ectodermique comme mentionné précédemment. Des rapports ultérieurs ont indiqué que *TP63* joue également un rôle important dans la tumorigenèse (Yao and Chen, 2012). À la différence de *TP53*, les mutations du gène *TP63* sont peu fréquentes dans les cancers, mais on observe des altérations de son expression, notamment une surexpression. Ainsi, une des altérations les plus partagées entre les carcinomes épidermoïdes du poumon, des VADS, de l'œsophage, du col de l'utérus et de la vessie est l'amplification de la région chromosomique entre 3q26 et 3q28, qui inclut le gène *TP63* ; cela est associé à une prédominance de l'ARNm codant l'isoforme ΔNp63α par rapport aux ARNm codant TAp63 (Campbell *et al.*, 2018). De manière similaire, selon les ensembles des données disponibles dans le portail cBioportal for Cancer Genomics (cbioportal.org), *TP63* est altérée ou amplifiée chez 47% des patients/échantillons atteints de carcinome des cellules squameuses (SCC) du poumon et chez 23% des patients/échantillons atteints de SCC des VADS (Gao *et al.*, 2013). Cependant, le rôle pro ou anti-tumoral de p63 demeure mal défini, surtout en ce qui concerne les fonctions distinctes des deux isoformes TAp63 et ΔNp63.

a. Rôle de l'isoforme TAp63

TAp63 est largement reconnu comme un suppresseur de la carcinogenèse et de la progression tumorale. Certains chercheurs estiment que l'expression forcée de TAp63 favorise l'apoptose consécutive au traitement chimiothérapeutique dans les cellules hépatiques. De plus, il a été démontré que TAp63 a la capacité d'activer à la fois les voies d'apoptose médiées par les récepteurs de la mort cellulaire (voie extrinsèque) et celles par le relargage du cytochrome c des mitochondries (voie intrinsèque), ce qui renforcent la sensibilité à la chimiothérapie ; en revanche, le blocage de la fonction de TAp63 conduit à une résistance accrue à la chimiothérapie (Gressner *et al.,* 2005).
D'autres rapports ont également indiqué que des agents génotoxiques, tels que l'irradiation ultraviolette (UV) conduisaient à une élévation des niveaux de protéines TAp63, et l'interaction avec Cables1 est impliqué dans la stabilité de l'isoforme TAp63 en le protégeant de la dégradation via le protéasome, ce qui favorise l'apoptose des

cellules en réponse aux agents génotoxiques (Wang *et al.*, 2010). Il semble alors qu'en réponse au stress causé par des dommages à l'ADN, les cellules favorisent une forte expression de TAp63, contribuant ainsi une série de réactions qui induisent l'apoptose cellulaire. Néanmoins, le rôle de TAp63 a fait l'objet de débats vu qu'une autre étude a signalé que les protéines TAp63 étaient également observées dans les noyaux d'une sous-population de cellules lymphoïdes et étaient présentes dans la plupart des lymphomes malins. En effet, les chercheurs ont constaté une prévalence élevée (33,2 ± 22,31%) de cellules néoplastiques immunoréactives pour TAp63 dans la plupart des lymphomes folliculaires de grade III (Pruneri *et al.*, 2005). Des données encore plus récentes montrent que TAp63α, qui induit l'apoptose dans de nombreux essais, peut favoriser la progression des tumeurs et les métastases chez les souris (Koster *et al.*, 2006).

b. Rôle de l'isoforme ΔNp63

Il est important de noter que ΔNp63α est l'isoforme prédominante présente dans l'épiderme humain adulte, et son expression est associée au compartiment prolifératif de la peau (Parsa *et al.*, 1999), mais jusqu'à présent son rôle dans les cancers est controversé (Mills, 2006; Chen *et al.*, 2018). Certaines études ont montré que des niveaux plus élevés de ΔNp63α pourraient favoriser la prolifération et l'invasion des cellules cancéreuses, ainsi que la résistance à la chimiothérapie, à travers divers mécanismes dans de nombreux types de tumeurs tels que les carcinomes épidermoïdes primaires des VADS, le cancer du sein et le cancer du poumon non à petites cellules (NSCLC) (Chung *et al.*, 2010; E *et al.*, 2013; Dang *et al.*, 2015; Fisher *et al.*, 2016). D'autres études ont suggéré un rôle de ΔNp63α dans la prévention des métastases et l'inhibition de la transition épithélio-mésenchymateuse au niveau des cellules cancéreuses humaines de la vessie (Tran *et al.*, 2013). De plus, il a été démontré que ΔNp63α est impliqué dans l'induction de l'arrêt du cycle cellulaire, de l'apoptose, et de la régulation des gènes cibles de p53 dans un modèle de lignée cellulaire dérivée d'un NSCLC (Dohn et al., 2001).

Barbieri *et al.* montrent que la perte de l'expression de p63 dans les cellules squameuses aboutit à une régulation à la hausse des gènes associés à l'invasion tumorale et la formation de métastases (N-cadhérine par exemple). Cet effet est précisément dû à la perte de l'isoforme ΔNp63α puisqu'une expression ectopique de

l'isoforme TAp63α chez la souris prédispose à une augmentation de l'expression de N-cadhérine, l'EMT et la dissémination métastatique (Barbieri *et al.*, 2006). Zhou *et al.* expliquent aussi que ΔNp63α exerce une fonction anti-tumorale au niveau des cellules du carcinome squameux cervical et ceci en montrant que ΔNp63α réduit la prolifération, régule l'EMT, supprime la migration, l'invasion ainsi que l'angiogenèse (Zhou *et al.*, 2020).

Pris ensemble, le rôle de p63 dans la tumorigenèse est complexe. L'expression de p63 et de ses isoformes respectives est beaucoup plus tissu-spécifique (exemple ΔNp63 dans les cellules basales de l'épithélium) que celle de p53, et par conséquent, l'impact de p63 sur la tumorigenèse est probablement spécifique à chaque type de tumeur.

La progression tumorale est souvent accompagnée de transition épithélio-mésenchymateuse. Ainsi, une tumeur dérivée d'une cellule épithéliale exprimant p63 (TAp63 et ΔNp63), comme une cellule cutanée, pourrait perdre l'expression de p63 en conséquence de cette transition (EMT), contrairement à une conséquence de l'initiation ou de la progression tumorale en elle-même (Mills, 2006).

L'équilibre entre les isoformes TAp63 et ΔNp63 semble jouer un rôle crucial dans la régulation des destinées cellulaires, telles que le maintien des cellules souches non engagées par rapport à la différenciation, la survie par rapport à l'apoptose, et la tumorigenèse par rapport à la suppression tumorale. Donc, la compréhension des rôles des interactions entre TAp63 et ΔNp63 pourrait probablement fournir des informations utiles pour le développement épithélial normal et la carcinogenèse.

Finalement, dévoiler le complexe réseau d'interactions entre les différentes isoformes de p63, en plus de déterminer comment ces protéines influencent les autres membres de la famille p53, représente des défis importants qui contribueront à mieux comprendre le rôle de p63 dans le cancer.

ΔNp63 dans les cancers des VADS

p63, et plus particulièrement l'isoforme prédominant ΔNp63α, est surexprimé dans 80% des cancers des VADS et semble jouer un rôle crucial dans leur évolution (Citro *et al.*, 2020). De nombreuses études ont été menées afin d'évaluer l'utilisation de p63 comme marqueur pronostique dans les carcinomes épidermoïdes, mais son rôle définitif dans la formation et la progression des tumeurs reste controversé. p63 est considéré dans la littérature comme un oncogène potentiel. Certaines études montrent que ΔNp63α favorise la prolifération, la migration et l'inflammation épithéliales squameuses dans les cancers des VADS (Rocco *et al.*, 2006; Yang *et al.*, 2011; Citro *et al.*, 2019). Une autre étude rapporte que la forte expression de p63 est associée à un phénotype plus agressif et à un mauvais pronostic dans ces cancers (Foschini *et al.*, 2004). De plus, plusieurs fonctions biochimiques de ΔNp63α ont été rapportées et pourraient médier l'oncogenèse induite par cette isoforme ; celles-ci comprennent l'activation de la signalisation de la β-caténine (Patturajan *et al.*, 2002), la régulation à la hausse de Hsp-70 (Wu *et al.*, 2005), la répression de la protéine pro-apoptotique IGFBP-3 (Barbieri *et al.*, 2005) et la suppression de l'apoptose dépendante de p73 (Rocco *et al.*, 2006).

Contrairement à un rôle dans la promotion de la tumorigenèse, l'expression de p63 est associée à un pronostic favorable dans la progression du cancer. Il a été démontré que des niveaux élevés de ΔNp63α sont associés à un pronostic favorable chez les patients atteints de carcinome épidermoïde de la tête et du cou (Zangen, Ratovitski and Sidransky, 2005). De manière importante, Barbieri *et al.* montrent grâce à une approche de perte de fonction que la perturbation de l'expression de p63 dans les lignées cellulaires épithéliales squameuses a conduit à la régulation négative des marqueurs de l'épithélium squameux, et à la diminution de la capacité des kératinocytes à se différencier (*in vitro*). La perte de p63 régule à la hausse l'expression de gènes associés à l'invasion tumorale et aux métastases qui s'accompagnent d'un changement vers une morphologie cellulaire mésenchymateuse. Ces données suggèrent que ΔNp63α agit pour maintenir le caractère épithélial dans les cellules qui l'expriment, et que la perte de son expression dans les tumeurs peut prédisposer à l'invasion et aux métastases (Barbieri *et al.*, 2006).

Il est donc possible que ΔNp63α agisse pour favoriser les premières étapes de la tumorigenèse en protégeant les cellules contre l'arrêt de la croissance et l'apoptose, tout en agissant en tant que suppresseur de métastases en maintenant le caractère épithélial des cellules cancéreuses.

Finalement, dans un modèle de cancer VADS HPV+, les niveaux d'expression de ΔNp63α (ARNm et protéine) sont significativement plus élevés dans les cancers VADS HPV+ où les oncoprotéines virales E6 et E7 régulent la transcription de ΔNp63α (en comparant à ceux HPV-) (Citro *et al.*, 2020). De plus, il est largement accepté que les cancers des VADS HPV+ répondent plus favorablement à la radiothérapie et ont un pronostic favorable par rapport aux cancers VADS HPV- (Gillison, 2004). Par conséquent, des études supplémentaires visant à définir l'expression de p63 dans les tumeurs des VADS HPV+ et son association à la survie ou la récurrence des patients sont nécessaires.

4. Activités transcriptionnelles de l'isoforme ΔNp63α

ΔNp63 est un facteur de transcription et son implication dans l'homéostasie épidermique et dans la pathogénèse du cancer épidermoïde est entre autres due à sa capacité de réguler l'expression de gènes cibles directs en se liant dans la région promotrice de ces gènes et en y interagissant avec d'autres cofacteurs de transcription. De plus, des études ont révélé que la plupart des sites génomiques de liaison de p63 sont situés au niveau de régions introniques et à une distance médiane de 27 kb du site d'initiation de la transcription, qui est une distribution qui caractérise les enhancers (Lin-Shiao *et al.*, 2019). Ceci a été prouvé également par Hamdan *et al.* qui montrent que la suppression de ΔNp63 affecte très fortement le programme de transcription des cellules pancréatiques et modifie leur identité moléculaire permettant ainsi d'émettre l'hypothèse que ΔNp63 occupe des super-enhancers (SE) (Hamdan and Johnsen, 2018).

Ainsi, p63 régule l'expression de nombreux gènes cibles impliqués dans plusieurs processus cellulaires impliquant la prolifération, la différenciation, la stratification et l'adhésion. Au cours des années, la compréhension des fonctions moléculaires de p63

a été facilitée par des expériences d'immunoprécipitation de la chromatine (ChIP) réalisées dans des kératinocytes humains primaires et immortalisés, ce qui a conduit à l'identification d'un nombre relativement important de cibles de p63 à l'échelle du génome (Kouwenhoven *et al.*, 2015). Par exemple, une étude réalisée par Lin-Shiao *et al.* identifie un certain nombre de gènes régulés à la hausse lors de l'expression ectopique de p63 et l'analyse par Gene Ontology (GO) montre un enrichissement dans l'expression de gènes impliqués dans l'adhésion cellulaire tels que *CDSN*, *LAD1* et *GJB4* (une caractéristique importante des cellules épithéliales pour la spécification de l'épithélium de chaque lignée). D'autres catégories concernaient également l'interféron, l'inflammation et les voies immunitaires, conformément aux rapports précédents montrant que p63 module le développement épidermique et des programmes d'inflammation et joue un rôle crucial dans le développement des lymphocytes T grâce à l'établissement de l'épithélium thymique (Lin-Shiao *et al.*, 2019).

Le panel de gènes régulés par ΔNp63α dans un contexte pathologique et notamment cancéreux a été décrit dans plusieurs publications. De façon intéressante, une étude visant à l'identification de cibles directes de ΔNp63α par RNA-seq et ChIP-seq dans le cancer du col de l'utérus a été réalisée montrant un enrichissement pour un ensemble de gènes impliqués dans la jonction cellulaire. De plus, certains gènes détectés étaient activés par ΔNp63α comme *CLDN1* (gène impliqué dans la jonction intercellulaire) et d'autres étaient réprimés comme *ZNF385B* et *NFATC1*. Une corrélation positive est observée entre l'expression de *CLDN1* et le taux de survie des patients alors qu'une corrélation négative est révélée lors de l'expression de *ZNF385B*. En revanche, la répression de *NFATC1* était associée à une diminution de la résistance au cisplatine favorisant ainsi l'apoptose (Zhou *et al.*, 2020). Ceci montre un rôle anti-tumoral de ΔNp63α qui est un régulateur important au niveau du cancer du col de l'utérus favorisant ainsi une meilleure compréhension des processus fondamentaux et constituant un pronostic qui pourra être associé ultérieurement à des cibles thérapeutiques adaptées.

De plus, l'influence de p63 sur les cellules de la réponse immunitaire adaptative a été démontrée dans une étude par Kubo *et al.*, dans laquelle p63 était liée à la production de TARC/CCL17 par différentes lignées de cellules épithéliales humaines, qui agit

comme une chimiokine qui attire les populations de lymphocytes T CD4+. Cela peut inclure à la fois des populations de lymphocytes T effecteurs activés et des lymphocytes T régulateurs (Tregs) ayant des rôles biologiques contrastés (Kubo *et al.*, 2008). De nombreuses études ont fourni des preuves de l'importance des cellules immunitaires dans le microenvironnement tumoral et l'effet de l'immunosuppression sur le développement du carcinome épidermoïde cutané (cSCC) (King *et al.*, 2019). Ainsi, Brantsch et al. ont démontré que la métastase du cSCC corrélait positivement avec l'immunosuppression et l'épaisseur de la tumeur, suggérant que l'évasion de l'immunité anti-tumorale peut favoriser la progression tumorale (Brantsch *et al.*, 2008). Chez les individus immunocompétents, les cSCC expriment un profil de chimiokines qui facilite le recrutement de cellules immunitaires dans l'environnement tumoral, mais de multiples mécanismes au sein du TME peuvent inhiber leur fonction. Par ailleurs, ce phénotype fortement inflammatoire est également observé dans d'autres SCC, tels que le carcinome épidermoïde des VADS, où ΔNp63α est fréquemment surexprimé (Davis, Van Waes and Allen, 2016).

En effet, à partir d'expériences menées sur des modèles *in vitro* et *in vivo* de carcinomes pancréatiques (pancreatic ductal adenocarcinomas PDA), les chercheurs ont découvert que ΔNp63α pouvait influencer le TME en stimulant l'expression de cytokines pro-inflammatoires, notamment l'IL-1α par les cellules cancéreuses du pancréas (Somerville *et al.*, no date).

Ceci peut être expliqué par le fait qu'une des fonctions majeures de l'épithélium squameux normal est de servir de barrière protectrice contre les agressions exogènes. En tant que tel, les voies inflammatoires doivent être étroitement régulées et prêtes à une réponse rapide dans ces tissus, et les cellules squameuses de l'épiderme sont connues pour exprimer de grandes quantités d'IL-1α à l'état stable (Hauser *et al.*, 1986). De plus, il a été précédemment démontré que ΔNp63α et le facteur de transcription « nuclear factor-kappa B » NF-kB régulent conjointement un ensemble commun de gènes cibles dans des modèles cellulaires de carcinome épidermoïde des VADS et qui comprend plusieurs gènes qui codent pour des cytokines inflammatoires. Cela a été validé d'une part *in vivo* où les chercheurs ont observé que l'augmentation du niveau nucléaire de ΔNp63α est associée à la présence de cellules inflammatoires infiltrées dans le derme des souris ainsi que dans des cellules cancéreuses des VADS (Yang *et al.*, 2011) et d'autre part grâce à une étude transcriptomique d'RNAseq

réalisée dans notre laboratoire et qui montre que les principales voies régulées à la baisse lors de l'extinction de ΔNp63α concernent les gènes impliqués dans la réponse immunitaire et la signalisation des cytokines (Mourtada *et al.*, 2023).

On peut donc conclure, à partir de ces résultats, que ΔNp63α joue un rôle dans la réponse immunitaire en modifiant la composition du microenvironnement tumoral et plus particulièrement en ce qui concerne les cellules immunitaires.

Finalement, il a été démontré que ΔNp63α régule l'expression de DKK3 (Dickkopf3), un membre de la famille des dickkopf, qui sont des protéines inhibitrices de la voie Wnt. Ainsi, dans un modèle cellulaire de cancer de l'œsophage, les chercheurs ont montré que ΔNp63α se fixe au niveau de la région en amont du promoteur de *DKK3* favorisant ainsi son expression (Kajiwara *et al.*, 2018). De plus, grâce à l'étude de RNAseq qu'on a réalisé dans le laboratoire, on a pu mettre en évidence que la régulation à la baisse de ΔNp63α dans un modèle de cancer de l'oropharynx HPV+ s'accompagne d'une diminution significative de l'expression de DKK3 (Mourtada *et al.*, 2023). Finalement, il convient de noter que DKK3 possède aussi un rôle controversé dans la tumorigenèse qui sera détaillé dans l'article de revue ci-dessous.

IV. Le Rôle Polyvalent de la Protéine Humaine Dickkopf-3 (DKK-3) dans le Développement, le Cancer et la Modulation Immunitaire

La protéine DKK3, également connue sous le nom de Dickkopf-3, est une protéine qui joue un rôle dans la régulation de la voie de signalisation Wnt, qui est importante pour le développement cellulaire et la croissance. DKK3 est impliquée dans la modulation de cette voie de signalisation, ce qui peut avoir des effets sur la prolifération cellulaire, la différenciation, et d'autres processus biologiques. A ce titre, plusieurs études mettent en évidence un rôle de DKK3 dans la régulation de la réponse immunitaire. DKK-3 assure ces différentes fonctions dans des contextes physiologiques comme pathologiques, comme dans le développement embryonnaire, la physiopathologie de certaines maladies, et notamment le cancer.

L'article de revue que j'ai rédigé et qui suit replace donc l'ensemble des propriétés structurales, biologiques et immunomodulatrices de DKK3 par rapport à ses fonctions physiologiques ainsi que son implication dans le cancer.

The Multifaceted Role of Human Dickkopf-3 (DKK-3) in Development, Immune Modulation and Cancer

Jana Mourtada[1,2], Chloé Thibaudeau[1,2] Bohdan Wasylyk[3,4,5,6] and Alain C. Jung[1,2]

1. Laboratoire de Biologie Tumorale, Institut de Cancérologie Strasbourg Europe, 17 Rue Albert Calmette, 6720 Strasbourg, France
2. Laboratoire STREINTH (Stress Response and Innovative Therapies), INSERM U1113 IRFAC, Université de Strasbourg, 3 av. Molière, 67200 Strasbourg, France
3. Institut de Génétique et de Biologie Moléculaire et Cellulaire (IGBMC), Illkirch, France
4. Institut National de la Santé et de la Recherche Médicale (INSERM) U 1258, Illkirch, France
5. Centre Nationale de la Recherche Scientifique (CNRS) UMR 7104, Illkirch, France
6. Université de Strasbourg, Illkirch, France

* Corresponding author : Dr. Alain Jung, Laboratoire de Biologie Tumorale, Institut de Cancérologie Strasbourg Europe, 67200 Strasbourg, France. Email: a.jung@icans.eu; Tel: +33 (0)3 88 27 53 67

Abstract: The human Dickkopf (DKK) family includes four main secreted proteins, DKK-1, DKK-2, DKK-3, and DKK-4, as well as the DKK-3 related protein soggy (Sgy-1 or DKKL1). These glycoproteins play crucial roles in various biological processes, and especially modulation of the Wnt signaling pathway. DKK-3 is distinct, with its multifaceted roles in development, stem cell differentiation and tissue homeostasis. Intriguingly, DKK-3 appears to have immunomodulatory functions and a complex role in cancer, acting as either a tumor suppressor or an oncogene, depending on the context. DKK-3 is a promising diagnostic and therapeutic target that can be modulated by epigenetic reactivation, gene therapy and DKK-3-blocking agents. However, further research is needed to optimize DKK-3-based therapies. In this review, we comprehensively describe the known functions of DKK-3 and highlight the importance of context in understanding and exploiting its roles in health and disease.

Keywords: Dickkopf (DKK) family, Wnt signaling pathway, DKK-3, Development, Immunomodulation, Cancer, Tumor suppressor, Oncogene, Therapy.

1. Sequence and structural properties of the DKK family of proteins

The human genome encodes four similar secreted dickkopf (DKK) proteins (DKK-1, DKK-2, DKK-3 and DKK-4) **(Figure 1)** and a distinct DKK-3-related protein known as Soggy (Sgy-1 or DKKL1). DKK proteins are glycosylated and harbor an N-terminal signal peptide as well as two conserved cysteine-rich domains (CRD1 and CRD2). CRD1 is located towards the N-terminus, and is uniquely found in the human DKK family of proteins [1]. Both CRD1 and CRD2 are required for receptor binding at the cell surface **(see below)**. DKK-3 is the most divergent family member. It has a shorter linker between its CRD1 and CRD2 (13 amino acids versus 51 to 56 for the others), lower homology (40% versus 50% between the others) [2,3], a higher molecular weight (38 kDa compared to 24 to 29 kDa [3]), and an additional Soggy domain[4] that resembles the N-terminal region of DKKL1. The functional significance of the Soggy domain remains unknown.

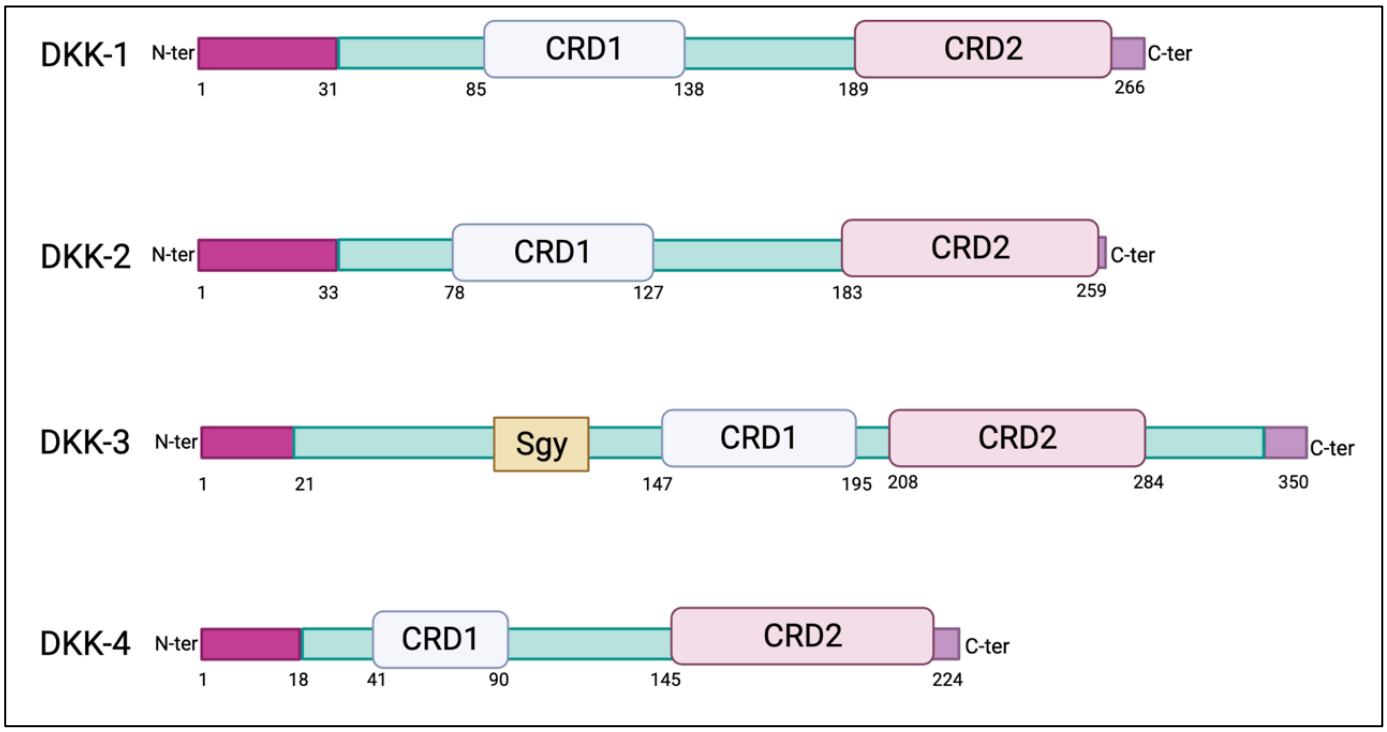

Figure 1- Schematic diagrams of individual DKK proteins.

CRD1/ CRD2: cysteine rich domain 1 or 2. Sgy: Soggy. Created with BioRender.com

2. DKKs modulate the Wnt signaling pathway through binding to the LRP5/6 and Krm1/2 co-receptors

DKK1 was initially discovered in Xenopus embryos as a crucial regulator of the Wnt/β-catenin signaling pathway, early embryonic development and head formation [5]. Wnt signaling includes three sub-pathways, namely the canonical as well as the non-canonical planar cell polarity (PCP) and Wnt/calcium pathways.

In the canonical pathway, Wnt regulates the stability and cellular localization of β-catenin. In the absence of Wnt signaling **(Figure 2, right panel)**, β-catenin is degraded through a sequence of events that involves : (1) binding to a multi-protein complex that contains Axin, the Glycogen Synthase Kinase 3β (GSK 3β) and adenomatous polyposis coli (APC), (2) phosphorylation by GSK 3β and CK1α, (3) ubiquitination by the β-transducin repeats-containing proteins (β-TrCP) E3-ubiquitin ligase (not shown) and (4) degradation by the proteasome. In the presence of Wnt **(Figure 2, left panel)**, β-catenin is stabilized by: (1) Wnt binding to the Frizzled receptors and the LRP5/6 (low density lipoprotein receptor-related protein 5/6) co-receptors (2) phosphorylation of disheveled leading to inhibition of the Axin/GSK 3β/APC complex, (3) accumulation of unphosphorylated β-catenin that is resistant to ubiquitination and degradation, (4) β-catenin translocation to the nucleus, association with the T-cell factor/lymphoid enhancer factor (TCF/LEF) transcription factors and regulation of Wnt target genes [6,7]

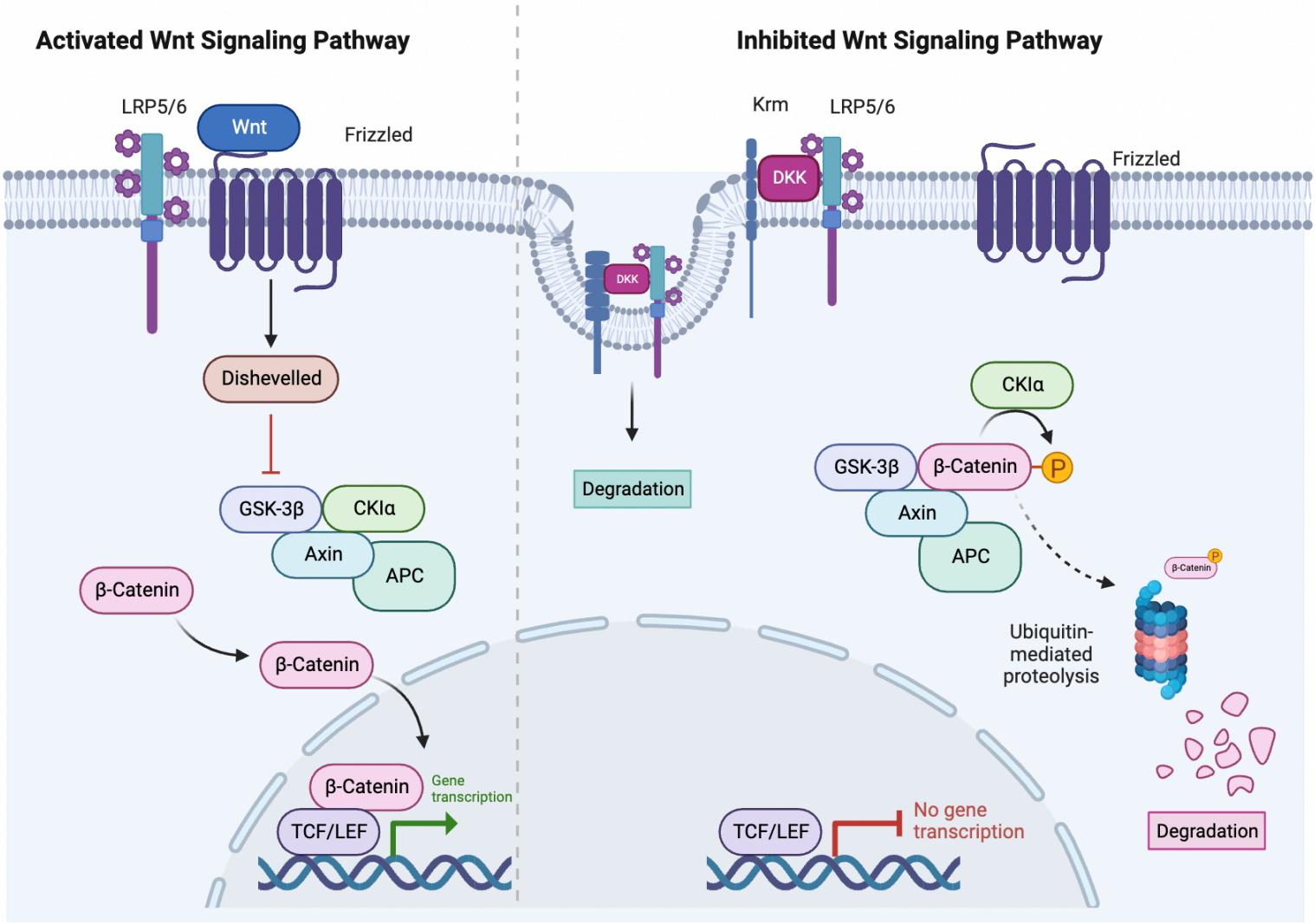

Figure 2- Canonical WNT signaling in the presence of WNT ligands (left panel) and inhibition by DKK (right panel).

Left panel: WNT binds to a receptor complex on the cell surface that is composed of Frizzled (FZD) and either lipoprotein receptor-related protein 5 (LRP5) or LRP6. This interaction leads to activation of Dishevelled (DVL) that then inhibits the axin-glycogen synthase kinase 3β (GSK3β)-adenomatous polyposis coli (APC)-casein kinase 1 (CK1) complex, leading to loss of β-catenin phosphorylation and degradation. β-catenin accumulates in the cytoplasm and translocates to the nucleus, where it activates the transcription factors T cell factor (TCF) and lymphoid enhancer factor (LEF). Right panel: Dickkopf (DKK) inhibits WNT-β-catenin signaling. DKK binds to LRP5/6, preventing its interaction with FZD. Additionally, it collaborates with kremen (Krm) to trigger internalization and degradation of the LRP6-DKK complex. Finally, the protein complex (DVL-GSK3β-APC-CK1-Axin) facilitated the phosphorylation of β-catenin leading to its ubiquitinylation and degradation by the proteasome (Adapted form Schunk et al., 2021). Created with BioRender.com

Canonical Wnt signaling is inhibited by DKK-1/-2 and -4 binding to the Wnt co-receptors LRP5/6 [8] **(Figure 2, right panel)**. LRP5/6 were initially discovered as plasma membrane receptors for DKK1 and DKK2, and LRP6 has been shown to be a co-receptor for Wnt signaling. Mao et al.[9] originally observed that DKK-1 binds specifically and with high affinity (10^{-10} M) to LRP6 expressed on 293T cells, and inhibits the Wnt pathway by impeding the formation of the Wnt-Frizzled-LRP complex. DKKs also inhibit Wnt signaling by binding with high affinity to Kremen proteins (Krm1 and Krm2), which results in formation of ternary complexes with LRP5/6, rapid endocytosis and degradation of LRP5/6 [10] **(Figure 2, right panel)**. Consistently, mice with a double knockout of Krm1 and Krm2 (Krm1/1 and Krm2/2) have elevated Wnt signaling, a bone mass phenotype and extra digits in the forelimbs. Notably, the growth of these ectopic digits is further amplified by loss of DKK expression, indicating that DKK1 and Kremen interact genetically during limb development [11].

DKK-3 differs from the other DKKs in the way it impinges on the Wnt signaling pathway. However, there are discordant findings. Nierhs and collaborators reported that DKK-3 does not bind to LRP6 or Kremen-2 co-receptors at the cell surface, consistent with the lack in its CRD2 of specific amino acids required for protein-protein interactions [12]. Similarly, Mao et al. reported that DKK-3 does not inhibit Wnt induction of transcription in 293T cells, suggesting that DKK-3 does not antagonize Wnt signaling [9]. Yet, several studies have reported that DKK-3 inhibits the Wnt signaling pathway by interacting with Kremen receptors. Mohammadpour et al. predicted, using bioinformatics models for docking analysis, that DKK-3 interacts with either or both the extracellular kringle and CUB domains of Kremen [13]. They proposed that the interaction with the CUB domain potentiates the Wnt pathway, leading to enhanced cell invasion and migration, whereas the interaction with either the kringle domain or both the kringle and CUB domains prevents Wnt signaling by inhibiting the nuclear translocation of β-catenin [14]. Xu et al., reported that DKK-3 and Kremen-1 interact functionally. Downregulation of Kremen-1 with siRNA reduced the protective ability of rDKK-3 in a mouse Intracerebral hemorrhage (ICH) model. In addition, DKK-3 and Kremen-1 co-localized in neurons and microglia after ICH [15]. Ferrari et al. reported that DKK-3 interact physically with Kremen-1 in human Breast Cancer-Cancer Associated Fibroblasts (BC-CAFs) and co-localizes in internal structures [16] leading to Kremen-1 destabilization, LRP5/6 stabilization and activation of Wnt signaling in a cell-autonomous manner.

In conclusion, DKK-3's properties are controversial and different from the other DKK family members, and due to the controversies about its ability to physically bind LRP5/6 and/or Kremen 1/2 at the cell surface, was considered by some authors to be an orphan ligand until the late 2010s'.

3. CKAP4 is the only known receptor for DKK-3

Quite recently, Kimura et al. [17] discovered that DKK-3, as well as the other DKKs, physically bind to CKAP4 (cytoskeleton-associated protein 4, also known as P63, CLIMP-63 or ERGIC-63). CKAP4 is a type II transmembrane protein that is primarily expressed in the endoplasmic reticulum (ER) and regulates its architecture [18]. Yet, a minor fraction of CKAP4 (less than 10% of the total) is transported to the plasma membrane of specific cell types, including pulmonary, vascular smooth muscle, and bladder epithelial cells [19]. CKAP4 is the only known protein that binds to the CRD1 domain [17], whereas LRP5/6 binds CRD2 [8,20] The CKAP4 extracellular domain-CRD1 interaction triggers the internalization of CKAP4 in a clathrin-dependent manner [17]. The functional consequences of DKK binding to CKAP4 on the cell membrane are poorly understood. Most notably DKK1 binding to CKAP4 triggers the intracellular PI3K/Akt signaling pathway [17], which is relevant for tumor progression [for review see [21] and references therein]. To date, and to the best of our knowledge, CKAP4 is the only known receptor for DKK-3.

4. DKK-3 has diverse biological roles

As mentioned earlier, DKK-3 is a divergent member of the DKK family. Intriguingly, it is expressed as both a secreted isoform and a cytoplasmic, non-secreted isoform called DKK-3b (D2p29). The *DKK-3b* transcript originates from an alternative transcriptional start site located in intron 2 of the *DKK-3* gene. DKK-3 and DKK-3b differ at the N-terminal 71 residues, which include the signal peptide sequence and N-glycosylation sites that direct DKK-3 to the secretory vesicle [22]. DKK-3b is an intracellular regulator of β-catenin signaling and cell proliferation. It impairs nuclear translocation of β-catenin through the formation of an extranuclear complex with β-

TrCP, thereby sequestering cytoplasmic, unphosphorylated β-catenin, and inhibiting Wnt/β-catenin signaling **(Figure 3A).**

Unlike other DKK members, DKK-3 has no major developmental function, and DKK-3 knock-out mice are viable and fertile. They display different phenotypes in behavior (increased velocity), elevated hematocrit and total hemoglobin concentration in blood, lower respiratory rates and higher titers of NK cells and IgM [23].

DKK-3 has additional roles, relating to cartilage degradation, cardiac hypertrophy, artheroprotection, pulmonary ventilation and oxidative stress **(Cell protection, Table 1)**. Snelling et al. demonstrated that incubation of primary human chondrocytes or chondrosarcoma cells with recombinant DKK-3 protects against *in vitro* cartilage degradation through enhanced TGF-β signaling, and DKK-3 expression is regulated by both injury and inflammatory cytokines [24]. Intracellular and extracellular DKK-3 play crucial roles in preventing cardiac hypertrophy [25] and promote the differentiation of stem cells into vascular smooth muscle cells [26], via the activation of several intracellular signaling pathways, including the ASK1/JNK/p38 [apoptosis signal-regulating kinase 1 (ASK1)-c-Jun N-terminal kinase (JNK)/p38] and MEK/ERK/ATF6 axes, respectively **(Figure 3B-C),**. Extracellular DKK-3 also serves as an atheroprotective cytokine, which stimulates the migration of HUVEC endothelial cells through the Wnt/Planar Cell Polarity (ROR2-Dvl1-Rac1-JNK) signaling pathway, potentially acting as a biomarker of endothelial integrity and repair [27] **(Figure 3D)**. DKK-3 can also influence cellular antioxidant defense mechanisms and protect cells from oxidative damage, since recombinant DKK-3 protects cultured astrocytes against oxidative stress [28]. However, in all these cases, the precise molecular mechanisms have not been elucidated.

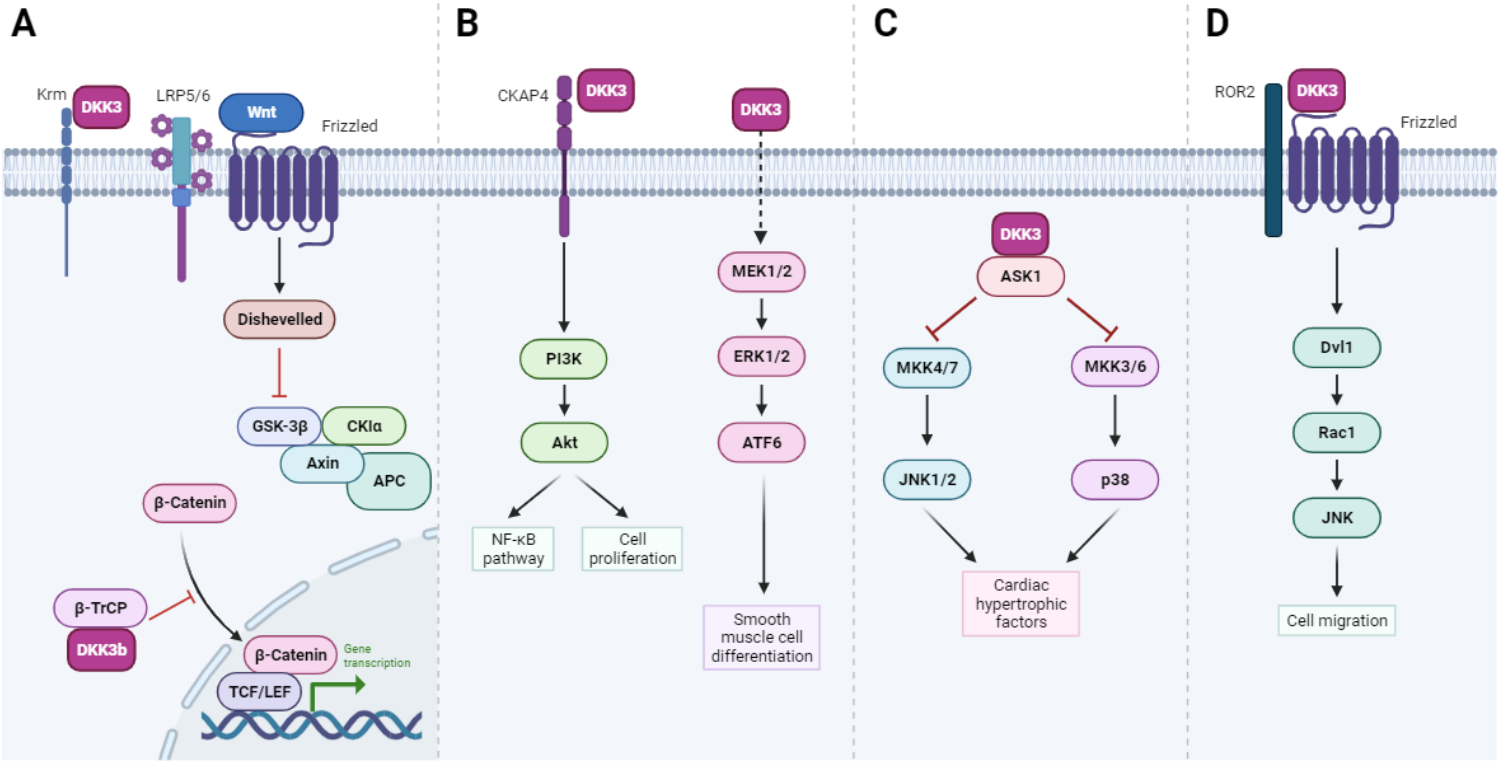

Figure 3- Pathways regulated by DKK3: insights into DKK-3 functions.

A- DKK-3b serves as an intracellular regulator of β-catenin signaling and cell proliferation. By forming an extranuclear complex with β-TrCP, DKK-3b impedes the nuclear translocation of β-catenin, leading to the cytoplasmic sequestration, unphosphorylated β-catenin and subsequent inhibition of Wnt/β-catenin signaling. **B-** *(left panel)* Secreted DKK-3 activates NF-κB signaling via a CKAP4-Akt-NF-κB axis. *(right panel)* Extracellular DKK-3 promotes the differentiation of stem cells into vascular smooth muscle cells through the activation of the MEK/ERK/ATF6 axis. **C-** Intracellular DKK-3 prevents cardiac hypertrophy through ASK1/JNK/p38 signaling pathway's activation. **D-** Extracellular DKK-3 stimulates the migration of HUVEC endothelial cells through the Wnt/Planar Cell Polarity (ROR2-Dvl1-Rac1-JNK) signaling pathway.

5. DKK-3 modulates the immune system

DKK-3 has diverse role in immunomodulation, that extends from differentiation of B-cells, immune peripheric tolerance, dendritic cell differentiation and inflammation **(Table 1).** DKK-3 is expressed at the highest levels in immune-privileged organs, such as embryo, placenta, eye, and brain [3], which is compatible with a role for DKK-3 in their immune tolerance. Ludwig et al. [29] provided evidence that DKK-3 acts as a modulator of B cell fate and function. They found that loss of DKK-3 in *DKK-3*$^{-/-}$ mice had significant impacts on various aspects of B cell biology. Specifically, it affected the maturation of B2 cells, which play a crucial role in adaptive immune responses. It also reduced the proliferation and self-maintenance ability of B1 cells in the periphery, thereby influencing the production of antibodies and cytokines involved in the innate immune response. Most importantly, DKK-3 has been shown to play a vital role in

establishing peripheral CD8 T-cell tolerance in a T-cell receptor (TCR) transgenic system. This is supported by the observation that DKK-3 expression is elevated in tolerant CD8 T cells, and it contributes to reducing the overall reactivity of CD8 T cells *in vitro* [30]. Interestingly, the same group also reported that an anti-DKK-3 neutralizing antibody, administered after transplantation of male MHC class-I mismatched embryoid bodies under the kidney capsule of sex-matched recipient mice, resulted in a higher occurrence of graft rejection. This suggests that DKK-3 is involved in the local microenvironment that protects transplanted MHC class-I mismatched embryo bodies from CD8+ T-cell-dependent rejection. In addition, they provided evidence that DKK-3 plays a role in regulating CD4+ T-cell-mediated autoimmune encephalomyelitis, by restricting T-cell activation and polarization, as well as moderating the activity of IFNγ in the central nervous system (CNS), leading to disease improvement [31]. Consistently, a machine learning approach proposed that high DKK-3 expression related to immunosuppression was associated with poor prognosis in glioblastoma [32]. DKK-3 also affects the functions of dendritic cells (DC), which play a crucial role in initiating and regulating immune responses. Secreted DKK-3 has been shown to induce differentiation of monocytes to DC-like cells [33]. DKK-3 is involved in inflammation, in that it reduces the intracerebral hemorrhage- related expression of TNF-α and IL-1β [15]. DKK-3 also reduces neuroinflammation and improves neuropathic pain, through the inhibition of p-ASK1, p-JNK, p-p38, the promotion of the transformation of microglia from pro-inflammatory type M1 to anti-inflammatory type M2, and decreased production of pro-inflammatory cytokines [34].

Further research is needed to fully characterize and understand the complex interplay between DKK-3 and the immune system, and to exploit these finding for immunomodulation therapies.

6. DKK-3 has a dual role in cancer, as either a tumor suppressor or an oncogene.

a. DKK-3 as a tumor suppressor

DKK-3, as implied by its other name, REIC (Reduced Expression in Immortalized Cells), is frequently downregulated in various tumor types, cancer cell lines, and immortalized cells [35], as expected for a tumor suppressor **(Table 1; Figure 4).** Its expression is commonly suppressed through hypermethylation of CpG islands in the DKK-3 locus in human cancer cells, including basal breast cancer, non-small cell lung cancer, gastric cancers and colon cancers [36,37]**.** Clinical trials are underway to explore the potential of REIC/DKK-3 gene therapy for prostate cancer [38] and liver cancer [39].

DKK-3 acts as a tumor suppressor through inhibition of the Wnt/β-Catenin signaling pathway. For instance, ectopic overexpression of DKK-3 has been shown to decrease cancer cell proliferation *in vitro* through the inhibition of the Wnt/β-catenin pathway [40,41]. DKK-3 strongly inhibits prostate cancer cell proliferation [42]. DKK-3 expression is significantly downregulated in invasive epithelial ovarian carcinoma compared to normal tissue, adenoma, and borderline tumors. Furthermore, DKK-3 inhibits proliferation of ovarian cancer cells. DKK-3 decreases the levels of active non-phosphorylated β-catenin, as well as P-glycoprotein, an important chemoresistance-regulating protein. DKK-3 acts as an inhibitor of chemoresistance, since reducing DKK-3 levels decreases resistance to chemotherapy with paclitaxel [43]. In lung cancer cells, DKK-3 downregulates the expression of survivin at the protein level, and DKK-3 overexpression decreases c-myc and MMP7, which are Wnt signaling effector genes that control the fate of cancer development, progression and metastasis [6]. In addition, DKK-3 inhibits cisplatin-resistant lung cancer cell growth in a xenograft model of nude mice. The authors show that DKK-3 enhances apoptosis and retards growth either alone or synergistically with cisplatin in resistant non-small cell lung cancer (NSCLC) cells [6] **(Figure 4, right panel).**

Interestingly, DKK-3 also exerts a tumor-suppressive function independently of Wnt signaling. An *in-silico* study predicted an interaction between DKK-3 and EGFR, in which DKK-3 could completely occupy the EGF binding domain of the EGFR. This

suggest that DKK-3 may possibly inhibit cancer proliferation by inhibiting both Wnt and EGFR signaling [14].

Another study based on blood samples from patients with ovarian cancer established a negative correlation between the serum levels of DKK-3 and the amount of circulating CD133+ cells, used as a glycoprotein marker for cancer stem cells (CSCs). Administration of DKK-3 increased both the transcript and protein levels of the epithelial marker E-cadherin and reduced mesenchymal markers (Vimentine, N-cadherin, and Snail) suggesting that DKK-3 inhibits the epithelial-mesenchymal transition (EMT). This observation is significant, since it suggests the combination of both of CD133+ and DKK-3 markers could have prognosis value **(Figure 4, left panel)** [44].

Consistently with the known function of DKK-3 as an immunomodulatory molecule (see above), REIC/DKK-3 may play a cytokine-like role in monocyte differentiation since the intratumor administration of full-length DKK-3 (FL-REIC) led to the induction of anti-cancer immunity towards prostate cancer cells, and inhibition of tumor growth *in vivo* [33]. Finally, our team has recently shown that DKK-3 expression is regulated by ΔNp63α in Human-Papillomavirus-positive oropharyngeal squamous cell carcinoma, and that secreted DKK-3 actives NF-κB signaling in macrophages through a CKAP4-Akt- NF-κB axis, without impacting Wnt signaling **(Figure 3B)** [45].

b. DKK-3 as an oncogene

DKK-3 expression is elevated and exhibits tumor-promoting functions in some cancers **(Table 1).** DKK-3 expression has been found to be high in squamous cell carcinoma of the head and neck, esophagus, and pancreatic ductal adenocarcinoma cell lines [46], and to promote cancer cell proliferation and migration **(Figure 4, right panel)**. Cytoplasmic levels of DKK-3 have been reported to increase during the carcinogenic transition of the oral epithelium, and to be higher in tissues samples of head and neck squamous cell carcinoma (HNSCC), where they correlate with β-catenin accumulation [47]. Moreover, and as mentioned earlier, DKK-3 has an immunomodulatory role that contributes to the establishment of peripheral T-cell tolerance [31]. Thus, DKK-3 could

contribute to limiting immune cell infiltration in the tumor microenvironment. In addition, it has been reported that DKK-3 is required for the pro-tumorigenic functions of cancer associated fibroblasts (CAFs), including matrix consolidation, and cancer cell growth and invasion [16]. High levels of stromal DKK-3 in Benign Prostatic Hyperplasia (BPH) and Prostate Cancer (PCa) have been reported to increase fibroblast proliferation, to promote myofibroblast differentiation and to contribute to the angiogenic switch by suppressing vessel-stabilizing factors like angiopoetin-1 (ANGPT1) [48] **(Figure 4, right panel).**

In conclusion, DKK-3 appears to have a dual role, acting either to promote or repress cancer depending on the specific tissue and/or cell context. The inhibitory effect of DKK-3 on the Wnt pathway implies a potential tumor suppressor role due to the prevalent pro-oncogenic impact of Wnt pathway overactivation. However, in other tumors DKK-3 has been implicated in immune suppression, in both Wnt signaling-dependent or independent manners.

	DKK3 function	Comment	Ref.
Cell protection	Cell adhesion, migration and invasion	Secreted DKK3 is part of the extracellular matrix and promotes cell adhesion, migration and invasion	49
	Chondroprotection	DKK3 prevents İnterleukin-1β/oncostatin-M driven proteoglycan loss of cartilage and is upregulated in osteoarthritis	24
	Protection against cardiac hypertrophy	DKK3 protects the heart against pressure overload-induced cardiac remodeling through the inhibition of the ASK1-JNK/p38 signaling pathway	50
	Smooth muscle cell (SMC) differentiation	DKK3 induces the expression of differentiated SMC markers (myocardin) through the activation of the ATF6 transcription factor	26
	Endothelium protection and repair	DKK3$^{-/-}$ mice have more atherosclerotic lesions. DKK3 stimulates endothelial cell migration through the Wnt/Planar Cell Polarity signaling pathway	27
	Protection against neuronal death	DKK3$^{-/-}$ ischemic mice have greater infarct size. DKK3 prevents astrocyte death via the upregulation of VEGF expression and the activation of VEGFR2	28
Immune response & inflammation	B cell fate and function	B1 cells have better proliferation and survival abilities whereas the development of B2 cells is impaired in DKK3$^{-/-}$ mice, which also show altered immune and cytokine responses	29
	Peripheral CD8 T cell tolerance	• DKK3 is expressed in tolerant T cells, where it reduces reactivity to host antigens. Blocking DKK3 leads to autologous skin grafts rejection. • DKK3$^{-/-}$ mice suffer from exacerbated experimental autoimmune encephalomyelitis with increased numbers of IFNγ-producing T cells in the central nervous system	30 31
	Anti-tumor immune response regulation	High expression of DKK3 in glioblastoma multiform correlates with poorer prognosis and decreased anti-tumor immunity.	32
	Regulation of inflammatory cytokines	DKK3 reduces the intracerebral hemorrhage-related expression of TNF-α and IL-1β	15
	Differentiation of monocytes to DCs	Human CD14^{+} monocytes grown with recombinant DKK3 differentiate into immature CD11c^{+}, CD40^{+}, CD86^{+}, HLADR^{+} DCs	33
	Microglia polarization and reduction of neuroinflammation	DKK3 inhibits the ASK-1/JNK/p38 pathway, favoring the transformation of type M1 to M2 microglia and the downregulation of TNF-α, IL-6 and IL-1β	15

Tumor suppressor function	Downregulated expression in cancer cells	DKK3 expression is lower in immortalized cell lines and 8 human tumor-derived cell lines	35
	DKK3 promoter is hypermethylated in cancer	The frequency of DKK3 promoter hypermethylation varies from 26% (pleural mesothelia) to 61% (breast carcinoma).	1,36
	Suppression of cell proliferation	The overexpression of DKK3 in hepatoma and cervical cancer cells diminishes cell proliferation in vitro	40,41
	Response to chemotherapy	• DKK3 loss is correlated with chemoresistance and adverse prognosis in ovarian cancer, and extracellular DKK3 reduces cell proliferation, migration, and response to paclitaxel in vitro • DKK3 siRNA-mediated dowregulation mediates lung cancer cell resistance to cisplatin, and DKK3 overexpression impairs cell proliferation and migration, induces apoptosis and increases cell sensitivity to cisplatin.	6,43
	Serum DKK3 is a prognosis biomarker	DKK3 levels are negatively correlated with the number of CD133+ circulating tumor cells in ovarian cancer	44
	Regulation of the tumor immune microenvironment	DKK3 expression correlates with infiltrating CD8+ lymphocytes and macrophages in HPV-positive HNSCC, and stimulates NF-κB signaling in macrophages	45
Oncogenic function	Stimulation of cell proliferation, migration and tumor growth	The expression of DKK3 is high in HNSCC, esophageal and pancreatic cell lines, where it stimulates cell proliferation and migration ion vitro. In xenograft models, DKK3 support tumor growth.	46
	Correlation with tumor progression	DKK3 expression was found to increase from normal oral mucosa in dysplasia and squamous cell carcinoma, and to correlate with the tissue proliferative index (Ki67)	47
	DKK3 has pro-tumorigenic function in tumor stroma	• The expression of DKK3 in the stroma of breast, colon and ovarian cancer is associated with poorer prognosis. DKK3 stimulates the β-catenin and YAP/TAZ signaling pathways in cancer-associated fibroblasts, increasing their extracellular matrix remodeling activity. • The knockdown of DKK3 in prostatic stromal cells decreases their proliferation, inhibits the fibroblast-to-myofibroblast differentiation, and contributes to blood vessel destabilization through the upregulation of ANGPT1.	16,48

Table 1- A comprehensive literature summary: Revealing the versatile role of human Dickkopf-3 (DKK-3) in development, immune Modulation, and cancer.

7. DKK-3 as a tool for cancer therapy

DKK-3 has a dual role in cancer, making its use as diagnostic/prognostic biomarker and/or as a therapeutic target complex and context-dependent. There are various strategies to increase DKK-3 levels, where it acts as a tumor suppressor. Epigenetic reactivation of DKK-3 expression through DNA hypomethylating reagents such as 5-Aza-20 -deoxycytidine (decitabine) have been proposed as potential therapeutics [51] **(Figure 4, left panel)**. Nevertheless, significant clinical challenges remain, such as non-selective cytotoxicity, limited bioavailability, and temporary activity since DNA methylation levels revert to normal once the drug is withdrawn [52]. Attempts have been made to express DKK-3 with an adenoviral vector (Ad-REIC) in cancer patients with low levels of DKK-3. DKK-3 expression has been shown to increase cancer cell apoptosis, in a phosphorylated JNK-dependent manner, via endoplasmic reticulum (ER) stress signaling. Interestingly, in non-cancer cells, a different ER stress response is observed, that leads to IL-7 expression and secretion, and NK cells activation of systemic anti-tumor immunity [53]. Ad-REIC has been shown in clinical trials (NCT01931046) with high-risk localized prostate cancer, to be safe with no apparent side effects [38] **(Figure 4, left panel)**. However, due to the need of local administration within the tumor and the need for imaging guidance, this therapy is limited to the treatment of solid tumors.

In contrast, DKK-3 expression is up-regulated in some cancers, such as squamous cell carcinoma of the head and neck and pancreatic ductal adenocarcinoma, and is correlated with poorer overall survival. DKK-3 could therefore be a druggable target and inhibitors are being developed [54,55]. Based on docking simulations, Katase et al. developed DKK-3 complementary peptides that significantly reduce DKK-3-driven Akt phosphorylation, cellular proliferation and migration of a human tongue cancer-derived cell line (HSC-3), as well as *in-vivo* tumor growth [56]. These therapeutic peptides are a promising approach for the development of anti-cancer agents, since they are relatively easy to develop and are inexpensive **(Figure 4, left panel)**. DKK-3-blocking monoclonal antibodies have also been developed and found to be effective against pancreatic ductal adenocarcinoma progression [57] **(Figure 4, left panel).**

In conclusion, DKK-3 is a promising target for cancer therapy. There are favorable facets that suggest that DKK-3 is a target of choice. It has functions in both cancer and immune cells, suggesting that targeting one factor could have multiple and perhaps synergistic effects. Furthermore, it is secreted, which suggest that it is more easily targeted and modulated. However, to fully exploit this promise, further investigations are needed to understand the different activities of DKK-3, and to optimize therapeutic strategies that take into account context and cancer-type dependence.

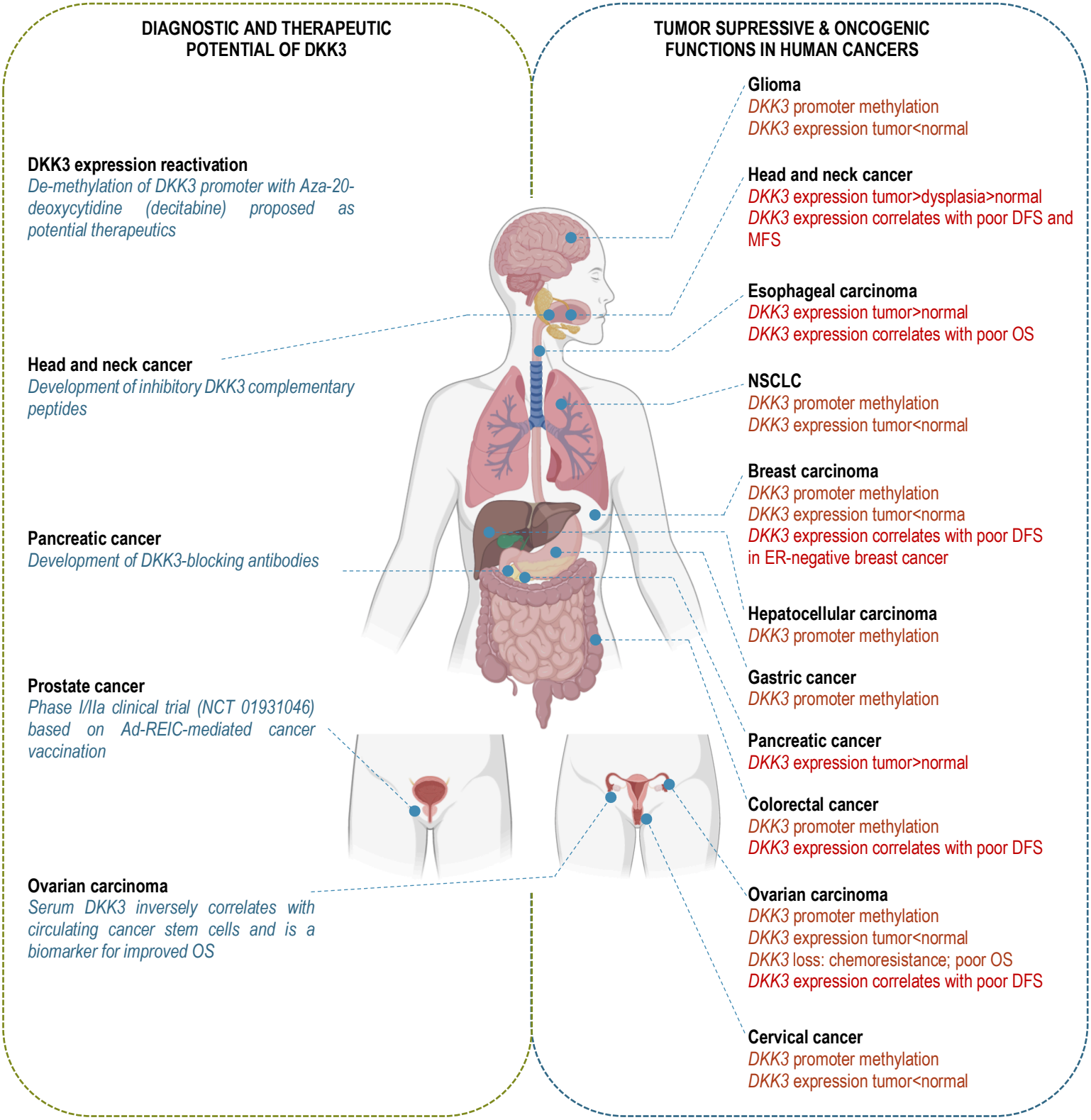

Figure 4- The Dual Role of DKK-3 in Cancer: Implications for Diagnosis, Prognosis, and Therapeutic Strategies. DKK3 has been reported to play a role in human cancer progression and/or response to treatment. However, its function has been described as tumor suppressive (green text; right panel) or oncogenic (red text; right panel) depending on the cellular and tissue context. In addition, DKK3 is a potential interesting tool, both as a prognostic biomarker or a druggable therapeutic target (left panel).

REFERENCES

(1) Veeck, J.; Dahl, E. Targeting the Wnt Pathway in Cancer: The Emerging Role of Dickkopf-3. *Biochim. Biophys. Acta BBA - Rev. Cancer* **2012**, *1825* (1), 18–28. https://doi.org/10.1016/j.bbcan.2011.09.003.

(2) Krupnik, V. E.; Sharp, J. D.; Jiang, C.; Robison, K.; Chickering, T. W.; Amaravadi, L.; Brown, D. E.; Guyot, D.; Mays, G.; Leiby, K.; Chang, B.; Duong, T.; Goodearl, A. D. J.; Gearing, D. P.; Sokol, S. Y.; McCarthy, S. A. Functional and Structural Diversity of the Human Dickkopf Gene Family. *Gene* **1999**, *238* (2), 301–313. https://doi.org/10.1016/S0378-1119(99)00365-0.

(3) Niehrs, C. Function and Biological Roles of the Dickkopf Family of Wnt Modulators. *Oncogene* **2006**, *25* (57), 7469–7481. https://doi.org/10.1038/sj.onc.1210054.

(4) Kajiwara, C.; Fumoto, K.; Kimura, H.; Nojima, S.; Asano, K.; Odagiri, K.; Yamasaki, M.; Hikita, H.; Takehara, T.; Doki, Y.; Morii, E.; Kikuchi, A. P63-Dependent Dickkopf3 Expression Promotes Esophageal Cancer Cell Proliferation via CKAP4. *Cancer Res.* **2018**, *78* (21), 6107–6120. https://doi.org/10.1158/0008-5472.CAN-18-1749.

(5) Kawano, Y.; Kypta, R. Secreted Antagonists of the Wnt Signalling Pathway. *J. Cell Sci.* **2003**, *116* (13), 2627–2634. https://doi.org/10.1242/jcs.00623.

(6) Wang, Z.; Ma, L.-J.; Kang, Y.; Li, X.; Zhang, X.-J. Dickkopf-3 (Dkk3) Induces Apoptosis in Cisplatin-Resistant Lung Adenocarcinoma Cells via the Wnt/β-Catenin Pathway. *Oncol. Rep.* **2015**, *33* (3), 1097–1106. https://doi.org/10.3892/or.2014.3704.

(7) Duchartre, Y.; Kim, Y.-M.; Kahn, M. The Wnt Signaling Pathway in Cancer. *Crit. Rev. Oncol. Hematol.* **2016**, *99*, 141–149. https://doi.org/10.1016/j.critrevonc.2015.12.005.

(8) Kikuchi, A.; Matsumoto, S.; Sada, R. Dickkopf Signaling, beyond Wnt-Mediated Biology. *Semin. Cell Dev. Biol.* **2022**, *125*, 55–65. https://doi.org/10.1016/j.semcdb.2021.11.003.

(9) Mao, B.; Wu, W.; Li, Y.; Hoppe, D.; Stannek, P.; Glinka, A.; Niehrs, C. LDL-Receptor-Related Protein 6 Is a Receptor for Dickkopf Proteins. *Nature* **2001**, *411* (6835), 321–325. https://doi.org/10.1038/35077108.

(10) Mao, B.; Wu, W.; Davidson, G.; Marhold, J.; Li, M.; Mechler, B. M.; Delius, H.; Hoppe, D.; Stannek, P.; Walter, C.; Glinka, A.; Niehrs, C. Kremen Proteins Are Dickkopf Receptors That Regulate Wnt/b-Catenin Signalling. **2002**, *417*.

(11) Nakamura, T.; Aoki, S.; Kitajima, K.; Takahashi, T.; Matsumoto, K.; Nakamura, T. Molecular Cloning and Characterization of Kremen, a Novel Kringle-Containing Transmembrane Protein. *Biochim. Biophys. Acta BBA - Gene Struct. Expr.* **2001**, *1518* (1–2), 63–72. https://doi.org/10.1016/S0167-4781(01)00168-3.

(12) Mao, B.; Niehrs, C. Kremen2 Modulates Dickkopf2 Activity during Wnt/lRP6 Signaling. *Gene* **2003**, *302* (1–2), 179–183. https://doi.org/10.1016/S0378-1119(02)01106-X.

(13) Mohammadpour, H.; Khalili, S.; Hashemi, Z. S. Kremen Is beyond a Subsidiary Co-Receptor of Wnt Signaling: An in Silico Validation. *Turk. J. Biol.* **2015**, *39*, 501–510. https://doi.org/10.3906/biy-1409-1.

(14) Mohammadpour, H.; Pourfathollah, A. A.; Nikougoftar Zarif, M.; Khalili, S. Key Role of Dkk3 Protein in Inhibition of Cancer Cell Proliferation: An in Silico Identification. *J. Theor. Biol.* **2016**, *393*, 98–104. https://doi.org/10.1016/j.jtbi.2015.12.029.

(15) Xu, Y.; Nowrangi, D.; Liang, H.; Wang, T.; Yu, L.; Lu, T.; Lu, Z.; Zhang, J. H.; Luo, B.; Tang, J. DKK3 Attenuates JNK and AP-1 Induced Inflammation via Kremen-1 and DVL-1 in Mice Following Intracerebral Hemorrhage. *J. Neuroinflammation* **2020**, *17* (1), 130. https://doi.org/10.1186/s12974-020-01794-5.

(16) Ferrari, N.; Ranftl, R.; Chicherova, I.; Slaven, N. D.; Moeendarbary, E.; Farrugia, A. J.; Lam, M.; Semiannikova, M.; Westergaard, M. C. W.; Tchou, J.; Magnani, L.; Calvo, F. Dickkopf-3 Links HSF1 and YAP/TAZ Signalling to Control Aggressive Behaviours in Cancer-Associated Fibroblasts. *Nat. Commun.* **2019**, *10*, 130. https://doi.org/10.1038/s41467-018-07987-0.

(17) Kimura, H.; Fumoto, K.; Shojima, K.; Nojima, S.; Osugi, Y.; Tomihara, H.; Eguchi, H.; Shintani, Y.; Endo, H.; Inoue, M.; Doki, Y.; Okumura, M.; Morii, E.; Kikuchi, A. CKAP4 Is a Dickkopf1 Receptor and Is Involved in Tumor Progression. *J. Clin. Invest.* **2016**, *126* (7), 2689–2705. https://doi.org/10.1172/JCI84658.

(18) Sandoz, P. A.; Denhardt-Eriksson, R. A.; Abrami, L.; Abriata, L. A.; Spreemann, G.; Maclachlan, C.; Ho, S.; Kunz, B.; Hess, K.; Knott, G.; S. Mesquita, F.; Hatzimanikatis, V.; van der Goot, F. G. Dynamics of CLIMP-63 S-Acylation Control ER Morphology. *Nat. Commun.* **2023**, *14* (1), 264. https://doi.org/10.1038/s41467-023-35921-6.

(19) Kikuchi, A.; Fumoto, K.; Kimura, H. The Dickkopf1-Cytoskeleton-Associated Protein 4 Axis Creates a Novel Signalling Pathway and May Represent a Molecular Target for Cancer Therapy. *Br. J. Pharmacol.* **2017**, *174* (24), 4651–4665. https://doi.org/10.1111/bph.13863.

(20) Aravind, L.; Koonin, E. V. A Colipase Fold in the Carboxy-Terminal Domain of the Wnt Antagonists – the Dickkopfs. *Curr. Biol.* **1998**, *8* (14), R477–R479. https://doi.org/10.1016/S0960-9822(98)70309-4.

(21) Bhavanasi, D.; Speer, K. F.; Klein, P. S. CKAP4 Is Identified as a Receptor for Dickkopf in Cancer Cells. *J. Clin. Invest.* **2016**, *126* (7), 2419–2421. https://doi.org/10.1172/JCI88620.

(22) Leonard, J. L.; Leonard, D. M.; Wolfe, S. A.; Liu, J.; Rivera, J.; Yang, M.; Leonard, R. T.; Johnson, J. P. S.; Kumar, P.; Liebmann, K. L.; Tutto, A. A.; Mou, Z.; Simin, K. J. The Dkk3 Gene Encodes a Vital Intracellular Regulator of Cell Proliferation. *PLOS ONE* **2017**, *12* (7), e0181724. https://doi.org/10.1371/journal.pone.0181724.

(23) Barrantes, I. del B.; Montero-Pedrazuela, A.; Guadaño-Ferraz, A.; Obregon, M.-J.; Martinez de Mena, R.; Gailus-Durner, V.; Fuchs, H.; Franz, T. J.; Kalaydjiev, S.; Klempt, M.; Hölter, S.; Rathkolb, B.; Reinhard, C.; Morreale de Escobar, G.; Bernal, J.; Busch, D. H.; Wurst, W.; Wolf, E.; Schulz, H.; Shtrom, S.; Greiner, E.; Hrabé de Angelis, M.; Westphal, H.; Niehrs, C. Generation and Characterization of Dickkopf3 Mutant Mice. *Mol. Cell. Biol.* **2006**, *26* (6), 2317–2326. https://doi.org/10.1128/MCB.26.6.2317-2326.2006.

(24) Snelling, S. J. B.; Davidson, R. K.; Swingler, T. E.; Le, L. T. T.; Barter, M. J.; Culley, K. L.; Price, A.; Carr, A. J.; Clark, I. M. Dickkopf-3 Is Upregulated in Osteoarthritis and Has a Chondroprotective Role. *Osteoarthritis Cartilage* **2016**, *24* (5), 883–891. https://doi.org/10.1016/j.joca.2015.11.021.

(25) Akazawa, H.; Komuro, I. Dickkopf-3: A Stubborn Protector of Cardiac Hypertrophy. *Cardiovasc. Res.* **2014**, *102* (1), 6–8. https://doi.org/10.1093/cvr/cvu051.

(26) Wang, X.; Karamariti, E.; Simpson, R.; Wang, W.; Xu, Q. Dickkopf Homolog 3 Induces Stem Cell Differentiation into Smooth Muscle Lineage via ATF6 Signalling. *J. Biol. Chem.* **2015**, *290* (32), 19844–19852. https://doi.org/10.1074/jbc.M115.641415.

(27) Yu, B.; Kiechl, S.; Qi, D.; Wang, X.; Song, Y.; Weger, S.; Mayr, A.; Le Bras, A.; Karamariti, E.; Zhang, Z.; del Barco Barrantes, I.; Niehrs, C.; Schett, G.; Hu, Y.; Wang, W.; Willeit, J.; Qu, A.; Xu, Q. A Cytokine-Like Protein Dickkopf-Related Protein 3 Is Atheroprotective. *Circulation* **2017**, *136* (11), 1022–1036. https://doi.org/10.1161/CIRCULATIONAHA.117.027690.

(28) Busceti, C. L.; Di Menna, L.; Bianchi, F.; Mastroiacovo, F.; Di Pietro, P.; Traficante, A.; Bozza, G.; Niehrs, C.; Battaglia, G.; Bruno, V.; Fornai, F.; Volpe, M.; Rubattu, S.; Nicoletti, F. Dickkopf-3 Causes Neuroprotection by Inducing Vascular Endothelial Growth Factor. *Front. Cell. Neurosci.* **2018**, *12*, 292. https://doi.org/10.3389/fncel.2018.00292.

(29) Ludwig, J.; Federico, G.; Prokosch, S.; Küblbeck, G.; Schmitt, S.; Klevenz, A.; Gröne, H.-J.; Nitschke, L.; Arnold, B. Dickkopf-3 Acts as a Modulator of B Cell Fate and Function. *J. Immunol.* **2015**, *194* (6), 2624–2634. https://doi.org/10.4049/jimmunol.1402160.

(30) Papatriantafyllou, M.; Moldenhauer, G.; Ludwig, J.; Tafuri, A.; Garbi, N.; Hollmann, G.; Küblbeck, G.; Klevenz, A.; Schmitt, S.; Pougialis, G.; Niehrs, C.; Gröne, H.-J.; Hämmerling, G. J.; Arnold, B.; Oelert, T. Dickkopf-3, an Immune Modulator in Peripheral CD8 T-Cell Tolerance. *Proc. Natl. Acad. Sci. U. S. A.* **2012**, *109* (5), 1631–1636. https://doi.org/10.1073/pnas.1115980109.

(31) Meister, M.; Papatriantafyllou, M.; Nordström, V.; Kumar, V.; Ludwig, J.; Lui, K. O.; Boyd, A. S.; Popovic, Z. V.; Fleming, T. H.; Moldenhauer, G.; Nawroth, P. P.; Gröne, H.-J.; Waldmann, H.; Oelert, T.; Arnold, B. Dickkopf-3, a Tissue-Derived Modulator of Local T-Cell Responses. *Front. Immunol.* **2015**, *6*, 78. https://doi.org/10.3389/fimmu.2015.00078.

(32) Han, M.-H.; Min, K.-W.; Noh, Y.-K.; Kim, J. M.; Cheong, J. H.; Ryu, J. I.; Won, Y. D.; Koh, S.-H.; Myung, J. K.; Park, J. Y.; Kwon, M. J. High DKK3 Expression Related to Immunosuppression Was Associated with Poor Prognosis in Glioblastoma: Machine Learning Approach. *Cancer Immunol. Immunother.* **2022**, *71* (12), 3013–3027. https://doi.org/10.1007/s00262-022-03222-4.

(33) Watanabe, M.; Kashiwakura, Y.; Huang, P.; Ochiai, K.; Futami, J.; Li, S.-A.; Takaoka, M.; Nasu, Y.; Sakaguchi, M.; Huh, N.-H.; Kumon, H. Immunological Aspects of REIC/Dkk-3 in Monocyte Differentiation and Tumor Regression. *Int. J. Oncol.* **2009**, *34* (3), 657–663. https://doi.org/10.3892/ijo_00000191.

(34) Zhang, L.-Q.; Gao, S.-J.; Sun, J.; Li, D.-Y.; Wu, J.-Y.; Song, F.-H.; Liu, D.-Q.; Zhou, Y.-Q.; Mei, W. DKK3 Ameliorates Neuropathic Pain via Inhibiting ASK-1/JNK/p-38-Mediated Microglia Polarization and Neuroinflammation. *J. Neuroinflammation* **2022**, *19*, 129. https://doi.org/10.1186/s12974-022-02495-x.

(35) Tsuji, T.; Miyazaki, M.; Sakaguchi, M.; Inoue, Y.; Namba, M. A REIC Gene Shows Down-Regulation in Human Immortalized Cells and Human Tumor-Derived Cell Lines. *Biochem. Biophys. Res. Commun.* **2000**, *268* (1), 20–24. https://doi.org/10.1006/bbrc.1999.2067.

(36) Hayashi, T.; Asano, H.; Toyooka, S.; Tsukuda, K.; Soh, J.; Shien, T.; Taira, N.; Maki, Y.; Tanaka, N.; Doihara, H.; Nasu, Y.; Huh, N.; Miyoshi, S. DNA Methylation Status of REIC/Dkk-3 Gene in Human Malignancies. *J. Cancer Res. Clin. Oncol.* **2012**, *138* (5), 799–809. https://doi.org/10.1007/s00432-012-1158-6.

(37) Veeck, J.; Bektas, N.; Hartmann, A.; Kristiansen, G.; Heindrichs, U.; Knüchel, R.; Dahl, E. Wnt Signalling in Human Breast Cancer: Expression of the Putative Wnt Inhibitor Dickkopf-

3 (DKK3) Is Frequently Suppressed by Promoter Hypermethylation in Mammary Tumours. *Breast Cancer Res. BCR* **2008**, *10* (5), R82. https://doi.org/10.1186/bcr2151.

(38) Kumon, H.; Ariyoshi, Y.; Sasaki, K.; Sadahira, T.; Araki, M.; Ebara, S.; Yanai, H.; Watanabe, M.; Nasu, Y. Adenovirus Vector Carrying REIC/DKK-3 Gene: Neoadjuvant Intraprostatic Injection for High-Risk Localized Prostate Cancer Undergoing Radical Prostatectomy. *Cancer Gene Ther.* **2016**, *23* (11), 400–409. https://doi.org/10.1038/cgt.2016.53.

(39) Oyama, A.; Shiraha, H.; Uchida, D.; Iwamuro, M.; Kato, H.; Takaki, A.; Ikeda, F.; Onishi, H.; Yasunaka, T.; Takeuchi, Y.; Wada, N.; Iwasaki, Y.; Sakata, M.; Okada, H.; Kumon, H. A Phase I/Ib Trial of Ad-REIC in Liver Cancer: Study Protocol. *Future Oncol.* **2019**, *15* (31), 3547–3554. https://doi.org/10.2217/fon-2019-0115.

(40) Lee, E.-J.; Jo, M.; Rho, S. B.; Park, K.; Yoo, Y.-N.; Park, J.; Chae, M.; Zhang, W.; Lee, J.-H. Dkk3, Downregulated in Cervical Cancer, Functions as a Negative Regulator of β-Catenin. *Int. J. Cancer* **2009**, *124* (2), 287–297. https://doi.org/10.1002/ijc.23913.

(41) Hsieh, S.-Y.; Hsieh, P.-S.; Chiu, C.-T.; Chen, W.-Y. Dickkopf-3/REIC Functions as a Suppressor Gene of Tumor Growth. *Oncogene* **2004**, *23* (57), 9183–9189. https://doi.org/10.1038/sj.onc.1208138.

(42) Romero, D.; Kypta, R. Dickkopf-3 Function in the Prostate. *Bioarchitecture* **2013**, *3* (2), 42–44. https://doi.org/10.4161/bioa.25243.

(43) Nguyen, Q. T. T.; Park, H. S.; Lee, T. J.; Choi, K.-M.; Park, J. Y.; Kim, D.; Kim, J. H.; Park, J.; Lee, E.-J. DKK3, Downregulated in Invasive Epithelial Ovarian Cancer, Is Associated with Chemoresistance and Enhanced Paclitaxel Susceptibility via Inhibition of the β-Catenin-P-Glycoprotein Signaling Pathway. *Cancers* **2022**, *14* (4), 924. https://doi.org/10.3390/cancers14040924.

(44) Nie, X.-C.; He, F.; Lan, C.; Niu, J.-M.; Xia, P. Combined Serum DKK3 and Circulating CD133 Cells as Prognostic Biomarkers for Ovarian Cancer Patients. *OncoTargets Ther.* **2021**, *14*, 427–434. https://doi.org/10.2147/OTT.S288191.

(45) Mourtada, J.; Lony, C.; Nicol, A.; De Azevedo, J.; Bour, C.; Macabre, C.; Roncarati, P.; Ledrappier, S.; Schultz, P.; Borel, C.; Burgy, M.; Wasylyk, B.; Mellitzer, G.; Herfs, M.; Gaiddon, C.; Jung, A. C. A Novel ΔNp63-Dependent Immune Mechanism Improves Prognosis of HPV-Related Head and Neck Cancer. *Front. Immunol.* **2023**, *14*.

(46) Katase, N.; Nishimatsu, S.-I.; Yamauchi, A.; Yamamura, M.; Terada, K.; Itadani, M.; Okada, N.; Hassan, N. M. M.; Nagatsuka, H.; Ikeda, T.; Nohno, T.; Fujita, S. DKK3 Overexpression Increases the Malignant Properties of Head and Neck Squamous Cell Carcinoma Cells. *Oncol. Res.* **2018**, *26* (1), 45–58. https://doi.org/10.3727/096504017X14926874596386.

(47) Fujii, M.; Katase, N.; Lefeuvre, M.; Gunduz, M.; Buery, R. R.; Tamamura, R.; Tsujigiwa, H.; Nagatsuka, H. Dickkopf (Dkk)-3 and β-Catenin Expressions Increased in the Transition from Normal Oral Mucosal to Oral Squamous Cell Carcinoma. *J. Mol. Histol.* **2011**, *42* (6), 499–504. https://doi.org/10.1007/s10735-011-9357-z.

(48) Zenzmaier, C.; Sampson, N.; Plas, E.; Berger, P. Dickkopf-related Protein 3 Promotes Pathogenic Stromal Remodeling in Benign Prostatic Hyperplasia and Prostate Cancer. *The Prostate* **2013**, *73* (13), 1441–1452. https://doi.org/10.1002/pros.22691.

(49) Kano, J.; Wang, H.; Zhang, H.; Noguchi, M. Roles of DKK3 in Cellular Adhesion, Motility, and Invasion through Extracellular Interaction with TGFBI. *FEBS J.* **2022**, *289* (20), 6385–6399. https://doi.org/10.1111/febs.16529.

(50) Zhang, Y.; Liu, Y.; Zhu, X.-H.; Zhang, X.-D.; Jiang, D.-S.; Bian, Z.-Y.; Zhang, X.-F.; Chen, K.; Wei, X.; Gao, L.; Zhu, L.-H.; Yang, Q.; Fan, G.-C.; Lau, W. B.; Ma, X.; Li, H. Dickkopf-3 Attenuates Pressure Overload-Induced Cardiac Remodelling. *Cardiovasc. Res.* **2014**, *102* (1), 35–45. https://doi.org/10.1093/cvr/cvu004.

(51) Hamzehzadeh, L.; Caraglia, M.; Atkin, S. L.; Sahebkar, A. Dickkopf Homolog 3 (DKK3): A Candidate for Detection and Treatment of Cancers? *J. Cell. Physiol.* **2018**, *233* (6), 4595–4605. https://doi.org/10.1002/jcp.26313.

(52) Mehdipour, P.; Murphy, T.; De Carvalho, D. D. The Role of DNA-Demethylating Agents in Cancer Therapy. *Pharmacol. Ther.* **2020**, *205*, 107416. https://doi.org/10.1016/j.pharmthera.2019.107416.

(53) Watanabe, M.; Nasu, Y.; Kumon, H. Adenovirus-Mediated REIC/Dkk-3 Gene Therapy: Development of an Autologous Cancer Vaccination Therapy (Review). *Oncol. Lett.* **2014**, *7* (3), 595–601. https://doi.org/10.3892/ol.2013.1777.

(54) KATASE, N.; LEFEUVRE, M.; GUNDUZ, M.; GUNDUZ, E.; BEDER, L. B.; GRENMAN, R.; FUJII, M.; TAMAMURA, R.; TSUJIGIWA, H.; NAGATSUKA, H. Absence of Dickkopf (Dkk)-3 Protein Expression Is Correlated with Longer Disease-Free Survival and Lower Incidence of Metastasis in Head and Neck Squamous Cell Carcinoma. *Oncol. Lett.* **2012**, *3* (2), 273–280. https://doi.org/10.3892/ol.2011.473.

(55) Zenzmaier, C.; Hermann, M.; Hengster, P.; Berger, P. Dickkopf-3 Maintains the PANC-1 Human Pancreatic Tumor Cells in a Dedifferentiated State. *Int. J. Oncol.* **2012**, *40* (1), 40–46. https://doi.org/10.3892/ijo.2011.1180.

(56) Katase, N.; Nishimatsu, S.; Yamauchi, A.; Okano, S.; Fujita, S. Establishment of Anti-DKK3 Peptide for the Cancer Control in Head and Neck Squamous Cell Carcinoma (HNSCC). *Cancer Cell Int.* **2022**, *22* (1), 352. https://doi.org/10.1186/s12935-022-02783-9.

(57) Zhou, L.; Husted, H.; Moore, T.; Lu, M.; Deng, D.; Liu, Y.; Ramachandran, V.; Arumugam, T.; Niehrs, C.; Wang, H.; Chiao, P.; Ling, J.; Curran, M. A.; Maitra, A.; Hung, M.-C.; Lee, J. E.; Logsdon, C. D.; Hwang, R. F. Suppression of Stromal-Derived Dickkopf-3 (DKK3) Inhibits Tumor Progression and Prolongs Survival in Pancreatic Ductal Adenocarcinoma. *Sci. Transl. Med.* **2018**, *10* (464), eaat3487. https://doi.org/10.1126/scitranslmed.aat3487.

OBJECTIF DE L'ÉTUDE

Les carcinomes épidermoïdes oropharyngés induits par le papillomavirus humain (HPV) définissent un sous-groupe clinique de cancer des VADS dont la prévalence augmente. Il se développent principalement à partir de l'épithélium de la base de la langue et des amygdales. On les trouve généralement chez des patients plus jeunes, qui fument et consomment moins d'alcool, et ils sont associés à une survie globale à 5 ans significativement meilleure (70-80%) par rapport aux tumeurs HPV-négatives.

Les tumeurs de l'oropharynx HPV+ présentent, elles aussi une hétérogénéité pronostique, avec une proportion de patients à risque élevé de dissémination métastatique. Une thérapie personnalisée pour la prise en charge des patients HPV+ à pronostic favorable et défavorable nécessite une meilleure compréhension des caractéristiques moléculaires des tumeurs des VADS liées au papillomavirus humain (HPV) et l'identification de biomarqueurs biologiquement pertinents. Ainsi, afin de mieux caractériser l'hétérogénéité des tumeurs de l'oropharynx HPV+ au niveau moléculaire, le laboratoire a analysé des données transcriptomiques précédemment générées à partir de 8 fragments tumoraux obtenus à partir d'une exérèse chirurgicale de patients avec une tumeur de l'oropharynx ayant un statut HPV+, et a identifié une signature moléculaire dépendante de ΔNp63α corrélée au pronostic des patients. ΔNp63α est une isoforme de la protéine p63 et fait partie de la famille des suppresseurs de tumeurs p53. Ainsi, en amont du début de mon travail de thèse, le laboratoire a initié une analyse fonctionnelle afin de caractériser le rôle que joue ΔNp63α dans l'agressivité tumorale et le pronostic des tumeurs de l'oropharynx liés au HPV et a pu mettre en évidence que ΔNp63α :

- Régule l'expression de facteurs impliqués dans la transition épithélio-mésenchymateuse.
- Inhibe la migration et l'invasion des cellules cancéreuses des VADS HPV+
- Augmente la sensibilité des cellules cancéreuses au traitement au cisplatine (chimiothérapie de référence dans ce type de cancer)
- Corréle avec une infiltration dans le microenvironnement tumoral par des cellules immunitaires, en particuliers par des lymphocytes T CD8.

Sur ces bases, mes travaux de thèse visent donc à déterminer plus précisément comment ΔNp63α régule le recrutement et/ou l'activation des cellules immunitaires ayant une activité anti-tumorale et contribuant à l'amélioration du pronostic des patients positifs au HPV et ceci à travers :

- Une étude transcriptomique par RNAseq sur un modèle cellulaire de cancers de l'oropharynx HPV+ (SCC090) dans lequel ΔNp63α a été invalidé par un siARN

- La validation du niveau des transcrits de certaines cibles de ΔNp63α impliquées dans l'activation de la réponse immunitaire

- Une analyse fonctionnelle de l'impact de ΔNp63α sur l'activation de la réponse immunitaire par activation de la phagocytose par des macrophages *in vitro*

- L'étude de la régulation d'une des cibles (DKK-3) par ΔNp63α identifiée par RNA-seq et son implication dans la réponse immunitaire anti-tumorale à travers une analyse fonctionnelle

- Étude de l'activation de l'axe DKK-3 -CKAP4- Akt -NFκB

RÉSULTATS

Une partie importante des résultats que j'ai obtenu sont présentés dans un article scientifique publié dans Frontiers Immunology, auquel j'ai contribué sous la direction des Drs. Alain C. JUNG et Christian GAIDDON.

Cet article expose les résultats que j'ai pu obtenir durant mon travail de thèse. Ceux-ci présentent l'implication du facteur de transcription ΔNp63α dans l'activation de la réponse immunitaire dans les cancers des VADS induits par le papillomavirus humain HPV, et notamment à travers la régulation de l'expression d'un immunomodulateur diffusible, DKK3.

Parmi les résultats présentés, j'ai généré ceux présentés en Figure 5, les résultats supplémentaires S5, S6 et S7 ainsi que la vidéo microscopie de phagocytose.

frontiers | Frontiers in Immunology

TYPE Original Research
PUBLISHED 25 October 2023
DOI 10.3389/fimmu.2023.1264093

OPEN ACCESS

EDITED BY
Ilda Patrícia Ribeiro,
University of Coimbra, Portugal

REVIEWED BY
Remya Raja,
Mayo Clinic Arizona, United States
Jozsef Dudas,
Innsbruck Medical University, Austria

*CORRESPONDENCE
Alain C. Jung
a.jung@icans.eu
Christian Gaiddon
gaiddon@unistra.fr

†These authors have contributed equally to this work and share first authorship

‡These authors have contributed equally to this work and share last authorship

RECEIVED 20 July 2023
ACCEPTED 29 September 2023
PUBLISHED 25 October 2023

CITATION
Mourtada J, Lony C, Nicol A, De Azevedo J, Bour C, Macabre C, Roncarati P, Ledrappier S, Schultz P, Borel C, Burgy M, Wasylyk B, Mellitzer G, Herfs M, Gaiddon C and Jung AC (2023) A novel ΔNp63-dependent immune mechanism improves prognosis of HPV-related head and neck cancer. *Front. Immunol.* 14:1264093. doi: 10.3389/fimmu.2023.1264093

A novel ΔNp63-dependent immune mechanism improves prognosis of HPV-related head and neck cancer

Jana Mourtada[1,2†], Christelle Lony[1,2†], Anaïs Nicol[3], Justine De Azevedo[1,2], Cyril Bour[1,2], Christine Macabre[1,2,4], Patrick Roncarati[5], Sonia Ledrappier[4], Philippe Schultz[6], Christian Borel[7], Mickaël Burgy[7], Bohdan Wasylyk[8,9,10,11], Georg Mellitzer[2], Michaël Herfs[5], Christian Gaiddon[2*‡] and Alain C. Jung[1,2,4*‡]

[1]Laboratoire de Biologie Tumorale, Institut de cancérologie Strasbourg Europe, Strasbourg, France, [2]Université de Strasbourg-Inserm, UMR_S 1113 IRFAC, Laboratory « Streinth », Strasbourg, France, [3]Laboratoire de Radiobiologie, Institut de cancérologie Strasbourg Europe, Strasbourg, France, [4]Tumorothèque du Centre Paul Strauss, Centre Paul Strauss, Strasbourg, France, [5]Laboratory of Experimental Pathology, GIGA-Cancer, University of Liège, Liège, Belgium, [6]Hôpitaux Universitaires de Strasbourg, Department of Otorhinolaryngology and Head and Neck Surgery, Strasbourg, France, [7]Department of Medical Oncology, Institut de cancérologie Strasbourg Europe, Strasbourg, France, [8]Department of Functional Genomics and Cancer, Institut de Génétique et de Biologie Moléculaire et Cellulaire (IGBMC), Illkirch-Graffenstaden, France, [9]Institut National de la Santé et de la Recherche Médicale (INSERM) U 1258, Illkirch-Graffenstaden, France, [10]Centre Nationale de la Recherche Scientifique (CNRS) UMR 7104, Illkirch-Graffenstaden, France, [11]Université de Strasbourg, Strasbourg, France

Background: Deconvoluting the heterogenous prognosis of Human Papillomavirus (HPV)-related oropharyngeal squamous cell carcinoma (OSCC) is crucial for enhancing patient care, given its rapidly increasing incidence in western countries and the adverse side effects of OSCC treatments.

Methods: Transcriptomic data from HPV-positive OSCC samples were analyzed using unsupervised hierarchical clustering, and clinical relevance was evaluated using Kaplan-Meier analysis. HPV-positive OSCC cell line models were used in functional analyses and phenotypic assays to assess cell migration and invasion, response to cisplatin, and phagocytosis by macrophages *in vitro*.

Results: We found, by transcriptomic analysis of HPV-positive OSCC samples, a ΔNp63 dependent molecular signature that is associated with patient prognosis. ΔNp63 was found to act as a tumor suppressor in HPV-positive OSCC at multiple levels. It inhibits cell migration and invasion, and favors response to chemotherapy. RNA-Seq analysis uncovered an unexpected regulation of genes, such as DKK3, which are involved in immune response-signalling pathways. In agreement with these observations, we found that ΔNp63 expression levels correlate with an enhanced anti-tumor immune environment in OSCC, and ΔNp63 promotes cancer cell phagocytosis by macrophages through a DKK3/NF-κB-dependent pathway.

10.3389/fimmu.2023.1264093

Conclusion: Our findings are the first comprehensive identification of molecular mechanisms involved in the heterogeneous prognosis of HPV-positive OSCC, paving the way for much-needed biomarkers and targeted treatment.

KEYWORDS

ΔNp63, immune response, human papillomavirus, oropharyngeal squamous cell carcinoma, tumor microenvironment

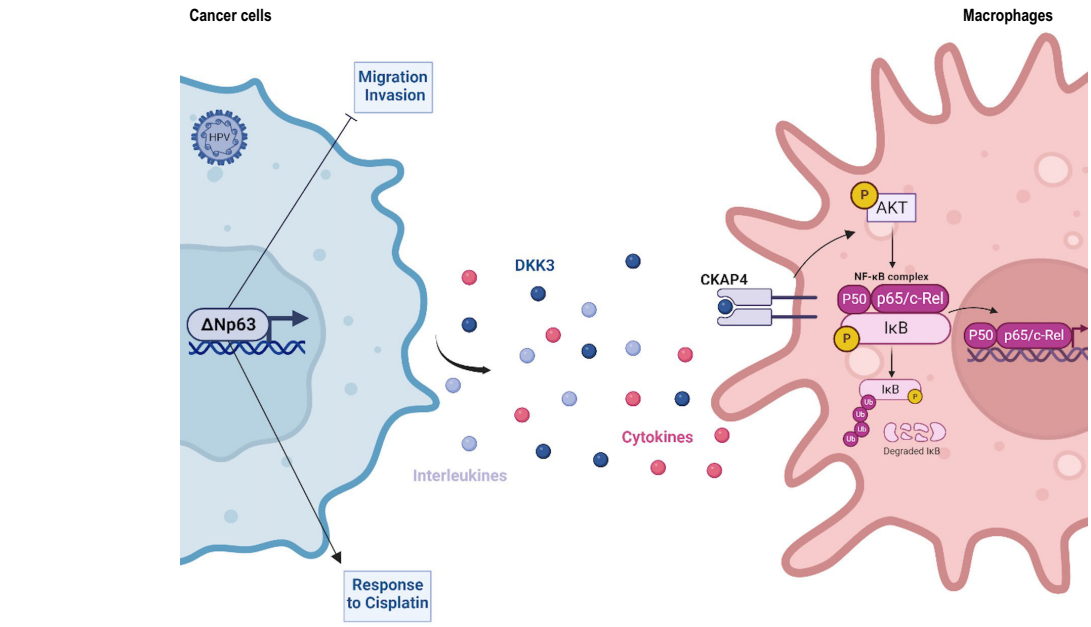

GRAPHICAL ABSTRACT

1 Introduction

There is a worldwide significant increase in the prevalence of Human Papillomavirus (HPV)-related oropharyngeal squamous cell carcinoma (OSCC) (1), which is now considered to be clinically distinct, with improved prognosis and specific biological features [see (2) and references therein]. Compared to HPV-negative Head and Neck Squamous Cell Carcinoma (HNSCC), the rate of metastatic spread is similar, but the target organs are different (3, 4). HPV tumor status is now included in the 8th edition for TNM staging and risk stratification (5). However, HPV-related OSCC is still treated therapeutically as HPV-negative HNSCC, with concomitant platinum-based chemoradiation therapy that causes severe acute and late toxicities (6, 7). Quality of life could be improved with therapeutic de-escalation, but there are no prognostic biomarkers to identify suitable patients (8). There is growing evidence for clinical heterogeneity of HPV-positive OSCC. For example, the molecularly defined "mesenchymal/inflamed" subgroup has longer overall survival than the "classical" (xenobiotic metabolism) subgroup (9). Higher expression of CD8 and/or PD-L1 in HPV-related OSCC tumors has been associated with improved prognosis (10, 11). However, the molecular mechanisms that drive improved prognosis need to be discovered.

We now report novel molecular processes that underly OSCC heterogeneous prognosis. They involve a differential expression of the ΔNp63 transcription factor and its antitumor activities. ΔNp63 is a member of the p53 family of transcription factors (12), which plays a major role in various cancers and is targeted by novel therapeutic approaches (13, 14). ΔNp63 lacks the N-terminal transactivation domain of TAp63, and is abundantly expressed in oral epithelium (15), as well as HNSCC (16), where it plays an oncogenic role in chemically-driven skin carcinogenesis (17). Here we show that ΔNp63 has a key role in a subset of HPV-related OSCC and significantly affects various cellular processes (*e.g.*, cell migration/invasion; response to cisplatin) that could account for differences in patient prognosis. Most importantly, our data provides evidence that ΔNp63 in cancer cells induces the expression of diffusible immunomodulators by cancer cells,

including Dickkopf-related protein 3 (DKK3), that activates the NF-κB signalling pathway in immune cells.

2 Materials and methods

2.1 Patient characteristics and tumor samples

Eight HPV-positive patients with OSCC samples and available transcriptomic data were included in this study. Patient description is shown in Supplementary Table S1. Patients' mean age is 59 years old and median follow-up is 130 months. Patients underwent initial surgery (Sainte Barbe clinic, Strasbourg) followed by chemoradiotherapy (Centre Paul Strauss) between 1993 and 1995. Transcriptomic data was previously generated using an Affymetrix GeneChip approach, as described in (18).

Gene expression analysis, immunohistochemistry and survival analyses were carried out on a cohort of 77 patients that were treated in Strasbourg, France (N=34; they include the 8 HPV-positive OSCC that generated the transcriptomic data), and Liège, Belgium (N=43) between 1993 and 2014. Patient description is shown in Supplementary Table S1. Patients' mean age is 60 years old and median follow-up is 37 months.

In all cases, tumor samples were collected at the time of surgery with the patients' informed consent, and stored in the "Centre Paul Strauss" tumor bank (Strasbourg, France) or the "Biothèque Hospitalo-Universitaire de Liège" (Liège, Belgium). A fragment was taken near the advancing edge of the primary tumor (avoiding its necrotic center), immediately frozen in liquid nitrogen, and stored at −70°C. The rest of the tumor was fixed in 6% buffered formalin and embedded in paraffin for histopathological analysis. Examination of sections adjacent to each tumor fragment showed that the percentage of tumor cells was over 70%. The TNM system of the UICC was used for tumor-node-metastasis staging (19). HPV-positivity is defined by the detection of both HPV16 viral genomic DNA [measured with the Multiplex HPV Genotyping kit (Multimetrix, Heidelberg, Germany)] and HPV16 E6/E7 transcript (measured by quantitative RT-PCR) as described in (18).

2.2 Data sets and bioinformatic analyses

2.2.1 Transcriptomics analysis

R and Bioconductor were used for the analysis of all data sets. The expression data obtained from microarrays Affymetrix HG-U133 plus 2.0 were obtained from HPV+ samples. Unsupervised analysis: A hierarchical classification allowed the observation of the distribution of samples. Ward's aggregation criterion and correlation distance were used. The Principal Component Analysis was realized with the R FactomineR (V1.29) package (20).

2.2.2 Differential analysis

The transcriptomic differential analysis was evaluated with a moderate t-test (R package limma V3.18.13) (21). The Bonferroni method was used for multiple corrections. Genes with a log fold change > 1 and an adjusted p-value< 0.05 were selected as differentially expressed. Results are presented as a heatmap (function heatmap, R package stats V3.0.2. R Core Team (2020). R: A language and environment for statistical computing. R Foundation for Statistical Computing, Vienna, Austria, https://www.R-project.org/.).

2.2.3 Meta-analysis

Public data sets were acquired from the public database Gene Expression Omnibus (GEO) where only the HPV+ samples extracted from the upper aerodigestive tract (oropharynx, hypopharynx, larynx and buccal cavity) were selected. Based on these criteria, three data sets were obtained. Two of these data sets come from GEO Database, Slebos et al. (22) (GSE3292) and Pyeon et al. (23) (GSE6791). The last one was from a collaboration. The data sets were preprocessed to ensure that they are comparable, and clusters of highly interconnected genes were found in the reference data set using the WCGNA R package (V1.70-3) (24, 25) based on an unsupervised analysis of gene expression profiles. Next, we investigated how these clusters are conserved in the three other data sets using the Preservation function module of the WGCNA package. This function outputs a Z-score which indicates high (>10), moderate (5<Z<10) or lower preservation (Z<5) of the modules in other data sets. Finally, we determined which genes are highly connected in both sets.

2.2.4 Analysis of the correlation between ΔNp63 and genes of signature identified by Barbieri et al.

Expression of Barbieri's signature genes (26) was analyzed in our data set. Correlation matrix of gene expression of these genes was calculated with the R package corrplot V0.73 and the function corrplot.

2.2.5 Estimation of tissue-infiltrating immune cell population

The R package MCPcounter (V1.2.0) (27) was used, based on the normalized gene expression matrix.

2.3 Cell lines and reagents

The SCC90 cell line was a kind gift from Prof. Susan Gollin (University of Pittsburgh). SCC90 cells originate from a HPV16-positive oropharyngeal (base of tongue) tumor, and express wild-type *TP53* (28). The SCC47 cell line was a kind gift from Prof. Thomas E. Carey (University of Michigan). SCC47 cells originate from an HPV16-positive carcinoma of the tongue, and express wild-type *TP53* (29). Cells were maintained at 37°C with 5% CO_2 and 90% humidity in Dulbecco's modified Eagle's medium (DMEM; PAN Biotech), supplemented with 10% fetal calf serum (FCS; Gibco), 10nM 4-(2-hydroxyethyl)-1-piperazineethanesulfonic acid (HEPES; PAN Biotech) and 1% non-essential amino acids (PAN Biotech). The THP-1 cell line was a kind gift from Elisabeth Martin (UMR1113, Strasbourg), and were maintained at 37°C with 5% CO_2 and 90%

humidity in Roswell Park Memorial Institute (RPMI) medium supplemented with 10% fetal bovine serum (Gibco).

2.4 siRNA and expression plasmid transfection

ΔNp63 and DKK3 downregulation was achieved by transfecting 15 nM of ΔNp63 siRNA (Eurogentec; sense strand: 5'-UGCCCAGACUCAAUUUAGU55-3'; antisense strand: 5'-ACUAAAUUGAGUCUGGGCA55-3') and 15 nM of DKK3 siRNA (Santa cruz Biotechnology; sc-41102) to $3E^{05}$ SCC90 cells using Lipofectamine RNAiMAX, according to the manufacturer's instructions. The Eurogentec SR-CL011-005 scrambled and Santa Cruz sc-37007siRNAs was used as a negative control for downregulation of ΔNp63 and DKK3, respectively. Total protein and RNA was extracted 48 h (DKK3) and 72 h (ΔNp63) post-transfection to assess gene and protein expression. CKAP4 downregulation was achieved by transfecting 15 nM of CKAP4 siRNA (Santa Cruz Biotechnology; sc-95758) to $5E^{05}$ THP-1 cells using Lipofectamine RNAiMAX, according to the manufacturer's instructions. Santa Cruz scrambled siRNA (sc-37007) was used as a negative control.

ΔNp63 overexpression was achieved by transfecting 0.5 µg of pcDNA3-ΔNp63 vector to $5E^{05}$ SCC90 cells using the jetPRIME® Polyplus-transfection reagent according to the manufacturer's instructions. Empty pcDNA3 was used as a negative control. Total protein and RNA was extracted 48 h post-transfection to assess gene and protein expression.

2.5 Gene expression assays

Gene expression assays in tumor samples were performed by extracting total RNA from 77 OSCC frozen tissues using the RNeasy kit (Qiagen), according to the manufacturer's instructions. The integrity of extracted RNA was verified on an Agilent 2100 Bioanalyser (Agilent Technologies). RNA was retro-transcribed using the Goscript reverse transcription system (Promega), and real-time quantitative PCR was performed using the LightCycler® 480 real-time PCR system (Roche). Specific primer pairs were used to measure the expression of the genes that encode ΔNp63, S100A9, THBS4, CD8α, GZMK and CD68 (see Supplementary Table S2 for primer sequences). RT-qPCR data was analyzed using LightCycler® 480 software. The expression levels of each gene were normalized to the geometric mean Ct values of 2 internal controls, *Ribosomal Protein Long P0* (*RPL0*) and *Ubiquitin B* (*UBB*).

Gene expression assays on cultured cells were performed by extracting total RNA from pelleted cells using a standard TRIZol procedure (TRI Reagent®: TR 118 Molecular Research Center), according to the manufacturer's instructions. RNA was retro-transcribed using the Goscript reverse transcription system (Promega), and real-time quantitative PCR was performed using the LightCycler® 480 real-time PCR system (Roche). *ΔNp63* and *DKK3* expression was measured with pairs of specific primers (see Supplementary Table S2 for primer sequences) and normalized to the expression of *RPLP0* using the $2^{-\Delta\Delta Ct}$ method.

Total RNA harvested from THP-1 cells was retro-transcribed using the High-Capacity cDNA Reverse Transcription Kits (Applied Biosystems), and real-time quantitative PCR was performed using the Applied Biosystems QuantStudio3. cDNA was diluted five times before being used as a template according to the provider instructions (4 µL/reaction) with FastStart Universal Probe Master Mix Taqman. Specific primers are used from TaqMan Gene Expression Assay (Applied Biosystems) to measure the expression of *CXCL10* (Hs00171042_m1), *CCL4* (Hs99999148_m1), *IL1B* (Hs00174097_m1) and normalized to the expression of *ACTB* (Hs01060665_g1) using the $2^{-\Delta\Delta Ct}$ method.

2.6 SDS-PAGE and western blot analysis

Total protein extraction was carried out by homogenizing $10E^{06}$ cells in 100 µL of 1X Laemmli lysis buffer [6.25 mM Tris (pH 6.8), 1% SDS, 1% DTT, protease and phosphatase inhibitors, Sigma]. 20 or 40 µg of total proteins were resolved by 6%-15% SDS-PAGE (depending on protein molecular weight) according to standard methods. Proteins were detected with primary antibodies raised against p63, p53, HPV16 E6, cleaved caspase 3 (Cas3*), DKK3, IKBα, IKBα-pS32, AKT, AKT-pS473, CKAP4 (see Supplementary Table S3 for clones, providers and concentrations). Depending on the host species, blots were probed with secondary antibodies (1/8000 anti-mouse IgG-HRP linked antibody, Cell Signalling 7076S; 1/8000 anti-rabbit IgG-HRP linked antibody, Cell Signalling 7074S). Proteins were visualized with enhanced chemiluminescence using the Clarity™ ECL Western blotting Substrate Bio-Rad reagent, according to the manufacturer instructions. Signals were acquired on a Pxi Imager (Syngene®) and quantified with the Genetools software (Syngene®).

2.7 Immunohistochemistry analysis and assessment

Immunohistochemical experiments were performed using a standard protocol extensively detailed previously (30, 31). The primary antibodies were as follows: anti-ΔNp63, anti-CD8, anti-CD68, anti-S100A7, anti-S100A9, anti-KRT6B and anti-THBS4 (see Supplementary Table S3 for clones references and concentrations). The mouse or rabbit EnVision detection system (Dako) was used for the secondary reaction according to supplier's recommendations. ΔNp63, S100A7, S100A9, KRT6B and THBS4 immunolabeled tissues were evaluated by histopathologists using a semi-quantitative score of the intensity (0: negative, 1: weak, 2: moderate, 3: intense) and extent (0: <5% positive cells, 1: 6–33%, 2: 34–66%, 3: >67%) of the staining, according to an arbitrary scale (30, 32). The multiplication of results acquired with the two scales allowed the obtention of a global score, ranging from 0 to 9. Tissue specimens with ΔNp63 scores below ≤4 and >4 were classified as $\Delta Np63^{low}$ and $\Delta Np63^{high}$, respectively. Regarding both CD8 and CD68 immunostainings, the number of positive cells per mm^2 was determined by computerized counts (QuPath 0.2.0) (33).

2.8 Cell migration and cell invasion assays

The analysis of the migratory properties of SCC90 and SCC47 cells were performed using Boyden chambers. For this purpose, the cells are seeded in 6-well plates and then transfected 24 h later with either siRNA or expression vector (see above). The culture medium of the transfected cells was first replaced by FCS-free DMEM for 3 h. Then, cells were detached from their support with trypsin, counted, and $8E^{04}$ cells were seeded in Thincert Cell Culture Inserts (Greiner Bio One) in 500 µL of FCS-free medium. Inserts were placed in the wells of a 24-well plate containing 750 µL of DMEM with 10% FCS, and cultures were incubated for 24 h at 37°C with 5% CO_2 and 90% humidity. After rinsing the inserts with 1X PBS, cells on the upper part of the insert were removed with a cotton-tipped swab, and cells that migrated through the filter to the lower part of the insert were fixed in 4% paraformaldehyde (PFA, Sigma-Aldrich) for 20 min at room temperature and stained with 1% crystal blue violet (Sigma). The filter of each chamber was then removed, mounted between slide and coverslip, and photographs were taken with a transmitted light microscope (Zeiss, Axio Imager.A1). The analysis of cell invasion was carried out in similar conditions, using matrigel-coated inserts (Corning® BioCoat® Matrigel®) and staining cells with a 1/50000 solution of DAPI (Sigma) for 20 min. In this case, photographs were taken with a Zeiss Axio Imager M2-Apotome2 fluorescence microscope.

2.9 *In vitro* cell viability analysis

2.9.1 MTT cell viability assays

A total of $1E^{04}$ cells were seeded per well in 96–well microplates (Falcon Multiwell, Dutscher), 24 h prior to treatment. Cisplatin (Mylan) at different concentrations (0; 0.1; 0.5; 1; 2.5; 7.5; 15; 30; 100 µM) was applied for 48 h in 100 µL of fresh medium. MTT assay was performed as previously described by replacing the cisplatin solution with fresh medium supplemented with 5 mg/L MTT (Sigma) for 1 h (34). Cells were lysed in DMSO 100% (100 µL/well). Absorbance measurements were performed at 550 nm with the LB942 Tristar2 Multimode Reader (Berthold Technologies). The calculation of the IC_{50} and IC_{75} was performed with the GraphpadPrism V5.02 software (Graphpad, Software, USA) using non-linear regression.

2.9.2 Resazurin (7-hydroxy-3H-phenoxazin-3-one) assays

SCC90 spheroids were obtained by seeding $5E^{03}$ cells in the wells of 96-well round-bottom microtest plates (Thermo Fisher Scientific), in 100 µL of culture medium. SCC90 cells were incubated for 24 h, and SCC47 cells were incubated for 48 h, at 37°C with 5% CO_2 and 90% humidity to form spheres. SCC90 spheroids were further incubated with 11 µL of cisplatin solution at various concentrations (0; 0.1; 0.5; 1; 2.5; 7.5; 15; 30; 100 µM) and one volume of a 10% resazurin in DMEM medium, for 48 h at 37°C with 5% CO_2 and 90% humidity. Absorbance measurements were performed at 550 nm with the LB942 Tristar2 Multimode Reader (Berthold Technologies).

2.10 RNA-sequencing and transcriptomic data analysis

RNA was extracted from SCC90 cells transfected with siRNA against ΔNp63 and TRIzol-mediated cell lysis. After extraction and RNA precipitation, supernatants were removed and the RNA pellet was washed with 75% EtOH, centrifuged at 9000× *g* for 5 min at 4°C, and again, 75% EtOH was added. Then, the RNA was resuspended in nuclease-free H_2O and quantified using a NanoDrop Spectrophotometer (Thermo Scientific, Waltham, MA, USA). To identify the deregulated genes, RNASeq was performed on extracted total RNAs. RNA-Seq libraries were generated from 600 ng of total RNA using TruSeq Stranded mRNA Library Prep Kit and TruSeq RNA Single Indexes kits A and B (Illumina, San Diego, CA), according to manufacturer's instructions. Briefly, following purification with poly-T oligo attached magnetic beads, the mRNA was fragmented using divalent cations at 94°C for 2 min. The cleaved RNA fragments were copied into first strand cDNA using reverse transcriptase and random primers. Strand specificity was achieved by replacing dTTP with dUTP during second strand cDNA synthesis using DNA Polymerase I and RNase H. Following addition of a single 'A' base and subsequent ligation of the adapter on double stranded cDNA fragments, the products were purified and enriched with PCR (30 sec at 98°C; [10 sec at 98°C, 30 sec at 60°C, 30 sec at 72°C] x 12 cycles; 5 min at 72°C) to create the cDNA library. Surplus PCR primers were further removed by purification using AMPure XP beads (Beckman-Coulter, Villepinte, France). The final libraries were checked for quality and quantified using capillary electrophoresis, and sequenced as single end read 1x50b on the Illumina HiSeq4000 platform according to manufacturer's instructions. Image analysis and base calling were performed using RTA 2.7.3 and bcl2fastq 2.17.1.14. The quantification of gene expressions was performed with the Kallisto algorithm (v 0.46.2) and default options. RNA-Seq analysis was assessed with R software (R version 4.0.3). The differential analysis was performed with DESeq2 R package (version 1.30.0). A significantly differentially expressed gene corresponds to a p-value inferior to 0.005 and a log2 fold change ≥ 1. Pathways enrichment analyses were performed using multiple databases (*e.g.*, DAVID, STRING, Reactome, TRAP, Biomarkers).

2.11 *In vitro* phagocytosis assay

SCC90 cells were seeded in 6-well plates and transfected with siΔNp63 (see above). Conditioned culture medium was harvested 48 h after transfection and filtered on 0.2 µm filters. THP-1 cells differentiation in macrophages was carried out by seeding $5E^{05}$ cells in wells of a 6-well microplate containing a coverslip, and by incubating them in a 162 nM PMA (phorbol 12-myristate 13-acetate; Sigma) solution in RPMI for 48 h. PMA solution was then

replaced by fresh medium (70% RPMI; 30% SCC90 conditioned medium), and further incubated for 24 h. Seventy two hours after transfection and the initiation of THP-1 differentiation, SCC90 cells were incubated for 30 min with 1 mM of CellTRacker™ Green CMFDA Dye (Thermofisher) in FCS-free DMEM, and THP-1 cells were incubated for 30 min with 1 mM of CellTRacker™ Deep Red Dye (Thermofisher) in FCS-free RPMI. After medium replacement by FCS-complemented DMEM, SCC90 cells were gently scraped in 1X PBS, centrifuged for 5 min at 800 rpm, resuspended in DMEM, and seeded on THP-1 cells in a 1:1 cell ratio (one well of each culture was used for cell numeration). Co-cultures were maintained at 37°C for 4h. Culture medium was then removed, coverslips were washed in 1X PBS and THP-1 cells were fixed in 4% PFA for 10 min at room temperature, and nuclei were labeled with a DAPI solution (1/20000) for 5 min. Coverslips were mounted in Calbiochem FluorSave™ reagent (Merck Millipore), and pictures were taken with a Zeiss Axio Imager M2-Apotome2 fluorescence microscope. Finally, in order to confirm the phagocytosis activity, a real time imaging approach was used using IncuCyte® S3 Live-Cell Analysis Instrument (SARTORIUS). THP-1 cells were seeded in a 6-well plate without coverslip and the phagocytosis experiment was carried out as described previously. Nine images per well from two technical replicates were taken every 10 min for 22 h using a 20X objective lens and then analyzed using the IncuCyte® Basic Software. Green channel acquisition time was 400 ms, whereas red channel acquisition time was 800 ms.

2.12 Immunocytofluorescent staining assays

THP-1 cells differentiation in macrophages was carried out by seeding $5E^{05}$ cells in wells of a 6-well microplate containing a coverslip, and by incubating them in a 162 nM PMA (phorbol 12-myristate 13-acetate; Sigma) solution in RPMI for 48 h. PMA solution was then replaced by fresh medium and further incubated for 6 h with 0.5 µg of DKK3 recombinant protein (rhDKK3). Culture medium was then removed, coverslips were washed in 1X PBS and cells were fixed in 4% PFA for 10 min at room temperature. Permeabilization was achieved using 0.1% Triton X-100 in PBS for 5 min at 4°C and then blocked in 5% NGS/PBS for 30 min at room temperature. Coverslips were then soaked with NF-κB p65 antibody (1/400) during 60 to 90 min at room temperature and washed in 1X PBS for 15 min before and after incubation with secondary fluorescent antibody (Alexa Fluor™ 488 Rabbit, Invitrogen) for 30 min in darkness. Nuclei were labeled with a DAPI solution (1/20 000) for 5 min. Coverslips were mounted in Calbiochem FluorSave™ reagent (Merck Millipore), and pictures were taken with a Zeiss Axio Imager M2-Apotome2 fluorescence microscope.

2.13 Statistical and survival analyses

Survival analyses were performed using MedCalc statistical software (http://www.medcalc.be/). A two-sample Wilcoxon rank-sum (Mann-Whitney) test was used to evaluate the association between the gene expression level of *S100A9* and *THBS4* and the occurrence of metastatic spread at 3 years, and the Liu method (maximization of the product of sensitivity and specificity) (35) was used to determine optimal cut-off values. A prediction score was then constructed by entering THBS4 and S100A9 cut-off values in a logistic regression model. This score was used to stratify patients and evaluate the impact of this stratification on metastasis-free survival at 3 years using a univariate Kaplan-Meier survival analysis and log-rank post-test. A multivariate Cox regression model including the THBS4/S100A9 prediction score and potential confounding factors (age; gender; tumor stage; history of tobacco smoking) was used to evaluate their influence on metastasis-free survival.

The hypothesis of normality (d'Agostino and Pearson test; Shapiro-Wilk test) and homogeneity of variances (Levene test for equality of variances) of other data sets were analyzed. If the sample did not meet at least one of these conditions, then a non-parametric test was used (Wilcoxon-Mann-Whitney test). Otherwise, parametric tests were used (Student t-test; ANOVA and Bonferroni post-test; ANOVA and Tukey post-test). Statistical tests were performed using GraphPad Prism 8. For all analyses, significance is represented in graphs using asterisks: *p<0.05; **p<0.01; ***p<0.001; ****p<0.0001.

3 Results

3.1 HPV-positive OSCC display molecular and prognostic heterogeneity is linked to differential expression of ΔNp63

We analyzed transcriptomic data from 8 tumor samples from patients with locally advanced HPV-16 positive OSCC. Unsupervised hierarchical clustering analysis distinguished two molecular groups (Figure 1A; Cluster 1 and Cluster 2), based on the differential expression of 148 genes (Supplementary Table S4). Interestingly, analysis of follow-up clinical data of the corresponding patients (Table 1) showed that Cluster 1 is associated with metastatic recurrence within 18 months and death within 3 years, and Cluster 2 with delayed metastatic spread (59 and 117 months after treatment) and longer survival (4/6 patients were still alive after 129 months). This shows that HPV-related OSCC can be separated into two clusters with different prognosis and molecular signatures.

The significance of the clustering analysis was evaluated by comparisons with three independent HNSCC data sets from GEO [« Mirghani et al. » (E-MTAB-2146) (36), Slebos et al. (GSE3292) (22) and Pyeon et al. (GSE6791) (23)], using weighted correlation network analysis (WGCNA) (see flowchart in Supplementary Figure S1A). Clusters of highly interconnected genes (*i.e.*, modules), corresponding to gene co-expression networks, were identified in both the reference and comparison data sets using unsupervised hierarchical clustering and dynamic tree cut analysis (modules are indicated by colors in Supplementary Figures S1B–G; connected modules are assigned identical colors). The analysis was

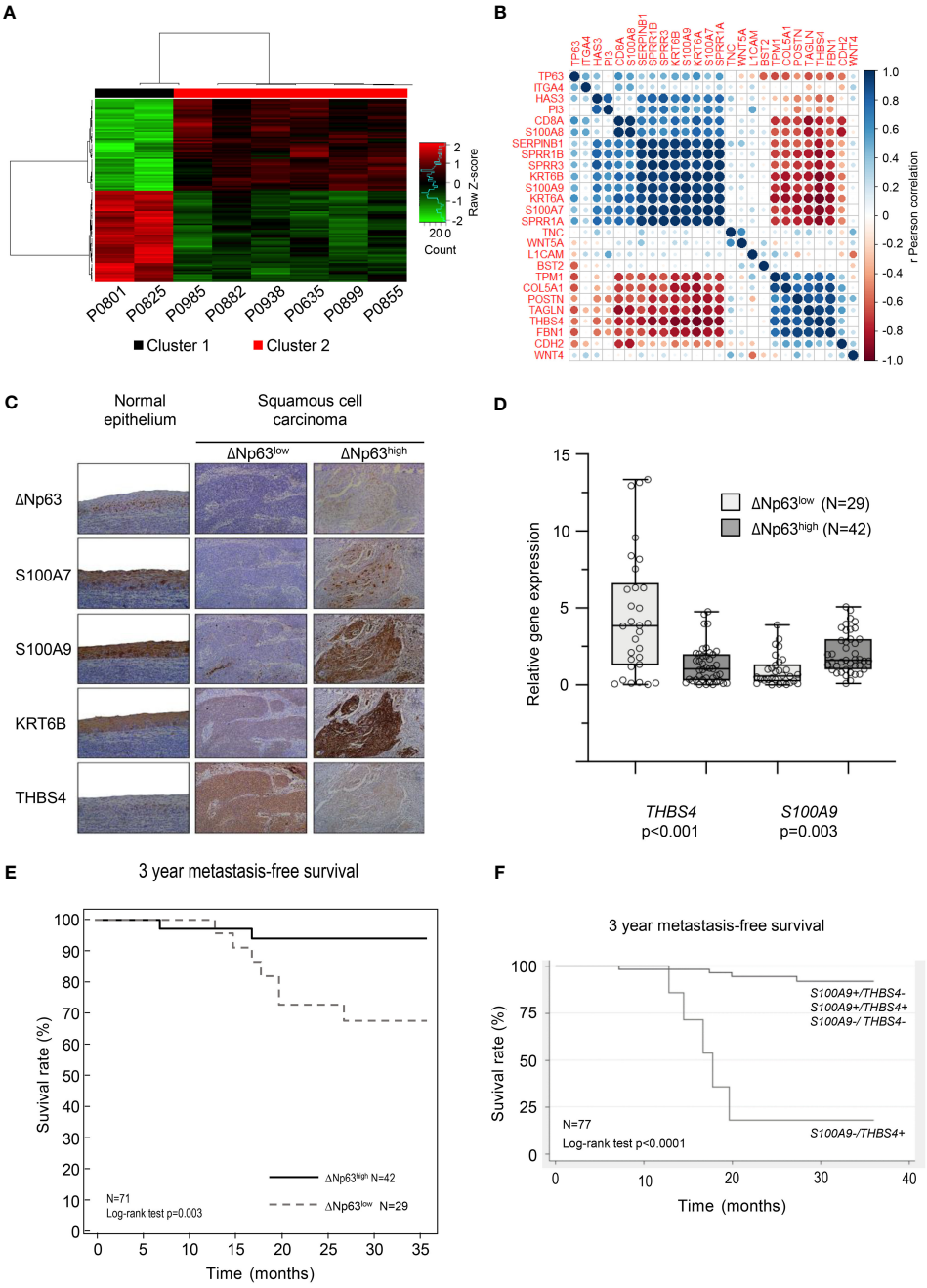

FIGURE 1
HPV-positive OSCC display molecular and prognostic heterogeneity that involves ΔNp63. **(A)** Dendograms and heat-map representation of unsupervised hierarchical Cluster 1 (poor prognosis) and Cluster 2 (good prognosis). **(B)** Correlation matrix of the expression of *TP63* and genes shown to be regulated by ΔNp63 by Barbieri et al. (26). **(C)** Immunohistochemistry analysis of the expression of ΔNp63 (using BC28 ab-172731 Antibody), S100A7, S100A9, KRT6B and THBS4. **(D)** Box-and-whisker plot (minimum to maximum, showing all points) representation of the expression of the *THBS4* and *S100A9* genes in ΔNp63^{low} and ΔNp63^{high} HPV-positive OSCC. **(E)** Kaplan-Meier analysis of the 3-year metastasis-free survival of patients stratified according to the expression of the *THBS4* and *S100A9* genes. **(F)** Kaplan-Meier analysis of the 3-year metastasis-free survival of patients stratified according to the expression of the *S100A9* and *THBS4* genes.

limited to probes that were expressed in the different data sets (*i.e.*, probes expressed in our data set and in publicly available data sets). The degree of conservation of gene modules between each pairwise comparison was assessed using a Z-score, which was established for each matching cluster (color; Supplementary Table S5; a Z-score > 10 indicates high conservation while a Z-score ranging from 5 to 10 indicates moderate conservation). 25/100 genes in the "purple module" of Slebos et al. (asterisk in Supplementary Figure S1B; italicized Z-score in Supplementary Table S5), 23/100 genes in the "red module" of Mirghani et al. (asterisk in Supplementary Figure S1D; italicized Z-score in Supplementary Table S5), and 17/100 and 15/100 genes, respectively, in the midnight blue and pink modules of Pyeon et al. (asterisks in Supplementary Figure S1F; italicized Z-score in Supplementary Table S5) were also found to be

10.3389/fimmu.2023.1264093

TABLE 1 Demographics of patients in Cluster 1 and Cluster 2.

	Cluster 1		Cluster 2					
Patient #	P0801	P0825	P0985	P0882	P0938	P0635	P0899	P0855
Gender	Male	Male	Male	Male	Male	Male	Female	Female
Age	53	61	82	58	48	42	75	54
Tobacco	Yes	Yes	NA	No	Yes	Yes	No	Yes
pT	T3	T3	T2	T3	T2	T3	T2	T2
pN	N3	N2b	N2c	N2a	N1	N2b	N1	N2b
Tumor stage	IV	IV	IV	IV	III	IV	III	IV
Treatment	Surg.+RT	Surg.+RT	Surg.+RT	Surg.+RT	Surg.+RT	Surg.+RT	Surg.+RT	Surg.+RT
Metastasis at 3 years	Yes	Yes	No	No	No	No	No	No
Metastasis-free survival	17 months	20 months	59 months	174 months	117 months	170 months	173 months	135 months
Overall survival	35 months	20 months	60 months	174 months	129 months	170 months	173 Months	135 months
5 years Overall survival	Deceased	Deceased	Deceased	Alive	Alive	Alive	Alive	Alive

Two and six patients were found in Cluster 1 and Cluster 2, respectively. Patient number (#), gender and age, tobacco consumption, pathological tumor size staging (pT), pathological lymph node invasion staging (pN), tumor stage, treatment [Surgery (Surg.); Radiotherapy (RT)], metastasis at 3 years (yes vs. no), metastasis-free survival (in months), overall survival (in months) and the 5-year overall survival status (alive vs. deceased) are shown. NA, not available.

downregulated in Cluster 2 (Supplementary Table S4; Gene names in bold). These observations, using three additional and independent transcriptomic data sets, support our initial finding of two transcriptomic profiles that correlate with distinct prognosis of HPV-positive OSCC patients.

Several genes that we found to be upregulated (*S100A7*, *S100A9*, *SPRR1A*, *SPRR1B*, *SPRR3*, *KRT6A*, *KRT6B*, *SERPINB1*; in bold in Supplementary Table S4) or downregulated (*THBS4*; in bold in Supplementary Table S4) in the good-prognosis Cluster 2 have been shown to be targets of the ΔNp63 transcription factor (26). We evaluated whether the expression of these targets and *TP63* are correlated in our data set. Correlation matrix analysis indicates that there is a correspondence (Figure 1B), suggesting that ΔNp63-dependent transcription could contribute to the different expression patterns of the two clusters. To evaluate if these RNA expression are also reflected at the protein level, we analyzed a separate collection of 71 formalin-fixed paraffin-embedded (FFPE) specimens from an independent cohort of HPV-positive OSCC patients (See Supplementary Table S1 for patient demographics). Using semi-quantitative scoring of immunohistochemistry stains, tumors were stratified into two groups with high or low ΔNp63 expression ($\Delta Np63^{high}$ (N=42) and $\Delta Np63^{low}$ (N=29), respectively; Figure 1C). Consistent with our transcriptomic data, $\Delta Np63^{high}$ tumors expressed relatively high levels of S100A7, S100A9 and KRTB6 proteins (Figure 1C). RT-qPCR analysis of RNA harvested from this later collection of HPV-positive OSCC samples (fresh-frozen samples, N=77, Supplementary Table S1) showed that *S100A9* is more highly expressed in $\Delta Np63^{high}$, and *THBS4* in $\Delta Np63^{low}$ HPV-positive OSCC (Figure 1D).

We then evaluated whether gene expression levels are different in metastatic and non-metastatic tumors in this larger cohort (N=77). Using median expression and a two-sample Wilcoxon rank-sum test, we found that *S100A9*, *SERPINB1* and *SPRR1A* are significantly more highly expressed in tumors with no metastatic spread within 3 years (Supplementary Table S6), whereas the expression of *THBS4* is significantly lower (Supplementary Table S6).

In order to assess prognostic power and maximize sensitivity and specificity, cut-off expression values were determined for each genes (see Supplementary Table S6 for detailed sensibility, specificity and area under the curve). An optimal predictor was found by combining the cut-off values of *THBS4* and *S100A9*. In a Kaplan-Meier analysis of 3-year metastasis-free survival, patients with low *S100A9* and high *THBS4* expression (*S100A9*-/*THBS4*+) were found to be at risk for metastatic progression (Log-rank test p-value<0.0001; Figure 1E). This predictor was found to be an independent prognostic marker in a Cox multivariate regression analysis that included potential confounding factors (including patient age and gender, tumor stage and history of tobacco smoking; Table 2). Interestingly, a Kaplan-Meier analysis of the 3-year metastasis-free survival of patients stratified according to ΔNp63 protein expression (Figure 1C) showed that $\Delta Np63^{low}$ HPV-positive OSCC are at higher risk for distant metastatic spread (log-rank test p-value=0.003; Figure 1F). Altogether, these observations show that ΔNp63 expression and a the *S100A9*/*THBS4* predictor define two distinct molecular and prognostic subgroups of HPV-related oropharyngeal tumors and suggest that ΔNp63 may play a role in tumor progression and response to therapy.

3.2 ΔNp63 regulates migration and invasion of HPV-positive head and neck cancer cells

Since ΔNp63 expression is correlated with distant metastatic relapse (Figure 1F), we tested whether it might regulate cell migration and invasion. SCC90 cells, that express high levels of ΔNp63 have lower migration and invasion abilities compared to

10.3389/fimmu.2023.1264093

TABLE 2 Multivariate analyses of the prognostic value of the S100A9/THBS4 predictor for the 3-year metastasis-free survival by a Cox regression model that includes potential confounding factors (including patient age and gender, tumor stage and history of tobacco smoking).

	3-year metastasis-free survival		
	Hazard ratio	95% CI	p-value
Predictor S100A9-/THBS4+ (N=7) vs. others (N=70)	24.22	4.23-138.81	**<0.0001**
Gender Male (N=51) vs. Female (N=26)	0.91	0.14-5.73	0.920
Age ≤ 59 years old (N=35) vs. > 59 years old (N=42)	0.65	0.15-2.84	0.564
Tumor stage Stage III/IV (N=66) vs. Stage I/II (N=11)	3.27	0.34-31.68	0.306
Tobacco Current/former (N=47) vs. never smoker (N=29)	11.23	1.04-120.82	**0.046**

Factors that are significantly associated with prognostic are shown with a bold p-value.

SCC47 cells, that express relatively low levels of ΔNp63 (Supplementary Figures S2A, B). Downregulation of ΔNp63 with a specific siRNA (siΔNp63; Supplementary Figure S2C) in sparse cultures of SCC90 cells resulted in greater cell flattening and coverage of the plate surface (Supplementary Figure S2D), and in the formation of smaller inner 3D spheroids (Figures 2A, B, especially days 3-6) with larger outer rims (Figure 2C). ΔNp63 silencing also resulted in increases in cell migration and invasion in transwell assays (Supplementary Figure S2E, Figures 2D, E, left graphs). Conversely, upregulation of ΔNp63 in SCC47 cells (Supplementary Figure S2F) resulted in changes in cell shape (Supplementary Figure S2G), and repression of cell migration (non-significant trend) and invasion (Supplementary Figure S2H, Figures 2D, E, right graphs). These observations show that ΔNp63 negatively regulates migration and invasion, and low levels of ΔNp63 are associated with increased migration and invasion in HPV-positive OSCC cells. This is consistent with increased risk for metastatic spread in tumors with low levels of ΔNp63 ($\Delta Np63^{low}$).

3.3 ΔNp63 is involved in the cell response to cisplatin and in cisplatin-induced cell apoptosis

To examine whether ΔNp63 expression affects carcinoma cell response to chemotherapy, we performed cell viability and spheroid assays using siRNA-transfected SCC90 cells treated with cisplatin. Decreased ΔNp63 expression led to decreased sensitivity to cisplatin in 2D-cultures (Supplementary Figures S3A, B). It also led to changes in spheroid morphology in 3D-cultures (Supplementary Figure S3C) as well as increased cell survival in 3D spheroids treated with increasing concentrations of cisplatin (Figure 2F). This shows that cells with lower ΔNp63 expression are more resistant to cisplatin-induced cytotoxicity. Downregulation of ΔNp63 in SCC90 cells decreases p53 protein expression (Figure 2G). This effect seems to be independent of HPV16 E6 oncoprotein, since E6 expression is not affected by ΔNp63 downregulation (Figure 2H). In addition, ΔNp63 knockdown decreases p53 induction by cisplatin (Figure 2I) as well as apoptosis (as measured by caspase 3 cleavage, Figure 2I). The effect on apoptosis appears to be mediated in part by p53, since p53 knockdown with p53 siRNA impaired, but did not completely abolish, caspase 3 cleavage (Supplementary Figure S4). Inversely, overexpression of ΔNp63 in SCC47 favored apoptosis induced by cisplatin (Figure 2J), which, however, did not correlate with increased expression of p53, suggesting that other factors could be involved. Overall, ΔNp63 expression levels affect apoptosis upon cisplatin treatment in cells in culture, suggesting that ΔNp63 levels affect sensitivity to platinum-based chemotherapy in HPV-positive carcinoma cells in human tumors.

3.4 ΔNp63 regulates the expression immune response genes and is linked to differences in the tumor immune landscape

In order to gain further insights into ΔNp63-dependent mechanisms in HPV-positive OSCC, we investigated the transcriptional program regulated by ΔNp63 in SCC90 cells. RNA-sequencing (RNA-seq) analysis was carried out on cells transfected with either scrambled or ΔNp63 siRNA. Using a $\log_2$ (fold change)>1 and adjusted p-value<0.05 as cut-offs, 690 genes were found to be differentially expressed (293 genes were downregulated and 397 upregulated) upon ΔNp63 inhibition. Pathway enrichment analysis using normalized transcriptomic data and the String software identified repressed (Figure 3A) and activated (Figure 3B) cellular functions. Most of the up-regulated genes were found to be involved in either development, epithelium/skin differentiation or cornification (Figure 3B; red and pink bars), as expected given the known role of ΔNp63 in keratinocyte differentiation and skin epithelium stratification. Consistent with the role of ΔNp63 in cell migration and invasion (Figures 2A–F), genes involved in movement and locomotion, as well as in the organization of the extracellular matrix, were significantly downregulated (Figure 3A; blue bars). More unexpectedly, the predominant downregulated pathways concern genes involved in the immune response and cytokine signalling (Figure 3A; light and dark green bars). The most downregulated genes (Figure 3C) include *RAB7B* (cellular response to interferon- γ; negative regulation of Toll-like receptor signalling; positive regulation of NF-κB signalling), *LCP1* (Interleukin-12-mediated signalling; T cell activation), *IL-33* (interleukin-33) and *DKK3* [inhibition of Wnt-signalling, interference with interferon-γ signalling and modulation of CD4+ and CD8+ T cell responses (37)]. Furthermore, one of the most upregulated genes is *CXCL-17* (involvement in monocyte, dendritic cell and macrophage chemotaxis; Figure 3D).

The clinical relevance of these observations was analyzed by correlating the expression of ΔNp63 and immune cell markers in HPV-positive OSCC samples. Immune-cell abundance in our initial cohort of 8 OSCC samples was analyzed by the MCP-counter

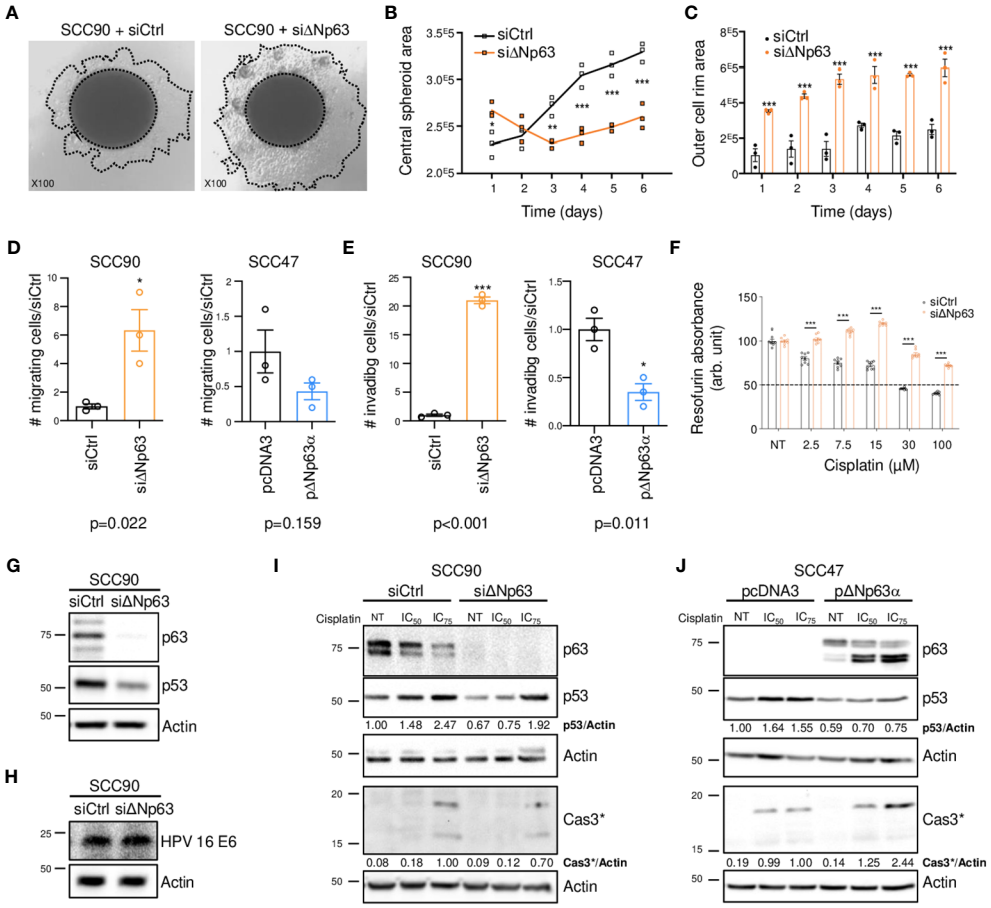

FIGURE 2
ΔNp63 regulates migration, invasion and response to cisplatin in HPV-positive head and neck cancer cells. **(A)** Spheroids of SCC90 cells transfected with scrambled or ΔNp63 siRNA. **(B)** Size of the central SCC90 spheroid area. Data is represented as individual replicates with mean connected (N=3). ANOVA and Bonferonni test: * p<0.05; ** p<0.01; *** p<0.001. **(C)** Size of the SCC90 spheroid outer cell rim area upon siRNA-mediated ΔNp63 downregulation. Data is represented as scatter plots with bars and mean +/- SEM (N=3). ANOVA and Bonferonni test: *** p<0.001. **(D)** Quantification of the migration of SCC90 and SCC47 cells upon ΔNp63 downregulation and upregulation, respectively (micrographs are shown in Supplementary Figures S2E, H). Data is represented as scatter plots with bars and mean +/- SEM (N≥3). Student t-test: * p<0.05. **(E)** Quantification of invasion of SCC90 and SCC47 cells upon ΔNp63 downregulation and upregulation, respectively (micrographs are shown in Supplementary Figures S2E, H). Data is represented as scatter plots with bars and mean +/- SEM (N≥3). Student t-test: * p<0.05. **(F)** Resazurin cell viability assay of SCC90 spheroids upon ΔNp63 inhibition. Data is represented as scatter plots with bars and mean +/- SEM (N=3). ANOVA and Bonferonni post-test: *** p<0.001. **(G, H)** Western blot analysis of ΔNp63, p53 **(G)** and HPV16 E6 **(H)** expression in siΔNp63-transfected SCC90 cells. **(I)** Western blot analysis of ΔNp63, p53 and cleaved caspase 3 (Cas3*) upon downregulation of ΔNp63 in SCC90 cells and treatment with cisplatin (IC_{50} = 2.8 μM; IC_{75} = 6.7 μM). p53 and Cas3* signals were quantified with respect to the actin loading control and normalized to non-treated siCtrl SCC90 cells or siCtrl SCC90 cells treated with the IC_{75} of cisplatin, respectively (quantification results are shown). **(J)** Western blot analysis of p63, p53 and cleaved caspase 3 (Cas3*) expression upon overexpression of ΔNp63 in SCC47 cells and treatment with cisplatin (IC_{50} = 2.7 μM; IC_{75} = 4.0 μM). p53 and Cas3* signals were quantified with respect to the actin loading control and normalized to non-treated siCtrl SCC90 cells or siCtrl SCC90 cells treated with the IC_{75} of cisplatin, respectively (quantification results are shown). (p63 was detected using 4A4 ab-735 Antibody)

method, which identifies immune cells based on specific gene signatures. Cluster 2 is clearly different from Cluster 1, and predicted to be enriched in myeloid dendritic cells, T cells, neutrophils, B and monocytic cell lineages and cytotoxic lymphocytes (Figure 4A). In order to confirm these observation, we quantified the expression of immune cell markers, including *CD8 α* (for CD8 T cells), *Granzyme K* (*GZMK*; for cytotoxic lymphocytes) and *CD68* (for macrophages). RT-qPCR analysis with RNA harvested from $\Delta Np63^{high}$ (N=10) *vs.* $\Delta Np63^{low}$ (N=19) HPV-positive fresh frozen samples showed that *GZMK* and *CD68* expression is higher in $\Delta Np63^{high}$ tumors (Figure 4B; ANOVA and Tukey post-test: * p<0.05). In addition, immunohistochemistry staining and automated signal quantification of CD8 α (Figure 4C) and CD68 (Figure 4D) in FFPE samples from $\Delta Np63^{high}$ and $\Delta Np63^{low}$ HPV-positive OSCC (N=+/-70) demonstrated that $\Delta Np63^{high}$ OSCC (N=43) had a significantly higher number of CD8 α -positive T cells (641 cells/mm^2 versus 347 cells/mm^2) compared to $\Delta Np63^{low}$ tumors (N=31) (Figure 4E; Mann-Whitney two-tailed p=0.0013). Similarly, $\Delta Np63^{high}$ OSCC (N=40) had an elevated number of CD68-positive macrophages (455 cells/mm^2versus 293 cells/mm^2) compared to $\Delta Np63^{low}$ tumors (N=30) (Figure 4E; Mann-Whitney two-tailed p=0.0051). These results provide compelling evidence for the contribution of the immune microenvironment to the prognosis of HPV-linked OSCC.

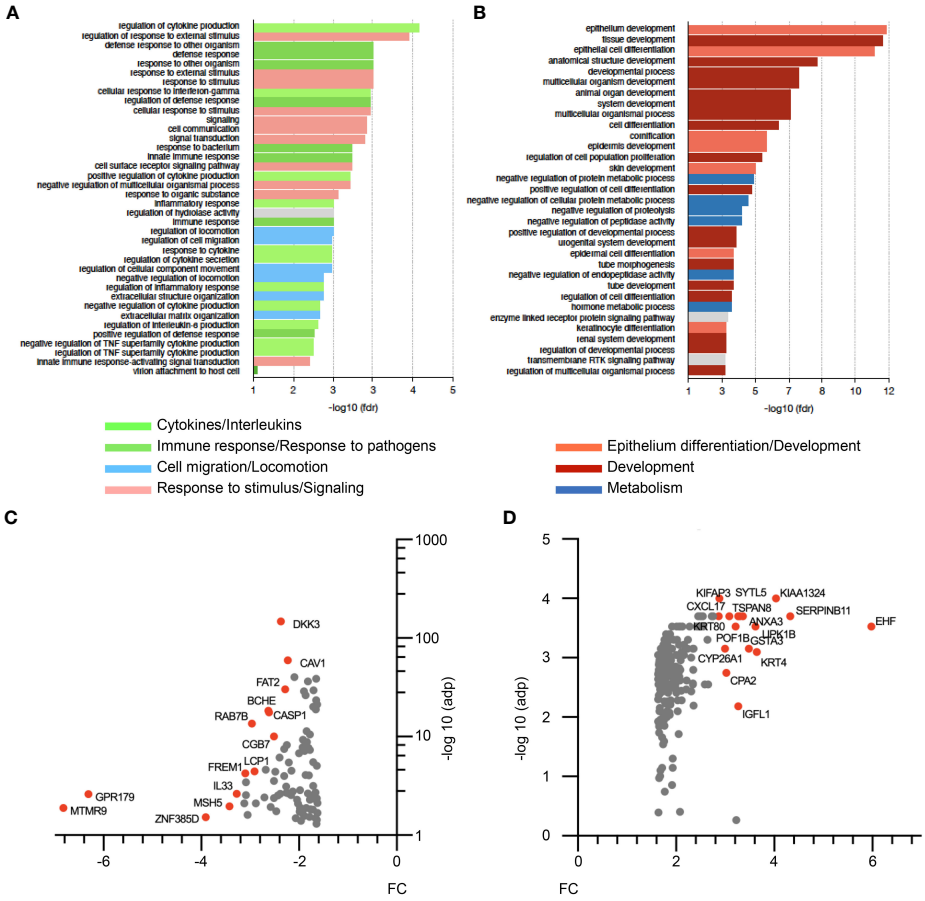

FIGURE 3
RNA-seq analysis of siΔNp63-transfected SCC90 cells. **(A)** Enrichment analysis of signalling pathways that are repressed upon siRNA-mediated ΔNp63 downregulation in SCC90 cells. **(B)** Enrichment analysis of signalling pathways that are activated upon siRNA-mediated ΔNp63 downregulation in SCC90 cells. **(C, D)** Top-100 downregulated **(C)** and upregulated **(D)** genes in siΔNp63-transfected SCC90 cells according to the fold change (FC) and the Log_{10}.adjusted p-value [log_{10}(adp)].

3.5 ΔNp63 regulates the uptake of HPV-positive head and neck cancer cells by macrophages

To explore the functional regulation of the immune response by ΔNp63, we carried out *in vitro* phagocytosis assays with THP-1-derived macrophages. THP-1 cells were stimulated with phorbol 12-myristate 13-acetate (PMA), labeled with a red fluorescent cell tracker dye and briefly co-cultivated (4 h) with SCC90 cells labeled with a green fluorescent cell tracker dye. ΔNp63 silencing in SCC90 cells decreased the percentage of THP-1 macrophages with green-labeled phagocytosis vesicles (Figure 4F) from 10.1% +/- 2.4 in siCtrl-SCC90 to 4.6% +/- 1.0 (Figure 4G; two tailed Student t-test p=0.021). Conversely, upregulation of ΔNp63 in SCC47 cells increased green label containing phagocytotic THP-1 macrophages (21.2% +/- 2.5), compared to mock-transfected SCC47 (9.1% +/- 2.8; Figure 4B; two tailed Student t-test p=0.005). Cancer cell phagocytosis was seen to occur by visualization with time-lapse video-microscopy (Video S1), which helps to rule out that the green vesicles were cell culture-related artifacts. These results show that ΔNp63 expression stimulates carcinoma-cell phagocytosis by macrophages.

3.6 ΔNp63 regulates cancer cell uptake by macrophages via DKK3 and the activation of a CKAP4-NF-κB axis

In order to study how ΔNp63 regulates the immune response, we investigated *DKK3*, which is one of the most significantly downregulated factors upon siRNA-mediated inhibition of ΔNp63 in SCC90 cells (Figure 3C; see above). We investigated this regulation further. We found that DKK3 expression depends on ΔNp63 in SCC90 cells at the transcriptional level (Figure 5A) and the protein level, both intracellularly (Figure 5B, upper panels) and extracellularly (Figure 5B, lower panels). These results suggest that ΔNp63 modulates DKK3 secretion by cancer cells, which could affect the properties of other cells, such as immune cells. We investigated whether DKK3 could stimulate THP-1 macrophages to phagocytose SCC90 cells, using *in vitro* phagocytosis assays. As a

10.3389/fimmu.2023.1264093

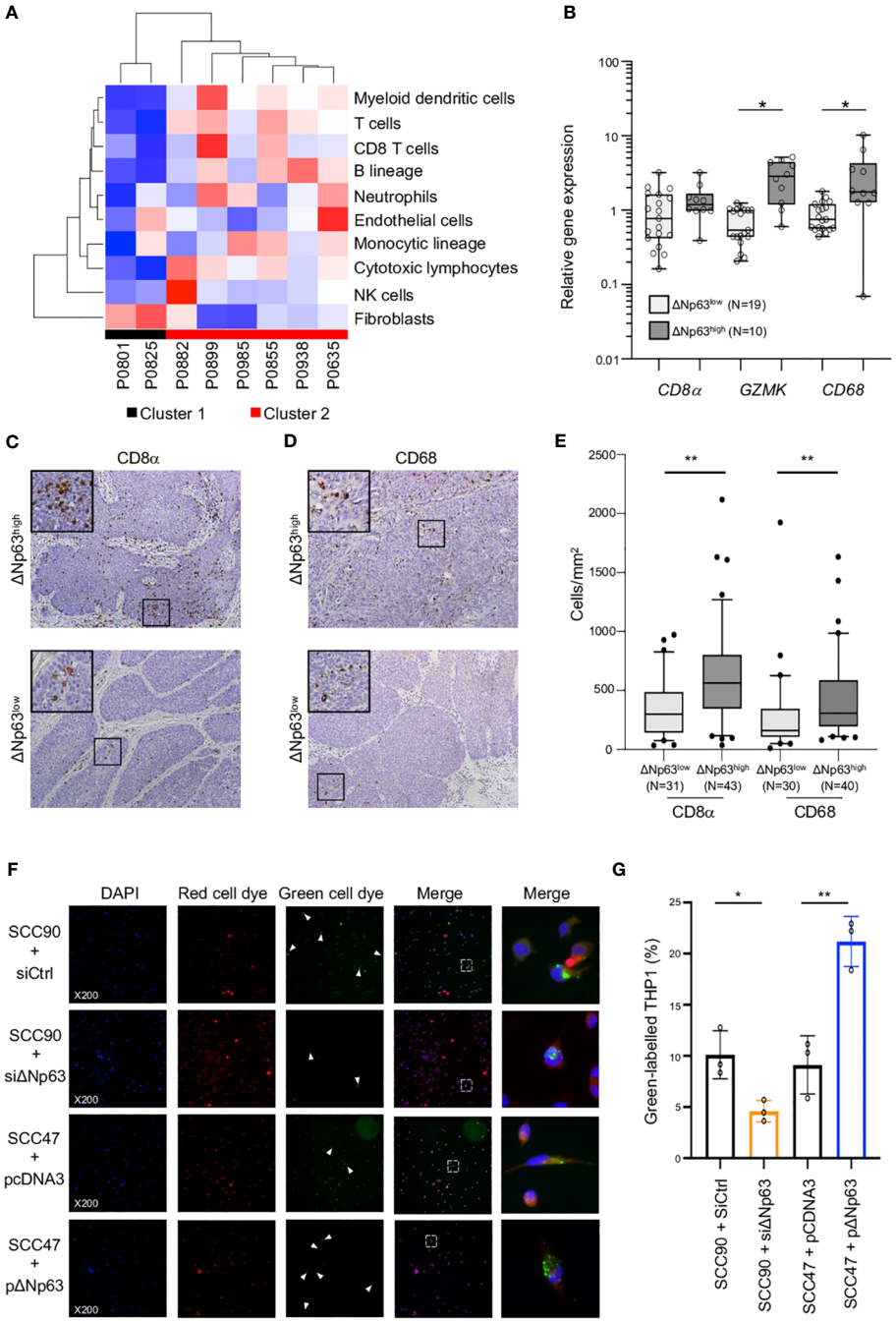

FIGURE 4
ΔNp63 is involved in the regulation of the immune response. **(A)** Deconvolution of the transcriptomic data (Figure 1A) and analysis of the abundance of 10 cell types in the tumor microenvironment of HPV-positive OSCC from Cluster 1 and Cluster 2. **(B)** Analysis of the expression of the CD8α, GZMK and CD68 genes in HPV-positive OSCC stratified according ΔNp63 levels ($\Delta Np63^{low}$ *vs.* $\Delta Np63^{high}$). Data is plotted as box plot (Box-and-whisker minimum to maximum, showing all points). ANOVA and Tukey post-test: * p<0.05. **(C, D)** Immunohistochemistry analysis of the expression of the CD8α **(C)** and CD68 **(D)** markers in formalin-fixed paraffin-embedded tumor samples of HPV-positive OSCC stratified according ΔNp63 expression. **(E)** Quantification of the number of CD8-positive T lymphocytes and CD68 macrophages (expressed as cells/mm^2) in whole slides from HPV-positive OSCC stratified according ΔNp63 expression. Data is plotted as Box-and-whisker plots with the median and 25th and 75th percentile. Mann-Whitney two-tailed test: ** p<0.01. **(F)** Analysis of the *in vitro* phagocytosis of green-labeled SCC90 or SCC47) cells by red-labeled THP-1 macrophages upon ΔNp63 inhibition (siΔNp63) or overexpression (pΔNp63α). DAPI, Red cell dye, Green cell dye and merge are shown. White arrowheads indicate green-labeled phagocytosis vesicles. Magnification: X200. A magnification (right panels) of the inset in the merge is shown. **(G)** Quantification of the proportion (%) of THP-1 macrophages that display green-labeled phagocytosis vesicles. Data is represented as scatter plots with bars and mean +/- SEM (N=3). Two-tailed Student t-test: * p<0.05; ** p<0.01.

control, we showed that DKK3 siRNA transfection downregulated intra- and extra-cellular levels of the DKK3 protein (Figure 5C, left and right panels, respectively). THP-1 macrophages were cultivated for 24 h with conditioned medium from siRNA-transfected SCC90, and were further briefly co-cultivated with transfected green-labelled SCC90 (Figure 5D). Silencing of DKK3 significantly decreased green-label incorporation in THP-1 macrophage from 18.7% +/- 3.5 in siCtrl-SCC90 to 12.1% +/- 1.4 (Figure 5E; Mann Whitney two tailed p=0.028). Altogether, these results indicate that ΔNp63 regulates cancer cell phagocytosis by macrophages through DKK3 expression and secretion.

In order to decipher the molecular mechanisms of THP-1 macrophage activation by DKK3, we studied whether DKK3 affects the nuclear localization of ß-catenin, since DKK3 activity has been shown to negatively regulate ß-catenin and Wnt-signalling (38). THP-1 macrophages were incubated with recombinant human DKK3 (rhDKK3) protein and immunocytofluorescently stained for ß-catenin. We did not observe a statistically significant change in the number of ß-catenin-positive nuclei of THP-1 cells treated 6 h with 0.5 µg of rhDKK3, compared to the negative control (*i.e.*, DMEM cell medium; Supplementary Figure S5), suggesting that nuclear localization of ß-catenin and Wnt signalling is not inhibited by rhDKK3. Consequently, we analyzed an alternative pathway, nuclear translocation of NF-κB, using p65 immunocytofluorescent staining. Interestingly, we found that incubation of THP-1 cells for 6 h with either Tumor Necrosis Factor-α (TNF-α; used as positive control) or 0.5 µg rhDKK3 triggered significant nuclear translocation of p65 (Figure 5F; Supplementary Figure S6A). As expected from activation of NF-κB, the expression levels of known NF-κB target genes, including *C-C Motif Chemokine Ligand 4* (*CCL4*), *C-X-C Motif Chemokine Ligand 10* (*CXCL10*), *Interleukin 1 beta* (*IL1B*) and *NF-Kappa-B Inhibitor Alpha* (IKBA), were found to be upregulated as early as 2 h after treatment with rhDKK3 (Supplementary Figure S6B). Strikingly, the proportion of THP-1 macrophages with p65-positive nuclei was found to be significantly lower (unpaired t-test p=0.034) after 6 h incubation with conditioned medium from siDKK3-transfected SCC90 cells (0.49+/-0.06; Figure 5G) compared to medium from siCtrl-SCC90 cells (0.90+/-0.12; Figure 5G). These observations show that extracellularly secreted DKK3 stimulates the NF-κB signalling pathway in THP-1 macrophages.

DKK3 was previously shown to bind to Cytoskeleton-Associated Protein 4 (CKAP4) on esophageal cancer cells (39), and DKK3 and CKAP4 were found to be required for the phosphorylation of the Akt serine/threonine kinase in HNSCC cell lines (40). In addition, Akt is known to be required for IκBα phosphorylation and degradation and subsequent NF-κB activation. We tested whether DKK3 has similar effects on THP-1 macrophages. Using western blot analysis of whole protein extracts from THP-1 macrophages, we observed that, as early as 30 min, DKK3 induced both Akt phosphorylation on serine S473, as well as IκBα phosphorylation on serine S32 (Figure 5H, left and right panels, respectively). Consistent with NF-κB nuclear translocation resulting from IκBα degradation, IκBα protein levels decreased following THP-1 incubation with DKK3. To further investigate the link between the CKAP4 receptor and NF-κB in THP-1 macrophages, we studied the consequences of CKAP4 receptor silencing on NF-κB nuclear translocation induced by DKK3. Using p65 immunocytofluorescent staining, we found that silencing of CKAP4 (Figure 5I) led to significantly fewer p65-positive nuclei in THP-1 cells following incubation with DKK3 for 6 h (Figure 5J, unpaired t-test p=0.02; Supplementary Figure S7). Altogether, these observations suggest that the expression of ΔNp63 in HPV-positive OSCC cells regulates NF-κB signalling in immune cells via the regulation of the expression of DKK3.

4 Discussion

4.1 ΔNp63 defines HPV-Positive OSCC molecular and prognostic heterogeneity

Multiple lines of evidence indicate that HPV-related OSCC are heterogeneous. Early on, Ang and collaborators (41) stratified HPV-positive patients into low and intermediate risk-of-death categories. Based on hierarchical clustering of transcriptomic data, HPV-positive HNSSC can be subdivided into two subgroups, HPV-classical (CL) and HPV-inflamed/mesenchymal (IMS) (9). The HPV-IMS subgroup has higher expression of mesenchymal-related and immune response genes and is associated with improved overall survival. However, the molecular mechanisms involved in causing this differential patient prognosis are still poorly understood. Similar to the previous report, our study also uncovers two molecular subgroups with distinct prognosis associated with distant metastasis. Importantly, our study finds that ΔNp63 makes a significant contribution to the different prognoses of the two groups. The ΔNp63 signature (ΔNp63-regulated genes) and high ΔNp63 protein levels were found to be biomarkers for good prognosis for HPV-related oropharyngeal cancer, the major site of HPV infection (42). Whether these findings are relevant for other sites of head and neck cancer remains to be determined.

There are rare instances of HPV infection in non-oropharyngeal head and neck locations. Interestingly, a recent meta-analysis found that HPV is associated with improved outcome in patients with laryngeal cancer (43). The contribution of ΔNp63 to the prognosis of these patients remains to be determined. HPV-related oropharyngeal cancer is mainly located in the lingual and palatine tonsils (42). In the remaining oral region, ΔNp63 expression in preneoplastic lesion has been reported to be associated with oral cancer risk (44). *TP53* mutations are rare in HPV-related OSCC but are frequently found in HPV-negative head and neck cancer (for review see (45)and references therein). The functional consequences of ΔNp63 expression in a mutant *TP53* background remains to be investigated.

The mechanisms that lead to differential expression of ΔNp63 in the two subgroups of HPV-positive tumors are not known, but could involve miR-203 expression or viral integration. Work by McKenna et al. suggests that the HPV16 E6 oncoprotein is indirectly involved in the regulation of miR-203 (46), and miR-203 regulates of the expression of ΔNp63 (47). The *TP63* genomic locus is a hotspot for HPV genome integration, resulting in genomic rearrangement and overexpression of local genes (48). These

10.3389/fimmu.2023.1264093

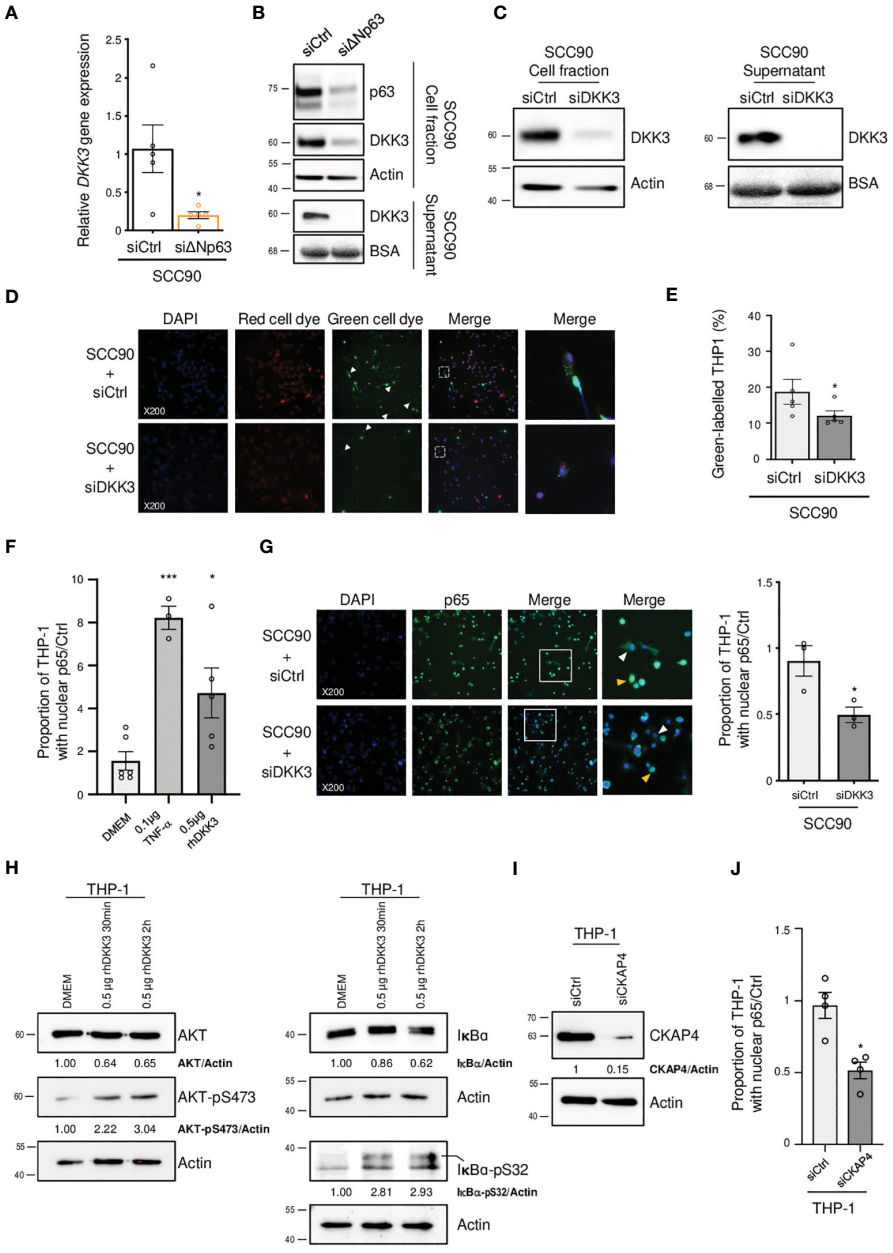

FIGURE 5
ΔNp63 regulates cancer cell uptake by macrophages via DKK3. **(A)** Analysis of the expression of the *DKK3* gene in siΔNp63-transfected SCC90 cells. Data is represented as scatter plots with bars and mean +/- SEM (N=4). Two-tailed Student t-test: * p<0.05. **(B)** Analysis of the expression of the DKK3 protein in the cellular (upper panels) and supernatant (lower panels) fractions of siΔNp63-transfected SCC90 cells (p63 was detected using 4A4 ab-735 Antibody). **(C)** Analysis of the expression of the DKK3 protein in the cellular (left panels) and supernatant (right panels) fractions of SCC90 cells transfected with an anti-DKK3 siRNA. **(D)** Analysis of the *in vitro* phagocytosis of green-labeled SCC90 cells by red-labeled THP-1 macrophages upon siRNA-mediated DKK3. DAPI, Red cell dye, Green cell dye and merge are shown. White arrowheads indicate green-labeled phagocytosis vesicles. Magnification: X200. A magnification (right panels) of the inset in the merge is shown. **(E)** Quantification of the proportion (%) of THP-1 macrophages that display green-labeled phagocytosis vesicles. Data is represented as scatter plots with bars and mean +/- SEM (N=4). Two-tailed Student t-test: p=0.029. **(F)** Quantification of the proportion of THP-1 macrophages that display p65-positive nuclei. THP-1 cells were incubated with DMEM (negative control), 0.1 µg of TNF-α or 0.5 µg of hrDKK4 for 6 h prior to staining (see also Supplementary Figure S6A). Data is represented as scatter plots with bars and mean +/- SEM (N≥3). ANOVA and Tukey post-test: *p<0.05; *** p<0.001. **(G)** Immunocytofluorescence analysis of the expression of p65 in THP-1 macrophages incubated with conditioned medium from siCtrl- (upper panels) or siDKK3- (lower panels) transfected SCC90 cells. DAPI, p65 staining and merge are shown. Magnification: X200. A magnification (right panels) of the inset in the merge is shown. White and yellow arrowheads highlight p65 staining in the cytoplasm and the nuclei, respectively. A quantification of the proportion of THP-1 macrophages with p65-positive nuclei is plotted in the graph. Data is represented as mean scatter plots with bars and +/- SEM (N=3). Two-tailed Student t-test: * p<0.05. **(H)** Western blot analysis of the expression of total and phosphorylated (pS473) AKT (left panels), and of total and phosphorylated (pS32) IκB-α in whole protein extracts from THP-1 cells incubated with rhDKK3 for 30 min and 2 h. AKT, AKT-pS473, IκB-α and IκB-α-pS32 signals were quantified with respect to the actin loading control and normalized to THP-1 macrophages incubated with DMEM (quantifications are shown). **(I)** Western blot analysis of CKAP4 expression in siCKAP4-transfected THP-1 macrophages. CKAP4 signals were quantified with respect to the actin loading control and normalized to siCtrl-transfected THP-1 macrophages (quantifications are shown). Shown blots are representative examples of three independent experiments. **(J)** A quantification of the proportion of siCtrl- and siCKAP4-transfected THP-1 macrophages with p65-positive nuclei upon incubation with 0.5 µg of rhDKK3 for 6 h. Data is represented as scatter plots with bars and mean +/- SEM (N=4). Two-tailed Student t-test: * p<0.05.

mechanisms that link HPV infection to the differential expression of ΔNp63 in tumors are interesting subjects for future studies.

We have found that high p63 is associated with good prognosis in OSCC. However, this is not always the case. p63 has a complex role in cancer, and can be oncogenic or tumor suppressive, depending on the cancer. For instance, high ΔNp63 expression correlates with poor patient outcome, tumor progression and/or metastasis in various cancers (49, 50). In contrast, low ΔNp63 expression correlates with high cancer progression in others (51, 52). An intriguing question is what determines these differences in ΔNp63's contribution to tumor progression.

4.2 ΔNp63 is involved in cell migration/invasion and response to cisplatin

Higher expression of ΔNp63 in HPV-positive OSCC cells favors apoptosis induced by cisplatin and reduces cell migration/invasion, which could account for differences in prognosis. Interestingly, similar observations on cell migration and invasion were recently reported for HPV-positive squamous cells of the uterine cervix (53). In addition, and similarly to our finding, ΔNp63 expression levels in HNSCC tumors have been correlated with response to chemotherapy: patients with complete or partial tumor response were reported to have 4-6-fold higher ΔNp63 levels compared to non-responders (54). An important question is how ΔNp63 stimulates the cisplatin response? A possibility might be that ΔNp63 could increase access of cisplatin to DNA by remodeling inaccessible chromatin regions as proposed by Yu et al. (55). Our results also indicate that the mechanisms involve p53, since silencing of ΔNp63 in SCC90 cells reduces p53 protein levels, which are associated with DNA damage caused by cisplatin (56). It seems that regulation of HPV E6 protein is not involved in this process. Intriguingly, the overexpression of ΔNp63 in SCC47 cells also resulted in p53 expression downregulation, rather than an upregulation, suggesting that other factors might be involved. This complex balance of the interplay between p53, p63 and p73 and of their respective TA and ΔN isoforms has been reported to be delicate, and to be tissue dependent (57). A more in-depth study is required to decipher the molecular mechanisms involving ΔNp63 expression modulation and their effect on p53 expression.

4.3 ΔNp63 regulates the expression of diffusible immunomodulators that control cancer cell phagocytosis via a DKK3/CKAP4/NF-κB-dependent mechanisms

Our results provide, to the best of our knowledge, the first demonstration that ΔNp63 expression correlates with lymphocyte infiltration of HPV-related OSCC and that ΔNp63 regulates macrophage activity. These effects on infiltration and macrophages could contribute to differences in HPV-positive OSCC prognosis. Furthermore, we dissected the underlying mechanisms and show that ΔNp63 exerts this activity via the expression of diffusible factors, notably DKK3, which induces a CKAP4/NF-κB pathway in macrophages. This is consistent with previous studies that suggest that ΔNp63 participates in the regulation of chemokines or cytokines, including CCL17 (58), CXCL2 and CCL2 (49). There is some understanding of how ΔNp63 regulates immune response genes: ΔNp63 physically interacts with the c-Rel transcription factor (59, 60), thereby regulating inflammatory and immune response genes, as well as NF-κB (61). Our results also show that ΔNp63 expression functionally activates HPV-positive OSCC cell phagocytosis by macrophages, and that this mechanism appears to involve DKK3. DKK3 is an atypical member of a family of glycoproteins (DKK1-4) that act as inhibitors of the Wnt/ß-catenin signalling pathway (62, 63). This pathway plays an important role in the differentiation and biological activity of macrophages (64). DKK3 is secreted into the extracellular space by mesenchymal stem cells, where it modulates peripheral T-cell tolerance (37, 65). Previous studies propose that DKK3 has a tumor-suppressor role, through its ability to induce dendritic cell differentiation and activation of T cells (66, 67). In this report, we have identified additional ΔNp63 regulated genes, such as IL-33 or LCP1, that should be investigated further for their contribution to immune modulation by ΔNp63.

4.4 DKK3 stimulates the canonical NF-κB signalling pathway through its CKAP4 receptor

We show here that, in THP-1 macrophages, DKK3 induces the phosphorylation of IκBα on the S32 residue, IκBα protein level downregulation, p65 nuclear translocation and the upregulation of known NF-κB targets genes. These observations indicate that DKK3 activates the canonical NF-κB signalling pathway (68), which is known to regulate the phagocytic activity of macrophages (69). NF-κB has previously been shown to upregulate *CCL4*, *IL1BI*, *IKBA* and *CXCL10* genes in response to lipopolysaccharide stimulation of THP-1 macrophages (70). Interestingly, CXCL10 secretion by monocytes/macrophages is known to play a chemotactic function on T lymphocytes (71). Intriguingly, we observed that $\Delta Np63^{high}$ OSCC have a higher infiltration of both CD68 macrophages and CD8 T lymphocytes. Our *in vitro* results and our observations in patient tumors suggest that ΔNp63 regulates immunostimulatory diffusible factors that could activate macrophages that could in turn contribute to the recruitment of T lymphocytes. However, how our *in vitro* observations reflect the situation in human tumors remains yet to be determined.

The only known receptor of DKK3 is the CKAP4 type II transmembrane protein, which binds all DKK family proteins (72, 73). Both DKK1 and DKK3 have been reported to activate the PI3K/Akt signalling pathway and to trigger Akt phosphorylation via binding to CKAP4 (40, 74). This is consistent with our results, which show that Akt is phosphorylated in THP-1 cells upon incubation with rhDKK3. Interestingly, Akt is known to activate the NF-κB-pathway via the phosphorylation of IκB kinase-α (IKKα) (75). In addition, DKK1 has been shown to induce the activation of NF-κB signalling via the CKAP4 receptor in multiple myeloid cells. We propose that a DKK3/CKAP4/NF-κB axis is responsible for the activation of THP-1 macrophages. Our results implicate the canonical NF-κB signalling in the effects of DKK3 on THP-1 cells, but we cannot exclude that additional molecular mechanisms are also involved.

This study establishes that in HPV-positive OSCC, the elevated expression of ΔNp63 in cancer cells favors the recruitment of anti-tumor immune cells, and more specifically the activation of macrophages via the transactivation and secretion of DKK3 that in turn binds to CKAP4 on macrophage membranes and induces the NF-κB pathway.

5 Conclusions

Our results demonstrate that ΔNp63 is a tumor suppressor in HPV-positive OSCC, and that it favors response to therapy and infiltration of immune cells, while reducing migration and invasion. The mechanisms involve intercellular communication mediated by peptides and proteins that are localized in membranes or secreted, such as DKK3. These peptides and proteins constitute an "exteriome" that functions exterior to cells. Components of the exteriome could potentially be very useful for the stratification of HPV-positive OSCC, since they are readily detectable. Serum DKK3 is an emerging diagnostic biomarker for colorectal (76) and some gynecological cancers (77). In ovarian cancers, lower DKK3 levels are associated with an increased risk of cancer and lymphatic metastasis (77). In addition, we found that the expression at the RNA level of *THBS4* together with *S100A9* is an independent prognostic signature that remains predictive of metastasis despite confounding factors that include patient age, tobacco consumption and tumor stage. We propose that DKK3, as well as *THBS4* + *S100A9*, could be used in addition to conventional clinical features, to identify patients who are eligible for therapeutic de-escalation.

Data availability statement

The datasets presented in this study can be found in online repositories. The names of the repository/repositories and accession number(s) can be found below: https://www.ebi.ac.uk/arrayexpress/, E-MTAB-1328 https://www.ncbi.nlm.nih.gov/geo/, GSE190046.

Ethics statement

The studies involving humans were approved by Comité de protection des personnes Est IV. The studies were conducted in accordance with the local legislation and institutional requirements. The participants provided their written informed consent to participate in this study. Ethical approval was not required for the studies on animals in accordance with the local legislation and institutional requirements because only commercially available established cell lines were used.

Author contributions

JM: Formal Analysis, Visualization, Writing – original draft, Investigation, Validation. CL: Formal Analysis, Investigation, Validation, Visualization, Writing – review & editing. AN: Formal Analysis, Investigation, Visualization, Writing – review & editing. JD: Investigation, Writing – review & editing. CBou: Investigation, Validation, Writing – review & editing. CM: Investigation, Validation, Writing – review & editing. PR: Investigation, Writing – review & editing. SL: Writing – review & editing, Resources. PS: Writing – review & editing. CBor: Writing – review & editing. MB: Writing – review & editing. BW: Writing – review & editing, Funding acquisition. GM: Writing – review & editing. MH: Writing – review & editing, Conceptualization, Investigation. CG: Conceptualization, Investigation, Writing – review & editing, Formal Analysis, Funding acquisition, Project administration, Supervision, Visualization. AJ: Conceptualization, Formal Analysis, Funding acquisition, Project administration, Supervision, Visualization, Writing – original draft.

Funding

The author(s) declare financial support was received for the research, authorship, and/or publication of this article. This work was financially supported by the Centre National pour la Recherche Scientifique (CNRS, France; CG), Alsace Contre le Cancer, the Cancéropole Est and the Conférence de Coordination Interrégionale Grand Est-Bourgogne Franche-Comté de la Ligue Contre le Cancer. The Streinth Team is also supported by the Association pour la Recherche sur le Cancer, European action COST Proteocure, the Interdisciplinary thematic Institute InnoVec, the IDEX Excellence grant from Unistra, Itmo Cancer, and the Institut National du Cancer. JM is financially supported by a PhD fellowship awarded by the French national "Ligue Contre le Cancer".

Acknowledgments

We thank Prof. Susan Gollin and Prof. Thomas E. Carey for sharing cell lines. RNA-sequencing was performed by the GenomEast platform, a member of the "France Génomique" consortium (ANR-10-INBS-0009). The authors express their gratitude to Aurélien De Reynies and Sylvie Job of the "Carte d'Identité des Tumeurs" program (Ligue Nationale contre le Cancer) for their valuable contribution to the bioinformatic characterization of the transcriptome of HPV-positive OSCC samples. We thank Dr. Gilles Travé for critically reading the manuscript. We thank Rob Simmons of IUT Louis Pasteur, Université de Strasbourg, for proofreading the manuscript.

Conflict of interest

The authors declare that the research was conducted in the absence of any commercial or financial relationships that could be construed as a potential conflict of interest.

The author(s) declared that they were an editorial board member of Frontiers, at the time of submission. This had no impact on the peer review process and the final decision.

Publisher's note

All claims expressed in this article are solely those of the authors and do not necessarily represent those of their affiliated organizations, or those of the publisher, the editors and the reviewers. Any product that may be evaluated in this article, or claim that may be made by its manufacturer, is not guaranteed or endorsed by the publisher.

Supplementary material

The Supplementary Material for this article can be found online at: https://www.frontiersin.org/articles/10.3389/fimmu.2023.1264093/full#supplementary-material

References

1. Gillison ML, Chaturvedi AK, Anderson WF, Fakhry C. Epidemiology of human papillomavirus-positive head and neck squamous cell carcinoma. *J Clin Oncol* (2015) 33(29):3235–42. doi: 10.1200/JCO.2015.61.6995

2. Powell SF, Vu L, Spanos WC, Pyeon D. The key differences between human papillomavirus-positive and -negative head and neck cancers: biological and clinical implications. *Cancers (Basel)* (2021) 13(20):5206. doi: 10.3390/cancers13205206

3. Huang SH, Perez-Ordonez B, Liu FF, Waldron J, Ringash J, Irish J, et al. Atypical clinical behavior of p16-confirmed HPV-related oropharyngeal squamous cell carcinoma treated with radical radiotherapy. *Int J Radiat Oncol Biol Phys* (2012) 82 (1):276–83. doi: 10.1016/j.ijrobp.2010.08.031

4. Ruzevick J, Olivi A, Westra WH. Metastatic squamous cell carcinoma to the brain: an unrecognized pattern of distant spread in patients with HPV-related head and neck cancer. *J Neurooncol* (2013) 112(3):449–54. doi: 10.1007/s11060-013-1075-9

5. Huang SH, O'Sullivan B. Overview of the 8th edition TNM classification for head and neck cancer. *Curr Treat Options Oncol* (2017) 18(7):40. doi: 10.1007/s11864-017-0484-y

6. Dong Y, Ridge JA, Li T, Lango MN, Churilla TM, Bauman JR, et al. Long-term toxicities in 10-year survivors of radiation treatment for head and neck cancer. *Oral Oncol* (2017) 71:122–8. doi: 10.1016/j.oraloncology.2017.05.009

7. Trotti A, Bellm LA, Epstein JB, Frame D, Fuchs HJ, Gwede CK, et al. Mucositis incidence, severity and associated outcomes in patients with head and neck cancer receiving radiotherapy with or without chemotherapy: a systematic literature review. *Radiother Oncol* (2003) 66(3):253–62. doi: 10.1016/S0167-8140(02)00404-8

8. Bigelow EO, Seiwert TY, Fakhry C. Deintensification of treatment for human papillomavirus-related oropharyngeal cancer: Current state and future directions. *Oral Oncol* (2020) 105:104652. doi: 10.1016/j.oraloncology.2020.104652

9. Keck MK, Zuo Z, Khattri A, Stricker TP, Brown CD, Imanguli M, et al. Integrative analysis of head and neck cancer identifies two biologically distinct HPV and three non-HPV subtypes. *Clin Cancer Res* (2015) 21(4):870–81. doi: 10.1158/1078-0432.CCR-14-2481

10. Badoual C, Hans S, Merillon N, Van Ryswick C, Ravel P, Benhamouda N, et al. PD-1-expressing tumor-infiltrating T cells are a favorable prognostic biomarker in HPV-associated head and neck cancer. *Cancer Res* (2013) 73(1):128–38. doi: 10.1158/0008-5472.CAN-12-2606

11. Jung AC, Guihard S, Krugell S, Ledrappier S, Brochot A, Dalstein V, et al. CD8-alpha T-cell infiltration in human papillomavirus-related oropharyngeal carcinoma correlates with improved patient prognosis. *Int J Cancer* (2013) 132(2):E26–36. doi: 10.1002/ijc.27776

12. Botchkarev VA, Flores ER. p53/p63/p73 in the epidermis in health and disease. *Cold Spring Harb Perspect Med* (2014) 4(8):a015248. doi: 10.1101/cshperspect.a015248

13. Fisher ML, Balinth S, Mills AA. DeltaNp63alpha in cancer: importance and therapeutic opportunities. *Trends Cell Biol* (2023) 33(4):280–92. doi: 10.1016/j.tcb.2022.08.003

14. Miller JJ, Gaiddon C, Storr T. A balancing act: using small molecules for therapeutic intervention of the p53 pathway in cancer. *Chem Soc Rev* (2020) 49 (19):6995–7014. doi: 10.1039/D0CS00163E

15. Nylander K, Coates PJ, Hall PA. Characterization of the expression pattern of p63 alpha and delta Np63 alpha in benign and Malignant oral epithelial lesions. *Int J Cancer* (2000) 87(3):368–72. doi: 10.1002/1097-0215(20000801)87:3<368::AID-IJC9>3.0.CO;2-J

16. Stransky N, Egloff AM, Tward AD, Kostic AD, Cibulskis K, Sivachenko A, et al. The mutational landscape of head and neck squamous cell carcinoma. *Science* (2011) 333(6046):1157–60. doi: 10.1126/science.1208130

17. Ramsey MR, Wilson C, Ory B, Rothenberg SM, Faquin W, Mills AA, et al. FGFR2 signaling underlies p63 oncogenic function in squamous cell carcinoma. *J Clin Invest* (2013) 123(8):3525–38. doi: 10.1172/JCI68899

18. Jung AC, Briolat J, Millon R, de Reynies A, Rickman D, Thomas E, et al. Biological and clinical relevance of transcriptionally active human papillomavirus (HPV) infection in oropharynx squamous cell carcinoma. *Int J Cancer* (2010) 126 (8):1882–94. doi: 10.1002/ijc.24911

19. Sobin LH, Fleming ID. TNM Classification of Malignant Tumors, fifth edition (1997). Union Internationale Contre le Cancer and the American Joint Committee on Cancer. *Cancer* (1997) 80(9):1803–4. doi: 10.1002/(sici)1097-0142(19971101)80:9<1803::aid-cncr16>3.0.co;2-9

20. Lê S, Josse J, Husson F. FactoMineR: an RPackage for multivariate analysis. *J Stat Soft* (2008) 25(1):1–18. doi: 10.18637/jss.v025.i01

21. Ritchie ME, Phipson B, Wu D, Hu Y, Law CW, Shi W, et al. limma powers differential expression analyses for RNA-sequencing and microarray studies. *Nucleic Acids Res* (2015) 43(7):e47. doi: 10.1093/nar/gkv007

22. Slebos RJ, Yi Y, Ely K, Carter J, Evjen A, Zhang X, et al. Gene expression differences associated with human papillomavirus status in head and neck squamous cell carcinoma. *Clin Cancer Res* (2006) 12(3 Pt 1):701–9. doi: 10.1158/1078-0432.CCR-05-2017

23. Pyeon D, Newton MA, Lambert PF, den Boon JA, Sengupta S, Marsit CJ, et al. Fundamental differences in cell cycle deregulation in human papillomavirus-positive and human papillomavirus-negative head/neck and cervical cancers. *Cancer Res* (2007) 67(10):4605–19. doi: 10.1158/0008-5472.CAN-06-3619

24. Langfelder P, Horvath S. WGCNA: an R package for weighted correlation network analysis. *BMC Bioinf* (2008) 9:559. doi: 10.1186/1471-2105-9-559

25. Langfelder P, Horvath S. Fast R functions for robust correlations and hierarchical clustering. *J Stat Softw* (2012) 46(11):i11. doi: 10.18637/jss.v046.i11

26. Barbieri CE, Tang LJ, Brown KA, Pietenpol JA. Loss of p63 leads to increased cell migration and up-regulation of genes involved in invasion and metastasis. *Cancer Res* (2006) 66(15):7589–97. doi: 10.1158/0008-5472.CAN-06-2020

27. Becht E, Giraldo NA, Lacroix L, Buttard B, Elarouci N, Petitprez F, et al. Estimating the population abundance of tissue-infiltrating immune and stromal cell populations using gene expression. *Genome Biol* (2016) 17(1):218. doi: 10.1186/s13059-016-1070-5

28. Ragin CC, Reshmi SC, Gollin SM. Mapping and analysis of HPV16 integration sites in a head and neck cancer cell line. *Int J Cancer* (2004) 110(5):701–9. doi: 10.1002/ijc.20193

29. Brenner JC, Graham MP, Kumar B, Saunders LM, Kupfer R, Lyons RH, et al. Genotyping of 73 UM-SCC head and neck squamous cell carcinoma cell lines. *Head Neck* (2010) 32(4):417–26. doi: 10.1002/hed.21198

30. Hubert P, Herman L, Roncarati P, Maillard C, Renoux V, Demoulin S, et al. Altered alpha-defensin 5 expression in cervical squamocolumnar junction: implication in the formation of a viral/tumour-permissive microenvironment. *J Pathol* (2014) 234 (4):464–77. doi: 10.1002/path.4435

31. Bruyere D, Monnien F, Colpart P, Roncarati P, Vuitton L, Hendrick E, et al. Treatment algorithm and prognostic factors for patients with stage I-III carcinoma of the anal canal: a 20-year multicenter study. *Mod Pathol* (2021) 34(1):116–30. doi: 10.1038/s41379-020-0637-6

32. Herfs M, Roncarati P, Koopmansch B, Peulen O, Bruyere D, Lebeau A, et al. A dualistic model of primary anal canal adenocarcinoma with distinct cellular origins, etiologies, inflammatory microenvironments and mutational signatures: implications for personalised medicine. *Br J Cancer* (2018) 118(10):1302–12. doi: 10.1038/s41416-018-0049-2

33. Bankhead P, Loughrey MB, Fernandez JA, Dombrowski Y, McArt DG, Dunne PD, et al. QuPath: Open source software for digital pathology image analysis. *Sci Rep* (2017) 7(1):16878. doi: 10.1038/s41598-017-17204-5

34. Gaiddon C, de Tapia M, Loeffler JP. The tissue-specific transcription factor Pit-1/GHF-1 binds to the c-fos serum response element and activates c-fos transcription. *Mol Endocrinol* (1999) 13(5):742–51. doi: 10.1210/mend.13.5.0275

35. Liu X. Classification accuracy and cut point selection. *Stat Med* (2012) 31 (23):2676–86. doi: 10.1002/sim.4509

36. Mirghani H, Ugolin N, Ory C, Lefevre M, Baulande S, Hofman P, et al. A predictive transcriptomic signature of oropharyngeal cancer according to HPV16 status exclusively. *Oral Oncol* (2014) 50(11):1025–34. doi: 10.1016/j.oraloncology.2014.07.019

37. Meister M, Papatriantafyllou M, Nordstrom V, Kumar V, Ludwig J, Lui KO, et al. Dickkopf-3, a tissue-derived modulator of local T-cell responses. *Front Immunol* (2015) 6:78. doi: 10.3389/fimmu.2015.00078

38. Lee EJ, Jo M, Rho SB, Park K, Yoo YN, Park J, et al. Dkk3, downregulated in cervical cancer, functions as a negative regulator of beta-catenin. *Int J Cancer* (2009) 124(2):287–97. doi: 10.1002/ijc.23913

39. Kajiwara C, Fumoto K, Kimura H, Nojima S, Asano K, Odagiri K, et al. p63-dependent dickkopf3 expression promotes esophageal cancer cell proliferation via CKAP4. *Cancer Res* (2018) 78(21):6107–20. doi: 10.1158/0008-5472.CAN-18-1749

40. Katase N, Kudo K, Ogawa K, Sakamoto Y, Nishimatsu SI, Yamauchi A, et al. DKK3/CKAP4 axis is associated with advanced stage and poorer prognosis in oral cancer. *Oral Dis* (2022). doi: 10.1111/odi.14277

41. Ang KK, Harris J, Wheeler R, Weber R, Rosenthal DI, Nguyen-Tan PF, et al. Human papillomavirus and survival of patients with oropharyngeal cancer. *N Engl J Med* (2010) 363(1):24–35. doi: 10.1056/NEJMoa0912217

42. Ferris RL, Westra W. Oropharyngeal carcinoma with a special focus on HPV-related squamous cell carcinoma. *Annu Rev Pathol* (2023) 18:515–35. doi: 10.1146/annurev-pathmechdis-031521-041424

43. Yang D, Shi Y, Tang Y, Yin H, Guo Y, Wen S, et al. Effect of HPV infection on the occurrence and development of laryngeal cancer: A review. *J Cancer* (2019) 10 (19):4455–62. doi: 10.7150/jca.34016

44. Saintigny P, El-Naggar AK, Papadimitrakopoulou V, Ren H, Fan YH, Feng L, et al. DeltaNp63 overexpression, alone and in combination with other biomarkers, predicts the development of oral cancer in patients with leukoplakia. *Clin Cancer Res* (2009) 15(19):6284–91. doi: 10.1158/1078-0432.CCR-09-0498

45. Zhou G, Liu Z, Myers JN. TP53 mutations in head and neck squamous cell carcinoma and their impact on disease progression and treatment response. *J Cell Biochem* (2016) 117(12):2682–92. doi: 10.1002/jcb.25592

46. McKenna DJ, McDade SS, Patel D, McCance DJ. MicroRNA 203 expression in keratinocytes is dependent on regulation of p53 levels by E6. *J Virol* (2010) 84 (20):10644–52. doi: 10.1128/JVI.00703-10

47. Melar-New M, Laimins LA. Human papillomaviruses modulate expression of microRNA 203 upon epithelial differentiation to control levels of p63 proteins. *J Virol* (2010) 84(10):5212–21. doi: 10.1128/JVI.00078-10

48. Kamal M, Lameiras S, Deloger M, Morel A, Vacher S, Lecerf C, et al. Human papilloma virus (HPV) integration signature in Cervical Cancer: identification of MACROD2 gene as HPV hot spot integration site. *Br J Cancer* (2021) 124(4):777–85. doi: 10.1038/s41416-020-01153-4

49. Kumar S, Wilkes DW, Samuel N, Blanco MA, Nayak A, Alicea-Torres K, et al. Delta Np63-driven recruitment of myeloid-derived suppressor cells promotes metastasis in triple-negative breast cancer. *J Clin Invest* (2018) 128(11):5095–109. doi: 10.1172/JCI99673

50. Massion PP, Taflan PM, Jamshedur Rahman SM, Yildiz P, Shyr Y, Edgerton ME, et al. Significance of p63 amplification and overexpression in lung cancer development and prognosis. *Cancer Res* (2003) 63(21):7113–21.

51. Quade BJ, Yang A, Wang Y, Sun D, Park J, Sheets EE, et al. Expression of the p53 homologue p63 in early cervical neoplasia. *Gynecol Oncol* (2001) 80(1):24–9. doi: 10.1006/gyno.2000.5953

52. Urist MJ, Di Como CJ, Lu ML, Charytonowicz E, Verbel D, Crum CP, et al. Loss of p63 expression is associated with tumor progression in bladder cancer. *Am J Pathol* (2002) 161(4):1199–206. doi: 10.1016/S0002-9440(10)64396-9

53. Zhou Y, Liu H, Wang J, Wang X, Qian L, Xu F, et al. DeltaNp63alpha exerts antitumor functions in cervical squamous cell carcinoma. *Oncogene* (2020) 39(4):905–21. doi: 10.1038/s41388-019-1033-x

54. Zangen R, Ratovitski E, Sidransky D. DeltaNp63alpha levels correlate with clinical tumor response to cisplatin. *Cell Cycle* (2005) 4(10):1313–5. doi: 10.4161/cc.4.10.2066

55. Yu X, Singh PK, Tabrejee S, Sinha S, Buck MJ. DeltaNp63 is a pioneer factor that binds inaccessible chromatin and elicits chromatin remodeling. *Epigenet Chromatin* (2021) 14(1):20. doi: 10.1186/s13072-021-00394-8

56. Sun CY, Zhang QY, Zheng GJ, Feng B. Phytochemicals: Current strategy to sensitize cancer cells to cisplatin. *BioMed Pharmacother* (2019) 110:518–27. doi: 10.1016/j.biopha.2018.12.010

57. Flores ER. The roles of p63 in cancer. *Cell Cycle* (2007) 6(3):300–4. doi: 10.4161/cc.6.3.3793

58. Kubo T, Ichimiya S, Tonooka A, Nagashima T, Kikuchi T, Sato N. p63 induces CD4+ T-cell chemoattractant TARC/CCL17 in human epithelial cells. *J Interferon Cytokine Res* (2008) 28(12):725–32. doi: 10.1089/jir.2008.0035

59. King KE, Ponnamperuma RM, Allen C, Lu H, Duggal P, Chen Z, et al. The p53 homologue DeltaNp63alpha interacts with the nuclear factor-kappaB pathway to modulate epithelial cell growth. *Cancer Res* (2008) 68(13):5122–31. doi: 10.1158/0008-5472.CAN-07-6123

60. Lu H, Yang X, Duggal P, Allen CT, Yan B, Cohen J, et al. TNF-alpha promotes c-REL/DeltaNp63alpha interaction and TAp73 dissociation from key genes that mediate growth arrest and apoptosis in head and neck cancer. *Cancer Res* (2011) 71(21):6867–77. doi: 10.1158/0008-5472.CAN-11-2460

61. Du J, Romano RA, Si H, Mattox A, Bian Y, Yang X, et al. Epidermal overexpression of transgenic DeltaNp63 promotes type 2 immune and myeloid inflammatory responses and hyperplasia via NF-kappaB activation. *J Pathol* (2014) 232(3):356–68. doi: 10.1002/path.4302

62. Klaus A, Birchmeier W. Wnt signalling and its impact on development and cancer. *Nat Rev Cancer* (2008) 8(5):387–98. doi: 10.1038/nrc2389

63. Veeck J, Dahl E. Targeting the Wnt pathway in cancer: the emerging role of Dickkopf-3. *Biochim Biophys Acta* (2012) 1825(1):18–28. doi: 10.1016/j.bbcan.2011.09.003

64. Malsin ES, Kim S, Lam AP, Gottardi CJ. Macrophages as a source and recipient of Wnt signals. *Front Immunol* (2019) 10:1813. doi: 10.3389/fimmu.2019.01813

65. Lu KH, Tounsi A, Shridhar N, Kublbeck G, Klevenz A, Prokosch S, et al. Dickkopf-3 contributes to the regulation of anti-tumor immune responses by mesenchymal stem cells. *Front Immunol* (2015) 6:645. doi: 10.3389/fimmu.2015.00645

66. Kinoshita R, Watanabe M, Huang P, Li SA, Sakaguchi M, Kumon H, et al. The cysteine-rich core domain of REIC/Dkk-3 is critical for its effect on monocyte differentiation and tumor regression. *Oncol Rep* (2015) 33(6):2908–14. doi: 10.3892/or.2015.3885

67. Mohammadpour H, Pourfathollah AA, Nikougoftar Zarif M, Tahoori MT. Effects of DKK-3, a Wnt signaling inhibitor, on dendritic cell phenotype and T cell polarization. *Immunopharmacol Immunotoxicol* (2015) 37(6):481–7. doi: 10.3109/08923973.2015.1089274

68. Zhang Q, Lenardo MJ, Baltimore D. 30 years of NF-kappaB: A blossoming of relevance to human pathobiology. *Cell* (2017) 168(1-2):37–57. doi: 10.1016/j.cell.2016.12.012

69. Dorrington MG, Fraser IDC. NF-kappaB signaling in macrophages: dynamics, crosstalk, and signal integration. *Front Immunol* (2019) 10:705. doi: 10.3389/fimmu.2019.00705

70. Sharif O, Bolshakov VN, Raines S, Newham P, Perkins ND. Transcriptional profiling of the LPS induced NF-kappaB response in macrophages. *BMC Immunol* (2007) 8:1. doi: 10.1186/1471-2172-8-1

71. Wang J, Vodovotz Y, Fan L, Li Y, Liu Z, Namas R, et al. Injury-induced MRP8/MRP14 stimulates IP-10/CXCL10 in monocytes/macrophages. *FASEB J* (2015) 29 (1):250–62. doi: 10.1096/fj.14-255992

72. Kikuchi A, Matsumoto S, Sada R. Dickkopf signaling, beyond Wnt-mediated biology. *Semin Cell Dev Biol* (2022) 125:55–65. doi: 10.1016/j.semcdb.2021.11.003

73. Li SX, Li J, Dong LW, Guo ZY. Cytoskeleton-associated protein 4, a promising biomarker for tumor diagnosis and therapy. *Front Mol Biosci* (2020) 7:552056. doi: 10.3389/fmolb.2020.552056

74. Kimura H, Fumoto K, Shojima K, Nojima S, Osugi Y, Tomihara H, et al. CKAP4 is a Dickkopf1 receptor and is involved in tumor progression. *J Clin Invest* (2016) 126 (7):2689–705. doi: 10.1172/JCI84658

75. Bai D, Ueno L, Vogt PK. Akt-mediated regulation of NFkappaB and the essentialness of NFkappaB for the oncogenicity of PI3K and Akt. *Int J Cancer* (2009) 125(12):2863–70. doi: 10.1002/ijc.24748

76. Safari E, Mosayebi G, Khorram S. Dkk-3 as a potential biomarker for diagnosis and prognosis of colorectal cancer. *Med J Islam Repub Iran* (2018) 32:86. doi: 10.14196/mjiri.32.86

77. Jiang T, Huang L, Wang S, Zhang S. Clinical significance of serum Dkk-3 in patients with gynecological cancer. *J Obstet Gynaecol Res* (2010) 36(4):769–73. doi: 10.1111/j.1447-0756.2010.01234.x

frontiers

Supplementary Material

Article Title A novel ΔNp63-dependent immune mechanism improves prognosis of HPV-related head and neck Cancer

Jana MOURTADA, Christelle LONY, Anaïs NICOL, Justine DE AZEVEDO, Cyril BOUR, Christine MACABRE, Patrick RONCARATI, Sonia LEDRAPPIER, Philippe SCHULTZ, Christian BOREL, Mickaël BURGY, Bohdan WASYLYK, Georg MELLITZER, Michaël HERFS, Christian GAIDDON*, Alain C. JUNG*

*** Correspondence:**

Dr Alain JUNG, Laboratoire de Biologie Tumorale, Institut de Cancérologie Strasbourg Europe, 17 rue Albert Calmette, F.67200 Strasbourg, FRANCE. Tel: +33 (0)3 88 27 53 67. Fax: +33 (0)3 88 26 35 38.
a.jung@icans.eu
Dr Christian GAIDDON, IRFAC INSERM U1113, 3 avenue Molière, F.67200 Strasbourg, FRANCE. Tel: +33 (0)3 88 27 53 67. Fax: +33 (0)3 88 26 35 38.
gaiddon@unistra.fr

1 Supplementary Tables

Supplementary Table 1: Patients' demographics. Two independent cohorts of patients with HPV-positive OSCC from the tumor banks of Strasbourg, France (N=34) and Liège, Belgium (N=43) were used for the validation of the transcriptomic data. 77 tumors specimens were used for gene expression assays by RT-qPCR. 71 FFPE samples were available for immunohistochemistry analyses. Patients' gender and age, history of tobacco smoking, pathological tumor size staging (pT), pathological lymph node invasion staging (pN), tumor stage, treatment, occurrence of metastasis within three years after treatment and 5-year overall survival are shown. Number and percentage (in brackets) for each cohort and combined cohorts are shown. NA: non available.

	HPV-positive OSCC Strasbourg (N=34)	**HPV-positive OSCC Liège (N=43)**	**HPV-positive OSCC Total (N=77)**
Gender			
Male	21 (62%)	30 (70%)	51 (66%)
Female	13 (38%)	13 (30%)	26 (34%)
Age			
Age<60 years	16 (47%)	19 (44%)	35 (45%)
Age≥60 years	18 (53%)	24 (56%)	42 (55%)
History of tobacco smoking			
Never smoker	9 (26%)	20 (47%)	29 (38%)
Former/current smoker	24 (71%)	23 (53%)	47 (61%)
NA	1 (3%)	0 (0%)	1 (1%)
Pathological tumor size staging (pT)			
T1	5 (15%)	5 (11.5%)	10 (13%)
T2	16 (47%)	27 (63%)	43 (56%)
T3	12 (35%)	6 (14%)	18 (23%)
T4	1 (3%)	5 (11.5%)	6 (8%)
Pathological lymph node staging (pN)			
N0	6 (18%)	9 (21%)	15 (19%)
N1	7 (20%)	12 (28%)	19 (25%)
N2a	4 (12%)	3 (7%)	7 (9%)
N2b	11 (32%)	14 (32.5%)	25 (32%)
N2c	4 (12%)	5 (11.5%)	9 (12%)
N3	2 (6%)	0 (0%)	2 (3%)
Tumor stage			
Stage I	1 (3%)	3 (7%)	4 (5%)
Stage II	1 (3%)	6 (14%)	7 (9%)
Stage III	11 (32%)	12 (28%)	23 (30%)
Stage IV	21 (62%)	22 (51%)	43 (56%)
Treatment			
Surgery	2 (6%)	8 (18.5%)	10 (13%)
Surgery + Radiotherapy	19 (56%)	14 (32.5%)	33 (43%)
Surgery + Chemoradiotherapy	13 (38%)	21 (49%)	34 (44%)
Metastasis at 3 years			
Yes	4 (12%)	5 (11.5%)	9 (12%)
No	29 (88%)	38 (88.5%)	67 (88%)
Overall survival at 5 years			
Alive	27 (80%)	30 (70%)	57 (84%)
Deceased	7 (20%)	13 (30%)	20 (26%)

Supplementary Table 2: List of oligonucleotide primer pairs. Gene of interest expression analysis was carried out by using a RT-qPCR approach. The names of analyzed gene are shown, as well as the 5'-to-3' sequence of forward and reverse oligonucleotide primers used in this study.

Gene name	Forward primer (5'-3')	Reverse primer (5'-3')
ΔNp63	ACGAGGAGCCGTTCTGAATC	ACCTGGAAAACAATGCCCAG
S100A7	GCCTGCTGACGATGATGAAG	ATGGCTCTGCTTGTGGTAGT
S100A9	GGACCTGGACACAAATGCAG	CTGTGATCTTGGCCACTGTG
KRT6B	TCTAGGTCCAGCTGCAGATG	GAGAGCAGAGAAAGCAGTGC
SERPINB1	AAGTTTGGCTCTGTTGGCTG	TCCCATGGCTATCAGGAGGA
SPRR1A	AGTTAGCATGCTGTCACCCT	CATCCTCAAATGCACCCGAG
SPRR1B	CTCTTCACACCAGGACCAGT	GCTCCTTGGTTTTGGGGATG
THBS4	GCAGACAGAGATGGCATTGG	ATCGGTGTCTTTCTGGTCGT
CD8a	AGGAAGTGAACCTGGTGGTG	CTCAGCAGACACTGCCACAT
GZMK	GTATTTTGGCAGGACCAGGA	CATTCCTGTGGGCTTTTTGT
CD68	ACTGAACCCCAACAAAACCA	TTGTACTCCACCGCCATGTA
DKK3	TTCATCCAGCAGTGTTGCTC	GGTGTGGGGTAGTGGAGAGA
RPLP0	GAAGGCTGTGGTGCTGATGG	CCGGATATGAGGCAGCAGTT
UBB	GCTTTGTTGGGTGAGCTTGT	CGAAGATCTGCATTTTGACCT
IKBα	CAGCAGACTCCACTCCACTT	GAGAGGGGTATTTCCTCGAA
ACTB	ATTGCCGACAGGATGCAGAA	GCTGATCCACATCTGCTGGAA

Supplementary Table 3: List of antibodies and experimental conditions. Protein of interest expression analysis was carried out by using Western Blot, immunohistochemistry or immunocytofluorescence approaches. Protein names are shown, as well as the references of used antibodies (including clone reference and provider) and the dilution at which they were used is shown.

	Protein	Provider	Antibody dilution
Western blot	Actine	mab150, Millipore	1/15000
	p63	4A4 ab-735, Abcam	1/500
	p53	DO-1 sc-126, santa Cruz	1/1000
	HPV16 E6	E6-6F4, Euromedex	1/500
	Cleaved caspase 3	9661L, Cell signaling	1/1000
	DKK3	ab-186409, Abcam	1/1000
	BSA	B2901, Sigma	1/2000
	anti-mouse IgG-HRP linked antibody	7076S, Cell Signaling	1/8000
	anti-rabbit IgG-HRP linked antibody	7074S, Cell Signaling	1/8000
	CKAP4	PA5-51455, Invitrogen	1/2500
	IKBα	14D4, Cell signaling	1/1000
	IKBα-Ps32	44D4, Cell signaling	1/1000
	AKT	92725, Cell signaling	1/1000
	AKT-pS473	4060L, Cell signaling	1/2000
Immunohistochemistry	p63	BC28 ab-172731, Abcam	1/150
	S100A7	HPA006997, Sigma-Aldrich	1/500
	S100A9	HPA004193, Sigma-Aldrich	1/10000
	KRT6B	17391-1-AP, Thermo Fisher Scientific	1/800

	THBS4	G-10, Santa Cruz Biotechnology	1/100
	CD8	SP57, Roche Tissue Diagnostics	1/1
	CD68	KP-1, Roche Tissue Diagnostics	1/1
Immunocytofluoresence	Anti-rabbit IgG Alexa Fluor 488	Invitrogen	1/1000
	NFκB P65	sc-372, Santa Cruz	1/400

Supplementary Table 4: List of 148 genes found to be differentially expressed in Cluster 1 and Cluster 2. Gene symbols, Gene names, gene id, $\log_2$ fold-change (logFC), average expression (AveExpr) and adjusted p-value (Adj.p.Val) are shown. Please note that only genes found to be deregulated with a logFC>1 and an Adj.p.Val<0.05 in our unsupervised hierarchical clustering analysis (Fig. 1A) are shown. Gene names highlighted in bold were previously shown to be transcriptionally regulated by ΔNp63 in Barbieri *et al.* (1).

Gene symbol	**Gene name**	**gene id**	**logFC (>1)**	**AveExpr**	**Adj.p.Val (< 0,05)**
S100A7	S100 calcium binding protein A7	6278	-8,12	9,73	5,54E-03
SPRR1A	small proline-rich protein 1A	6698	-6,89	10,19	2,94E-04
SPRR1B	small proline-rich protein 1B	6699	-6,32	10,18	5,15E-03
SPRR1A	small proline-rich protein 1A	6698	-6,14	9,90	4,96E-03
CLCA4	chloride channel accessory 4	22802	-6,13	7,48	4,54E-02
SPRR3	small proline-rich protein 3	6707	-5,44	10,80	1,32E-02
TMPRSS11E	transmembrane protease, serine 11E	28983	-5,17	7,10	2,05E-02
C10orf99	chromosome 10 open reading frame 99	387695	-5,03	6,89	4,98E-02
CLCA2	chloride channel accessory 2	9635	-5,02	7,08	2,86E-02
SBSN	suprabasin	374897	-4,90	7,63	4,98E-02
CRNN	cornulin	49860	-4,79	7,64	4,78E-02
CLCA2	chloride channel accessory 2	9635	-4,75	7,69	3,47E-02
IVL	involucrin	3713	-4,73	7,65	4,96E-03
SPINK5	serine peptidase inhibitor, Kazal type 5	11005	-4,45	8,88	4,02E-02
FAM83C	family with sequence similarity 83, member C	128876	-4,41	6,26	4,65E-02
CLCA2	chloride channel accessory 2	9635	-4,29	6,97	4,59E-02
RHCG	Rh family, C glycoprotein	51458	-4,21	8,02	4,78E-02
GBP6	guanylate binding protein family, member 6	163351	-4,21	6,72	2,77E-02
GJB6	gap junction protein, beta 6, 30kDa	10804	-4,19	7,01	2,62E-02
KRT6B	keratin 6B	3854	-4,18	11,21	8,39E-03
SPRR3	small proline-rich protein 3	6707	-4,16	11,77	1,48E-02
SPRR2C	small proline-rich protein 2C (pseudogene)	6702	-4,14	5,38	2,70E-02
TGM3	transglutaminase 3	7053	-4,08	6,66	8,39E-03
TGM1	transglutaminase 1	7051	-3,90	7,15	3,26E-02
CYP2E1	cytochrome P450, family 2, subfamily E, polypeptide 1	1571	-3,75	6,19	2,76E-02
KRT6A	keratin 6A	3853	-3,40	11,21	8,80E-03
S100A9	S100 calcium binding protein A9	6280	-3,36	11,61	4,35E-02

CCR7	chemokine (C-C motif) receptor 7	1236	-3,21	5,51	4,43E-02
IL1RN	interleukin 1 receptor antagonist	3557	-3,20	8,27	4,37E-02
IL1RN	interleukin 1 receptor antagonist	3557	-3,14	9,44	4,35E-02
KRT6B	keratin 6B	3854	-3,02	11,22	2,62E-02
SELL	selectin L	6402	-2,97	6,92	3,48E-02
DSG3	desmoglein 3	1830	-2,95	9,15	2,00E-02
GRHL3	grainyhead-like 3 (Drosophila)	57822	-2,89	5,87	4,35E-02
ZNF750	zinc finger protein 750	79755	-2,72	5,37	4,83E-02
GJB5	gap junction protein, beta 5, 31.1kDa	2709	-2,69	6,52	4,02E-02
DSG3	desmoglein 3	1830	-2,67	9,28	4,35E-02
NLRC3	NLR family, CARD domain containing 3	197358	-2,65	5,06	3,47E-02
TTC22	tetratricopeptide repeat domain 22	55001	-2,43	7,10	2,86E-02
ZBED2	zinc finger, BED-type containing 2	79413	-2,31	5,12	4,98E-02
ANKRD22	ankyrin repeat domain 22	118932	-2,26	7,76	1,63E-02
SERPINB1	serpin peptidase inhibitor, clade B (ovalbumin), member 1	1992	-2,21	8,02	1,32E-02
SERPINB1	serpin peptidase inhibitor, clade B (ovalbumin), member 1	1992	-2,13	8,89	2,62E-02
ANKRD22	ankyrin repeat domain 22	118932	-2,09	6,77	4,65E-02
PRKCB	protein kinase C, beta	5579	-2,07	5,44	4,98E-02
LCK	LCK proto-oncogene, Src family tyrosine kinase	3932	-2,06	7,10	3,48E-02
HLA-DOB	major histocompatibility complex, class II, DO beta	3112	-2,03	5,54	4,02E-02
ANXA1	annexin A1	301	-1,99	11,50	4,81E-02
GJB3	gap junction protein, beta 3, 31kDa	2707	-1,96	7,55	1,13E-02
DAPP1	dual adaptor of phosphotyrosine and 3-phosphoinositides	27071	-1,95	5,32	3,99E-02
IL2RB	interleukin 2 receptor, beta	3560	-1,91	7,48	2,15E-02
ITGAL	integrin, alpha L (antigen CD11A (p180), lymphocyte function-associated antigen 1; alpha polypeptide)	3683	-1,86	6,11	3,47E-02
EPHA1	EPH receptor A1	2041	-1,81	5,85	2,70E-02
LCK	LCK proto-oncogene, Src family tyrosine kinase	3932	-1,80	6,04	4,59E-02
ERO1L	ERO1-like (S. cerevisiae)	30001	-1,78	7,23	4,59E-02
GJB3	gap junction protein, beta 3, 31kDa	2707	-1,76	7,14	2,62E-02
SEPT1	septin 1	1731	-1,75	5,13	2,45E-02
ARHGAP15	Rho GTPase activating protein 15	55843	-1,70	6,81	4,78E-02
DAPP1	dual adaptor of phosphotyrosine and 3-phosphoinositides	27071	-1,61	6,02	4,83E-02
PTPRC	protein tyrosine phosphatase, receptor type, C	5788	-1,60	8,57	4,78E-02
EVI2B	ecotropic viral integration site 2B	2124	-1,50	7,20	4,98E-02
DUSP28	dual specificity phosphatase 28	285193	-1,50	5,18	5,00E-02
SPN	sialophorin	6693	-1,44	4,22	4,54E-02
MAP4K1	mitogen-activated protein kinase kinase kinase kinase 1	11184	-1,40	5,18	3,47E-02

RHOF	ras homolog family member F (in filopodia)	54509	-1,38	4,11	4,78E-02
ZNF101	zinc finger protein 101	94039	-1,38	4,66	4,65E-02
LINC00324	long intergenic non-protein coding RNA 324	284029	-1,33	4,16	3,87E-02
FYB	FYN binding protein	2533	-1,32	7,65	4,78E-02
HMGCR	3-hydroxy-3-methylglutaryl-CoA reductase	3156	-1,25	6,60	4,65E-02
ZNF200	zinc finger protein 200	7752	-1,22	5,76	4,35E-02
GAS7	growth arrest-specific 7	8522	1,13	3,76	4,78E-02
GABRB2	gamma-aminobutyric acid (GABA) A receptor, beta 2	2561	1,21	2,30	3,47E-02
CALD1	caldesmon 1	800	1,26	2,81	4,78E-02
DDX43	DEAD (Asp-Glu-Ala-Asp) box polypeptide 43	55510	1,39	2,78	4,78E-02
ZNF853	zinc finger protein 853	54753	1,39	3,44	4,35E-02
LAMA4	laminin, alpha 4	3910	1,44	3,60	4,78E-02
SSPN	sarcospan	8082	1,44	4,41	4,43E-02
SGCD	sarcoglycan, delta (35kDa dystrophin-associated glycoprotein)	6444	1,46	3,17	4,37E-02
MFGE8	milk fat globule-EGF factor 8 protein	4240	1,47	6,68	4,59E-02
PCDHB16	protocadherin beta 16	57717	1,48	2,74	4,96E-02
TANC1	tetratricopeptide repeat, ankyrin repeat and coiled-coil containing 1	85461	1,51	3,32	4,37E-02
MAGI2-AS3	MAGI2 antisense RNA 3	1E+08	1,57	4,23	3,29E-02
CALD1	caldesmon 1	800	1,57	4,40	2,70E-02
ETV1	ets variant 1	2115	1,59	3,92	4,42E-02
MEIS3P1	Meis homeobox 3 pseudogene 1	4213	1,59	5,66	4,35E-02
ANTXR1	anthrax toxin receptor 1	84168	1,59	3,37	4,78E-02
CORIN	corin, serine peptidase	10699	1,60	3,10	3,07E-02
SV2A	synaptic vesicle glycoprotein 2A	9900	1,60	3,54	3,47E-02
RPRD1A	regulation of nuclear pre-mRNA domain containing 1A	55197	1,62	4,28	4,37E-02
TRIL	TLR4 interactor with leucine-rich repeats	9865	1,63	3,78	4,63E-02
TRO	trophinin	7216	1,64	2,85	2,76E-02
DKK3	dickkopf WNT signaling pathway inhibitor 3	27122	1,64	3,16	4,54E-02
FZD3	frizzled class receptor 3	7976	1,65	3,65	4,23E-02
TRIL	TLR4 interactor with leucine-rich repeats	9865	1,68	3,34	3,87E-02
ARHGEF10	Rho guanine nucleotide exchange factor (GEF) 10	9639	1,70	3,55	3,07E-02
ACAA2	acetyl-CoA acyltransferase 2	10449	1,71	7,39	4,78E-02
BHLHE41	basic helix-loop-helix family, member e41	79365	1,80	7,10	4,63E-02
CAPS	calcyphosine	828	1,83	3,63	4,79E-02
TRO	trophinin	7216	1,87	3,18	2,86E-02
CLCN4	chloride channel, voltage-sensitive 4	1183	1,90	3,38	1,35E-02
SCG2	secretogranin II	7857	1,92	3,04	1,14E-02
PDE10A	phosphodiesterase 10A	10846	1,92	3,65	1,51E-02
DUXAP10	double homeobox A pseudogene 10	503639	1,96	4,68	4,78E-02

ST8SIA2	ST8 alpha-N-acetyl-neuraminide alpha-2,8-sialyltransferase 2	8128	2,00	2,82	3,47E-02
MARVELD1	MARVEL domain containing 1	83742	2,00	6,34	4,34E-02
CAPS	calcyphosine	828	2,00	5,24	2,00E-02
CALD1	caldesmon 1	800	2,02	3,51	2,86E-02
CALD1	caldesmon 1	800	2,05	3,76	2,11E-02
ACTA2	actin, alpha 2, smooth muscle, aorta	59	2,10	9,81	4,78E-02
COL8A2	collagen, type VIII, alpha 2	1296	2,15	6,63	4,35E-02
TMTC1	transmembrane and tetratricopeptide repeat containing 1	83857	2,16	5,56	3,92E-02
TNFRSF19	tumor necrosis factor receptor superfamily, member 19	55504	2,19	3,39	1,48E-02
TRO	trophinin	7216	2,20	4,12	2,86E-02
FZD3	frizzled class receptor 3	7976	2,21	4,23	4,11E-02
CALD1	caldesmon 1	800	2,31	6,53	4,78E-02
COL8A2	collagen, type VIII, alpha 2	1296	2,31	6,92	4,35E-02
LTBP2	latent transforming growth factor beta binding protein 2	4053	2,31	8,26	3,87E-02
COL6A1	collagen, type VI, alpha 1	1291	2,39	5,12	3,47E-02
LOXL1	lysyl oxidase-like 1	4016	2,47	8,09	3,47E-02
RGS16	regulator of G-protein signaling 16	6004	2,51	4,77	1,63E-02
ENAH	enabled homolog (Drosophila)	55740	2,51	5,12	4,35E-02
COL6A1	collagen, type VI, alpha 1	1291	2,58	6,09	4,35E-02
FGFR1	fibroblast growth factor receptor 1	2260	2,59	5,48	4,62E-02
FGFR1	fibroblast growth factor receptor 1	2260	2,61	6,88	4,78E-02
BMPR1B	bone morphogenetic protein receptor, type IB	658	2,71	3,39	2,49E-02
SNED1	sushi, nidogen and EGF-like domains 1	25992	2,75	4,61	4,63E-02
SGCD	sarcoglycan, delta (35kDa dystrophin-associated glycoprotein)	6444	2,83	3,96	4,02E-02
BMPR1B	bone morphogenetic protein receptor, type IB	658	2,83	3,05	1,13E-02
LAMP5	lysosomal-associated membrane protein family, member 5	24141	2,87	5,34	2,70E-02
GRP	gastrin-releasing peptide	2922	2,88	3,79	1,48E-02
NTM	neurotrimin	50863	2,95	4,62	8,80E-03
ACTG2	actin, gamma 2, smooth muscle, enteric	72	3,11	5,71	2,15E-02
NTM	neurotrimin	50863	3,13	6,95	4,35E-02
LOC339260	uncharacterized LOC339260	339260	3,27	3,63	5,15E-03
PAX7	paired box 7	5081	3,29	3,16	5,15E-03
COL1A2	collagen, type I, alpha 2	1278	3,40	5,93	4,62E-02
ITGBL1	integrin, beta-like 1 (with EGF-like repeat domains)	9358	3,43	4,48	1,51E-02
ITGBL1	integrin, beta-like 1 (with EGF-like repeat domains)	9358	3,47	5,31	4,02E-02
ITGBL1	integrin, beta-like 1 (with EGF-like repeat domains)	9358	3,61	4,42	4,98E-02
FN1	fibronectin 1	2335	3,76	6,05	2,62E-02
TIMP3	TIMP metallopeptidase inhibitor 3	7078	3,91	8,26	1,48E-02

TIMP3	TIMP metallopeptidase inhibitor 3	7078	3,98	6,84	4,96E-03
THBS4	thrombospondin 4	7060	4,00	6,86	3,74E-02
C1QTNF3	C1q and tumor necrosis factor related protein 3	114899	4,23	5,12	2,43E-02
TIMP3	TIMP metallopeptidase inhibitor 3	7078	4,30	7,21	1,86E-02
TIMP3	TIMP metallopeptidase inhibitor 3	7078	4,45	6,66	1,35E-02
FIBIN	fin bud initiation factor homolog (zebrafish)	387758	4,62	5,41	2,62E-02
COMP	cartilage oligomeric matrix protein	1311	5,42	5,14	4,35E-02

Supplementary Table 5: Meta-analysis and two-two comparison of our tumor transcriptomic data with independent publicly available data sets. Our transcriptomic data set was compared to data sets from Slebos *et al*. (2), Mirghani *et al*. (3) and Pyeon *et al*. (4), which allowed the recovery of gene modules named with colors. The Z-score, correlation coefficient (Corr.) and p-value of the two-two comparisons are shown. The modules showing the most genes in common with Cluster 2 are shown in italic.

Modules	***vs.* Slebos *et al.***			***vs*. Mirgani *et al.***			***vs.* Pyeon *et al.***		
	Z-score	**Corr.**	**p-value**	**Z-score**	**Corr.**	**p-value**	**Z-score**	**Corr.**	**p-value**
Blue				5.34	0.14	0.012			
Red	21.53	0.34	9.4 E $^{-07}$	*13.62*	*0.38*	*5E^{-08}*	11.56	0.25	0.00029
Brown	10	0.45	5.4E^{-20}	18.07	0.41	4.8 E $^{-12}$	10.30	0.47	6.4 E -^{15}
Cyan				5.56	0.25	0.014	8.32	0.41	9.7 E $^{-5}$
Pink				7.42	0.25	0.002	*8.19*	*0.2*	*0.0088*
Yellow							8.10	0.23	0.00054
Turquoise				10.20	0.37	1.1 E $^{-17}$	6.67	0.22	3.5 E $^{-6}$
Midnight Blue				5.39	0.21	0.043	*6.05*	*0.21*	*0.054*
Salmon							5.51	0.29	0.0056
Green				12.32	0.46	4 E $^{-14}$			
Purple	*7.45*	*0.23*	*0.0026*						

Supplementary Table 6: Analysis of the correlation of gene expression with metastasis occurrence. The expression of the *KRT6B*, *S100A7*, *S100A9*, *SERPINB1*, *SPRR1A*, *SPRR1B* and *THBS4* genes was measured by RT-qPCR in patient tumor samples (N=77; Table S4). The median expression (Med) in metastatic (Meta) and non-metastatic (Non-meta) lesions is shown. Median expressions were compared using a two-sample Wilcoxon rank-sum test, and differences were considered statistically significant when $p<0.05$ (shown in bold). A ROC-curve analysis of the relationship between expression and the occurrence of metastatic relapse within 3 years was carried out, and optimal cut-off values were determined. The predictive power of these values was assessed by determining their sensibility, specificity and area under the curve (AUC).

Gene name	RT-qPCR Med. Non-Meta.	RT-qPCR Med. Meta.	p-value	Sensibility	Specificity	AUC
KRT6B	1.01	0.27	0.24	0.84	0.56	0.70
S100A7	1.06	0.13	0.06	0.85	0.56	0.70
S100A9	1.04	0.14	**0.02**	0.94	0.56	0.75
SERPINB1	1.05	0.29	**0.01**	0.93	0.75	0.84
SPRR1A	1.04	0.07	**0.04**	0.83	0.75	0.79
SPRR1B	1.00	1.16	0.78	/	/	/
THBS4	0.95	2.65	**0.02**	0.78	0.72	0.75

2 Supplementary Figures

Figure S1

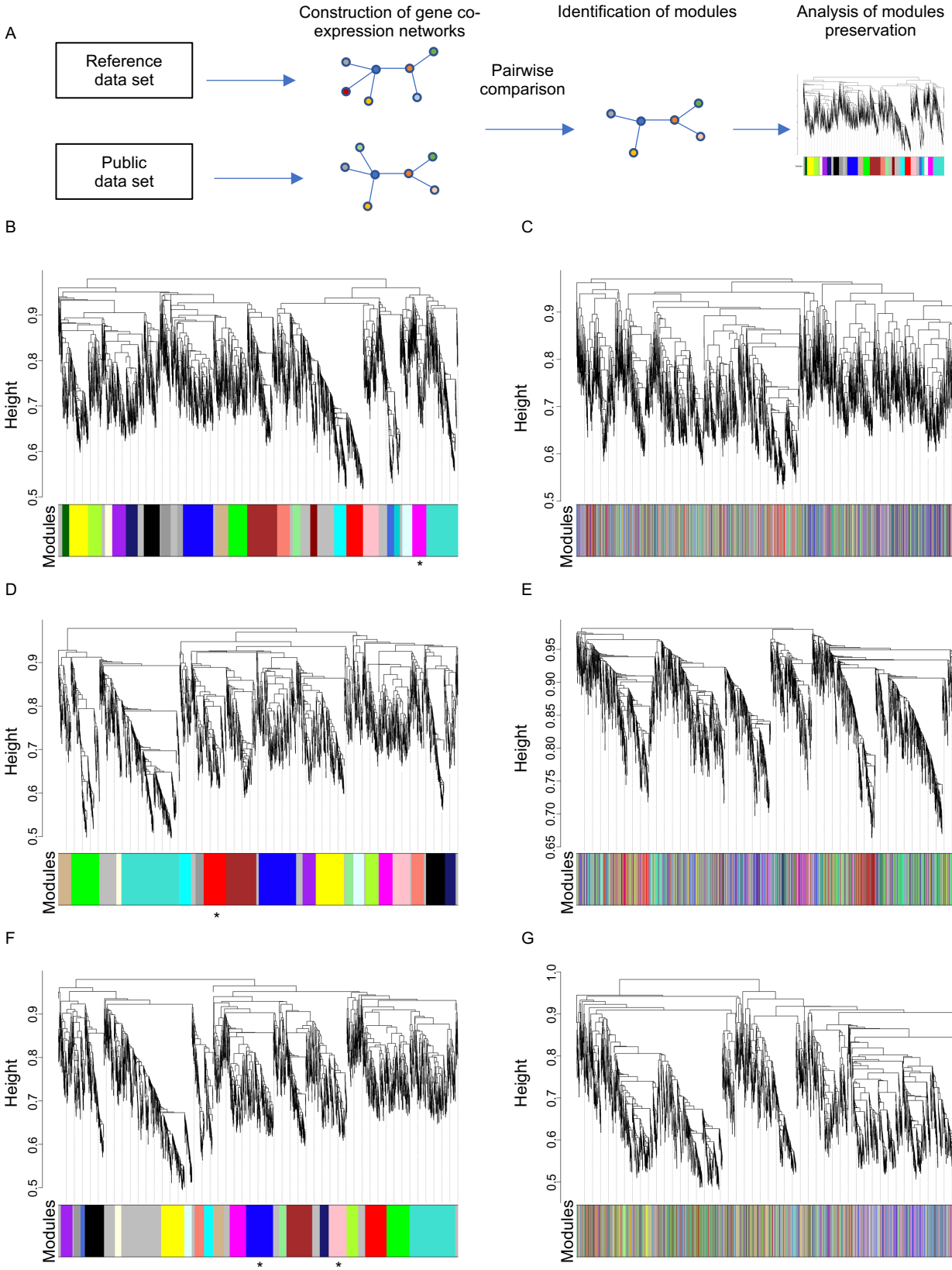

Supplementary Figure 1. The ΔNp63-dependent molecular signature is consistently retrieved in independent transcriptomic data sets.

(A)Flowchart of the WGCNA. Gene co-expression networks (depicted as connected dots) are identified in both data sets. A pairwise comparison and hierarchical clustering analysis of these networks allows the identification of highly interconnected clusters of genes called modules. A dynamic tree cut analysis and dendogram is established for each data set (Figures S1B-G). Their pairwise comparison matching clusters allow the identification of the most preserved ones (see also Table S3). (B-G) Meta-analysis comparing our HPV-positive OSCC transcriptomic data set to independent publicly available data sets was carried out. Gene dendograms and inferred module colors are shown for our data set (B; D; F) and data sets previously reported by Slebos et al. (2) (C), Mirghani et al. (3) (E) and Pyeon et al. (4) (G). Asterisks highlight the purple (B), red (D), and blue and pink modules (E).

Figure S2

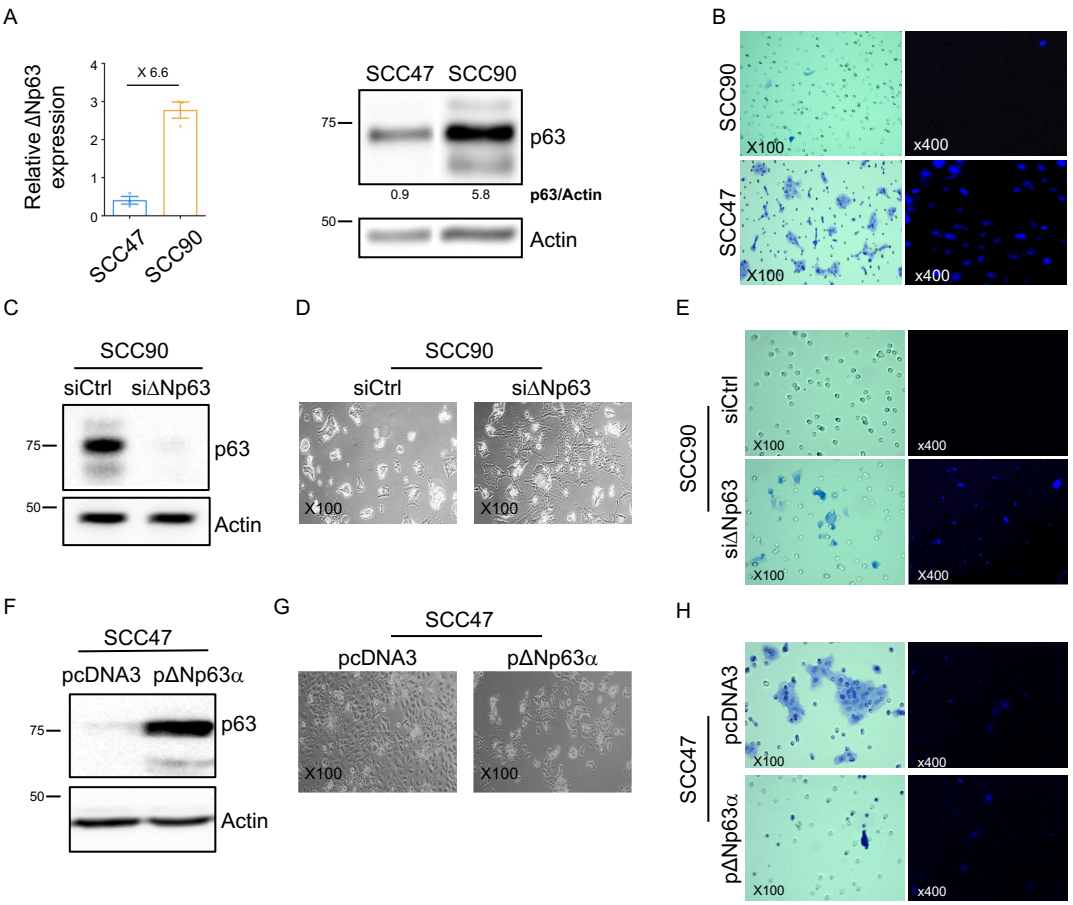

Figure S3

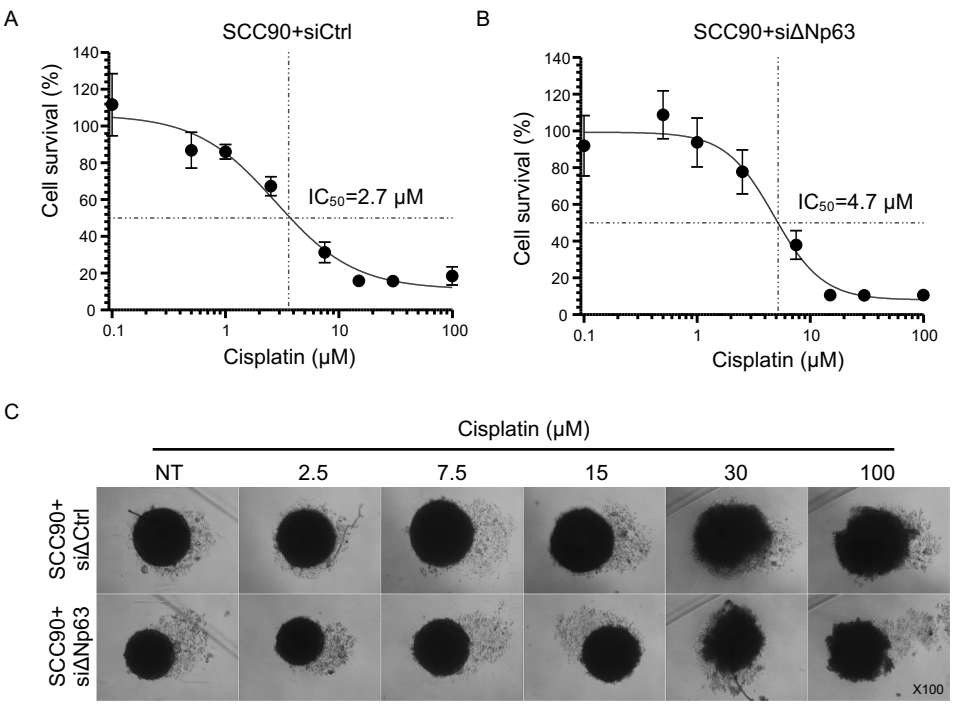

Supplementary Figure 2. Modulation of ΔNp63 expression in SCC90 and SCC47 cell line models

(A) Analysis of the ΔNp63 gene (RT-qPCR) and protein (western blot) expression in SCC47 and SCC90 HPV-positive cell line models. RT-qPCR data is shown as scatter plots with bars and mean +/- SEM (N=3). ΔNp63 protein signals were quantified with respect to the actin loading control, and quantification results (p63/Actin) are shown below the blot. (B) Analysis of the migration (left panel) and invasion (right panel) abilities of the SCC90 (upper panels) and SCC47 (lower panels) cells, as evaluated using a trans-well chamber assay. Magnification (100X; 400X) is shown. (C) siRNA-mediated downregulation of ΔNp63 expression in SCC90 cells. (D) Morphology of SCC90 cells upon downregulation of ΔNp63. Magnification (100X) is shown. (E) Analysis of the migration (left panels) and invasion (right panels) properties of SCC90 cells upon ΔNp63 downregulation using a transwell assay. Magnification (100X; 40X) is shown. (F) Western blot analysis of the expression of ΔNp63 in SCC47 cells transfected with a ΔNp63 expression vector. (G) Morphology of ΔNp63-overexpressing SCC47 cells. Magnification (100X) is shown. (H) Analysis of the migration (left panels) and invasion (right panels) properties of SCC47 cells upon ΔNp63 upregulation using a transwell assay. Magnification (100X; 40X) is shown.

Supplementary Figure 3. ΔNp63 is involved in the cellular response to cisplatin and in genotoxic-induced cell apoptosis.

(A-B) Analysis of SCC90 cell survival upon treatment with growing concentrations of cisplatin, using a MTT-based cell viability assay, after transfection with scrambled (siCtrl; A) or anti-ΔNp63 (siΔNp63; B) siRNAs. Results are plotted as sigmoid curves and the cisplatin IC_{50} in both conditions is shown. (C) Morphology of spheroids of SCC90 cells transfected with scrambled or ΔNp63 siRNA and treated with increasing concentration of cisplatin

Figure S4

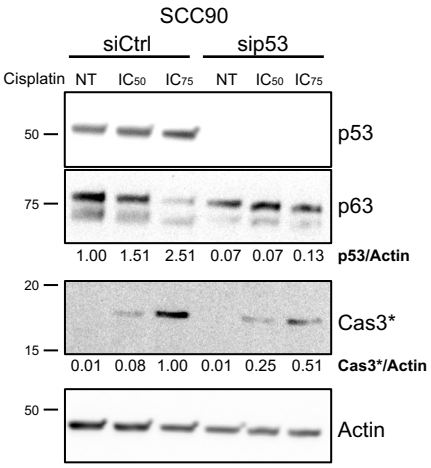

Figure S5

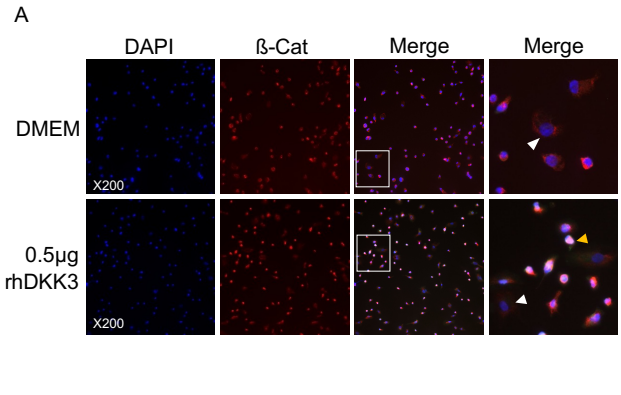

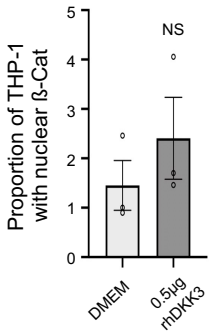

Figure S6

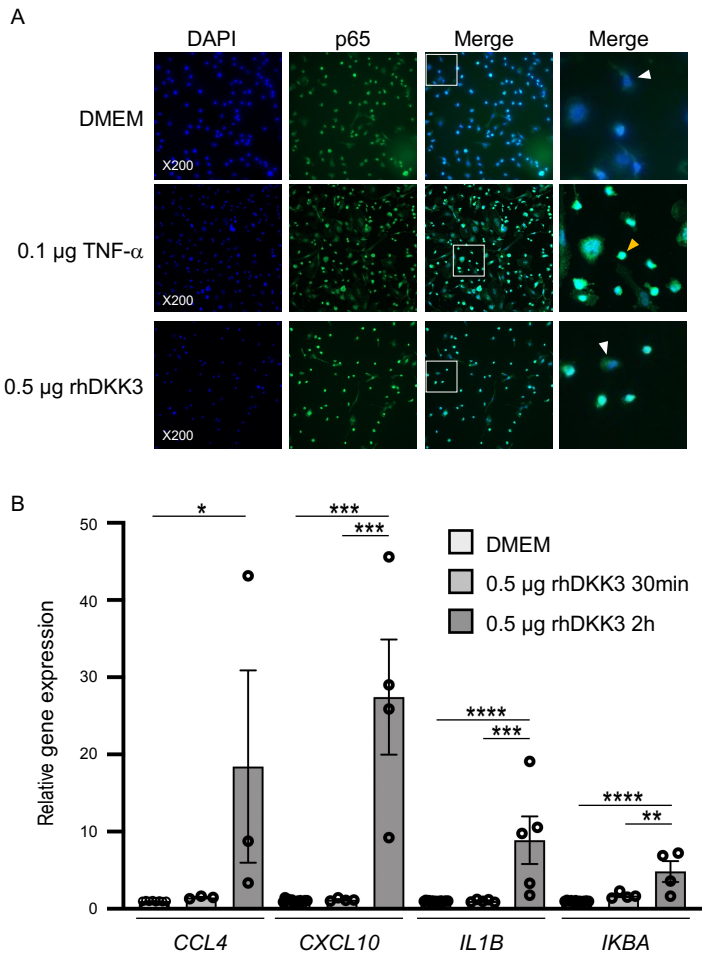

Supplementary Figure 4. p53 partially mediates cisplatin-induced apoptosis in SCC90 cells.

Western blot analysis of p53, ΔNp63 and cleaved caspase 3 (Cas3*) expression upon siRNA-mediated downregulation of p53 in SCC90 cells and treatment with cisplatin (IC_{50}=2.8μM; IC_{75}=6.7μM). p53 and Cas3* signals were quantified with respect to the actin loading control and normalized to non-treated siCtrl SCC90 cells or siCtrl SCC90 cells treated with the IC_{75} of cisplatin, respectively. Quantification results (p63/Actin; Cas3*/Actin) are shown below the blot.

Supplementary Figure 5. DKK3 does not impact Wnt-signalling in THP-1 macrophages.

(A) Immunocytofluorescence staining of ß-catenin (ß-cat) expression in THP-1 macrophages incubated with DMEM (negative control) or 0.5 μg of hrDKK4 for 6h prior to staining. DAPI, ß-cat staining and merge are shown. Magnification: X200. A magnification (right panels) of the inset in the merge is shown. White and yellow arrowheads highlight ß-cat staining in the cytoplasm and the nuclei, respectively. (B) A quantification of the proportion of THP-1 macrophages with ß-cat-positive nuclei is plotted in a graph. Data is represented as scatter plots with bars and mean +/- SEM (N=3). NS: Non-significant.

Supplementary Figure 6. DKK3 activates NF-κB signaling in THP-1 macrophages.

Immunocytofluorescence staining of p65 expression in THP-1 macrophages incubated with DMEM (negative control), 0.1μg of TNF-α or 0.5 μg of hrDKK4 for 6 h prior to staining. DAPI, p65 staining and merge are shown. Magnification: X200. A magnification (right panels) of the inset in the merge is shown. White and yellow arrowheads highlight p65 staining in the cytoplasm and the nuclei, respectively. (B) Analysis of the expression of the *CCL4*, *CXCL10*, *IL1B* and *IKBA* genes in THP-1 macrophages incubated with DMEM (negative control), 0.1μg of TNF-α or 0.5 μg of hrDKK4 for 30 min and 2 h. Data is represented as as scatter plots with bars and mean +/- SEM (N≥3). One-way ANOVA and Tuckey post-test: * $p<0.05$; ** $p<0.01$; *** $p<0.001$; **** $p<0.0001$.

Figure S7

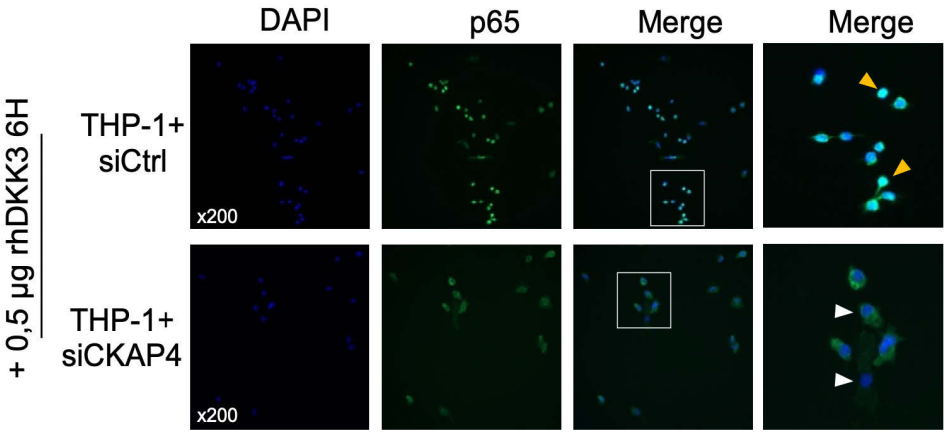

Supplementary Figure 7. CKAP4 is required for the DKK3-dependent activation of NF-κB signaling in THP-1 macrophages.

Immunocytofluorescence staining of p65 expression in THP-1 macrophages transfected with either scrambled (siCtrl) or anti-CKAP4 (siCKAP4) siRNAs, and incubated with DMEM (negative control) or 0.5 µg of hrDKK4 for 6 h prior to staining. DAPI, p65 staining and merge are shown. Magnification: X200. A magnification (right panels) of the inset in the merge is shown. White and yellow arrowheads highlight p65 staining in the cytoplasm and the nuclei, respectively.

Supplemental Video S1. In vitro time-lapse analysis of the phagocytosis of SCC90 cells by THP-1 macrophages

Green-labelled SCC90 cells were co-cultured with red-labelled THP-1 macrophages, cultures were analyzed using a time-lapse video-microscopy approach. Images were acquired every 10min for 22h and 20min using the 20X objective of a IncuCyte® S3 Live-Cell Analysis Instrument.

References

1. Barbieri CE, Tang LJ, Brown KA, Pietenpol JA. Loss of p63 leads to increased cell migration and up-regulation of genes involved in invasion and metastasis. Cancer Res. 2006;66(15):7589-97.
2. Slebos RJ, Yi Y, Ely K, Carter J, Evjen A, Zhang X, et al. Gene expression differences associated with human papillomavirus status in head and neck squamous cell carcinoma. Clin Cancer Res. 2006;12(3 Pt 1):701-9.
3. Mirghani H, Ugolin N, Ory C, Lefevre M, Baulande S, Hofman P, et al. A predictive transcriptomic signature of oropharyngeal cancer according to HPV16 status exclusively. Oral Oncol. 2014;50(11):1025-34.
4. Pyeon D, Newton MA, Lambert PF, den Boon JA, Sengupta S, Marsit CJ, et al. Fundamental differences in cell cycle deregulation in human papillomavirus-positive and human papillomavirus-negative head/neck and cervical cancers. Cancer Res. 2007;67(10):4605-19.

RÉSULTATS ANNEXES

1. ΔNp63α régule l'expression de DKK-3 : Une régulation directe ?

Nous avons montré que ΔNp63α régule l'expression de DKK-3 au niveau transcriptionnel et protéique, à la fois à l'intérieur et à l'extérieur des cellules SCC090 (voir Mourtada *et al.* ; Figure 5). De manière intéressante, une étude antérieure menée dans un modèle de cancer de l'œsophage a démontré que ΔNp63α se lie à une région en amont du promoteur de *DKK-3* et régule son expression (Kajiwara *et al.*, 2018). Par conséquent, il serait intéressant de déterminer si ΔNp63α régule directement ou indirectement l'expression de DKK-3 dans notre modèle cellulaire.

Pour répondre à cette question, nous avons effectué une analyse bio-informatique de la région promotrice du gène codant DKK-3. Cette analyse a révélé la présence de deux sites consensus de réponse à ΔNp63, qui sont répétés 11 fois sur une plage de 9000 paires de bases en amont du site d'initiation de la transcription de *DKK-3* **(Figure S1-A).** Nous avons ensuite dessiné des amorces oligonucléotidiques et les avons utilisées dans une expérience d'immunoprécipitation de chromatine (ChIP) à partir de cellules SCC090, en utilisant un anticorps spécifique de ΔNp63. À partir de 5 couples d'amorces dessinés, 3 ont été retenus lors de l'évaluation de leur efficacité par PCR quantitative. Ces 3 amorces sont spécifiques des sites de fixation II, IX et X de p63. IRF6 étant un contrôle positif de fixation de ΔNp63 et la myoglobine exon 2 un contrôle négatif.

Cependant, lors de l'analyse de l'enrichissement de ces régions en amont du promoteur de *DKK-3* (comme calculé dans la section "Matériels et Méthodes"), on observe une légère réduction du pourcentage d'enrichissement entre la condition contrôle (AC anti-IgG) et la condition ΔNp63 (AC anti-ΔNp63) pour les sites p63 X (F2R2) et p63 RE II (F2R2), ainsi qu'une légère augmentation pour le site p63 RE II (F1R1) **(Figure S1-B).** Toutefois, il convient de noter que ce dernier n'a pas été pris en considération en raison des valeurs élevées des Ct obtenues en qPCR. Ceci suggère que ΔNp63 ne se lie pas au promoteur de *DKK-3* sur ces sites, en particulier sur le site X, qui a été décrit dans la littérature comme étant une cible directe de ΔNp63 dans un modèle de cancer de l'œsophage. En conclusion, nos analyses indiquent que, du moins pour les sites que j'ai pu étudier dans la lignée SCC090, la régulation de l'expression transcriptionnelle de DKK-3 par ΔNp63 est indirecte.

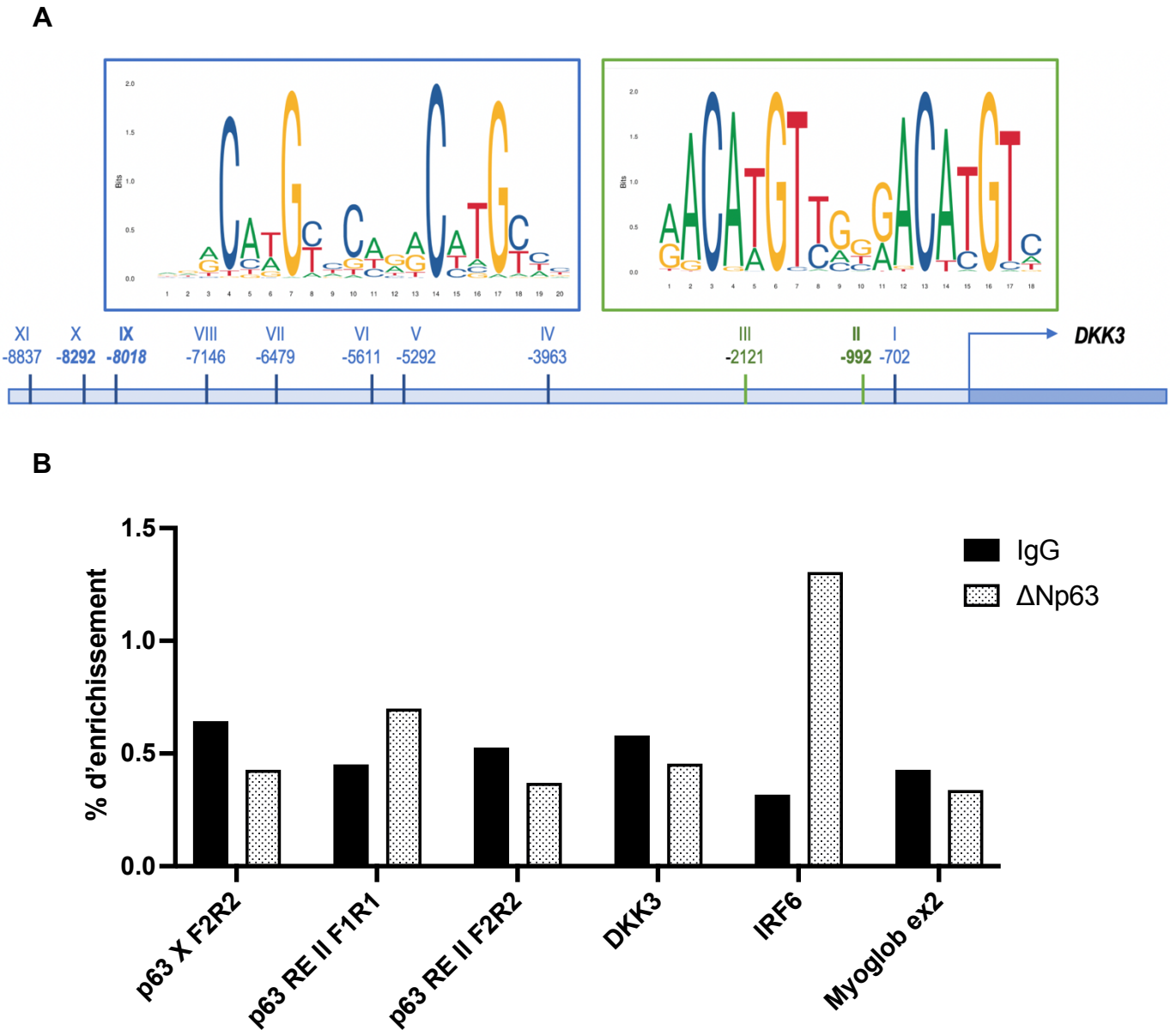

Figure S1- A. Des sites potentiels de réponse à ΔNp63 ont été identifié dans le locus génomique de DKK-3 : MA0525.1 (encart bleu) et MA0525.2 (encart vert), situé dans la région en amont d'environ 9 kb du site d'initiation de la transcription de DKK-3. La séquence consensus de p63 est représentée graphiquement sous la forme d'un logo de séquence obtenu à partir du site web JASPAR. **B.** Analyse de la précipitation de la chromatine à l'aide des cellules SCC090. La chromatine a été précipitée avec des anticorps IgG de contrôle et anti-ΔNp63 (BC28) et les fragments d'ADN génomiques purifiés ont été analysé par qPCR. Des amorces ciblant le promoteur de IRF6 et de la Myoglobine ont été utilisés respectivement comme contrôle positif et négatif. Aucune amplification n'est observée avec les amorces spécifiques des régions II, IX et X.

2. Rôle de DKK-3 dans la régulation de la voie Wnt

Certaines études montrent que DKK-3 bloque la translocation nucléaire de la β-caténine inhibant alors l'expression des gènes cibles de la voie Wnt. De plus, des liens ont été établis entre la voie Wnt et l'activation de la voie NF-κB, ce qui joue un rôle dans l'activation de la réponse immunitaire innée. Ainsi, et afin d'analyser les mécanismes moléculaires impliqués dans l'activation des macrophages THP-1 par DKK-3, nous avons étudié la translocation nucléaire de la β-caténine par immunocytofluorescence au niveau des macrophages THP-1 incubés avec la protéine recombinante humaine DKK-3 (rhDKK3). Cependant, nous n'avons pas observé de changement statistiquement significatif dans le nombre de noyaux positifs pour la β-caténine au niveau des cellules THP-1 traitées pendant 6 heures avec 0,5 µg de rhDKK3, par rapport au témoin négatif (c'est-à-dire, le milieu cellulaire DMEM), ce qui suggère que la localisation nucléaire de la β-caténine et la signalisation Wnt ne sont pas inhibées par la rhDKK3 **(voir Mourtada *et al.,* Figure S5).**

En parallèle de l'analyse de la translocation de la β-caténine, nous avons utilisé le système de rapporteur à la luciférase (TOPFLASH) pour mesurer l'induction de la signalisation Wnt canonique dépendante de la β-caténine. Le vecteur rapporteur TOPFLASH est composé de trois motifs consensus multimérisés de liaison du facteur de transcription TCF/LEF, clonés en amont du gène de la luciférase de luciole. L'induction de l'activité luciférase à partir de ce rapporteur dépend fortement de la présence à la fois de la β-caténine et de TCF. Dans le vecteur FOPFLASH, les sites de liaison à TCF sont mutés et non fonctionnels. Ce vecteur est donc utilisé comme contrôle négatif. Par conséquent, le ratio d'expression entre TOPFLASH et FOPFLASH (T/F) fournit une mesure précise de l'activité transcriptionnelle spécifique aux voies canoniques de Wnt.

De ce fait, nous avons évalué l'activité de la β-caténine dans deux modèles cellulaires distincts. Dans un premier modèle, nous avons réalisé une transfection des macrophages THP-1 avec soit un plasmide d'expression β-caténine/TCF (p-CTRL positif) soit un plasmide d'expression DKK-3 ou un plasmide vide servant de contrôle négatif. Dans un second modèle, ces mêmes conditions expérimentales ont été

reproduites avec la lignée HEK293, qui est utilisée comme une lignée contrôle de l'activation de la voie Wnt par le plasmide β-caténine/TCF.

Lors de la comparaison des rapports d'expression T/F entre les différentes conditions, nous n'avons pas observé d'impact significatif de DKK-3 sur la voie Wnt dans les deux lignées cellulaires (THP-1 et HEK). Toutefois, il est important de noter que ces résultats ne permettent pas de conclure définitivement pour la lignée THP-1, car même le contrôle positif d'activation de la voie Wnt n'a pas induit l'effet attendu. Cette observation pourrait s'expliquer par un taux de transfection potentiellement insuffisant dans les THP-1, bien que d'autres facteurs ne soient pas exclus.

En revanche, dans la lignée contrôle HEK, la transfection avec le plasmide DKK-3 n'a pas engendré de modification significative des niveaux de β-caténine nucléaire, avec des rapports T/F de 2,75 et 3,10 pour les conditions plasmide vide et plasmide-DKK-3, respectivement. Cependant, il est important de noter que la voie Wnt a été activée avec succès en présence du contrôle positif, comme en témoigne un rapport de 66,51 (p-CTRL). Par conséquent, il semble que DKK-3 n'inhibe pas la voie Wnt dans cette lignée cellulaire **(Figure S2).**

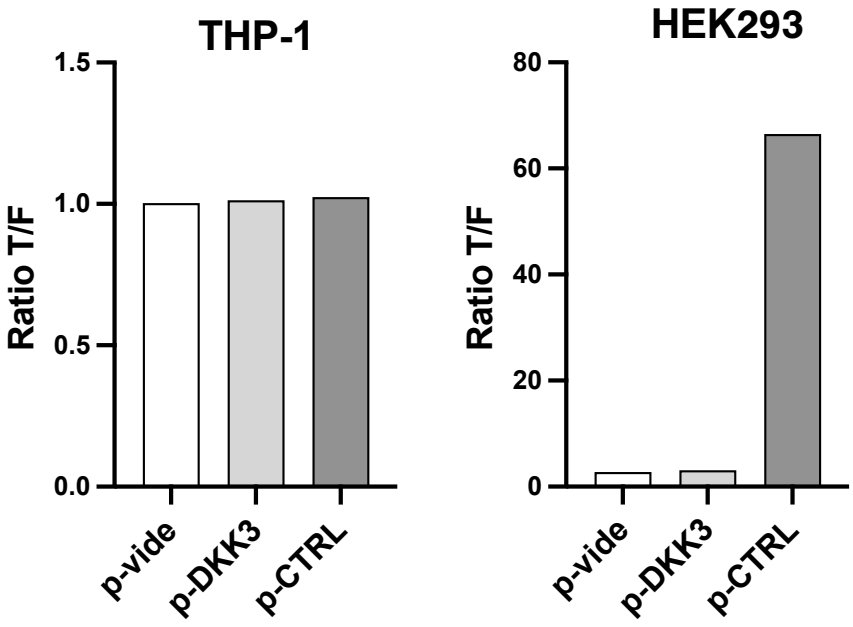

Figure S2- Activité de la luciférase mesurée dans les cellules THP-1 et HEK293 transfectées par un plasmide vide ou un plasmide DKK-3. Les résultats sont représentés sous forme de ratio TOP/FOPflash.

3. Effet de la surexpression de DKK-3 sur l'activité phagocytaire des macrophages THP-1

Comme mentionné précédemment dans notre étude (Mourtada *et al.* ; Figure 4 et 5), ΔNp63 régule la phagocytose des cellules cancéreuses par les macrophages via l'expression et la sécrétion de DKK-3 : l'inhibition de l'expression de DKK-3 par siARN réduit significativement la phagocytose des cellules cancéreuses (SCC090) par les macrophages (THP-1).

Ainsi, nous avons voulu vérifier si l'effet opposé est observé lorsqu'on surexprime DKK-3. Cette étude a été réalisée sur les deux lignées cellulaires de cancer de l'oropharynx HPV+ (SCC090 et SCC47) transfectées par un plasmide d'expression de DKK-3. Nous avons vérifié que la transfection des cellules par un plasmide d'expression p-DKK-3 augmentait les niveaux d'expression intra- et extracellulaire de la protéine DKK-3 dans les deux lignées cellulaires (pour les détails de l'expérimentation, voir Mourtada *et al*.).

Dans une expérience de phagocytose *in vitro*, on observe une tendance à l'augmentation du pourcentage de phagocytose par les macrophages THP-1, des cellules cancéreuses (SCC090 et SCC47) surexprimant DKK-3 sans que celle-ci soit statistiquement significative **(Figure S3)**. Ceci pourrait suggérer que les niveaux basaux d'expression de DKK-3 dans nos modèles cellulaires sont suffisants pour activer un certain niveau de phagocytose *in vitro* par les macrophages ; et que les effets sur la stimulation de la phagocytose consécutifs à une augmentation des niveaux d'expression de DKK-3 est plus difficile à mettre en évidence de manière statistiquement significative.

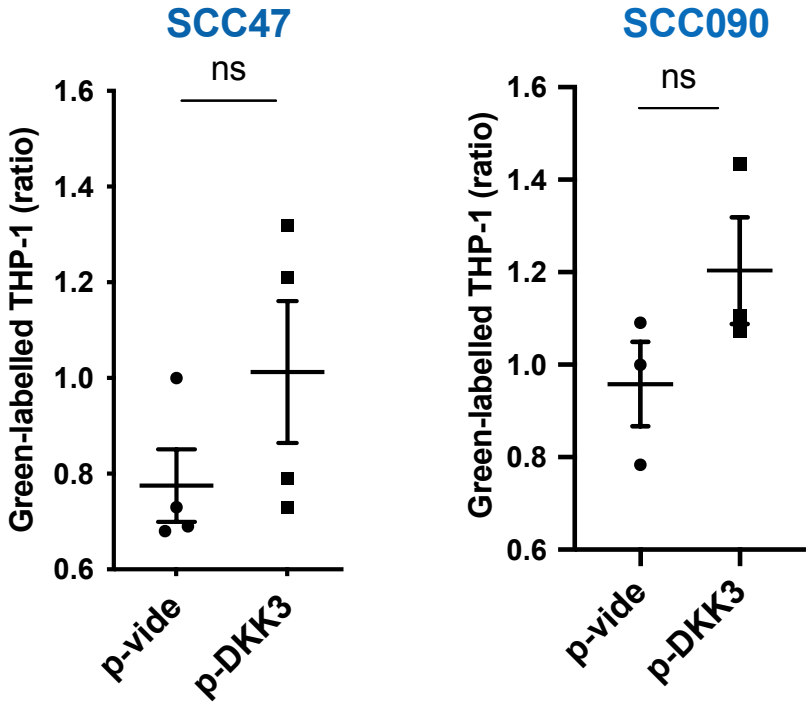

Figure S3- Taux de phagocytose des cellules SCC47 et SCC090 transfectées par un plasmide DKK-3 (versus vide) par les macrophages THP-1.

4. Phagocytose par vidéo microscopie direct (pHrodo®)

Afin de pouvoir valider la phagocytose des macrophages *in vitro*, nous avons optimisé et utilisé l'équipement d'imagerie en temps réel IncuCyte™ et utilisé le colorant pHrodo® Red Cell Labeling Dye for Incucyte®. Il s'agit d'un réactif permettant de marquer des cellules entières avec un fluorophore sensible au pH exploitant l'environnement acide du phagosome pour quantifier la phagocytose. Ainsi, lorsque les cellules marquées au pHrodo® se trouvent dans la solution extracellulaire neutre (pH 7,4) et sont englouties par les phagocytes pour entrer dans le phagosome acide (pH 4,5-5,5), une augmentation significative de la fluorescence est observée. En l'absence de phagocytes, l'intensité de fluorescence des cellules marquées reste faible. L'analyse d'image et la quantification de la fluorescence ont été réalisées avec le logiciel automatisé IncuCyte™ Basic.

Dans le but d'optimiser les conditions expérimentales, deux concentrations du colorant pHrodo ont été testés (15 et 30 µg/mL), d'une part dans un pH neutre (en présence du

milieu de culture pH=7,4) et d'autre part dans un pH acide (en présence d'un tampon Citrate pH=4) afin de mimer l'acidité du phagosome. Les paramètres d'analyses par l'IncuCyte™ ont été ajustés pour éliminer les risques de faux positifs.

Après avoir pris en compte diverses conditions d'optimisation, nous avons procédé à l'étude de la phagocytose en suivant les protocoles fournis, et en utilisant des conditions expérimentales similaires à celles appliquées dans notre étude antérieure de la phagocytose avec des traceurs cellulaires (rouges et verts, comme décrit dans Mourtada *et al.* ; Figure 4 et Figure 5). Bien que cette expérience n'ait été réalisée qu'une seule fois, les résultats obtenus semblent indiquer qu'en moyenne, l'intensité totale des objets rouges internalisés (reflétant la phagocytose) serait réduite lorsque les macrophages THP-1 sont incubés avec des SCC090 transfectées avec un siARN ciblant DKK-3 par rapport à ceux incubés avec des SCC090 transfectées avec un siARN contrôle, et ce pendant une période de 48 heures **(voir Figure S4).**

Ainsi, ces résultats préliminaires sont cohérents avec nos premières constatations sur la diminution du taux de phagocytose en absence de DKK-3, écartant la possibilité que les vésicules vertes observées en immunofluorescence soient des artefacts liés à la culture cellulaire. Ils correspondent également aux résultats précédemment observés lors des tests de phagocytose *in vitro*, ce qui renforce l'efficacité de notre système expérimental et confirme le rôle de DKK-3 dans la stimulation de la phagocytose par les macrophages THP-1 *in vitro*.

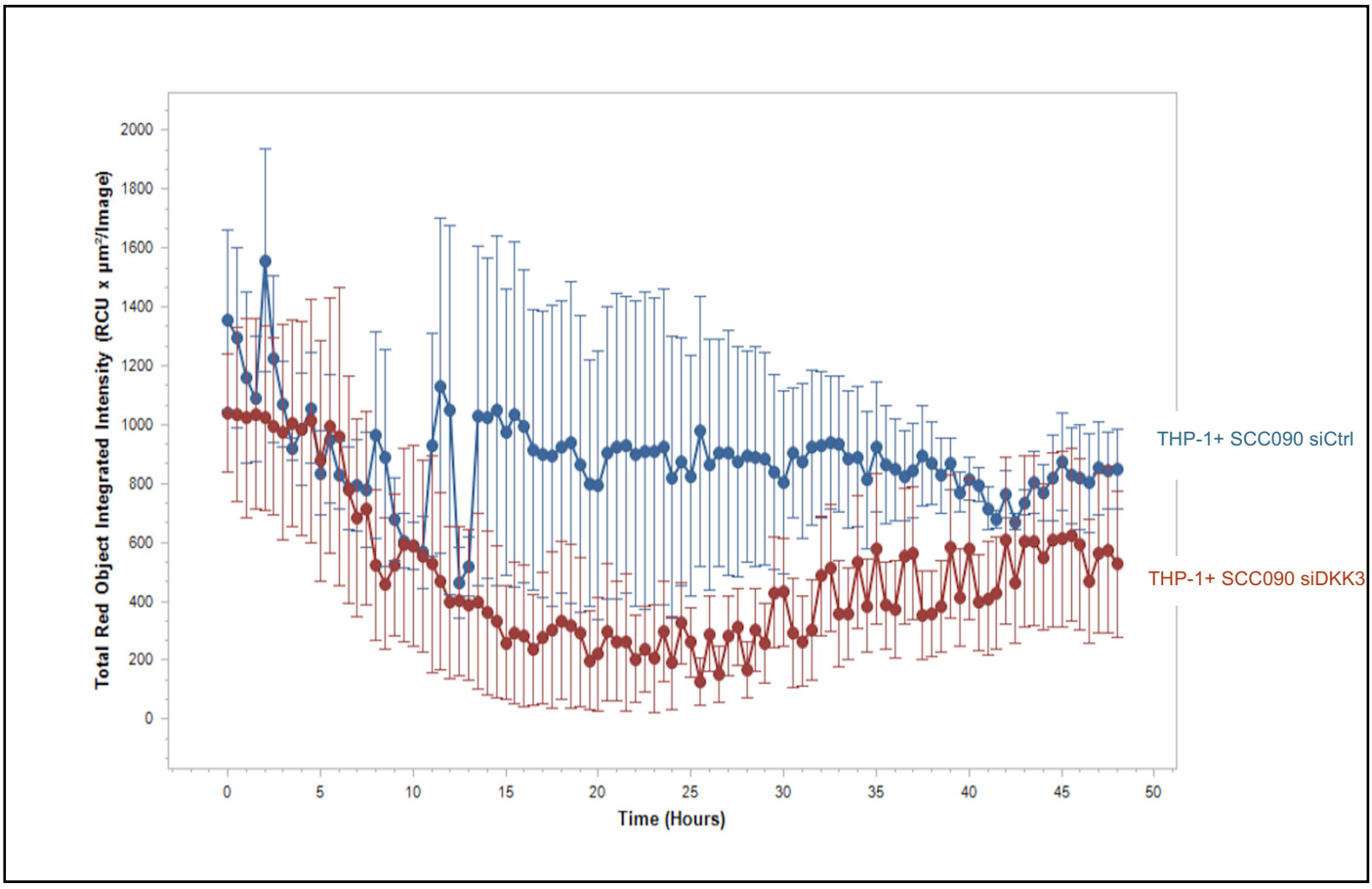

Figure S4- Taux de phagocytose des cellules SCC090 transfectées avec un siARN anti-DKK-3 versus contrôle par les macrophages THP-1. Ce taux est représenté sous forme d'intensité totale d'objets rouge intégrés indiquant un shift du pH vers l'acide signifiant qu'un phénomène de phagocytose a eu lieu.

5. ΔNp63α régule l'expression de certains gènes codant l'inflammasome

Nous avons étudié le programme transcriptionnel régulé par ΔNp63α par séquençage d'ARN (RNA-seq) dans notre modèle cellulaire de cancer de l'oropharynx HPV+ transfectés avec soit un siARN ΔNp63α, soit un siARN témoins (données de RNAseq présentées dans le papier Mourtada *et al.* ; Figure 3). L'analyse de l'enrichissement des voies de signalisation/processus cellulaire à l'aide des données transcriptomiques normalisées et du logiciel STRING a identifié des fonctions cellulaires réprimées et d'autres activées. Comme mentionné dans notre article (Mourtada *et al.* ; Figure 3), les voies principalement réprimées concernent les gènes impliqués dans la réponse immunitaire et la signalisation des cytokines. Parmi ces gènes, nous observons une diminution de l'expression de *NLRP1* et *CASP1*, qui selon les données de la littérature, sont impliqués dans la formation et l'activité de l'inflammasome. L'inflammasome est un complexe multiprotéique tubulaire induit par les PAMPs (Pathogen-associated

Molecular Patterns) et/ou DAMPs (Damage-Associated Molecular Patterns), régule la réponse immunitaire innée et est impliqué dans la maturation et le relargage extracellulaire des interleukines IL-1β et IL-18. Grâce au logiciel STRING nous avons pu mettre en évidence un réseau d'interaction entre NLRP1 et CASP1 et d'autres protéines impliquées dans la régulation et l'activation de l'inflammasome, tels que GBP1 ; GBP3 ; GBP4 et GBP6 **(Figure S5).** Par conséquent, j'ai validé l'effet de l'inhibition de l'expression de ΔNp63α sur la diminution des niveaux transcriptionnels de *CASP1* et de *NLRP1* et j'ai testé cet effet sur les niveaux transcriptionnels de *GBP3, GBP6* ainsi que les gènes codant les interleukines IL-1β et IL-18. De manière intéressante, l'inhibition de ΔNp63α diminue significativement les niveaux transcriptionnels de *GBP3* et *GBP6* et montre une tendance à la diminution mais non significative pour les interleukines 1β et 18 **(Figure S6).** On peut donc conclure que l'extinction de ΔNp63α diminue l'expression d'un certain nombre de gènes codant des facteurs constitutifs ou régulant l'inflammasome, mais n'a pas d'impact significatif sur les niveaux d'expression des ARNm d'IL1β et IL-18.

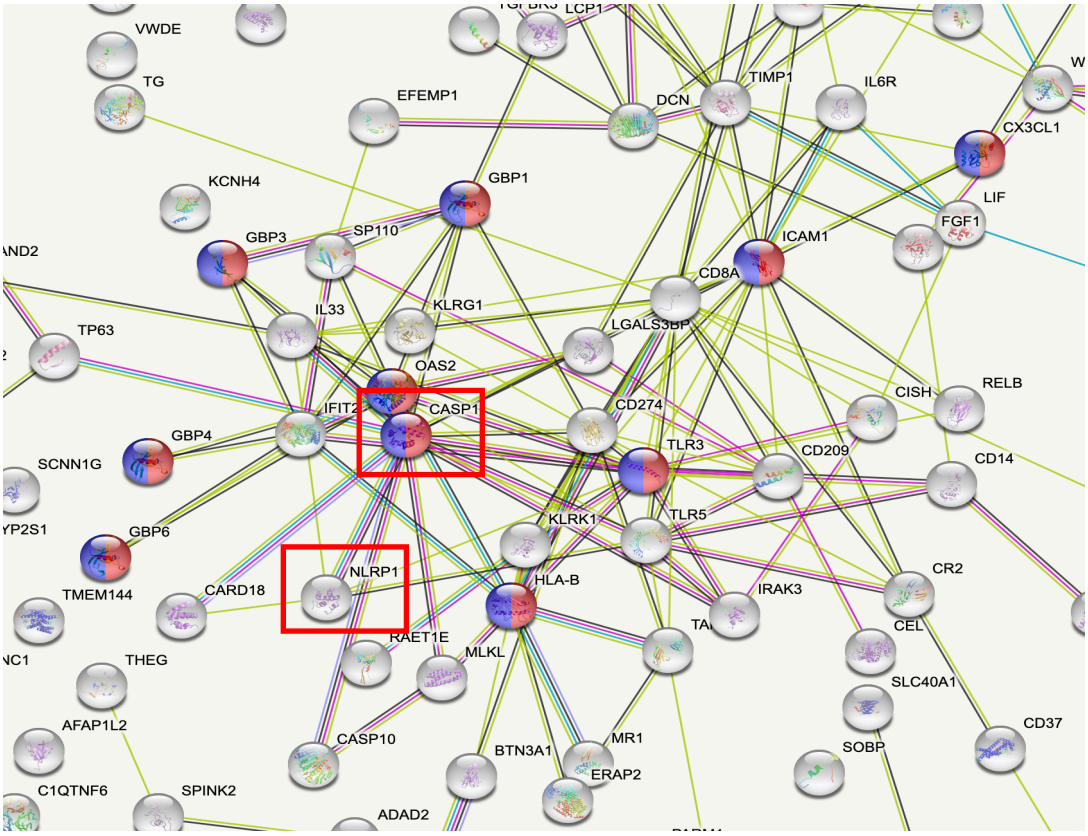

Figure S5- Réseau d'interaction entre la CASP1 et NLRP1 et d'autres protéines, obtenu grâce au logiciel STRING.

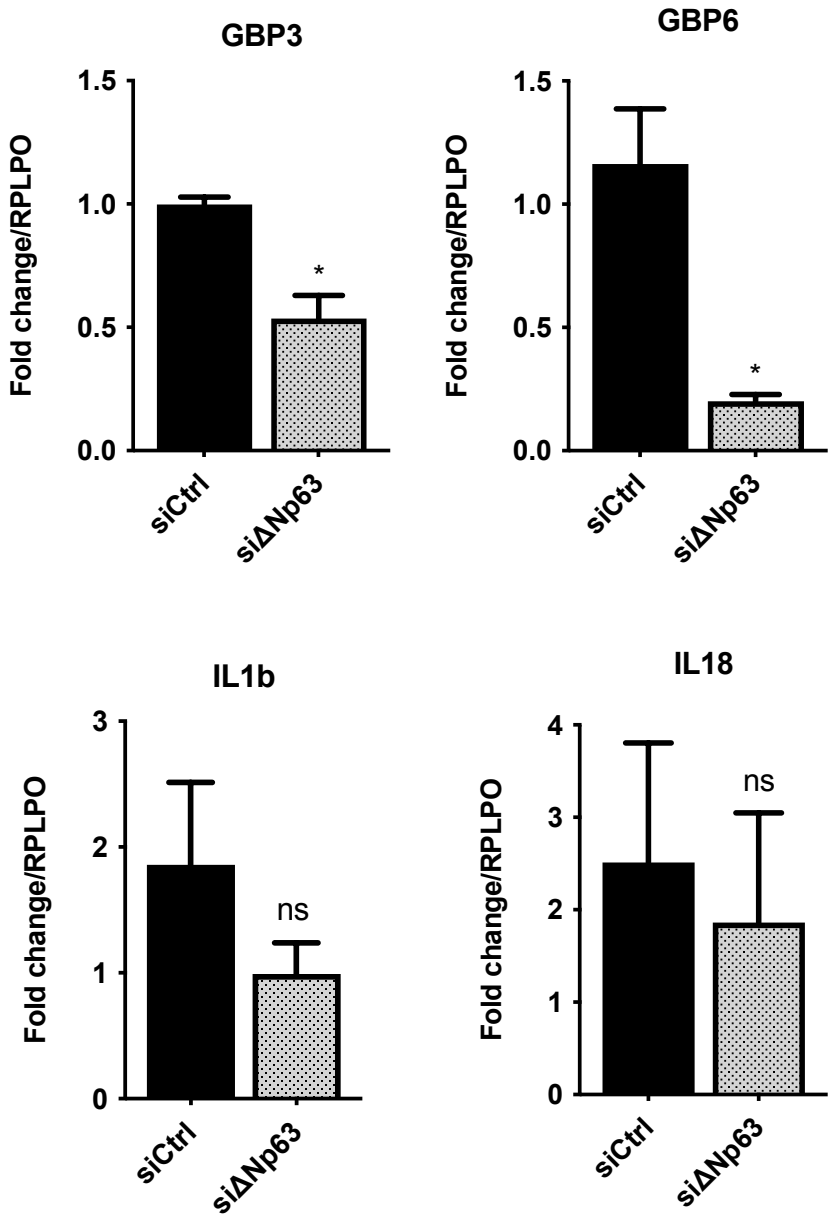

Figure S6- Niveau d'expression des transcrits GBP3, GBP6, IL1β et IL18 dans les SCC090 transfectées par un siARN anti-ΔNp63. Ces résultats sont normalisés au gène de référence RPLP0. (* p<0,05)

6. Lignée stable SCC090 sh-p63

En complément de l'extinction de ΔNp63 par un siARN (effet transitoire ; inhibition partielle de l'expression) et afin d'établir un système plus robuste d'extinction de p63, nous avons généré des clones stables de SCC090 avec une séquence sh-p63 (ainsi que des clones contrôles sh-vide). Les séquences sh utilisées sont conçues pour réduire l'expression des isoformes TA et ΔNp63. En revanche, nos données montrent que l'isoforme prédominante de p63 exprimée dans les cellules SCC090 est ΔNp63α. L'extinction de p63 dans des clones stables pour 4 séquences a été analysée par western blot, mais seul le clone sh-p63-6 se caractérise par une diminution satisfaisante de l'expression de ΔNp63 **(Figure S7).**

a. P63 régule l'expression de certaines cytokines

Pour étudier l'impact de la délétion de ΔNp63 dans la lignée SCC090 sur l'expression de cytokines jouant un rôle essentiel dans l'immunité innée, j'ai utilisé des membranes pré-imprimées avec des anticorps ciblant 80 cytokines différentes (cytokine array) afin d'analyser la composition du milieu conditionné des cellules transfectées soit par un sh-vide, soit par un sh-p63.

Cette étude m'a permis de mettre en évidence en réalisant 4 réplicats biologiques, une diminution significative de l'expression de la cytokine TNFRSF11B et une tendance à la baisse d'expression de 4 cytokines (CCL26, CCL11, TIMP1 et TIMP2) en absence de ΔNp63 **(Figure S8).**

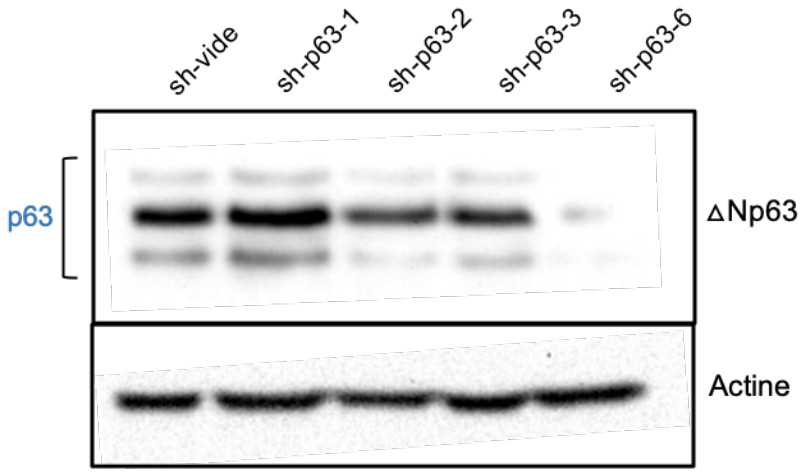

Figure S7- Validation de la diminution stable par sh de l'expression protéique de p63

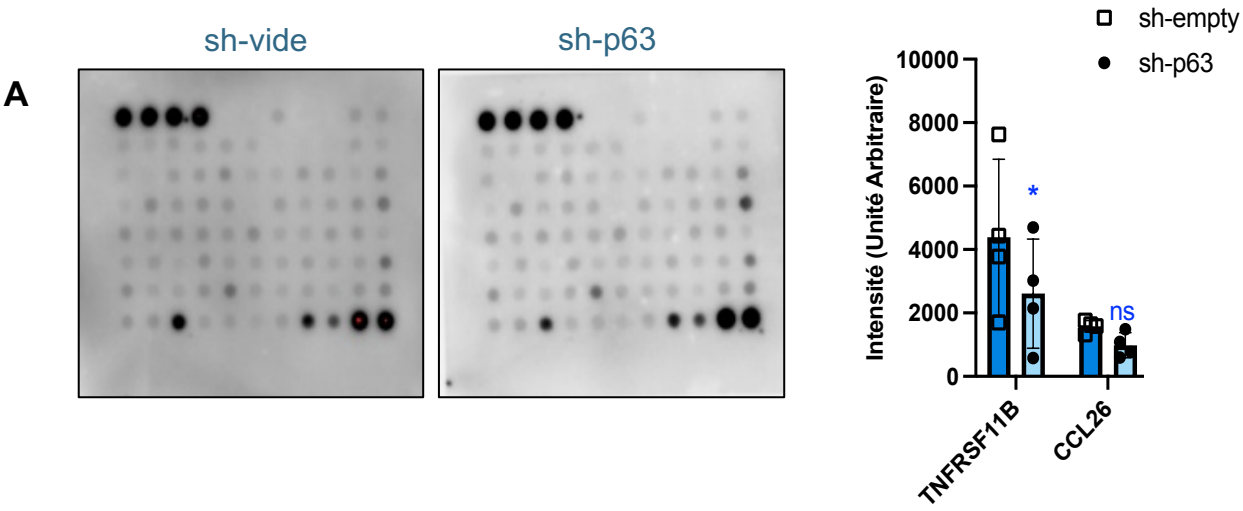

Liste et position des cytokines sur le cytokine array :

	A	B	C	D	E
1	Pos	Pos	Pos	Pos	Neg
2	I-309	IL-1α	IL-1β	IL-2	IL-3
3	IL-12 p40/p70	IL-13	IL-15	IFN-γ	MCP-1
4	MIP-1δ	RANTES	SCF	SDF-1	TARC
5	Oncostatin M	Thrombopoietin	VEGF	PDGF-BB	Leptin
6	FGF-4	FGF-6	FGF-7	FGF-9	Flt-3 Ligand
7	IGFBP-3	IGFBP-4	IL-16	IP-10	LIF
8	NT-4	Osteopontin	Osteoprotegerin	PARC	PIGF

F	G	H	I	J	K
Neg	ENA-78	GCSF	GM-CSF	GRO	GRO-α
IL-4	IL-5	IL-6	IL-7	IL-8	IL-10
MCP-2	MCP-3	MCSF	MDC	MIG	MIP-1b
TGF-β1	TNF-α	TNF-β	EGF	IGF-I	Angiogenin
BDNF	BLC	Ck β 8-1	Eotaxin	Eotaxin-2	Eotaxin-3
Fractalkine	GCP-2	GDNF	HGF	IGFBP-1	IGFBP-2
LIGHT	MCP-4	MIF	MIP-3α	NAP-2	NT-3
TGF-β2	TGF-β3	TIMP-1	TIMP-2	Pos	Pos

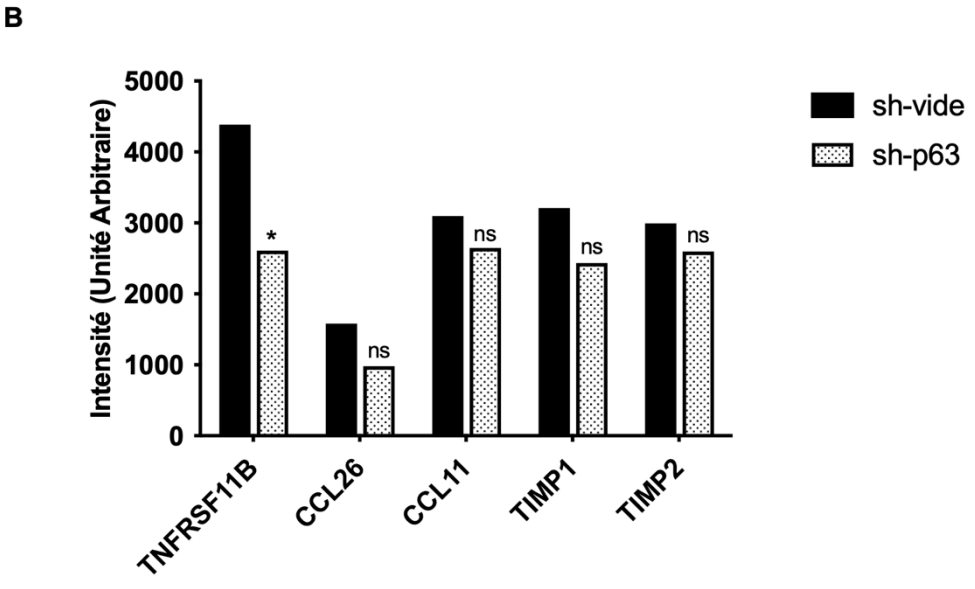

Figure S8- Analyse des membranes de cytokines array des cellules SCC090 transfectées par un sh-vide et un sh-p63**. A.** Les membranes montrent un léger changement dans l'intensité d'expression de quelques cytokines. L'intensité des points ont été quantifié grâce au calcul de leur aire sur ImageJ et comparés aux contrôles positifs et négatifs. **B.** L'analyse montre une diminution de la cytokine TNFRSF11B, et une tendance à la diminution mais non significative des cytokines CCL26, TIMP1 et TIMP2.

b. P63 régule l'expression transcriptionnelle de TNFRSF11B, CCL26, CCL11, TIMP1 et TIMP2

Afin de valider les résultats obtenus par cytokine array, j'ai testé, par RT-PCR quantitative, les niveaux des transcrits codant ces cytokines dans des cellules SCC090 transfectées stablement avec un sh-p63 (versus sh-vide). De manière intéressante, j'observe une diminution significative de l'expression des ARNm de ces cytokines en l'absence d'expression de p63 **(Figure S9)**. Ceci nous permet donc de confirmer le rôle que joue ΔNp63 dans la régulation de l'expression de certaines cytokines qui peuvent jouer un rôle majeur dans l'inflammation, le recrutement et l'activation de la réponse immunitaire.

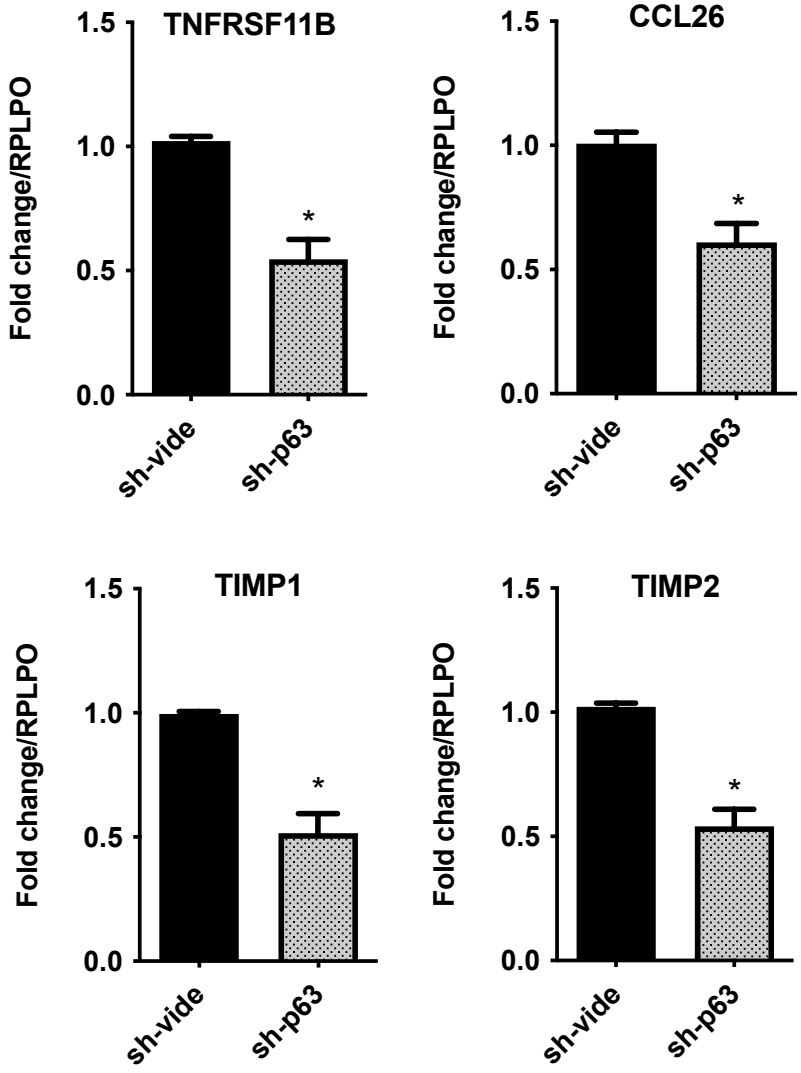

Figure S9- Niveau d'expression des transcrits TNFRSF11B, CCL26, TIMP1 et TIMP2 dans les SCC090 transfectées par un sh-p63. Ces résultats sont normalisés au gène de référence RPLP0. (* p<0,05)

MATÉRIELS & MÉTHODES

Cette partie comprend l'ensemble des matériels et méthodes des résultats annexes qui ne sont pas présentés dans l'article scientifique.

1. Immunoprécipitation de la chromatine

L'immunoprécipitation de la chromatine (ChIP) permet de cartographier la distribution *in vivo* des protéines associées à l'ADN génomique. Son principe repose sur l'enrichissement de fragments de chromatine associés à un antigène d'intérêt présent à la surface de ces protéines. Dans le cadre de notre étude, la ChIP a été réalisée en suivant les instructions du kit Magna ChIP™ (Millipore).

Celui-ci consiste en cinq grandes étapes : la préparation du lysat cellulaire et la réticulation à l'ADN (par liaison covalente) des protéines qui lui sont liées par le paraformaldéhyde (PFA) en ajoutant 275 µL de PFA dans 10 mL du milieu de culture (soit 37% du volume final) pendant exactement 10 minutes à température ambiante; La fragmentation de l'ADN génomique par sonication à bain (Bioruptor) à 4 ℃ pendant 12 minutes (mode high) pour obtenir des fragments de taille appropriée exploitables en PCR quantitative (200-1000pb) ; L'immunoprécipitation des fragments de chromatine liée à la protéine d'intérêt en incubant les échantillons de chromatine avec des billes couplées à un anticorps spécifique de la protéine d'intérêt (dans notre cas : un anticorps anti-ΔNp63 et un anticorps anti-IgG servant de contrôle négatif); la dénaturation des protéines et l'annulation de la réticulation, suivie de la purification de l'ADN en utilisant les réactifs et colonnes du kit Magna ChIP; la détection d'une séquence d'ADN spécifique par qPCR dans les échantillons de ChIP, ainsi que dans les échantillons d'input (chromatine fragmentée non immunoprécipitée) qui servent de contrôles.

Des amorces oligonucléotidiques spécifiques de la région en amont du enhancer du gène codant IRF6 et de la région promotrice du gène codant la Myoglobine ex2 sont respectivement utilisés dans notre étude comme un contrôle positif et négatif. Les séquences des amorces sont les suivantes :

Nom du gène	Amorce sens (5'-3')	Amorce anti-sens (5'-3')
IRF6	ACCGGCAGCATTTCTAGTTC	ACTGGGCTGAGATGAGCTTC
Myoglobine exon 2	AAGTTTGACAAGTTCAAGCACCTG	TGGCACCATGCTTCTTTAAGTC
P63 X	CCCTCCAGTTCGGCATTAGT	AGCCCTGGTTGAGCATTCAT
P63 RE II (F1R1)	TCGCTCCTTAGTCATCCTCCA	CAGGAGGGACAAGCCTCAAG
P63 RE II (F2R2)	ACACACGTGCAAGAAAATACGG	CCATCACCCTTGAAACGCAG
DKK3	CCATCCTGCCTTGAAACCCA	AGCAAGTTACAGGCAGGAACT

Tableau supplémentaire 1 - Liste des couples oligonucléotidiques des amorces utilisées dans l'analyse d'immunoprécipitation de la chromatine

La détection des séquences spécifiques d'ADN est réalisée par PCR quantitative, o nous détectons les Ct (Cycle threshold) de chaque séquence amplifiée afin de déterminer le % d'enrichissement par rapport à l'input (chromatine non immunoprécipitée) pour chaque ChIP. Celui-ci peut être calculé par la formule ci-dessous :

$$\% \text{ Input} = 2^{(Ct\text{Input} - 6.64 - Ct\text{ChIP})} \times 100$$

Enfin, les % d'enrichissement par rapport à l'input obtenus dans les différents échantillons seront comparés à celui obtenu dans la condition contrôle (ChIP avec anticorps anti-IgG).

2. Étude de l'activité de la Firefly luciférase

L'activation de la voie Wnt canonique a été mesurée avec des constructions de rapporteurs TOPFLASH. Le vecteur rapporteur TOPFLASH est composé de trois motifs consensus multimérisés de liaison du facteur de transcription TCF/LEF, clonés en amont du gène de la luciférase de luciole. L'induction de l'activité luciférase à partir de ce rapporteur dépend fortement de la présence à la fois de la β-caténine et de TCF. Brièvement, après avoir ensemencé et cultivé les cellules (HEK293) dans une plaque 24 puits à raison de 150,000 cellules/puits, les cellules ont été transfectées avec 100 ng/puits d'un plasmide rapporteur Luciférase de luciole (TOP ou contrôle avec sites mutés FOP), 10 ng d'un plasmide rapporteur Luciférase de rénilla (pRL-null) qui sera constitutivement exprimée et sert de contrôle interne pour normaliser, et 500 ng de

plasmides d'expression DKK-3 ou contrôle (plasmide vide). Les cellules ont été incubées pendant 48 heures, puis lysées pour mesurer l'expression du gène rapporteur luciférase à l'aide d'un luminomètre, tout en suivant le protocole et le matériel du kit Promega Dual-Luciferase® Reporter Assay System.

3. Analyse de l'activité phagocytaire *in vitro*

Cette expérimentation a été réalisée dans les mêmes conditions que celles décrites dans l'article scientifique, mais en surexprimant DKK3 grâce à un plasmide d'expression dans les cellules SCC090 ou SCC47, à raison de 2ug/puits pour 300,000cellules/puits et pendant 72h.

4. Quantification de la phagocytose par technique pHrodo Red Cell Labeling

Cette expérience a été réalisée en mesurant la fluorescence de la sonde pHrodo® Red Cell Labeling Kit for Incucyte de chez Sartorius. Les monocytes THP-1 ont été ensemencés dans une plaque 96 puits à raison de 7,000 cellules/puits et différenciés en macrophage par 162nM de PMA (phorbol 12-myristate 13-acetate2 Sigma). Les cellules SCC090 ont également été ensemencées dans une plaque 6 puits à raison de 300,000 cellules/puits et transfecté par un siRNA DKK-3 à une concentration finale de 15 nM pendant 48h. Le milieu conditionné des cellules transfectées est ensuite filtré sur filtre 0.2 μm et ajouté sur les macrophages après différenciation à raison de 30% du volume final de milieu de culture, pendant 24h avant la co-culture. Concernant la co-culture, les cellules cibles sont marquées avec le kit de marquage cellulaire pHrodo® et ceci en débutant par des étapes de lavage du culôt cellulaire avec les tampons de lavages pHrodo (composants C et D) qui sont préalablement chauffé à 37° dans un bain marie. Le colorant de marquage cellulaire (composant A) préalablement dilué dans du DMSO à 30μg/ml (concentration choisie lors de l'optimisation de l'expérimentation) est ensuite ajouter à notre suspension cellulaire (concentration cellulaire choisie afin d'obtenir un ratio 1 :1 entre les cellules cibles et les cellules effectrices) pendant 1 heure à 37°C. Ensuite, une étape d'élimination de l'excès du colorant est réalisée grâce à des centrifugations et resuspension du culôt cellulaire dans du milieu de culture. Ces cellules sont ensuite ajoutées aux cellules effectrices à raison de 50μL/puit. La vidéo microscopie a été réalisé sur l'IncuCyte S3

Live-Cell Analysis Instrument (SARTORIUS). Des images ont été prise toutes les 30 minutes pendant 48h en utilisant l'objectif 20X et un temps d'acquisition de 450ms pour le canal rouge. Pour générer les métriques, nous avons créé une définition d'analyse de base adaptée au type de cellules, aux conditions de l'essai et à la magnification sélectionnée. A savoir que le seuil de fluorescence choisi dans notre protocole est de 5 RCU (suivre les étapes du protocole du fournisseur pour plus de détail sur l'analyse et la génération des données).

5. Établissement d'une lignée stable sh-p63

La lignée humaine SCC090 a été infectée avec les virus produits par les cellules PHOENIX-Ampho (version humaine) qui ont été préalablement transfectées par les plasmides pSuper retro puro sh BC039815, type B : TP63-1, TP63-2, TP63-3 et TP63-6 (versus pSuper retro puro sh-vide : VEC-PRT-0002, type A). Le sh contient le gène de résistance à la puromycine. L'inhibition de l'expression par shRNA est basé sur les séquences p63-1, 5′-AACAGCCATGCCCAGTATGTA-3′ et p63-2, 5′-AAAGCAGCAAGTTTCGGACAG-3 (Barbieri et *al.*). Ces vecteurs nous ont été gracieusement fourni par le laboratoire de Jennifer Pientenpol (Vanderbilt University Medical Center, Nashville, TN 37232, USA). Les lignées modifiées ont ensuite été testées afin de vérifier l'extinction des niveaux d'ARNm et de protéines de p63. La lignée SCC090 sh-p63-6 a été retenue (diminution d'environ 90% de l'expression de p63, voir résultat ci-dessous) et des clones ont été établis afin d'obtenir des cellules homogènes ayant toutes intégrées le sh-p63 en question. L'établissement des clones a été réalisé par ensemencement des cellules à raison de 1000 cellules/boite de 10 cm pour qu'elles puissent pousser et former des clones isolés, et une fois les clones apparaissent, on les isole par trypsinisation de chaque clone et ensemencement dans un puit de plaque 6 puits. Enfin, afin de booster la prolifération cellulaire, on a suivi une technique proposée par Boh Wazylyk et qui consiste d'ensemencer ce clone avec des cellules sauvages SCC090 et réaliser une sélection à la puromycine 2 jours après.

6. Mesure de la libération de cytokines à l'aide de Cytokine array

Les membranes de cytokines array (ab133998-Human Cytokine Antibody Array-Membrane- abcam) sont composées de 80 anticorps dirigés contre différentes cytokines et chimiokines. Les membranes ont été bloquées avec 2mL de tampon de

blocage à température ambiante pendant 30 min, selon les recommandations du fournisseur. Les membranes ont été ensuite incubées avec le milieu conditionné des SCC090 transfectées par un sh-p63 ou un sh-vide à 4°C over night (ce milieu a été centrifugé pendant 5 minutes à 800rpm afin de récupérer le surnageant). Des étapes de lavages sont ensuite réalisées, suivi d'une incubation des membranes avec des anti-cytokines couplés à la biotine pendant 1,5h à température ambiante. Finalement une incubation avec de la streptavidine conjugué au HRP est réalisé pendant 2 h à température ambiante suivi d'une détection par chimioluminescence en utilisant des tampons de détections C et D à des volumes égaux (1 :1) selon les recommandations du fournisseur. (Suivre le protocole du fournisseur pour plus de détails).

7. Analyse de l'expression de gènes par RTqPCR

L'analyse de l'expression de gènes impliqués dans l'inflammasome a été réalisé de manière similaire à celle présentée dans notre article (Mourtada *et al.,* voie ci-dessus). En bref, les cellules SCC090 ont été transfectées par 15nM de siRNA anti-ΔNp63 pendant 72h en utilisant la Lipofectamine RNAiMAX, tout en suivant les instructions du fournisseur. Une extraction d'ARN est réalisée selon la technique standard TRIZol Chloroforme et la rétrotranscription (RT) grâce au kit High-Capacity cDNA Reverse Transcription Kits (Applied Biosystems). Une PCR quantitative a été réalisée en utilisant le LightCycler 480 real-time PCR system (Roche). Les niveaux d'expression des gènes ont été normalisés à un contrôle interne RPLP0 (Ribosomal Protein Long P0).

Les séquences des amorces utilisées sont les suivantes :

Nom du gène	Amorce sens (5'-3')	Amorce anti-sens (5'-3')
GBP3	CAGAAACCCTCCAGGAGCTG	AGCTGGGCCGCTAATTTCTT
GBP6	GGTGCTATAGAGCAGGGTGAC	GTGAGCTCCGTCACATAATGC
IL1β	AAACCTCTTCGAGGCACAAGG	ACTGGCGAGCTCAGGTACT
IL18	TGCCAACTCTGGCTGCTAAA	TTGTTGCGAGAGGAAGCGAT
RPLP0	GAAGGCTGTGGTGCTGATGG	CCGGATATGAGGCAGCAGTT

Tableau supplémentaire 2- Liste des couples oligonucléotidiques des amorces utilisées dans l'analyse d'expression des gènes de l'inflammasome.

Pour les lignées SCC090 sh-p63 et sh-vide, la PCR quantitative a été réalisée sur l'Applied Biosystems QuantStudio3. Les cDNA ont été dilué 5 fois et utilisés avec les sondes FastStart Universal Probe Master Mix Taqman. Des amorces spécifiques ont été utilisé de TaqMan Gene Expression Assay (Applied Biosytems) pour mesurer l'expression de TNFRSF11B (Hs00900358_m1), CCL26 (Hs00171146_m1), TIMP1 (Hs00171558_m1) et TIMP2 (Hs00234278_m1) et normalisé à l'expression de RPLP0 (Hs99999902_m1)

DISCUSSION

Le cancer des voies aérodigestives supérieures (VADS) se classe au sixième rang parmi les cancers les plus fréquents, provoquant près de 500 000 décès dans le monde chaque année. Les deux étiologies principales de ces cancers sont clairement liées à la consommation de tabac et d'alcool et/ou à une infection par le papillomavirus humain (HPV). Alors que l'incidence des cancers de la tête et du cou non liés à l'HPV est en baisse, on observe une augmentation significative de l'incidence des cancers positifs à l'HPV au cours des dernières décennies. De nombreuses études ont mis en évidence des différences moléculaires (taux de mutations, régulation de l'expression génique, etc…) et cliniques (réponses au traitement ; taux de survie des patients) entre les patients atteints de cancer des VADS, positifs et négatifs à l'égard d'HPV. En effet, il a été observé que les patients ayant des tumeurs de l'oropharynx HPV+ ont une meilleure survie par rapport aux patients avec des tumeurs de l'oropharynx HPV- (Gillison *et al.*, 2008). Néanmoins, parmi les patients positifs au HPV, il existe également une diversité en ce qui concerne la survie : on observe deux groupes distincts de patients avec des taux variables de métastases à distance (Ang *et al.*, 2010b). Les mécanismes moléculaires responsables de cette différence de pronostic des patients demeuraient donc, jusqu'à présent, non élucidés.

1. Diversité moléculaire et pronostique chez les patients HPV+

Notre équipe a révélé que le sous-groupe clinique des patients HPV+ montre une diversité sur le plan moléculaire et pronostic. Initialement, nous avons mis en évidence grâce à une analyse par Affymetrix GeneChip que les tumeurs de l'oropharynx HPV+ expriment des niveaux plus élevés de gènes liés à la réponse immunitaire. De plus, nous avons détecté une infiltration plus importante des tumeurs HPV+ par des lymphocytes T CD8 cytotoxiques comparé aux tumeurs HPV-, et cette infiltration est corrélée à un pronostic amélioré **(Figure 9A)** (Jung *et al.*, 2013). Ces constatations s'accordent avec les conclusions de Ang *et al.*, qui démontrent que les patients atteints de tumeurs HPV+ étaient considérés comme présentant un faible risque de décès, à l'exception des fumeurs présentant un stade ganglionnaire élevé (N2b à N3), qui étaient plutôt classés comme étant à risque intermédiaire, tandis que les patients souffrant de tumeurs HPV- étaient classés comme étant à haut risque de décès (Ang *et al.*, 2010b). De plus, l'infiltration des tumeurs par les lymphocytes T CD8+ a été associée à un pronostic favorable dans plusieurs types de tumeurs, suggérant qu'elle

pourrait servir de biomarqueur prédictif pour l'immunothérapie du cancer (Fridman *et al.*, 2012). Keck *et al.* ont identifié deux sous-types moléculaires distincts au sein des tumeurs HPV+ : le sous-type classical et le sous-type inflammé-mésenchymateux. Ce dernier se caractérise par un phénotype immunitaire fortement activé, ce qui est confirmé par l'infiltration de lymphocytes T CD8+ en immunohistochimie présentant une tendance à une meilleure survie par rapport au sous-type classical (Keck *et al.*, 2015).

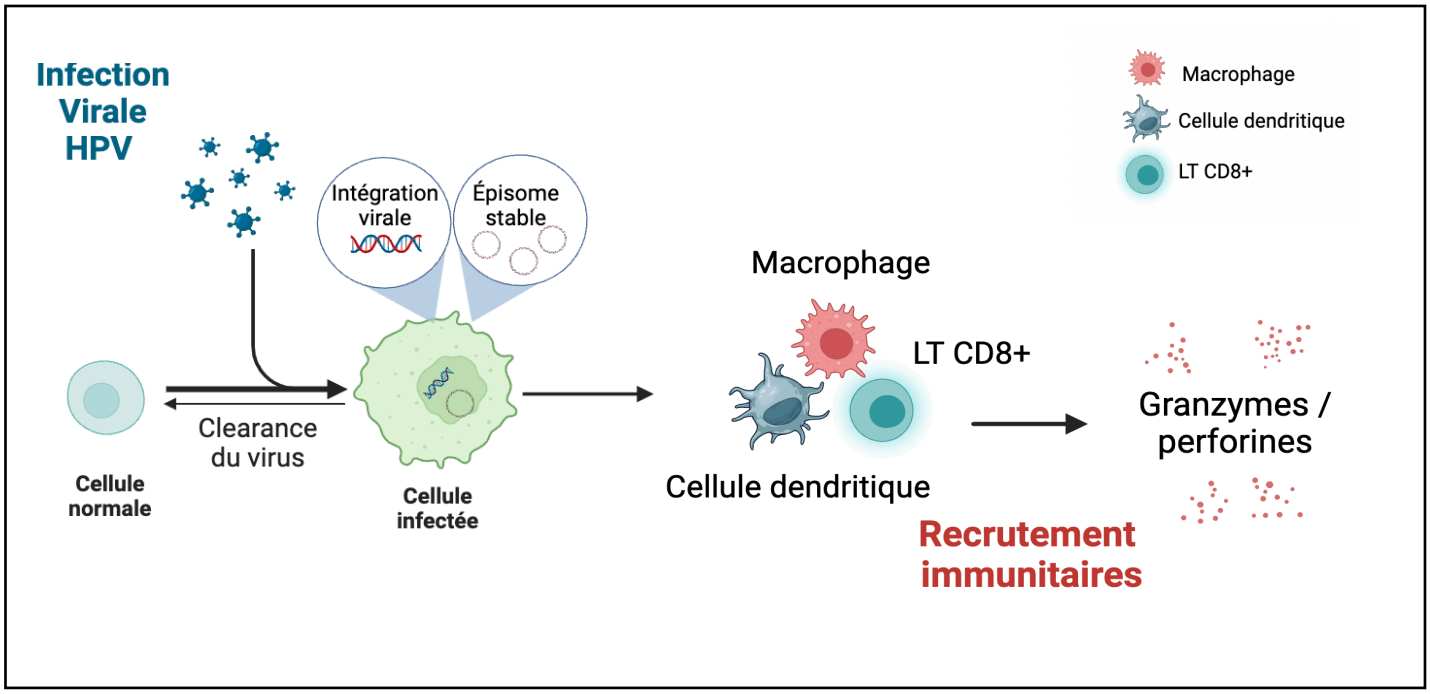

Figure 9A- Infiltration des tumeurs HPV+, par des cellules du système immunitaire tel que les lymphocytes T CD8 cytotoxiques

Nos résultats, en accord avec la littérature nous ont motivé à réaliser une analyse de regroupement hiérarchique non supervisée sur des données transcriptomiques de 8 échantillons de tumeurs provenant de patients atteints de carcinomes épidermoïdes oropharyngés localement avancés et positifs au HPV-16. Cette analyse nous a permis de distinguer deux groupes moléculaires sur la base de l'expression différentielle de 148 gènes (Cluster 1 et Cluster 2). L'analyse des données cliniques de suivi des patients correspondants a montré qu'ils sont classés en deux groupes : ceux qui sont associés à un mauvais pronostic (récurrence métastatique dans les 18 mois et décès

dans les 3 ans) et ceux qui sont associés à un bon pronostic (dissémination métastatique retardée et survie plus longue des patients). Pour mieux comprendre, nous avons analysé cette signature moléculaire hétérogène à l'origine de cette différence de pronostic, et nous avons identifié une signature moléculaire qui se caractérise par l'expression opposée des gènes S100A7, S100A9, KRT6B, et THBS4 entre ces deux groupes. De manière intéressante, ces mêmes gènes ont été identifiés dans une analyse transcriptomique de modèles de lignées cellulaires des VADS négatifs au HPV, où ils sont régulés au niveau transcriptionnel par le facteur de transcription ΔNp63 (Barbieri *et al.*, 2006). Suggérant que ΔNp63 puisse jouer un rôle dans la progression tumorale et/ou la réponse au traitement dans les cancers ORL.

De plus, il a été clairement démontré dans plusieurs ensembles de données omiques indépendantes qu'il existe une grande variabilité des niveaux d'expression de p63 au sein des tumeurs HPV+. Les résultats d'une étude menée par Glathar *et al.* suggèrent que p63 joue un rôle essentiel dans la régulation de gènes et de voies de signalisation impliqués dans la malignité liée au HPV. Cette régulation concerne notamment des voies telles que la signalisation PI3K, WNT et le contrôle du cycle cellulaire, et elle a été étudiée à la fois dans des modèles de culture cellulaire précliniques et à partir de données tumorales. Ils suggèrent donc un rôle de p63 dans la régulation de la signalisation PI3K et la signalisation mTOR dans les cancers des VADS HPV+ conférant ainsi un rôle oncogène de p63 dans leur modèle d'étude. De manière importante, leur analyse transcriptomique par RNAseq lors de la suppression de p63 montre un enrichissement des voies d'adhérence cellulaire et de kératinisation. Ceci est en accord avec nos données qui révèlent une surexpression de gènes impliqués dans le développement et la différenciation de l'épithélium cutané ou la cornification [(Mourtada *et al.*, 2023) ;Figure 3B]. Cependant, contrairement à nos données, la faible expression de p63 est associée à un enrichissement des gènes associés à la réponse immunitaire (Glathar *et al.*, 2022). Cette divergence pourrait s'expliquer par une régulation différentielle de p63 dans les différents sous-types moléculaires, à savoir le sous-type classical et le sous-type inflammé-mésenchymateux (Keck *et al.*, 2015). Ainsi, il est plausible de formuler l'hypothèse suivante : le modèle d'étude de Glathar *et al.*, qui repose sur des lignées cellulaires issues de tumeurs de la cavité buccale et de l'hypopharynx, pourrait représenter un sous-type classical caractérisé par une moindre activation de la réponse immunitaire, favorisant ainsi la régulation des

voies de signalisation par p63 impliquées dans la carcinogenèse. En revanche, notre modèle dérivant d'une lignée oropharyngée suggère une association au sous-type IMS, marqué par une activation de la réponse immunitaire et le recrutement de lymphocytes T CD8+. Il est toutefois essentiel de noter que notre étude repose sur une petite cohorte et sur une analyse RNAseq réalisée sur un seul modèle de lignée cellulaire avec une diminution transitoire de l'expression de ΔNp63 par un si ΔNp63, contrairement à la diminution stable de ΔNp63 par shRNA utilisée dans le modèle de Glathar *et al.* Ceci nécessite donc la réalisation d'une étude sur une plus grande cohorte de tumeurs des VADS HPV+ tout en réalisant une analyse approfondit des sous-types moléculaires et leur implication dans les effets observés sur le pronostic.

Les raisons pour lesquelles l'expression de ΔNp63 est différentiellement régulée dans les deux sous-groupes de tumeurs HPV+ ne sont pas comprises à l'heure actuelle. D'après les travaux de McKenna *et al.*, il semble que la protéine HPV16 E6 soit impliquée dans la régulation de ΔNp63 dans les tumeurs HPV+ par le biais du processus suivant : en général, p53 agit en tant que régulateur positif de la transcription du micro-ARN miR203, qui à son tour réprime la transcription de ΔNp63. Cependant, dans les cellules HPV+, E6 dégrade p53, ce qui entraîne une réduction de l'expression de miR203 et, par conséquent, une augmentation de la transcription de ΔNp63 (McKenna *et al.*, 2010) **(Figure 9B)**. De plus, le locus génomique *TP63* est un site d'intégration du génome HPV dans les cancers des VADS, ce qui peut entrainer des réarrangements génomiques et une surexpression de p63 (Kamal *et al.*, 2021). Néanmoins, ces propositions ne sont à ce jour que des hypothèses, et il conviendrait de vérifier expérimentalement leur pertinence sur des échantillons de tumeurs humaines.

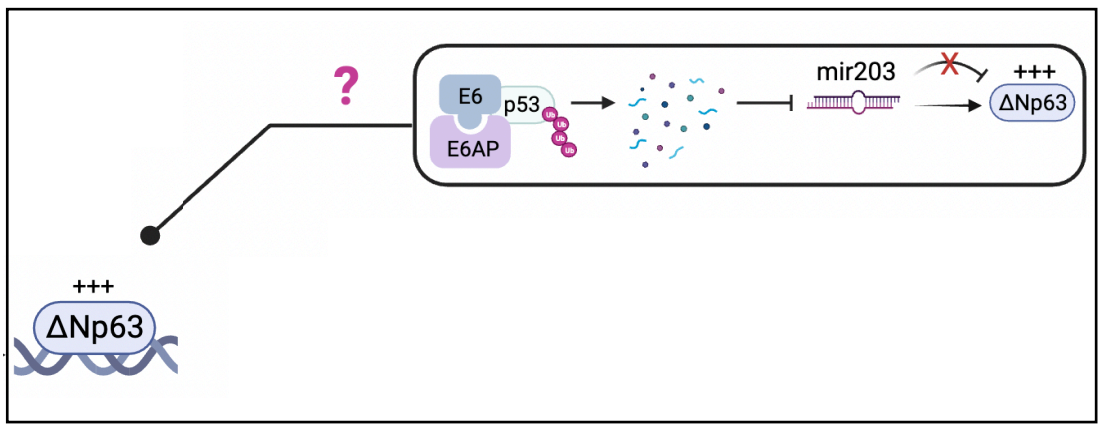

Figure 9B- Hypothèse sur l'expression différentielle de ΔNp63

2. Le rôle de ΔNp63 dans la différence de pronostic

Une analyse de Kaplan-Meier portant sur la survie sans métastases à 3 ans des patients, stratifiés en fonction de l'expression de la protéine ΔNp63, a montré que les patients atteints de cancer de l'oropharynx HPV+ présentant une faible expression de ΔNp63 courent un risque plus élevé de propagation métastatique à distance. Par conséquent, notre laboratoire s'est intéressé à l'étude des mécanismes moléculaires impliqués dans l'agressivité des cancers expliquant le pronostic observé chez ces patients, en mettant l'accent sur le rôle de ΔNp63.

3. ΔNp63 : un acteur clé dans la régulation immunitaire

Nous avons découvert que ΔNp63 régule négativement la migration et l'invasion dans nos modèles cellulaires de cancers de l'oropharynx HPV+. De plus, ΔNp63 augmente la sensibilité au cisplatine, suggérant ainsi le rôle suppresseur de tumeur de ΔNp63 dans les tumeurs oropharyngés HPV+ **(Figure 9C)**. Des résultats similaires concernant la migration, l'invasion et la réponse au traitement ont récemment été observés dans les cellules squameuses du col de l'utérus HPV+ (Zhou *et al.*, 2020).

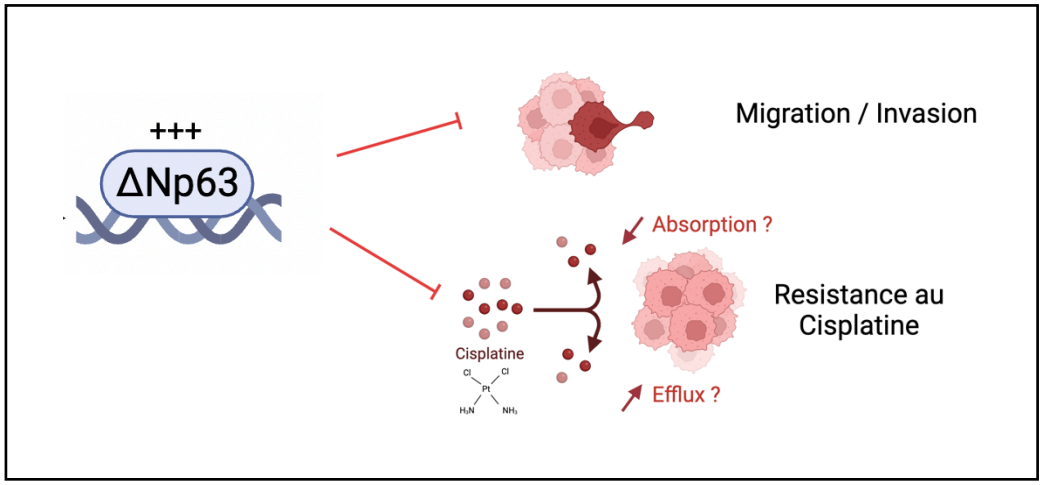

Figure 9C- Rôle de ΔNp63 dans l'inhibition de la migration, l'invasion et la résistance au cisplatine

Le facteur de transcription p63, un régulateur principal du développement cutané, fonctionne à la fois en tant qu'activateur et répresseur de la transcription génique (King *et al.*, 2003). Comme mentionné précédemment, p63 régule l'expression de groupes de gènes liés à l'interféron et à l'inflammation, ce qui a un impact sur le développement épidermique et les processus inflammatoires. De plus, p63 joue un rôle essentiel dans le développement des lymphocytes T en contribuant à la formation de l'épithélium thymique (Candi *et al.*, no date). En outre, il a été observé que p63 permet la sécrétion de TARC/CCL17, agissant comme une chimiokine qui attire diverses populations de lymphocytes T CD4+, dans différentes lignées de cellules épithéliales humaines (Kubo *et al.*, 2008).

De manière similaire, nous avons démontré que ΔNp63 régule un certain nombre de gènes tel que S100A7 et S100A9 considérés comme des « damage-associated molecular patterns » (DAMPs), qui sont des molécules de danger endogènes libérés par les cellules endommagées ou mourantes, et qui activent le système immunitaire inné en interagissant avec les récepteurs de reconnaissance de motifs (PRR) (Roh and Sohn, 2018) **(Figure 9D).**

4. L'implication de ΔNp63 dans le recrutement immunitaire

Nous avons analysé le microenvironnement immunitaire tumoral dans nos modèles de tumeurs oropharyngés HPV+ par MCP Counter. Nos résultats montrent que dans le groupe de patients présentant un pronostic favorable, associé à une expression élevée de ΔNp63, nous retrouvons une expression plus élevée de marqueurs cellulaires associés aux cellules immunitaires (ex. cellules dendritiques, lymphocytes, macrophages...). De plus, nous avons pu constater que les patients atteints de carcinome oropharyngé HPV+ avec une expression élevée de ΔNp63 se caractérisent par une expression importante du marqueur CD8α par immunohistochimie, ainsi qu'une expression élevée des marqueurs de la réponse immunitaire de *GZMK, IRF5* et *CD68* par RT-qPCR. Nous avons aussi précédemment démontré que les tumeurs des VADS HPV+ sont caractérisées par une infiltration des lymphocytes T CD8α+ dans le microenvironnement tumoral (Jung *et al.*, 2013). Ces résultats sont en accord avec les données de Keck *et al.* qui montrent aussi un phénotype immunitaire

fortement activé, confirmé par l'infiltration de lymphocytes T CD8+ et associée à un pronostic favorable dans les sous-types IMS (HPV+ et HPV-) des cancers des VADS (Keck *et al.*, 2015). De plus, Badoual *et al.* montrent que les tumeurs des VADS HPV+ présentent des niveaux élevés de cellules PD-1+ et que le nombre total des lymphocytes T PD-1+CD4+ et PD-1+CD8+ est corrélé à une meilleure survie globale par rapport aux tumeurs présentant des faibles niveaux d'infiltration immunitaire (Badoual *et al.*, 2013). Ces données supportent la présence locale d'une immunité spécifique aux cellules T dirigée contre le HPV16 dans les HNSCC HPV16+, impliquant ainsi un rôle dans la réponse antitumorale, et soutient le développement de l'immunothérapie pour les cancers des VADS (Heusinkveld *et al.*, 2011).

Nous avons étudié le programme transcriptionnel dépendant de ΔNp63 dans notre modèle de carcinome oropharyngé HPV+ par RNA-seq afin de mieux comprendre les mécanismes moléculaires qu'il régule. Nous avons pu mettre en évidence que les voies de signalisation les plus dérégulées en absence de ΔNp63 concernent des gènes impliqués dans la réponse immunitaire ainsi que les voies de signalisations et de production des cytokines **(Figure 9D).** Cela est cohérent avec des études précédentes suggérant que ΔNp63 participe à la régulation de certaines chimiokines ou cytokines comme CXCL2 et CCL22 dans des modèles murins et humains de cancer triple négatif du sein (TNBC) (Kumar *et al.*, 2018) et à la production de TARC/CCL17 qui agit comme une chimiokine qui attire les lymphocyte T CD4+ dans des cellules épithéliales humaines (Kubo et al., 2008) . Des résultats d'expériences menées sur des modèles *in vitro* et *in vivo* de carcinomes pancréatiques (pancreatic ductal adenocarcinomas PDA) montrent aussi que ΔNp63α peut promouvoir l'inflammation stromale au niveau du microenvironnement tumoral, en stimulant l'expression de cytokines pro-inflammatoires, notamment l'IL-1α par les cellules cancéreuses du pancréas (Somerville *et al.*, no date). De plus, des études antérieures ont établi que ΔNp63α et le facteur de transcription NF-κB co-régulent un ensemble de gènes cibles commun dans des modèles cellulaires de carcinome épidermoïde des VADS, parmi lesquels figurent plusieurs gènes codant pour des cytokines inflammatoires tels que l'IL-6 et l'IL-8 (Yang *et al.*, 2011). Parmi les gènes dont l'expression est perturbée en raison de la diminution de ΔNp63 dans les cellules SCC090, j'ai pu démontrer que certains sont responsables de la production de protéines impliquées dans la formation de l'inflammasome, comme NLRP-1 **(Figure 9D)**. L'inflammasome, un complexe

multiprotéique, activé en réponse à des signaux de danger, facilite l'activation de la caspase-1, ce qui entraîne la sécrétion de cytokines pro-inflammatoires telles que l'interleukine IL-1β et l'IL-18. Les inflammasomes ont des rôles essentiels, mais contrastés, en facilitant l'immunité anti-tumorale ou en induisant des facteurs oncogènes. Dans la plupart des rapports cités, les preuves suggérant que l'inflammasome NLRP3 contribue à la progression du cancer *in vivo* demeurent préliminaires et nécessitent une confirmation supplémentaire. Il a été suggéré que l'activation de l'inflammasome dans les tumeurs dépend spécifiquement du contexte tissulaire pour déterminer si l'inhibition ou l'activation de la tumorigenèse en résulte (Moossavi *et al.*, 2018). Dans un modèle de carcinome squameux des VADS, l'inflammasome NLRP3 a été surexprimé et associé à la carcinogénèse ainsi qu'à l'activation de l'auto-renouvèlement des cellules souches cancéreuse (Huang *et al.*, 2017). De manière importante, les protéines associées à l'inflammasome, notamment NLRP3, IL-1β, IL-18, ASC et la caspase-1 sont fortement exprimés dans un modèle de carcinome épidermoïde oropharyngé HPV+ par rapport aux amygdales normales. En revanche, il n'y a pas d'association significative entre l'expression des protéines de l'inflammasome et l'infection par le papillomavirus humain HPV dans le cancer de l'oropharynx (Takano *et al.*, 2016). Ainsi d'autres études sont nécessaires pour aborder les mécanismes moléculaires responsables de la production, l'activation et la modulation des inflammasomes et pour déterminer leur rôle thérapeutique potentiel dans les tumeurs humaine.

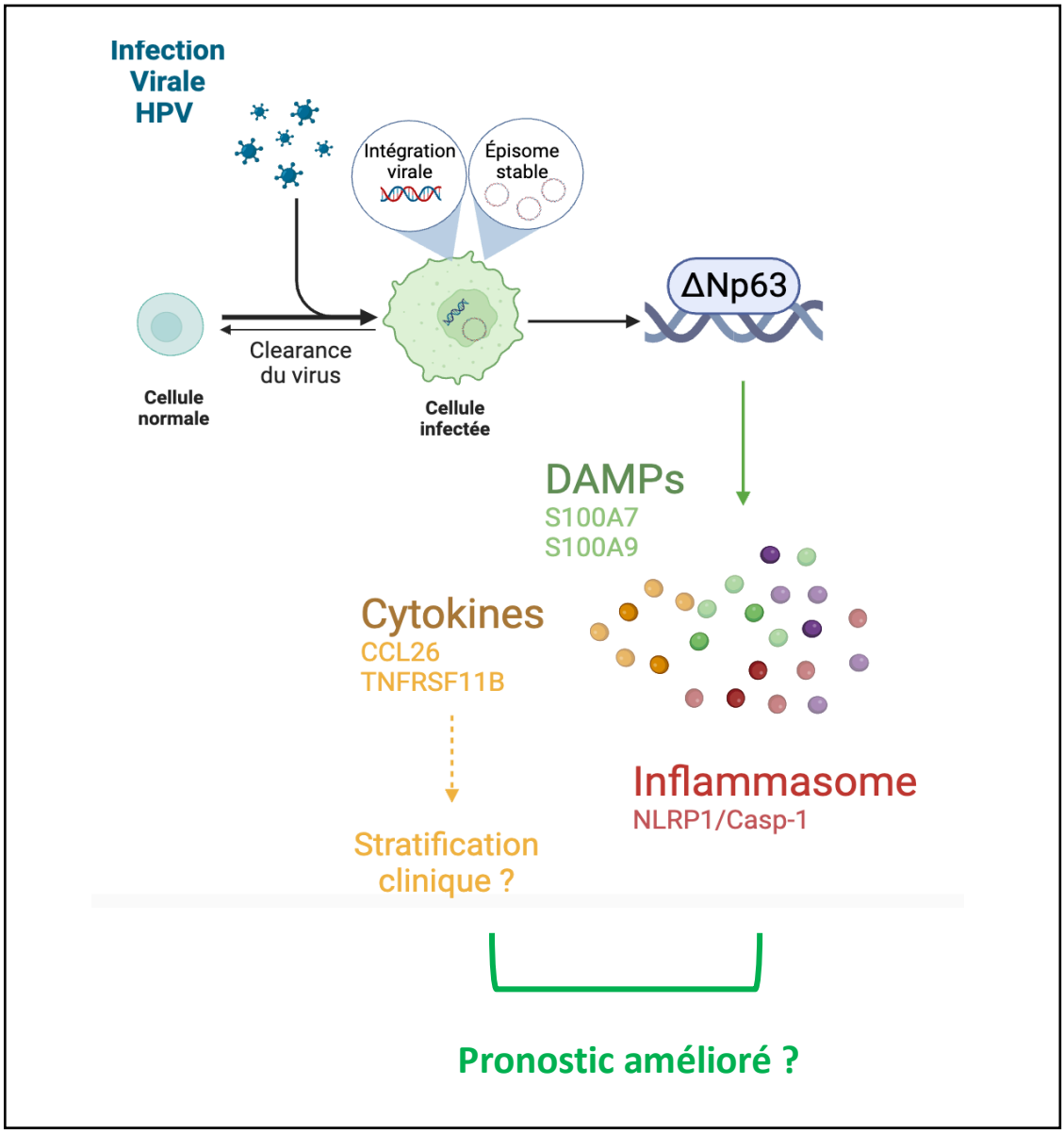

Figure 9D- ΔNp63 est impliqué dans le recrutement immunitaire à travers la régulation de l'expression de facteurs de dangers (DAMPs), de certaines cytokines et de facteurs impliqués dans la formation de l'inflammasome.

Une étude du rôle fonctionnel de ΔNp63 dans l'activation de la phagocytose par les macrophages *in vitro* m'a permis de mieux comprendre son implication dans le recrutement et l'activation d'une réponse immunitaire anti-tumorale. Nous avons mis en évidence que ΔNp63 favorise l'infiltration de lymphocyte T CD8+, régule l'expression de gènes impliqués dans des réponses inflammatoires et dans la production des cytokines et régule l'activité phagocytaire des macrophages *in-vitro*. Ces résultats confèrent un rôle suppresseur de tumeur à ΔNp63 dans nos modèles de cancers de l'oropharynx HPV+ pouvant, au moins partiellement, expliquer la différence

de pronostic observée. Ces résultats sont en accord avec des études sur les carcinomes épidermoïdes de la tête et du cou qui montrent que ΔNp63α est associé à un pronostic favorable chez les patients (Zangen, Ratovitski and Sidransky, 2005) et que la perte de son expression dans les tumeurs peut prédisposer à l'invasion et aux métastases (Barbieri *et al.*, 2006). Cependant dans un modèle de cancer triple négatif du sein (TNBC), l'activation des chimiokines CXCL2 et CCL22 est associée à la progression et les métastases des tumeurs (Kumar *et al.*, 2018). Par conséquent, ces résultats suggèrent que ΔNp63α a un impact sur la réponse immunitaire en modifiant la composition du microenvironnement tumoral, et que cet impact est variable en fonction du tissu atteint. Ainsi, il est important de noter que son rôle oncogénique ou suppresseur de tumeur dépend fortement du contexte tumoral.

En outre, ΔNp63α régule l'expression de DKK3 (Dickkopf3), un membre de la famille des Dickkopf, qui sont des protéines inhibitrices de la voie Wnt. Cependant, bien que DKK-3 est décrit comme un inhibiteur de la voie Wnt (Veeck *et al.*, 2008), certaines études ont démontré que DKK-3 n'a aucune fonction antagoniste sur la signalisation Wnt (review Mourtada *et al.* en préparation). Ainsi Mao *et al.* ont signalé que les cellules épithéliales rénales HEK-293T qui coexpriment Wnt1, Frizzled, Kremen2 et DKK3 n'induisent pas l'activation du rapporteur Wnt Luciférase (TOPFLASH) (Mao *et al.*, 2001). De manière similaire, notre modèle d'étude basé sur un système de rapporteur à luciférase n'a pas permis de mettre en évidence cette propriété inhibitrice de la voie Wnt. Cependant, nous avons observé une cytotoxicité induite par la transfection des macrophages THP-1. Par conséquent, il serait intéressant d'étudier l'activation de la voie Wnt en mesurant les niveaux d'expression des gènes cibles de la voie Wnt, tels que la Cyclin D1 et cMyc, dans les macrophages THP-1 traités avec la protéine recombinante DKK-3 rhDKK3, par RT-qPCR. Nous pourrions également inclure un contrôle positif d'activation de la voie Wnt en traitant les macrophages THP-1 avec un activateur de la voie Wnt, le chlorure de lithium (LiCl). Ces résultats nous permettront de parvenir à une conclusion plus robuste quant à l'implication de DKK-3 dans la voie Wnt dans le contexte de notre étude.

5. ΔNp63 régule l'expression de facteurs diffusibles immunomodulateurs qui contrôlent la phagocytose des cellules cancéreuse par des mécanismes dépendants de l'axe DKK3/CKAP4/ NF-κB

Nous avons démontré que ΔNp63 favorise la phagocytose *in vitro* par les macrophages et ceci à travers l'expression de facteurs diffusibles tel que DKK-3 qui induit l'activation de la voie NF-κB dans les macrophages via son récepteur CKAP4 **(Figure 9E).** NF-κB est un régulateur central des réponses immunitaires innées et est essentiel pour de nombreuses fonctions que jouent les macrophages et d'autres cellules immunitaires innées dans l'orchestration de la réponse inflammatoire aux agents pathogènes. De plus, la fixation de DKK-3 sur son récepteur CKAP4 active la voie de signalisation PI3K/Akt provoquant ainsi l'activation de la voie NF-κB canonique par phosphorylation d'IκB kinase-α (IKKα). Ceci est cohérent avec des résultats de la littérature qui montrent que DKK1 se lie à CKAP4 et déclenche la voie de signalisation intracellulaire PI3K/Akt (Kimura *et al.*, 2016). Cependant cette fonction a été montrée comme pertinente pour la progression tumorale. Il serait donc crucial d'explorer la relation directe entre l'axe DKK3/CKAP4 et l'activation de la phagocytose par les macrophages dans notre modèle d'étude. Une stratégie possible consisterait à inhiber les récepteurs CKAP4 sur les macrophages THP-1 en présence de DKK-3, puis à évaluer l'activité phagocytaire de ces macrophages en comparant les conditions avec et sans CKAP4. Il a été démontré que DKK-3 affecte la fonction des cellules dendritiques (DC), qui jouent un rôle crucial dans l'initiation et la régulation des réponses immunitaires. En effet, des études ont montré que la protéine REIC/DKK3 sécrétée induit la différenciation des monocytes en cellules semblables à des cellules dendritiques, montrant son rôle dans l'activation et la modulation de la réponse immunitaire.

Nous pourrions donc envisager d'effectuer une étude *in vivo* pour renforcer la robustesse de nos résultats. Pour cela, des souris immunocompétentes pourraient être utilisées, dans lesquelles nous effectuerions des greffes de cellules tumorales HPV+ (modèle syngénique mERRL95 : kératinocytes primaires d'oropharynx de souris exprimant les oncoprotéines E6 et E7 d'HPV16 et hRAS (Vermeer *et al.*, 2016)), ayant subi une réduction stable de l'expression de DKK-3 grâce à un sh-DKK3. Cette approche nous permettrait d'analyser la progression tumorale ainsi que le

microenvironnement immunitaire de la tumeur en évaluant l'infiltration des cellules immunitaires et l'activation des macrophages.

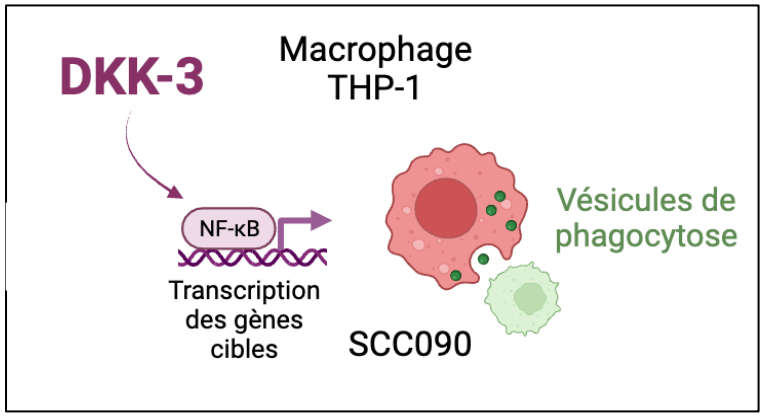

Figure 9E- ΔNp63 régule l'expression de DKK-3 qui est impliqué dans l'activation de la phagocytose *in vitro* à travers la voie NF-κB

6. P63 régule l'expression de cytokines

Nous avons mis en évidence, grâce à des membranes à cytokines, que p63 régule l'expression d'un certain nombre de cytokines. Ces données ont été validé par RT PCR quantitative montrant une diminution significative du niveau d'expression de ces cytokines en absence de p63. Celles-ci regroupent TNFRSF11B (facteur de nécrose tumorale-membre de la superfamille 11B), CCL26 (chimiokine C-C motif ligand 26), TIMP1 et TIMP2 (inhibiteur des métalloprotéinases tissulaires 1 et 2). Ces cytokines jouent différents rôles dans le contexte de la régulation de l'inflammation et de la progression tumorale **(Figure 9D)**. Il convient de noter que le rôle précis de ces cytokines peut varier en fonction du contexte spécifique, y compris le type de cancer et le microenvironnement tumoral. Leur expression peut être associée à des processus inflammatoires, à la réponse immunitaire et à la progression tumorale, et leur influence dépendra des interactions complexes entre ces facteurs dans le contexte de la maladie. Des études réalisées sur ces cytokines et leurs implications dans les différents types de cancers ont révélées que TNFRSF11B favorise les phénotypes agressifs des cellules de carcinome gastrique en activant la voie de signalisation Wnt/β-caténine et en stimulant la prolifération cellulaire, la migration, l'invasion *in vitro* ainsi que la capacité tumorigène *in vitro* et *in vivo* (Luan *et al.*, 2020).

Selon certaines études, la chimiokine CCL26 (Eotaxine-3) est impliquée dans la progression du cancer du côlon en régulant la transition épithélio-mésenchymateuse et régule l'expression protéique de TIMP1 (Sun, Li and Jiang, 2022). Une expression élevée des éotaxines se produit dans des tumeurs telles que le cancer du sein (Thomas *et al.*, 2019), le cancer colorectal (Cho *et al.*, 2015) et les carcinomes épidermoïdes buccaux (Lorena *et al.*, 2003), où elle est associée au recrutement d'éosinophiles dans la niche tumorale. Cependant, le rôle des éosinophiles dans les tumeurs n'est pas clair (Sakkal *et al.*, no date), car ils présentent à la fois des caractéristiques pro- et anti-cancéreuses selon le type de tumeur. Lin *et al.* ont constaté que CCL26 est surexprimée dans les fibroblastes hépatiques liés au cancer, et sa surexpression favorise la croissance et l'invasion des tumeurs hépatiques (Lin *et al.*, 2019). Cependant, très peu d'études révèlent un rôle spécifique de TNFRS11B et de CCL26 dans les cancers des VADS.

TIMP-1 et TIMP-2 sont couramment identifiés dans les carcinomes épidermoïdes de la tête et du cou. Les TIMPs sont sécrétés par les fibroblastes et se trouvent à des niveaux élevés dans le sérum (Rosenthal and Matrisian, 2006). Les études identifient généralement qu'une surexpression de TIMP-1 est associée à l'invasion et aux métastases dans les cancers des VADS (Kurahara *et al.*, 1999; O-Charoenrat, Rhys-Evans and Eccles, 2001). Cependant, des niveaux sériques élevés de TIMP-1 sont plus fortement associés à un pronostic défavorable chez les patients atteints de tumeurs négatives pour le HPV que chez ceux atteints de tumeurs HPV+ dans un modèle de cancer épidermoïde de l'oropharynx (Carpén *et al.*, 2019). TIMP-2, une protéine plasmatique largement exprimée dans le compartiment stromal des tissus normaux, possède des fonctions inhibitrices de la croissance tumorale et de l'angiogenèse dans un contexte tumoral (Stetler-Stevenson, 2008). Ainsi, Peeney *et al.* ont démontré que TIMP-2 inhibe la croissance tumorale et les métastases dans un modèle murin de cancer triple négatif du sein (Peeney *et al.*, 2020). Cependant, TIMP-2 pourrait également jouer un rôle dans la prolifération, l'invasion et la chimiorésistance du cancer de l'ovaire (Escalona *et al.*, 2020). Finalement, une expression plus élevée de TIMP-2 et une activité accrue des métalloprotéinases sont associées à la présence du HPV dans des lignées cellulaires de carcinome du col de l'utérus humain. Cela suggère que le HPV pourrait jouer un rôle dans la régulation de l'expression de MMP

et de TIMP-2 (da Silva Cardeal *et al.*, 2006). Des travaux supplémentaires seront donc nécessaires pour élucider le rôle de des TIMPs dans les cancers des VADS HPV induits.

Il serait donc pertinent d'approfondir notre compréhension sur l'implication de chacune de ces cytokines dans les cancers des VADS positifs à l'HPV et d'évaluer leur utilisation potentielle en tant que biomarqueurs pronostiques. Il est prévu de réaliser cette évaluation en utilisant des biopsies liquides de patients prélevées dans le cadre d'une étude ancillaire à l'essai clinique DETECT-HPV, porté par Unicancer. Ceci pourrait être envisageable grâce à la surveillance des niveaux d'expression sériques des cytokines en parallèle des niveaux d'ADN circulant (ADN ct) d'HPV, au cours du suivi post-thérapeutique de patients atteints d'un cancer de l'oropharynx HPV-induit. Ce dernier peut être évalué en tant que biomarqueur plasmatique aisé à utiliser pour déterminer précocement l'efficacité du traitement et la survenue de rechutes, compte tenu de l'utilisation croissante de traitements très spécifiques et couteux tels que les immunothérapies. La cinétique de l'ADN ct d'HPV est clairement corrélée à l'échec ou à la réussite du traitement, et cette caractéristique serait plus précoce que les critères classiques d'évaluation de la réponse dans les tumeurs solides (RECIST) (Hanna *et al.*, 2018; Chera *et al.*, 2019; Veyer *et al.*, 2019). Selon différentes études déjà publiées sur le ct ADN d'HPV dans les carcinomes squameux oropharyngés induit par HPV, ce biomarqueur présente une sensibilité et une spécificité très élevées, récemment estimées à 89 et 97%, respectivement (Chera *et al.*, 2019). Donc l'étude du ct ADN d'HPV avant et après traitement et l'évaluation de la positivité des patients pourrait être corrélé à l'expression des cytokines que nous avons identifiées, qui elles-mêmes sont potentiellement corrélées avec l'expression de p63 et plus particulièrement à l'expression de l'isoforme prédominant ΔNp63. ΔNp63 et les cytokines, dont il régule l'expression, pourraient ainsi être valorisés comme facteurs de stratification clinique et thérapeutique **(Figure 9F)**.

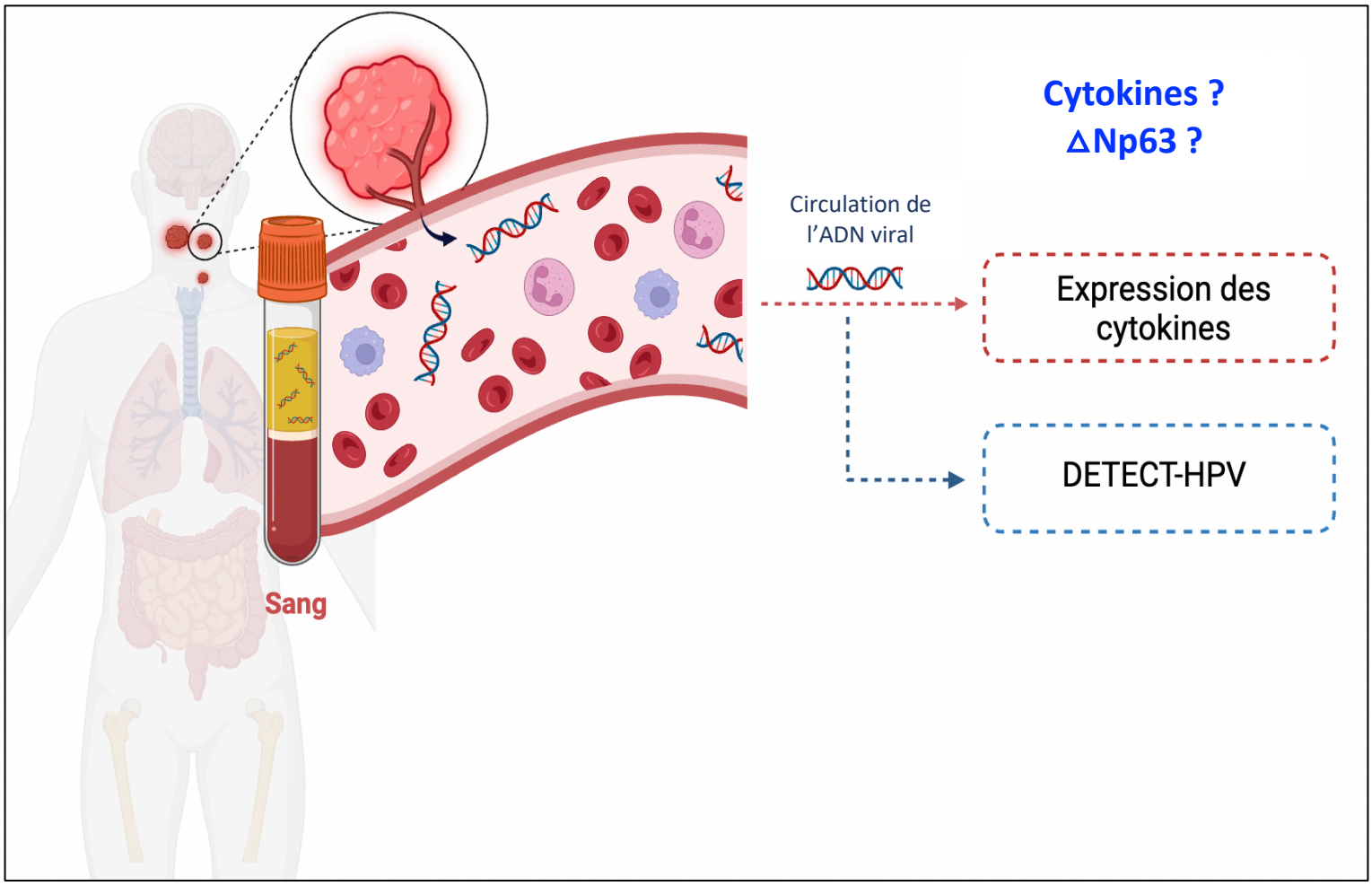

Figure 9F- Étude de ΔNp63 et de certaines cytokines dont il régule l'expression, en tant que biomarqueurs de stratification clinique et thérapeutique ?

SCHÉMA DE SYNTHÈSE

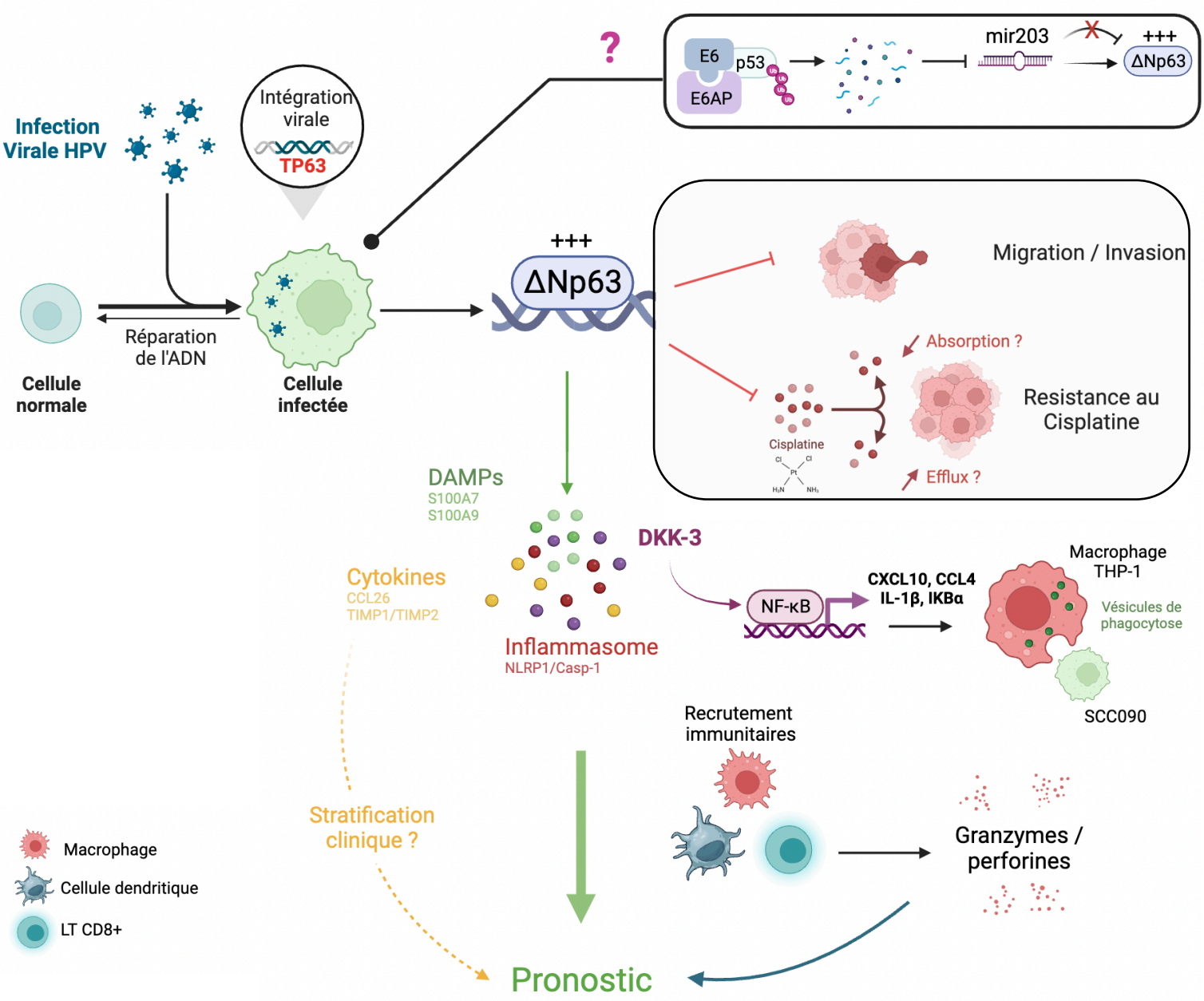

BIBLIOGRAPHIE

Defossez G, Le Guyader-Peyrou S, Uhry Z, et al.EstimationsNationales de l'Incidence et de la Mortalité par Cancer en FranceMétropolitaine Entre 1990 et 2018. Volume 1– Tumeurs solides. Saint-Maurice (Fra): Santé Publique France; 2019:372

Cowppli-Bony A, Uhry Z, Remontet L, et al. Survie des personnes atteintes de cancer en France, 1989-2013. Etude à partir des registres des cancers du réseau Francim. Par tumeurs solides. Saint-Maurice: Institut de veille sanitaire 2016; pp. 274

Alizadeh, A.A. *et al.* (2000) 'Distinct types of diffuse large B-cell lymphoma identified by gene expression profiling', *Nature*, 403(6769), pp. 503–511. Available at: https://doi.org/10.1038/35000501.

Androphy, E.J. *et al.* (1987) 'Identification of the HPV-16 E6 protein from transformed mouse cells and human cervical carcinoma cell lines', *The EMBO journal*, 6(4), pp. 989–992.

Ang, K.K. *et al.* (2010a) 'Human Papillomavirus and Survival of Patients with Oropharyngeal Cancer', *The New England journal of medicine*, 363(1), pp. 24–35. Available at: https://doi.org/10.1056/NEJMoa0912217.

Ang, K.K. *et al.* (2010b) 'Human Papillomavirus and Survival of Patients with Oropharyngeal Cancer', *New England Journal of Medicine*, 363(1), pp. 24–35. Available at: https://doi.org/10.1056/NEJMoa0912217.

Badoual, C. *et al.* (2006) 'Prognostic Value of Tumor-Infiltrating CD4+ T-Cell Subpopulations in Head and Neck Cancers', *Clinical Cancer Research*, 12(2), pp. 465–472. Available at: https://doi.org/10.1158/1078-0432.CCR-05-1886.

Badoual, C. *et al.* (2013) 'PD-1–Expressing Tumor-Infiltrating T Cells Are a Favorable Prognostic Biomarker in HPV-Associated Head and Neck Cancer', *Cancer Research*, 73(1), pp. 128–138. Available at: https://doi.org/10.1158/0008-5472.CAN-12-2606.

Barbieri, C.E. *et al.* (2005) 'IGFBP-3 is a direct target of transcriptional regulation by DeltaNp63alpha in squamous epithelium', *Cancer Research*, 65(6), pp. 2314–2320. Available at: https://doi.org/10.1158/0008-5472.CAN-04-3449.

Barbieri, C.E. *et al.* (2006) 'Loss of p63 leads to increased cell migration and up-regulation of genes involved in invasion and metastasis', *Cancer Research*, 66(15), pp. 7589–7597. Available at: https://doi.org/10.1158/0008-5472.CAN-06-2020.

Bauman, J.E. *et al.* (2020) 'Phase I Study of Ficlatuzumab and Cetuximab in Cetuximab-Resistant, Recurrent/Metastatic Head and Neck Cancer', *Cancers*, 12(6), p. 1537. Available at: https://doi.org/10.3390/cancers12061537.

Blot, W.J. *et al.* (1988) 'Smoking and drinking in relation to oral and pharyngeal cancer', *Cancer Research*, 48(11), pp. 3282–3287.

Bougeard, G. *et al.* (2003) 'The Rapp-Hodgkin syndrome results from mutations of the TP63 gene', *European journal of human genetics: EJHG*, 11(9), pp. 700–704. Available at: https://doi.org/10.1038/sj.ejhg.5201004.

Brantsch, K.D. *et al.* (2008) 'Analysis of risk factors determining prognosis of cutaneous squamous-cell carcinoma: a prospective study', *The Lancet. Oncology*, 9(8), pp. 713–720. Available at: https://doi.org/10.1016/S1470-2045(08)70178-5.

Bray, F. *et al.* (2018) 'Global cancer statistics 2018: GLOBOCAN estimates of incidence and mortality worldwide for 36 cancers in 185 countries', *CA: A Cancer Journal for Clinicians*, 68(6), pp. 394–424. Available at: https://doi.org/10.3322/caac.21492.

Brooks, P.J. and Theruvathu, J.A. (2005) 'DNA adducts from acetaldehyde: implications for alcohol-related carcinogenesis', *Alcohol (Fayetteville, N.Y.)*, 35(3), pp. 187–193. Available at: https://doi.org/10.1016/j.alcohol.2005.03.009.

Burtness, B. *et al.* (2019) 'Pembrolizumab alone or with chemotherapy versus cetuximab with chemotherapy for recurrent or metastatic squamous cell carcinoma of the head and neck (KEYNOTE-048): a randomised, open-label, phase 3 study', *The Lancet*, 394(10212), pp. 1915–1928. Available at: https://doi.org/10.1016/S0140-6736(19)32591-7.

Busceti, C.L. *et al.* (2018) 'Dickkopf-3 Causes Neuroprotection by Inducing Vascular Endothelial Growth Factor', *Frontiers in Cellular Neuroscience*, 12, p. 292. Available at: https://doi.org/10.3389/fncel.2018.00292.

Cai, B.-H. *et al.* (2022) 'P63 and P73 Activation in Cancers with p53 Mutation', *Biomedicines*, 10(7), p. 1490. Available at: https://doi.org/10.3390/biomedicines10071490.

Campbell, J.D. *et al.* (2018) 'Genomic, Pathway Network, and Immunologic Features Distinguishing Squamous Carcinomas', *Cell Reports*, 23(1), pp. 194-212.e6. Available at: https://doi.org/10.1016/j.celrep.2018.03.063.

Candi, E. *et al.* (2006) 'Differential roles of p63 isoforms in epidermal development: selective genetic complementation in p63 null mice', *Cell Death and Differentiation*, 13(6), pp. 1037–1047. Available at: https://doi.org/10.1038/sj.cdd.4401926.

Candi, E. *et al.* (no date) '⌬Np63 regulates thymic development through', *CELL BIOLOGY* [Preprint].

Carpén, T. *et al.* (2019) 'High levels of tissue inhibitor of metalloproteinase-1 (TIMP-1) in the serum are associated with poor prognosis in HPV-negative squamous cell oropharyngeal cancer', *Cancer Immunology, Immunotherapy*, 68(8), pp. 1263–1272. Available at: https://doi.org/10.1007/s00262-019-02362-4.

Carroll, D.K. *et al.* (2006) 'p63 regulates an adhesion programme and cell survival in epithelial cells', *Nature Cell Biology*, 8(6), pp. 551–561. Available at: https://doi.org/10.1038/ncb1420.

Carvalho, A.L. *et al.* (2005) 'Trends in incidence and prognosis for head and neck cancer in the United States: A site-specific analysis of the SEER database', *International Journal of Cancer*, 114(5), pp. 806–816. Available at: https://doi.org/10.1002/ijc.20740.

Celli, J. *et al.* (1999) 'Heterozygous Germline Mutations in the p53 Homolog p63 Are the Cause of EEC Syndrome', *Cell*, 99(2), pp. 143–153. Available at: https://doi.org/10.1016/S0092-8674(00)81646-3.

Chan, W.M. *et al.* (2004) 'How Many Mutant p53 Molecules Are Needed To Inactivate a Tetramer?', *Molecular and Cellular Biology*, 24(8), pp. 3536–3551. Available at: https://doi.org/10.1128/MCB.24.8.3536-3551.2004.

Chaturvedi, A.K. *et al.* (2015) 'NHANES 2009-2012 findings: association of sexual behaviors with higher prevalence of oral oncogenic human papillomavirus infections in U.S. men', *Cancer research*, 75(12), pp. 2468–2477. Available at: https://doi.org/10.1158/0008-5472.CAN-14-2843.

Chen, Y. *et al.* (2018) 'A double dealing tale of p63: an oncogene or a tumor suppressor', *Cellular and Molecular Life Sciences*, 75(6), pp. 965–973. Available at: https://doi.org/10.1007/s00018-017-2666-y.

Chera, B.S. *et al.* (2019) 'Rapid Clearance Profile of Plasma Circulating Tumor HPV Type 16 DNA during Chemoradiotherapy Correlates with Disease Control in HPV-Associated Oropharyngeal Cancer', *Clinical Cancer Research*, 25(15), pp. 4682–4690. Available at: https://doi.org/10.1158/1078-0432.CCR-19-0211.

Cho, H. *et al.* (2015) 'Eosinophils in Colorectal Neoplasms Associated with Expression of CCL11 and CCL24', *Journal of Pathology and Translational Medicine*, 50(1), pp. 45–51. Available at: https://doi.org/10.4132/jptm.2015.10.16.

Chung, C.H. *et al.* (2004) 'Molecular classification of head and neck squamous cell carcinomas using patterns of gene expression', *Cancer Cell*, 5(5), pp. 489–500. Available at: https://doi.org/10.1016/S1535-6108(04)00112-6.

Chung, J. *et al.* (2010) 'SATB2 augments ΔNp63α in head and neck squamous cell carcinoma', *EMBO reports*, 11(10), pp. 777–783. Available at: https://doi.org/10.1038/embor.2010.125.

Citro, S. *et al.* (2019) 'Synergistic antitumour activity of HDAC inhibitor SAHA and EGFR inhibitor gefitinib in head and neck cancer: a key role for ΔNp63α', *British Journal of Cancer*, 120(6), pp. 658–667. Available at: https://doi.org/10.1038/s41416-019-0394-9.

Citro, S. *et al.* (2020) 'Human Papilloma Virus Increases ΔNp63α Expression in Head and Neck Squamous Cell Carcinoma', *Frontiers in Cellular and Infection Microbiology*, 10, p. 143. Available at: https://doi.org/10.3389/fcimb.2020.00143.

Cripps, C. *et al.* (2010) 'Epidermal growth factor receptor targeted therapy in stages III and IV head and neck cancer', *Current Oncology*, 17(3), pp. 37–48.

Dang, T.T. *et al.* (2015) 'ΔNp63α Promotes Breast Cancer Cell Motility through the Selective Activation of Components of the Epithelial-to-Mesenchymal Transition Program', *Cancer Research*, 75(18), pp. 3925–3935. Available at: https://doi.org/10.1158/0008-5472.CAN-14-3363.

Davis, R.J., Van Waes, C. and Allen, C.T. (2016) 'Overcoming barriers to effective immunotherapy: MDSCs, TAMs, and Tregs as mediators of the immunosuppressive microenvironment in head and neck cancer', *Oral Oncology*, 58, pp. 59–70. Available at: https://doi.org/10.1016/j.oraloncology.2016.05.002.

De Laurenzi, V. *et al.* (2000) 'Induction of neuronal differentiation by p73 in a neuroblastoma cell line', *The Journal of Biological Chemistry*, 275(20), pp. 15226–15231. Available at: https://doi.org/10.1074/jbc.275.20.15226.

Della Gatta, G. *et al.* (2008) 'Direct targets of the TRP63 transcription factor revealed by a combination of gene expression profiling and reverse engineering', *Genome Research*, 18(6), pp. 939–948. Available at: https://doi.org/10.1101/gr.073601.107.

Denaro, N. *et al.* (2014) 'State-of-the-Art and Emerging Treatment Options in the Management of Head and Neck Cancer: News from 2013', *Oncology*, 86(4), pp. 212–229. Available at: https://doi.org/10.1159/000357712.

DiGiuseppe, S. *et al.* (2016) 'Incoming human papillomavirus type 16 genome resides in a vesicular compartment throughout mitosis', *Proceedings of the National Academy of Sciences*

of the United States of America, 113(22), pp. 6289–6294. Available at: https://doi.org/10.1073/pnas.1600638113.

DiMaio, D. and Petti, L.M. (2013) 'The E5 proteins', *Virology*, 445(1–2), pp. 99–114. Available at: https://doi.org/10.1016/j.virol.2013.05.006.

Dohn, M., Zhang, S. and Chen, X. (2001) 'p63alpha and DeltaNp63alpha can induce cell cycle arrest and apoptosis and differentially regulate p53 target genes', *Oncogene*, 20(25), pp. 3193–3205. Available at: https://doi.org/10.1038/sj.onc.1204427.

Doorbar, J. (2005) 'The papillomavirus life cycle', *Journal of Clinical Virology*, 32, pp. 7–15. Available at: https://doi.org/10.1016/j.jcv.2004.12.006.

Doorbar, J. *et al.* (2015) 'Human papillomavirus molecular biology and disease association', *Reviews in Medical Virology*, 25(Suppl Suppl 1), pp. 2–23. Available at: https://doi.org/10.1002/rmv.1822.

Duijf, P.H.G., van Bokhoven, H. and Brunner, H.G. (2003) 'Pathogenesis of split-hand/split-foot malformation', *Human Molecular Genetics*, 12 Spec No 1, pp. R51-60. Available at: https://doi.org/10.1093/hmg/ddg090.

Dyson, N. *et al.* (1989) 'The Human Papilloma Virus-16 E7 Oncoprotein Is Able to Bind to the Retinoblastoma Gene Product', *Science*, 243(4893), pp. 934–937. Available at: https://doi.org/10.1126/science.2537532.

E, K. *et al.* (2013) 'Association of RASSF1A and p63 with poor recurrence-free survival in node-negative stage I-II non-small cell lung cancer.', *Clinical Cancer Research : an Official Journal of the American Association for Cancer Research*, 19(5), pp. 1204–1212. Available at: https://doi.org/10.1158/1078-0432.ccr-12-2848.

Escalona, R.M. *et al.* (2020) 'TIMP-2 regulates proliferation, invasion and STAT3-mediated cancer stem cell-dependent chemoresistance in ovarian cancer cells', *BMC Cancer*, 20(1), p. 960. Available at: https://doi.org/10.1186/s12885-020-07274-6.

Fakhry, C. *et al.* (2008) 'Improved survival of patients with human papillomavirus-positive head and neck squamous cell carcinoma in a prospective clinical trial', *Journal of the National Cancer Institute*, 100(4), pp. 261–269. Available at: https://doi.org/10.1093/jnci/djn011.

Farkona, S., Diamandis, E.P. and Blasutig, I.M. (2016) 'Cancer immunotherapy: the beginning of the end of cancer?', *BMC Medicine*, 14(1), p. 73. Available at: https://doi.org/10.1186/s12916-016-0623-5.

Ferlay, J. *et al.* (2015) 'Cancer incidence and mortality worldwide: Sources, methods and major patterns in GLOBOCAN 2012: Globocan 2012', *International Journal of Cancer*, 136(5), pp. E359–E386. Available at: https://doi.org/10.1002/ijc.29210.

Ferlay, J. *et al.* (2018) 'Cancer incidence and mortality patterns in Europe: Estimates for 40 countries and 25 major cancers in 2018', *European Journal of Cancer*, 103, pp. 356–387. Available at: https://doi.org/10.1016/j.ejca.2018.07.005.

Ferrari, N. *et al.* (2019) 'Dickkopf-3 links HSF1 and YAP/TAZ signalling to control aggressive behaviours in cancer-associated fibroblasts', *Nature Communications*, 10, p. 130. Available at: https://doi.org/10.1038/s41467-018-07987-0.

Ferris, R.L. (2015) 'Immunology and Immunotherapy of Head and Neck Cancer', *Journal of Clinical Oncology*, 33(29), pp. 3293–3304. Available at: https://doi.org/10.1200/JCO.2015.61.1509.

Ferris, R.L. *et al.* (2016) 'Nivolumab for Recurrent Squamous-Cell Carcinoma of the Head and Neck', *New England Journal of Medicine*, 375(19), pp. 1856–1867. Available at: https://doi.org/10.1056/NEJMoa1602252.

Ferris, R.L. *et al.* (2022) 'Phase I Trial of Cetuximab, Radiotherapy, and Ipilimumab in Locally Advanced Head and Neck Cancer', *Clinical Cancer Research: An Official Journal of the American Association for Cancer Research*, 28(7), pp. 1335–1344. Available at: https://doi.org/10.1158/1078-0432.CCR-21-0426.

Fisher, M.L. *et al.* (2016) 'Transglutaminase Interaction with α6/β4-Integrin Stimulates YAP1-Dependent ΔNp63α Stabilization and Leads to Enhanced Cancer Stem Cell Survival and Tumor Formation', *Cancer Research*, 76(24), pp. 7265–7276. Available at: https://doi.org/10.1158/0008-5472.CAN-16-2032.

Foon, K.A. *et al.* (2004) 'Preclinical and clinical evaluations of ABX-EGF, a fully human anti-epidermal growth factor receptor antibody', *International Journal of Radiation Oncology*Biology*Physics*, 58(3), pp. 984–990. Available at: https://doi.org/10.1016/j.ijrobp.2003.09.098.

Foschini, M.P. *et al.* (2004) 'Pattern of p63 expression in squamous cell carcinoma of the oral cavity', *Virchows Archiv*, 444(4), pp. 332–339. Available at: https://doi.org/10.1007/s00428-003-0969-x.

Freedman, N.D. *et al.* (2008) 'Fruit and vegetable intake and head and neck cancer risk in a large United States prospective cohort study', *International Journal of Cancer*, 122(10), pp. 2330–2336. Available at: https://doi.org/10.1002/ijc.23319.

Freed-Pastor, W.A. and Prives, C. (2012) 'Mutant p53: one name, many proteins', *Genes & Development*, 26(12), pp. 1268–1286. Available at: https://doi.org/10.1101/gad.190678.112.

Fridman, W.H. *et al.* (2012) 'The immune contexture in human tumours: impact on clinical outcome', *Nature Reviews. Cancer*, 12(4), pp. 298–306. Available at: https://doi.org/10.1038/nrc3245.

Fujii, M. *et al.* (2011) 'Dickkopf (Dkk)-3 and β-catenin expressions increased in the transition from normal oral mucosal to oral squamous cell carcinoma', *Journal of Molecular Histology*, 42(6), pp. 499–504. Available at: https://doi.org/10.1007/s10735-011-9357-z.

Galati, L. *et al.* (2022) 'HPV and head and neck cancers: Towards early diagnosis and prevention', *Tumour Virus Research*, 14, p. 200245. Available at: https://doi.org/10.1016/j.tvr.2022.200245.

Ganti, K. *et al.* (2015) 'The Human Papillomavirus E6 PDZ Binding Motif: From Life Cycle to Malignancy', *Viruses*, 7(7), pp. 3530–3551. Available at: https://doi.org/10.3390/v7072785.

Gao, J. *et al.* (2013) 'Integrative analysis of complex cancer genomics and clinical profiles using the cBioPortal', *Science Signaling*, 6(269), p. pl1. Available at: https://doi.org/10.1126/scisignal.2004088.

Garber, M.E. *et al.* (2001) 'Diversity of gene expression in adenocarcinoma of the lung', *Proceedings of the National Academy of Sciences of the United States of America*, 98(24), pp. 13784–13789. Available at: https://doi.org/10.1073/pnas.241500798.

Garcia, J. *et al.* (2020) 'Bevacizumab (Avastin®) in cancer treatment: A review of 15 years of clinical experience and future outlook', *Cancer Treatment Reviews*, 86, p. 102017. Available at: https://doi.org/10.1016/j.ctrv.2020.102017.

Gillison, M.L. *et al.* (2000) 'Evidence for a causal association between human papillomavirus and a subset of head and neck cancers', *Journal of the National Cancer Institute*, 92(9), pp. 709–720. Available at: https://doi.org/10.1093/jnci/92.9.709.

Gillison, M.L. (2004) 'Human papillomavirus-associated head and neck cancer is a distinct epidemiologic, clinical, and molecular entity', *Seminars in Oncology*, 31(6), pp. 744–754. Available at: https://doi.org/10.1053/j.seminoncol.2004.09.011.

Gillison, M.L. *et al.* (2008) 'Distinct risk factor profiles for human papillomavirus type 16-positive and human papillomavirus type 16-negative head and neck cancers', *Journal of the National Cancer Institute*, 100(6), pp. 407–420. Available at: https://doi.org/10.1093/jnci/djn025.

Gillison, M.L. *et al.* (2012) 'Prevalence of Oral HPV Infection in the United States, 2009–2010', *JAMA*, 307(7), pp. 693–703. Available at: https://doi.org/10.1001/jama.2012.101.

Gillison, M.L. *et al.* (2014) 'Eurogin Roadmap: Comparative epidemiology of HPV infection and associated cancers of the head and neck and cervix', *International Journal of Cancer*, 134(3), pp. 497–507. Available at: https://doi.org/10.1002/ijc.28201.

Gillison, M.L. *et al.* (2015) 'Epidemiology of Human Papillomavirus–Positive Head and Neck Squamous Cell Carcinoma', *Journal of Clinical Oncology*, 33(29), pp. 3235–3242. Available at: https://doi.org/10.1200/JCO.2015.61.6995.

Gillison, M.L. *et al.* (2019) 'Radiotherapy plus cetuximab or cisplatin for human papillomavirus (HPV)-positive oropharyngeal cancer: a randomized, multicenter, non-inferiority clinical trial', *Lancet (London, England)*, 393(10166), pp. 40–50. Available at: https://doi.org/10.1016/S0140-6736(18)32779-X.

Gillison, M.L., Chaturvedi, A.K. and Lowy, D.R. (2008) 'HPV Prophylactic Vaccines and the Potential Prevention of Noncervical Cancers in Both Men and Women', *Cancer*, 113(10 Suppl), pp. 3036–3046. Available at: https://doi.org/10.1002/cncr.23764.

Glathar, A.R. *et al.* (2022) 'p63 Directs Subtype-Specific Gene Expression in HPV+ Head and Neck Squamous Cell Carcinoma', *Frontiers in Oncology*, 12. Available at: https://www.frontiersin.org/articles/10.3389/fonc.2022.879054 (Accessed: 26 October 2023).

Glisson, B.S. *et al.* (2020) 'Safety and Clinical Activity of MEDI0562, a Humanized OX40 Agonist Monoclonal Antibody, in Adult Patients with Advanced Solid Tumors', *Clinical Cancer Research: An Official Journal of the American Association for Cancer Research*, 26(20), pp. 5358–5367. Available at: https://doi.org/10.1158/1078-0432.CCR-19-3070.

Gong, J. *et al.* (2018) 'Development of PD-1 and PD-L1 inhibitors as a form of cancer immunotherapy: a comprehensive review of registration trials and future considerations', *Journal for Immunotherapy of Cancer*, 6, p. 8. Available at: https://doi.org/10.1186/s40425-018-0316-z.

Graham, S.V. (2017) 'The human papillomavirus replication cycle, and its links to cancer progression: a comprehensive review', *Clinical Science*, 131(17), pp. 2201–2221. Available at: https://doi.org/10.1042/CS20160786.

Grégoire, V. *et al.* (2010) 'Squamous cell carcinoma of the head and neck: EHNS–ESMO–ESTRO Clinical Practice Guidelines for diagnosis, treatment and follow-up', *Annals of Oncology*, 21, pp. v184–v186. Available at: https://doi.org/10.1093/annonc/mdq185.

Gressner, O. *et al.* (2005) 'TAp63α induces apoptosis by activating signaling via death receptors and mitochondria', *The EMBO Journal*, 24(13), pp. 2458–2471. Available at: https://doi.org/10.1038/sj.emboj.7600708.

Guha, N. *et al.* (2007) 'Oral Health and Risk of Squamous Cell Carcinoma of the Head and Neck and Esophagus: Results of Two Multicentric Case-Control Studies', *American Journal of Epidemiology*, 166(10), pp. 1159–1173. Available at: https://doi.org/10.1093/aje/kwm193.

Guizard, A.-V.N. *et al.* (2017) 'Diagnosis and management of head and neck cancers in a high-incidence area in France', *Medicine*, 96(26), p. e7285. Available at: https://doi.org/10.1097/MD.0000000000007285.

Hamdan, F.H. and Johnsen, S.A. (2018) 'DeltaNp63-dependent super enhancers define molecular identity in pancreatic cancer by an interconnected transcription factor network', *Proceedings of the National Academy of Sciences*, 115(52), pp. E12343–E12352. Available at: https://doi.org/10.1073/pnas.1812915116.

Hamid, O. *et al.* (2022) 'First-in-human study of an OX40 (ivuxolimab) and 4-1BB (utomilumab) agonistic antibody combination in patients with advanced solid tumors', *Journal for Immunotherapy of Cancer*, 10(10), p. e005471. Available at: https://doi.org/10.1136/jitc-2022-005471.

Han, M.-H. *et al.* (2022) 'High DKK3 expression related to immunosuppression was associated with poor prognosis in glioblastoma: machine learning approach', *Cancer Immunology, Immunotherapy*, 71(12), pp. 3013–3027. Available at: https://doi.org/10.1007/s00262-022-03222-4.

Hanna, G.J. *et al.* (2018) *Frameshift events predict anti–PD-1/L1 response in head and neck cancer*. American Society for Clinical Investigation. Available at: https://doi.org/10.1172/jci.insight.98811.

Harris, C.C. (1993) 'p53: at the crossroads of molecular carcinogenesis and risk assessment', *Science (New York, N.Y.)*, 262(5142), pp. 1980–1981. Available at: https://doi.org/10.1126/science.8266092.

zur Hausen, H. (2002) 'Papillomaviruses and cancer: from basic studies to clinical application', *Nature Reviews. Cancer*, 2(5), pp. 342–350. Available at: https://doi.org/10.1038/nrc798.

Hauser, C. *et al.* (1986) 'Interleukin 1 is present in normal human epidermis', *Journal of Immunology (Baltimore, Md.: 1950)*, 136(9), pp. 3317–3323.

Hayashi, T. *et al.* (2012) 'DNA methylation status of REIC/Dkk-3 gene in human malignancies', *Journal of Cancer Research and Clinical Oncology*, 138(5), pp. 799–809. Available at: https://doi.org/10.1007/s00432-012-1158-6.

Hecht, S.S. (1999) 'Tobacco Smoke Carcinogens and Lung Cancer', *Journal of the National Cancer Institute*, 91(14).

Hennessey, P.T., Westra, W.H. and Califano, J.A. (2009) 'Human Papillomavirus and Head and Neck Squamous Cell Carcinoma', *Journal of Dental Research*, 88(4), pp. 300–306. Available at: https://doi.org/10.1177/0022034509333371.

Herfs, M. *et al.* (2012) 'A discrete population of squamocolumnar junction cells implicated in the pathogenesis of cervical cancer', *Proceedings of the National Academy of Sciences*, 109(26), pp. 10516–10521. Available at: https://doi.org/10.1073/pnas.1202684109.

Heusinkveld, M. *et al.* (2011) 'The detection of circulating human papillomavirus-specific T cells is associated with improved survival of patients with deeply infiltrating tumors', *International Journal of Cancer*, 128(2), pp. 379–389. Available at: https://doi.org/10.1002/ijc.25361.

Hsieh, S.-Y. *et al.* (2004) 'Dickkopf-3/REIC functions as a suppressor gene of tumor growth', *Oncogene*, 23(57), pp. 9183–9189. Available at: https://doi.org/10.1038/sj.onc.1208138.

Huang, C.-F. *et al.* (2017) 'NLRP3 inflammasome activation promotes inflammation-induced carcinogenesis in head and neck squamous cell carcinoma', *Journal of Experimental & Clinical Cancer Research*, 36(1), p. 116. Available at: https://doi.org/10.1186/s13046-017-0589-y.

Huang, E. *et al.* (2003) 'Gene expression predictors of breast cancer outcomes', *Lancet (London, England)*, 361(9369), pp. 1590–1596. Available at: https://doi.org/10.1016/S0140-6736(03)13308-9.

Ihrie, R.A. *et al.* (2005) 'Perp is a p63-regulated gene essential for epithelial integrity', *Cell*, 120(6), pp. 843–856. Available at: https://doi.org/10.1016/j.cell.2005.01.008.

Jeon, S., Allen-Hoffmann, B.L. and Lambert, P.F. (1995) 'Integration of human papillomavirus type 16 into the human genome correlates with a selective growth advantage of cells.', *Journal of Virology*, 69(5), pp. 2989–2997.

Johnson, D.E. *et al.* (2020) 'Head and neck squamous cell carcinoma', *Nature reviews. Disease primers*, 6(1), p. 92. Available at: https://doi.org/10.1038/s41572-020-00224-3.

Jung, A.C. *et al.* (2010) 'Biological and clinical relevance of transcriptionally active human papillomavirus (HPV) infection in oropharynx squamous cell carcinoma', *International Journal of Cancer*, 126(8), pp. 1882–1894. Available at: https://doi.org/10.1002/ijc.24911.

Jung, A.C. *et al.* (2013) 'CD8-alpha T-cell infiltration in human papillomavirus-related oropharyngeal carcinoma correlates with improved patient prognosis', *International Journal of Cancer*, 132(2), pp. E26-36. Available at: https://doi.org/10.1002/ijc.27776.

Kaghad, M. *et al.* (1997) 'Monoallelically Expressed Gene Related to p53 at 1p36, a Region Frequently Deleted in Neuroblastoma and Other Human Cancers', *Cell*, 90(4), pp. 809–819. Available at: https://doi.org/10.1016/S0092-8674(00)80540-1.

Kajiwara, C. *et al.* (2018) 'p63-Dependent Dickkopf3 Expression Promotes Esophageal Cancer Cell Proliferation via CKAP4', *Cancer Research*, 78(21), pp. 6107–6120. Available at: https://doi.org/10.1158/0008-5472.CAN-18-1749.

Kamal, M. *et al.* (2021) 'Human papilloma virus (HPV) integration signature in Cervical Cancer: identification of MACROD2 gene as HPV hot spot integration site', *British Journal of Cancer*, 124(4), pp. 777–785. Available at: https://doi.org/10.1038/s41416-020-01153-4.

Kammertoens, T., Schüler, T. and Blankenstein, T. (2005) 'Immunotherapy: target the stroma to hit the tumor', *Trends in Molecular Medicine*, 11(5), pp. 225–231. Available at: https://doi.org/10.1016/j.molmed.2005.03.002.

Kano, J. *et al.* (2022) 'Roles of DKK3 in cellular adhesion, motility, and invasion through extracellular interaction with TGFBI', *The FEBS Journal*, 289(20), pp. 6385–6399. Available at: https://doi.org/10.1111/febs.16529.

Katase, N. *et al.* (2018) 'DKK3 Overexpression Increases the Malignant Properties of Head and Neck Squamous Cell Carcinoma Cells', *Oncology Research*, 26(1), pp. 45–58. Available at: https://doi.org/10.3727/096504017X14926874596386.

Keam, S.J. (2023) 'Tremelimumab: First Approval', *Drugs*, 83(1), pp. 93–102. Available at: https://doi.org/10.1007/s40265-022-01827-8.

Keck, M.K. *et al.* (2015) 'Integrative Analysis of Head and Neck Cancer Identifies Two Biologically Distinct HPV and Three Non-HPV Subtypes', *Clinical Cancer Research*, 21(4), pp. 870–881. Available at: https://doi.org/10.1158/1078-0432.CCR-14-2481.

Kimura, H. *et al.* (2016) 'CKAP4 is a Dickkopf1 receptor and is involved in tumor progression', *Journal of Clinical Investigation*, 126(7), pp. 2689–2705. Available at: https://doi.org/10.1172/JCI84658.

King, K.E. *et al.* (2003) 'ΔNp63α functions as both a positive and a negative transcriptional regulator and blocks in vitro differentiation of murine keratinocytes', *Oncogene*, 22(23), pp. 3635–3644. Available at: https://doi.org/10.1038/sj.onc.1206536.

King, K.E. *et al.* (2019) 'Intersection of the p63 and NF-κB pathways in epithelial homeostasis and disease', *Molecular Carcinogenesis*, 58(9), pp. 1571–1580. Available at: https://doi.org/10.1002/mc.23081.

Koster, M.I. *et al.* (2006) 'Reactivation of developmentally expressed p63 isoforms predisposes to tumor development and progression', *Cancer Research*, 66(8), pp. 3981–3986. Available at: https://doi.org/10.1158/0008-5472.CAN-06-0027.

Kouwenhoven, E.N. *et al.* (2015) 'Transcription factor p63 bookmarks and regulates dynamic enhancers during epidermal differentiation', *EMBO Reports*, 16(7), pp. 863–878. Available at: https://doi.org/10.15252/embr.201439941.

Kouwenhoven, E.N., van Bokhoven, H. and Zhou, H. (2015) 'Gene regulatory mechanisms orchestrated by p63 in epithelial development and related disorders', *Biochimica et Biophysica Acta (BBA) - Gene Regulatory Mechanisms*, 1849(6), pp. 590–600. Available at: https://doi.org/10.1016/j.bbagrm.2015.03.003.

Kubo, T. *et al.* (2008) 'p63 induces CD4+ T-cell chemoattractant TARC/CCL17 in human epithelial cells', *Journal of Interferon & Cytokine Research: The Official Journal of the International Society for Interferon and Cytokine Research*, 28(12), pp. 725–732. Available at: https://doi.org/10.1089/jir.2008.0035.

Kumar, S. *et al.* (2018) 'ΔNp63-driven recruitment of myeloid-derived suppressor cells promotes metastasis in triple-negative breast cancer', *The Journal of Clinical Investigation*, 128(11), pp. 5095–5109. Available at: https://doi.org/10.1172/JCI99673.

Kunst, C. *et al.* (2016) 'The p53 family in hepatocellular carcinoma', *Translational Cancer Research*, 5(6), pp. 632–638. Available at: https://doi.org/10.21037/11030.

Kurahara, S. *et al.* (1999) 'Expression of MMPS, MT-MMP, and TIMPs in squamous cell carcinoma of the oral cavity: correlations with tumor invasion and metastasis', *Head & Neck*, 21(7), pp. 627–638. Available at: https://doi.org/10.1002/(sici)1097-0347(199910)21:7<627::aid-hed7>3.0.co;2-2.

Lahmamssi, C. *et al.* (2020) 'Désescalade thérapeutique dans les cancers de l'oropharynx induit par les HPV : mise au point', *Cancer/Radiothérapie*, 24(3), pp. 258–266. Available at: https://doi.org/10.1016/j.canrad.2019.12.003.

Lane, D.P. (1992) 'p53, guardian of the genome', *Nature*, 358(6381), pp. 15–16. Available at: https://doi.org/10.1038/358015a0.

LeBoeuf, M. *et al.* (2010) 'Hdac1 and Hdac2 act redundantly to control p63 and p53 functions in epidermal progenitor cells', *Developmental cell*, 19(6), pp. 807–818. Available at: https://doi.org/10.1016/j.devcel.2010.10.015.

Lee, E.-J. *et al.* (2009) 'Dkk3, downregulated in cervical cancer, functions as a negative regulator of β-catenin', *International Journal of Cancer*, 124(2), pp. 287–297. Available at: https://doi.org/10.1002/ijc.23913.

Lee, N.C.J. *et al.* (2018) 'Patterns of failure in high-metastatic node number human papillomavirus-positive oropharyngeal carcinoma', *Oral Oncology*, 85, pp. 35–39. Available at: https://doi.org/10.1016/j.oraloncology.2018.08.001.

Leemans, C.R., Braakhuis, B.J.M. and Brakenhoff, R.H. (2011) 'The molecular biology of head and neck cancer', *Nature Reviews Cancer*, 11(1), pp. 9–22. Available at: https://doi.org/10.1038/nrc2982.

Leoyklang, P., Siriwan, P. and Shotelersuk, V. (2006) 'A mutation of the p63 gene in non-syndromic cleft lip', *Journal of Medical Genetics*, 43(6), p. e28. Available at: https://doi.org/10.1136/jmg.2005.036442.

Liao, H. *et al.* (2021) 'CAN017, a novel anti-HER3 antibody, exerted great potency in mouse avatars of esophageal squamous cell carcinoma with NRG1 as a biomarker', *American Journal of Cancer Research*, 11(4), pp. 1697–1708.

Lin, F. *et al.* (2019) 'Association of CCL11, CCL24 and CCL26 with primary biliary cholangitis', *International Immunopharmacology*, 67, pp. 372–377. Available at: https://doi.org/10.1016/j.intimp.2018.12.026.

Lin, J., Teresky, A.K. and Levine, A.J. (1995) 'Two critical hydrophobic amino acids in the N-terminal domain of the p53 protein are required for the gain of function phenotypes of human p53 mutants', *Oncogene*, 10(12), pp. 2387–2390.

Lin-Shiao, E. *et al.* (2019) 'p63 establishes epithelial enhancers at critical craniofacial development genes', *Science Advances*, 5(5), p. eaaw0946. Available at: https://doi.org/10.1126/sciadv.aaw0946.

Liu, C. *et al.* (2018) 'The molecular mechanisms of increased radiosensitivity of HPV-positive oropharyngeal squamous cell carcinoma (OPSCC): an extensive review', *Journal of Otolaryngology - Head & Neck Surgery*, 47(1), p. 59. Available at: https://doi.org/10.1186/s40463-018-0302-y.

Lo Nigro, C. *et al.* (2017) 'Head and neck cancer: improving outcomes with a multidisciplinary approach', *Cancer Management and Research*, 9, pp. 363–371. Available at: https://doi.org/10.2147/CMAR.S115761.

Lorena, S. *et al.* (2003) 'Eotaxin expression in oral squamous cell carcinomas with and without tumour associated tissue eosinophilia', *Oral Diseases*, 9(6), pp. 279–283. Available at: https://doi.org/10.1034/j.1601-0825.2003.00958.x.

Luan, F. *et al.* (2020) 'TNFRSF11B activates Wnt/β-catenin signaling and promotes gastric cancer progression', *International Journal of Biological Sciences*, 16(11), pp. 1956–1971. Available at: https://doi.org/10.7150/ijbs.43630.

Ludwig, J. *et al.* (2015) 'Dickkopf-3 Acts as a Modulator of B Cell Fate and Function', *The Journal of Immunology*, 194(6), pp. 2624–2634. Available at: https://doi.org/10.4049/jimmunol.1402160.

Lyhne, N.M. *et al.* (2015) 'The DAHANCA 6 randomized trial: Effect of 6 vs 5 weekly fractions of radiotherapy in patients with glottic squamous cell carcinoma', *Radiotherapy and Oncology*, 117(1), pp. 91–98. Available at: https://doi.org/10.1016/j.radonc.2015.07.004.

Mangiulli, M. *et al.* (2009) 'Identification and functional characterization of two new transcriptional variants of the human p63 gene', *Nucleic Acids Research*, 37(18), pp. 6092–6104. Available at: https://doi.org/10.1093/nar/gkp674.

Mao, B. *et al.* (2001) 'LDL-receptor-related protein 6 is a receptor for Dickkopf proteins', *Nature*, 411(6835), pp. 321–325. Available at: https://doi.org/10.1038/35077108.

Martín-Hernán, F. *et al.* (2013) 'Oral cancer, HPV infection and evidence of sexual transmission', *Medicina Oral, Patología Oral y Cirugía Bucal*, 18(3), pp. e439–e444. Available at: https://doi.org/10.4317/medoral.18419.

McGrath, J.A. (2001) 'Hay-Wells syndrome is caused by heterozygous missense mutations in the SAM domain of p63', *Human Molecular Genetics*, 10(3), pp. 221–229. Available at: https://doi.org/10.1093/hmg/10.3.221.

McKenna, D.J. *et al.* (2010) 'MicroRNA 203 Expression in Keratinocytes Is Dependent on Regulation of p53 Levels by E6', *Journal of Virology*, 84(20), pp. 10644–10652. Available at: https://doi.org/10.1128/JVI.00703-10.

McKeon, F. (2004) 'p63 and the epithelial stem cell: more than status quo?', *Genes & Development*, 18(5), pp. 465–469. Available at: https://doi.org/10.1101/gad.1190504.

McKian, K.P. and Haluska, P. (2009) 'Cixutumumab', *Expert opinion on investigational drugs*, 18(7), pp. 1025–1033. Available at: https://doi.org/10.1517/13543780903055049.

Mehanna, H. *et al.* (2010) 'Oropharyngeal carcinoma related to human papillomavirus', *BMJ*, 340, p. c1439. Available at: https://doi.org/10.1136/bmj.c1439.

Mehanna, H. *et al.* (2019) 'Radiotherapy plus cisplatin or cetuximab in low-risk human papillomavirus-positive oropharyngeal cancer (De-ESCALaTE HPV): an open-label randomised controlled phase 3 trial', *Lancet (London, England)*, 393(10166), pp. 51–60. Available at: https://doi.org/10.1016/S0140-6736(18)32752-1.

Meister, M. *et al.* (2015) 'Dickkopf-3, a Tissue-Derived Modulator of Local T-Cell Responses', *Frontiers in Immunology*, 6, p. 78. Available at: https://doi.org/10.3389/fimmu.2015.00078.

Melino, G. (2003) 'Functional regulation of p73 and p63: development and cancer', *Trends in Biochemical Sciences*, 28(12), pp. 663–670. Available at: https://doi.org/10.1016/j.tibs.2003.10.004.

Michaud, D.S. *et al.* (2014) 'High-risk HPV types and head and neck cancer', *International Journal of Cancer*, 135(7), pp. 1653–1661. Available at: https://doi.org/10.1002/ijc.28811.

Mills, A.A. *et al.* (1999) ‘p63 is a p53 homologue required for limb and epidermal morphogenesis’, *Nature*, 398(6729), pp. 708–713. Available at: https://doi.org/10.1038/19531.

Mills, A.A. (2006) ‘p63: oncogene or tumor suppressor?’, *Current Opinion in Genetics & Development*, 16(1), pp. 38–44. Available at: https://doi.org/10.1016/j.gde.2005.12.001.

Mishra, A. and Meherotra, R. (2014) ‘Head and Neck Cancer: Global Burden and Regional Trends in India’, *Asian Pacific Journal of Cancer Prevention*, 15(2), pp. 537–550. Available at: https://doi.org/10.7314/APJCP.2014.15.2.537.

Missero, C. and Antonini, D. (2014) ‘Crosstalk among p53 family members in cutaneous carcinoma’, *Experimental Dermatology*, 23(3), pp. 143–146. Available at: https://doi.org/10.1111/exd.12320.

Moossavi, M. *et al.* (2018) ‘Role of the NLRP3 inflammasome in cancer’, *Molecular Cancer*, 17(1), p. 158. Available at: https://doi.org/10.1186/s12943-018-0900-3.

Mourtada, J. *et al.* (2023) ‘A novel ΔNp63-dependent immune mechanism improves prognosis of HPV-related head and neck cancer’, *Frontiers in Immunology*, 14. Available at: https://www.frontiersin.org/articles/10.3389/fimmu.2023.1264093 (Accessed: 27 October 2023).

Moutafi, M. *et al.* (2023) ‘Phase II Window Study of Olaparib Alone or with Cisplatin or Durvalumab in Operable Head and Neck Cancer’, *Cancer Research Communications*, 3(8), pp. 1514–1523. Available at: https://doi.org/10.1158/2767-9764.CRC-23-0051.

Nagel, R. *et al.* (2013) ‘Treatment response of HPV-positive and HPV-negative head and neck squamous cell carcinoma cell lines’, *Oral Oncology*, 49(6), pp. 560–566. Available at: https://doi.org/10.1016/j.oraloncology.2013.03.446.

Nekulova, M. *et al.* (2013) ‘Characterization of specific p63 and p63-N-terminal isoform antibodies and their application for immunohistochemistry’, *Virchows Archiv*, 463(3), pp. 415–425. Available at: https://doi.org/10.1007/s00428-013-1459-4.

Nguyen, Q.T.T. *et al.* (2022) ‘DKK3, Downregulated in Invasive Epithelial Ovarian Cancer, Is Associated with Chemoresistance and Enhanced Paclitaxel Susceptibility via Inhibition of the β-Catenin-P-Glycoprotein Signaling Pathway’, *Cancers*, 14(4), p. 924. Available at: https://doi.org/10.3390/cancers14040924.

Nie, X.-C. *et al.* (2021) ‘Combined Serum DKK3 and Circulating CD133 Cells as Prognostic Biomarkers for Ovarian Cancer Patients’, *OncoTargets and therapy*, 14, pp. 427–434. Available at: https://doi.org/10.2147/OTT.S288191.

Nylander, K. *et al.* (2002) ‘Differential expression of p63 isoforms in normal tissues and neoplastic cells’, *The Journal of Pathology*, 198(4), pp. 417–427. Available at: https://doi.org/10.1002/path.1231.

O-Charoenrat, P., Rhys-Evans, P.H. and Eccles, S.A. (2001) ‘Expression of matrix metalloproteinases and their inhibitors correlates with invasion and metastasis in squamous cell carcinoma of the head and neck’, *Archives of Otolaryngology--Head & Neck Surgery*, 127(7), pp. 813–820.

Osada, M. *et al.* (2005) ‘Differential Recognition of Response Elements Determines Target Gene Specificity forp53 and p63’, *Molecular and Cellular Biology*, 25(14), pp. 6077–6089. Available at: https://doi.org/10.1128/MCB.25.14.6077-6089.2005.

Osterburg, C. and Dötsch, V. (2022) 'Structural diversity of p63 and p73 isoforms', *Cell Death & Differentiation*, 29(5), pp. 921–937. Available at: https://doi.org/10.1038/s41418-022-00975-4.

Ozbun, M.A. (2002) 'Human Papillomavirus Type 31b Infection of Human Keratinocytes and the Onset of Early Transcription', *Journal of Virology*, 76(22), pp. 11291–11300. Available at: https://doi.org/10.1128/JVI.76.22.11291-11300.2002.

Pai, S.I. and Westra, W.H. (2009) 'Molecular pathology of head and neck cancer: implications for diagnosis, prognosis, and treatment', *Annual Review of Pathology*, 4, pp. 49–70. Available at: https://doi.org/10.1146/annurev.pathol.4.110807.092158.

Papatriantafyllou, M. *et al.* (2012) 'Dickkopf-3, an immune modulator in peripheral CD8 T-cell tolerance', *Proceedings of the National Academy of Sciences of the United States of America*, 109(5), pp. 1631–1636. Available at: https://doi.org/10.1073/pnas.1115980109.

Parfenov, M. *et al.* (2014) 'Characterization of HPV and host genome interactions in primary head and neck cancers', *Proceedings of the National Academy of Sciences*, 111(43), pp. 15544–15549. Available at: https://doi.org/10.1073/pnas.1416074111.

Parsa, R. *et al.* (1999) 'Association of p63 with proliferative potential in normal and neoplastic human keratinocytes', *The Journal of Investigative Dermatology*, 113(6), pp. 1099–1105. Available at: https://doi.org/10.1046/j.1523-1747.1999.00780.x.

Patturajan, M. *et al.* (2002) 'DeltaNp63 induces beta-catenin nuclear accumulation and signaling', *Cancer Cell*, 1(4), pp. 369–379. Available at: https://doi.org/10.1016/s1535-6108(02)00057-0.

Peeney, D. *et al.* (2020) 'TIMP-2 suppresses tumor growth and metastasis in murine model of triple-negative breast cancer', *Carcinogenesis*, 41(3), pp. 313–325. Available at: https://doi.org/10.1093/carcin/bgz172.

Pellegrini, G. *et al.* (2001) 'p63 identifies keratinocyte stem cells', *Proceedings of the National Academy of Sciences of the United States of America*, 98(6), pp. 3156–3161. Available at: https://doi.org/10.1073/pnas.061032098.

Perou, C.M. *et al.* (2000) 'Molecular portraits of human breast tumours', *Nature*, 406(6797), pp. 747–752. Available at: https://doi.org/10.1038/35021093.

Petitjean, A. *et al.* (2007) 'Impact of mutant p53 functional properties on TP53 mutation patterns and tumor phenotype: lessons from recent developments in the IARC TP53 database', *Human Mutation*, 28(6), pp. 622–629. Available at: https://doi.org/10.1002/humu.20495.

Pignon, J.-P. *et al.* (2009) 'Meta-analysis of chemotherapy in head and neck cancer (MACH-NC): An update on 93 randomised trials and 17,346 patients', *Radiotherapy and Oncology*, 92(1), pp. 4–14. Available at: https://doi.org/10.1016/j.radonc.2009.04.014.

Pozniak, C.D. *et al.* (2002) 'p73 Is Required for Survival and Maintenance of CNS Neurons', *The Journal of Neuroscience*, 22(22), pp. 9800–9809. Available at: https://doi.org/10.1523/JNEUROSCI.22-22-09800.2002.

Propping, P. *et al.* (2000) 'ADULT syndrome allelic to limb mammary syndrome (LMS)?', *American Journal of Medical Genetics*, 90(2), pp. 179–182.

Pruneri, G. *et al.* (2005) 'The transactivating isoforms of p63 are overexpressed in high-grade follicular lymphomas independent of the occurrence of p63 gene amplification', *The Journal of Pathology*, 206(3), pp. 337–345. Available at: https://doi.org/10.1002/path.1787.

Punt, S. *et al.* (2016) 'A beneficial tumor microenvironment in oropharyngeal squamous cell carcinoma is characterized by a high T cell and low IL-17+ cell frequency', *Cancer Immunology, Immunotherapy*, 65, pp. 393–403. Available at: https://doi.org/10.1007/s00262-016-1805-x.

Qi, Z. *et al.* (2019) 'Single-cell sequencing and its applications in head and neck cancer', *Oral Oncology*, 99, p. 104441. Available at: https://doi.org/10.1016/j.oraloncology.2019.104441.

Raff, A.B. *et al.* (2013) 'The Evolving Field of Human Papillomavirus Receptor Research: a Review of Binding and Entry', *Journal of Virology*, 87(11), pp. 6062–6072. Available at: https://doi.org/10.1128/JVI.00330-13.

Ramaswamy, S. *et al.* (2001) 'Multiclass cancer diagnosis using tumor gene expression signatures', *Proceedings of the National Academy of Sciences of the United States of America*, 98(26), pp. 15149–15154. Available at: https://doi.org/10.1073/pnas.211566398.

Rinne, T. *et al.* (2006) 'Pattern of p63 mutations and their phenotypes--update', *American Journal of Medical Genetics. Part A*, 140(13), pp. 1396–1406. Available at: https://doi.org/10.1002/ajmg.a.31271.

Rinne, T., Brunner, H.G. and van Bokhoven, H. (2007) 'p63-associated disorders', *Cell Cycle (Georgetown, Tex.)*, 6(3), pp. 262–268. Available at: https://doi.org/10.4161/cc.6.3.3796.

Rocco, J.W. *et al.* (2006) 'p63 mediates survival in squamous cell carcinoma by suppression of p73-dependent apoptosis', *Cancer Cell*, 9(1), pp. 45–56. Available at: https://doi.org/10.1016/j.ccr.2005.12.013.

Roh, J.S. and Sohn, D.H. (2018) 'Damage-Associated Molecular Patterns in Inflammatory Diseases', *Immune Network*, 18(4), p. e27. Available at: https://doi.org/10.4110/in.2018.18.e27.

Roman, A. and Munger, K. (2013) 'The papillomavirus E7 proteins', *Virology*, 445(1–2), pp. 138–168. Available at: https://doi.org/10.1016/j.virol.2013.04.013.

Romano, R.-A. *et al.* (2009) 'An active role of the DeltaN isoform of p63 in regulating basal keratin genes K5 and K14 and directing epidermal cell fate', *PloS One*, 4(5), p. e5623. Available at: https://doi.org/10.1371/journal.pone.0005623.

Romano, R.-A. *et al.* (2012) 'ΔNp63 knockout mice reveal its indispensable role as a master regulator of epithelial development and differentiation', *Development (Cambridge, England)*, 139(4), pp. 772–782. Available at: https://doi.org/10.1242/dev.071191.

Romano, R.-A., Birkaya, B. and Sinha, S. (2007) 'A functional enhancer of keratin14 is a direct transcriptional target of deltaNp63', *The Journal of Investigative Dermatology*, 127(5), pp. 1175–1186. Available at: https://doi.org/10.1038/sj.jid.5700652.

Rosenthal, E.L. and Matrisian, L.M. (2006) 'MATRIX METALLOPROTEASES IN HEAD AND NECK CANCER', *Head & neck*, 28(7), pp. 639–648. Available at: https://doi.org/10.1002/hed.20365.

Rowhani-Rahbar, A. *et al.* (2009) 'Antibody responses in oral fluid following administration of prophylactic human papillomavirus vaccines', *The Journal of Infectious Diseases*, 200(9), pp. 1452–1455. Available at: https://doi.org/10.1086/606026.

Sakkal, S. *et al.* (no date) 'Eosinophils in Cancer: Favourable or Unfavourable?', *Current Medicinal Chemistry*, 23(7), pp. 650–666.

Saloura, V. *et al.* (2014) 'Correlation of T-cell inflamed phenotype with mesenchymal subtype, expression of PD-L1, and other immune checkpoints in head and neck cancer.', *Journal of Clinical Oncology*, 32(15_suppl), pp. 6009–6009. Available at: https://doi.org/10.1200/jco.2014.32.15_suppl.6009.

Sapp, M. and Bienkowska-Haba, M. (2009) 'Viral entry mechanisms: human papillomavirus and a long journey from extracellular matrix to the nucleus', *The FEBS journal*, 276(24), pp. 7206–7216. Available at: https://doi.org/10.1111/j.1742-4658.2009.07400.x.

Sauer, M. *et al.* (2008) 'C-terminal diversity within the p53 family accounts for differences in DNA binding and transcriptional activity', *Nucleic Acids Research*, 36(6), pp. 1900–1912. Available at: https://doi.org/10.1093/nar/gkn044.

Scheffner, M. *et al.* (1992) 'Targeted degradation of the retinoblastoma protein by human papillomavirus E7-E6 fusion proteins.', *The EMBO Journal*, 11(7), pp. 2425–2431. Available at: https://doi.org/10.1002/j.1460-2075.1992.tb05307.x.

Segre, J.A. (2006) 'Epidermal barrier formation and recovery in skin disorders', *The Journal of Clinical Investigation*, 116(5), pp. 1150–1158. Available at: https://doi.org/10.1172/JCI28521.

da Silva Cardeal, L.B. *et al.* (2006) 'Higher expression and activity of metalloproteinases in human cervical carcinoma cell lines is associated with HPV presence', *Biochemistry and Cell Biology = Biochimie Et Biologie Cellulaire*, 84(5), pp. 713–719. Available at: https://doi.org/10.1139/o06-084.

Smith, E.M. *et al.* (2004) 'Age, sexual behavior and human papillomavirus infection in oral cavity and oropharyngeal cancers', *International Journal of Cancer*, 108(5), pp. 766–772. Available at: https://doi.org/10.1002/ijc.11633.

Smotkin, D. and Wettstein, F.O. (1986) 'Transcription of human papillomavirus type 16 early genes in a cervical cancer and a cancer-derived cell line and identification of the E7 protein', *Proceedings of the National Academy of Sciences of the United States of America*, 83(13), pp. 4680–4684. Available at: https://doi.org/10.1073/pnas.83.13.4680.

Snelling, S.J.B. *et al.* (2016) 'Dickkopf-3 is upregulated in osteoarthritis and has a chondroprotective role', *Osteoarthritis and Cartilage*, 24(5), pp. 883–891. Available at: https://doi.org/10.1016/j.joca.2015.11.021.

Somerville, T.D. *et al.* (no date) 'Squamous trans-differentiation of pancreatic cancer cells promotes stromal inflammation', *eLife*, 9, p. e53381. Available at: https://doi.org/10.7554/eLife.53381.

Sørlie, T. *et al.* (2001) 'Gene expression patterns of breast carcinomas distinguish tumor subclasses with clinical implications', *Proceedings of the National Academy of Sciences of the United States of America*, 98(19), pp. 10869–10874. Available at: https://doi.org/10.1073/pnas.191367098.

Spence, T. *et al.* (2016) 'HPV Associated Head and Neck Cancer', *Cancers*, 8(8), p. 75. Available at: https://doi.org/10.3390/cancers8080075.

Srivastava, R.M. *et al.* (2017) 'CD137 Stimulation Enhances Cetuximab-Induced Natural Killer: Dendritic Cell Priming of Antitumor T-Cell Immunity in Patients with Head and Neck Cancer', *Clinical Cancer Research: An Official Journal of the American Association for Cancer Research*, 23(3), pp. 707–716. Available at: https://doi.org/10.1158/1078-0432.CCR-16-0879.

St Guily, J.L. *et al.* (2011) 'Human papillomavirus genotype distribution in oropharynx and oral cavity cancer in France—The EDiTH VI study', *Journal of Clinical Virology*, 51(2), pp. 100–104. Available at: https://doi.org/10.1016/j.jcv.2011.03.003.

Stein, A.P. *et al.* (2015) 'Prevalence of human papillomavirus in oropharyngeal cancer: a systematic review', *Cancer journal (Sudbury, Mass.)*, 21(3), pp. 138–146. Available at: https://doi.org/10.1097/PPO.0000000000000115.

Stetler-Stevenson, W.G. (2008) 'Tissue Inhibitors of Metalloproteinases in Cell Signaling: Metalloproteinase-Independent Biological Activities', *Science Signaling*, 1(27), pp. re6–re6. Available at: https://doi.org/10.1126/scisignal.127re6.

Stransky, N. *et al.* (2011) 'The Mutational Landscape of Head and Neck Squamous Cell Carcinoma', *Science (New York, N.Y.)*, 333(6046), pp. 1157–1160. Available at: https://doi.org/10.1126/science.1208130.

Sun, A., Li, Y. and Jiang, X. (2022) 'CCL26 silence represses colon cancer by inhibiting the EMT signaling pathway', *Tissue and Cell*, 79, p. 101937. Available at: https://doi.org/10.1016/j.tice.2022.101937.

Syrjänen, K.J. *et al.* (1983) 'Immunohistochemical demonstration of Human papilloma virus (HPV) antigens in oral squamous cell lesions', *British Journal of Oral Surgery*, 21(2), pp. 147–153. Available at: https://doi.org/10.1016/0007-117X(83)90060-4.

Takano, K. *et al.* (2016) 'Expression of Inflammasome-Associated Proteins in Human Oropharyngeal Squamous Cell Carcinoma'. Available at: https://doi.org/10.1159/000441884.

Talamini, R. *et al.* (2002) 'Combined effect of tobacco and alcohol on laryngeal cancer risk: a case-control study', *Cancer causes & control: CCC*, 13(10), pp. 957–964. Available at: https://doi.org/10.1023/a:1021944123914.

Thomas, J.K. *et al.* (2019) 'CC chemokines are differentially expressed in Breast Cancer and are associated with disparity in overall survival', *Scientific Reports*, 9(1), p. 4014. Available at: https://doi.org/10.1038/s41598-019-40514-9.

Thomas, J.T. and Laimins, L.A. (1998) 'Human Papillomavirus Oncoproteins E6 and E7 Independently Abrogate the Mitotic Spindle Checkpoint', *Journal of Virology*, 72(2), pp. 1131–1137. Available at: https://doi.org/10.1128/jvi.72.2.1131-1137.1998.

Thurlow, J.K. *et al.* (2010) 'Spectral Clustering of Microarray Data Elucidates the Roles of Microenvironment Remodeling and Immune Responses in Survival of Head and Neck Squamous Cell Carcinoma', *Journal of Clinical Oncology* [Preprint]. Available at: https://doi.org/10.1200/JCO.2009.24.8724.

Tran, M.N. *et al.* (2013) 'The p63 protein isoform ΔNp63α inhibits epithelial-mesenchymal transition in human bladder cancer cells: role of MIR-205', *The Journal of Biological Chemistry*, 288(5), pp. 3275–3288. Available at: https://doi.org/10.1074/jbc.M112.408104.

Truong, A.B. *et al.* (2006) 'p63 regulates proliferation and differentiation of developmentally mature keratinocytes', *Genes & Development*, 20(22), pp. 3185–3197. Available at: https://doi.org/10.1101/gad.1463206.

Truong, A.B. and Khavari, P.A. (2007) 'Control of keratinocyte proliferation and differentiation by p63', *Cell Cycle (Georgetown, Tex.)*, 6(3), pp. 295–299. Available at: https://doi.org/10.4161/cc.6.3.3753.

Tsang, C.M. *et al.* (2020) 'Translational genomics of nasopharyngeal cancer', *Seminars in Cancer Biology*, 61, pp. 84–100. Available at: https://doi.org/10.1016/j.semcancer.2019.09.006.

Tsuji, T. *et al.* (2000) 'A REIC Gene Shows Down-Regulation in Human Immortalized Cells and Human Tumor-Derived Cell Lines', *Biochemical and Biophysical Research Communications*, 268(1), pp. 20–24. Available at: https://doi.org/10.1006/bbrc.1999.2067.

Vakonaki, E. *et al.* (2012) 'Overexpression and ratio disruption of ΔNp63 and TAp63 isoform equilibrium in endometrial adenocarcinoma: correlation with obesity, menopause, and grade I/II tumors', *Journal of Cancer Research and Clinical Oncology*, 138(8), pp. 1271–1278. Available at: https://doi.org/10.1007/s00432-012-1200-8.

Van Bokhoven, H. *et al.* (2001) 'p63 Gene Mutations in EEC Syndrome, Limb-Mammary Syndrome, and Isolated Split Hand–Split Foot Malformation Suggest a Genotype-Phenotype Correlation', *The American Journal of Human Genetics*, 69(3), pp. 481–492. Available at: https://doi.org/10.1086/323123.

Veeck, J. *et al.* (2008) 'Wnt signalling in human breast cancer: expression of the putative Wnt inhibitor Dickkopf-3 (DKK3) is frequently suppressed by promoter hypermethylation in mammary tumours', *Breast Cancer Research : BCR*, 10(5), p. R82. Available at: https://doi.org/10.1186/bcr2151.

Veeck, J. and Dahl, E. (2012) 'Targeting the Wnt pathway in cancer: The emerging role of Dickkopf-3', *Biochimica et Biophysica Acta (BBA) - Reviews on Cancer*, 1825(1), pp. 18–28. Available at: https://doi.org/10.1016/j.bbcan.2011.09.003.

Vermeer, D.W. *et al.* (2016) 'Metastatic model of HPV+ oropharyngeal squamous cell carcinoma demonstrates heterogeneity in tumor metastasis', *Oncotarget*, 7(17), pp. 24194–24207. Available at: https://doi.org/10.18632/oncotarget.8254.

Vermorken, J.B. *et al.* (2008) 'Platinum-Based Chemotherapy plus Cetuximab in Head and Neck Cancer', *New England Journal of Medicine*, 359(11), pp. 1116–1127. Available at: https://doi.org/10.1056/NEJMoa0802656.

Veyer, D. *et al.* (2019) 'HPV detection and genotyping of head and neck cancer biopsies by molecular testing with regard to the new oropharyngeal squamous cell carcinoma classification based on HPV status', *Pathology*, 51(4), pp. 421–425. Available at: https://doi.org/10.1016/j.pathol.2019.02.002.

Viens, L.J. *et al.* (2016) 'Human Papillomavirus-Associated Cancers - United States, 2008-2012', *MMWR. Morbidity and mortality weekly report*, 65(26), pp. 661–666. Available at: https://doi.org/10.15585/mmwr.mm6526a1.

de Villiers, E.-M. *et al.* (2004) 'Classification of papillomaviruses', *Virology*, 324(1), pp. 17–27. Available at: https://doi.org/10.1016/j.virol.2004.03.033.

Vogelstein, B., Lane, D. and Levine, A.J. (2000) 'Surfing the p53 network', *Nature*, 408(6810), pp. 307–310. Available at: https://doi.org/10.1038/35042675.

Vousden, K.H. and Prives, C. (2009) 'Blinded by the Light: The Growing Complexity of p53', *Cell*, 137(3), pp. 413–431. Available at: https://doi.org/10.1016/j.cell.2009.04.037.

Walter, V. *et al.* (2013) 'Molecular subtypes in head and neck cancer exhibit distinct patterns of chromosomal gain and loss of canonical cancer genes', *PloS One*, 8(2), p. e56823. Available at: https://doi.org/10.1371/journal.pone.0056823.

Wang, N. *et al.* (2010) 'Cables1 protects p63 from proteasomal degradation to ensure deletion of cells after genotoxic stress', *EMBO reports*, 11(8), pp. 633–639. Available at: https://doi.org/10.1038/embor.2010.82.

Wang, X. *et al.* (2015) 'Dickkopf Homolog 3 Induces Stem Cell Differentiation into Smooth Muscle Lineage via ATF6 Signalling', *Journal of Biological Chemistry*, 290(32), pp. 19844–19852. Available at: https://doi.org/10.1074/jbc.M115.641415.

Wang, Z. *et al.* (2015) 'Dickkopf-3 (Dkk3) induces apoptosis in cisplatin-resistant lung adenocarcinoma cells via the Wnt/β-catenin pathway', *Oncology Reports*, 33(3), pp. 1097–1106. Available at: https://doi.org/10.3892/or.2014.3704.

Werness, B.A. (no date) 'The E6 Oncoprotein Encoded by Human Papillomavirus Types 16 and 18 Promotes the Degradation of ~53'.

Westfall, M.D. *et al.* (2003) 'The ΔNp63α Phosphoprotein Binds the p21 and 14-3-3σ Promoters In Vivo and Has Transcriptional Repressor Activity That Is Reduced by Hay-Wells Syndrome-Derived Mutations', *Molecular and Cellular Biology*, 23(7), pp. 2264–2276. Available at: https://doi.org/10.1128/MCB.23.7.2264-2276.2003.

Westra, W.H. *et al.* (2008) 'Inverse relationship between human papillomavirus-16 infection and disruptive p53 gene mutations in squamous cell carcinoma of the head and neck', *Clinical Cancer Research: An Official Journal of the American Association for Cancer Research*, 14(2), pp. 366–369. Available at: https://doi.org/10.1158/1078-0432.CCR-07-1402.

Wong, I.C.K., Ng, Y.-K. and Lui, V.W.Y. (2014) 'Cancers of the lung, head and neck on the rise: perspectives on the genotoxicity of air pollution', *Chinese Journal of Cancer*, 33(10), pp. 476–480. Available at: https://doi.org/10.5732/cjc.014.10093.

Wu, G. *et al.* (2005) 'DeltaNp63alpha up-regulates the Hsp70 gene in human cancer', *Cancer Research*, 65(3), pp. 758–766.

Wu, S.-Y. and Chiang, C.-M. (2007) 'The Double Bromodomain-containing Chromatin Adaptor Brd4 and Transcriptional Regulation', *Journal of Biological Chemistry*, 282(18), pp. 13141–13145. Available at: https://doi.org/10.1074/jbc.R700001200.

Xu, Y. *et al.* (2020) 'DKK3 attenuates JNK and AP-1 induced inflammation via Kremen-1 and DVL-1 in mice following intracerebral hemorrhage', *Journal of Neuroinflammation*, 17(1), p. 130. Available at: https://doi.org/10.1186/s12974-020-01794-5.

Yang, A. *et al.* (1998) 'p63, a p53 Homolog at 3q27–29, Encodes Multiple Products with Transactivating, Death-Inducing, and Dominant-Negative Activities', *Molecular Cell*, 2(3), pp. 305–316. Available at: https://doi.org/10.1016/S1097-2765(00)80275-0.

Yang, A. *et al.* (1999) 'p63 is essential for regenerative proliferation in limb, craniofacial and epithelial development', *Nature*, 398(6729), pp. 714–718. Available at: https://doi.org/10.1038/19539.

Yang, A. *et al.* (2000) 'p73-deficient mice have neurological, pheromonal and inflammatory defects but lack spontaneous tumours', *Nature*, 404(6773), pp. 99–103. Available at: https://doi.org/10.1038/35003607.

Yang, X. *et al.* (2011) 'ΔNp63 Versatilely Regulates a Broad *NF-κB* Gene Program and Promotes Squamous Epithelial Proliferation, Migration, and Inflammation', *Cancer Research*, 71(10), pp. 3688–3700. Available at: https://doi.org/10.1158/0008-5472.CAN-10-3445.

Yao, J.-Y. and Chen, J.-K. (2012) 'Roles of p63 in epidermal development and tumorigenesis', *Biomedical Journal*, 35(6), pp. 457–463. Available at: https://doi.org/10.4103/2319-4170.104410.

Ying, H. *et al.* (2005) 'DNA-binding and transactivation activities are essential for TAp63 protein degradation', *Molecular and Cellular Biology*, 25(14), pp. 6154–6164. Available at: https://doi.org/10.1128/MCB.25.14.6154-6164.2005.

Yu, B. *et al.* (2017) 'A Cytokine-Like Protein Dickkopf-Related Protein 3 Is Atheroprotective', *Circulation*, 136(11), pp. 1022–1036. Available at: https://doi.org/10.1161/CIRCULATIONAHA.117.027690.

Yu, P. *et al.* (2005) 'Intratumor depletion of CD4+ cells unmasks tumor immunogenicity leading to the rejection of late-stage tumors', *The Journal of Experimental Medicine*, 201(5), pp. 779–791. Available at: https://doi.org/10.1084/jem.20041684.

Zangen, R., Ratovitski, E.A. and Sidransky, D. (2005) 'ΔNp63α Levels Correlate with Clinical Tumor Response to Cisplatin', *Cell Cycle*, 4(10), pp. 1313–1315. Available at: https://doi.org/10.4161/cc.4.10.2066.

Zenzmaier, C. *et al.* (2013) 'Dickkopf-related protein 3 promotes pathogenic stromal remodeling in benign prostatic hyperplasia and prostate cancer', *The Prostate*, 73(13), pp. 1441–1452. Available at: https://doi.org/10.1002/pros.22691.

Zhang, Y. *et al.* (2014) 'Dickkopf-3 attenuates pressure overload-induced cardiac remodelling', *Cardiovascular Research*, 102(1), pp. 35–45. Available at: https://doi.org/10.1093/cvr/cvu004.

Zheng, Z.-M. and Baker, C.C. (2006) 'Papillomavirus genome structure, expression, and post-transcriptional regulation', *Frontiers in Bioscience-Landmark*, 11(3), pp. 2286–2302. Available at: https://doi.org/10.2741/1971.

Zhou, Y. *et al.* (2020) 'ΔNp63α exerts antitumor functions in cervical squamous cell carcinoma', *Oncogene*, 39(4), pp. 905–921. Available at: https://doi.org/10.1038/s41388-019-1033-x.

Zilfou, J.T. and Lowe, S.W. (2009) 'Tumor Suppressive Functions of p53', *Cold Spring Harbor Perspectives in Biology*, 1(5), p. a001883. Available at: https://doi.org/10.1101/cshperspect.a001883.

ANNEXE

Tumor-Suppressive and Immunomodulating Activity of miR-30a-3p and miR-30e-3p in HNSCC Cells and Tumoroids

Ombline Conrad [1] , Mickaël Burgy [1,2] , Sophie Foppolo [1] , Aude Jehl [1] , Alicia Thiéry [3], Sébastien Guihard [4], Romain Vauchelles [1], Alain C. Jung [5,6], **Jana Mourtada** [5] , Christine Macabre [5,6], Sonia Ledrappier [5,6], Marie-Pierre Chenard [7], Mihaela-Alina Onea [7], Aurélien Danic [8], Thomas Dourlhes [8], Claire Thibault [8],Philippe Schultz [8], Monique Dontenwill [1] and Sophie Martin [1,*]

Dans cet article publié par Conrad et al., j'ai participé à la mise en place et à l'optimisation du protocole de phagocytose.

Résumé : Les carcinomes épidermoïdes de la tête et du cou (HNSCC) sont des tumeurs hétérogènes, bien connues pour leur nature récidivante fréquente. Afin de lutter contre les récidives, il est urgent de disposer de biomarqueurs pour le diagnostic précoce, le pronostic ou la prédiction de la réponse au traitement. Les miARN peuvent avoir un impact profond sur la physiologie normale et favoriser l'oncogenèse. Parmi tous les miARN, la famille miR-30 est fréquemment régulée à la baisse dans les HNSCC. Ici, nous avons déterminé comment les niveaux des brins passagers 3p de miR-30a et miR-30e affectent le comportement tumoral et clarifié leur rôle fonctionnel dans le LA-HNSCC. Dans une étude rétrospective, les niveaux de miR-30a-3p et miR-30e-3p ont été déterminés chez 110 patients et corrélés à la survie globale, à la rechute locorégionale et aux métastases à distance. miR-30a/e-3p ont été exprimés dans des lignées cellulaires HNSCC et des tumeurs dérivées de patients HNSCC (PDT) afin d'étudier leur effet sur les cellules tumorales et leur microenvironnement. Les deux miARN ont une valeur pronostique, car une faible expression de miR-30a/e-3p est corrélée à un pronostic défavorable et réduit la survie globale. Une faible expression de miR-30a/e-3p est associée à un délai plus court jusqu'à la rechute locorégionale et à un délai plus court jusqu'à la métastase, respectivement. L'expression de miR-30a/e-3p régule à la baisse le TGF-βR1 et le BMPR2 et atténue la survie et la motilité des HNSCC. Les résultats ont été confirmés dans les PDT. Enfin, les sécrétomes des cellules HNSCC transfectées par miR-30a/e-3p activent les macrophages de type M1, qui exercent une activité phagocytaire plus forte à l'égard des cellules tumorales. L'expression des miR-30a/e-3p peut discriminer des sous-groupes de patients HNSCC LA- ayant des pronostics différents, ce qui en fait de bons candidats comme biomarqueurs de pronostic. En outre, en ciblant les membres de la famille TGF-β et en générant un microenvironnement immunitaire favorable, ils pourraient devenir une alternative aux médicaments anti-TGF-β à utiliser en combinaison avec les inhibiteurs de points de contrôle immunitaire.

International Journal of
Molecular Sciences

MDPI

Article

Tumor-Suppressive and Immunomodulating Activity of miR-30a-3p and miR-30e-3p in HNSCC Cells and Tumoroids

Ombline Conrad [1], Mickaël Burgy [1,2], Sophie Foppolo [1], Aude Jehl [1], Alicia Thiéry [3], Sébastien Guihard [4], Romain Vauchelles [1], Alain C. Jung [5,6], Jana Mourtada [5], Christine Macabre [5,6], Sonia Ledrappier [5,6], Marie-Pierre Chenard [7], Mihaela-Alina Onea [7], Aurélien Danic [8], Thomas Dourlhes [8], Claire Thibault [8], Philippe Schultz [8], Monique Dontenwill [1] and Sophie Martin [1,*]

1 Laboratory of Bioimaging and Pathology, University of Strasbourg, UMR7021 CNRS, 67401 Illkirch, France; ombline.conrad@etu.unistra.fr (O.C.); m.burgy@icans.eu (M.B.); sophie.foppolo@unistra.fr (S.F.); monique.dontenwill@unistra.fr (M.D.)
2 Department of Medical Oncology, Institut de Cancérologie Strasbourg Europe, 67200 Strasbourg, France
3 Department of Public Health, Institut de Cancérologie Strasbourg Europe, 67200 Strasbourg, France
4 Department of Radiotherapy, Institut de Cancérologie Strasbourg Europe, 67200 Strasbourg, France
5 Laboratory STREINTH, Inserm IRFAC U1113, Université de Strasbourg, 67200 Strasbourg, France; a.jung@icans.eu (A.C.J.)
6 Laboratory of Tumor Biology, Institut de Cancérologie Strasbourg Europe, 67200 Strasbourg, France
7 Department of Pathology, Strasbourg University Hospital, 67200 Strasbourg, France; marie-pierrette.chenard@chru-strasbourg.fr (M.-P.C.)
8 Department of Otolaryngology and Cervico-Facial Surgery, Strasbourg University Hospital, 67200 Strasbourg, France; philippe.schultz@chru-strasbourg.fr (P.S.)
* Correspondence: sophie.martin@unistra.fr; Tel.: +33-36-885-4197; Fax: +33-36-885-4313

Abstract: Head and neck squamous cell carcinomas (HNSCCs) are heterogeneous tumors, well known for their frequent relapsing nature. To counter recurrence, biomarkers for early diagnosis, prognosis, or treatment response prediction are urgently needed. miRNAs can profoundly impact normal physiology and enhance oncogenesis. Among all of the miRNAs, the miR-30 family is frequently downregulated in HNSCC. Here, we determined how levels of the 3p passenger strands of miR-30a and miR-30e affect tumor behavior and clarified their functional role in LA-HNSCC. In a retrospective study, levels of miR-30a-3p and miR-30e-3p were determined in 110 patients and correlated to overall survival, locoregional relapse, and distant metastasis. miR-30a/e-3p were expressed in HNSCC cell lines and HNSCC patient-derived tumoroids (PDTs) to investigate their effect on tumor cells and their microenvironment. Both miRNAs were found to have a prognosis value since low miR-30a/e-3p expression correlates to adverse prognosis and reduces overall survival. Low expression of miR-30a/e-3p is associated with a shorter time until locoregional relapse and a shorter time until metastasis, respectively. miR-30a/e-3p expression downregulates both TGF-βR1 and BMPR2 and attenuates the survival and motility of HNSCC. Results were confirmed in PDTs. Finally, secretomes of miR-30a/e-3p-transfected HNSCC activate M1-type macrophages, which exert stronger phagocytic activities toward tumor cells. miR-30a/e-3p expression can discriminate subgroups of LA-HNSCC patients with different prognosis, making them good candidates as prognostic biomarkers. Furthermore, by targeting members of the TGF-β family and generating an immune-permissive microenvironment, they may emerge as an alternative to anti-TGF-β drugs to use in combination with immune checkpoint inhibitors.

Keywords: head and neck cancers; microRNA; tumoroid; biomarkers; phagocytosis

Citation: Conrad, O.; Burgy, M.; Foppolo, S.; Jehl, A.; Thiéry, A.; Guihard, S.; Vauchelles, R.; Jung, A.C.; Mourtada, J.; Macabre, C.; et al. Tumor-Suppressive and Immunomodulating Activity of miR-30a-3p and miR-30e-3p in HNSCC Cells and Tumoroids. *Int. J. Mol. Sci.* **2023**, *24*, 11178. https://doi.org/10.3390/ijms241311178

Academic Editors: Donald J. Buchsbaum and Peter Hamar

Received: 2 June 2023
Revised: 30 June 2023
Accepted: 3 July 2023
Published: 6 July 2023

1. Introduction

Head and neck squamous cell carcinoma (HNSCC) develops from epithelial cells of the upper aerodigestive tract, including the oral cavity, pharynx, and larynx. HNSCC is the seventh most common cancer worldwide and is the leading cause of cancer death with

approximately 900,000 new cases per year and 450,000 deaths estimated [1]. Despite its severity and increasing prevalence within society (+25% in the last decade), there is little awareness of this cancer from the public. The main risk factors are tobacco and alcohol consumption. HNSCC from the oropharynx is mainly due to human papillomavirus (HPV) infection [2]. Patients diagnosed in the early stages of the disease have an 80–90% survival rate with good quality of life after single-modality treatment, mainly surgery or radiotherapy. Unfortunately, most tumors (60% of newly diagnosed patients) are not diagnosed until they are locally advanced (LA-HNSCC: stage III or IV of UICC 8th edition) or metastasized. Late detection limits the effectiveness of combined modality therapy involving a primary surgery followed by radiotherapy and/or chemotherapy [3–5]. High recurrence rates (secondary primary tumors, locoregional recurrence, and distant metastasis occurring in 20–30% of patients) hamper the success of multimodal therapeutic procedures leading to poor prognosis with an overall 5-year survival rate of <50% [6]. In clinicopathological practice, it is difficult to assign patients into classes of risk since no reliable biomarkers are available to predict the outcome of HNSCC. In contrast to other cancers, multidisciplinary treatment decisions for patients suffering from HNSCC are still based on TNM staging and anatomical localization.

HNSCC is well known for its heterogeneity, anatomical diversity, and relapsing nature. To counter recurrence and resistance, but also to identify biomarkers for early diagnosis, prognosis, or treatment response prediction, an improved understanding and characterization of these tumors are needed. The human genome project showed that non-coding RNAs, such as miRNAs, are transcribed and function in normal and pathological cells [7,8]. miRNAs are endogenous, small non-coding RNAs of 19–25 nucleotides. They fine-tune gene expression by binding to the 3′ untranslated region of the target mRNA, leading to mRNA degradation or mRNA translational repression [9]. Over the past decade, several studies have shown that dysregulation of miRNAs can profoundly impact normal physiology and enhance oncogenesis [10,11]. Analysis of miRNA signature and TCGA has revealed that the miR-30 family is frequently downregulated in HNSCC [12,13]. The miR-30 family contains six miRNAs (miR-30a/b/c1/c2/d/e) encoded by six genes located on three distinct loci of the human genome (chromosome 1 for miR-30e/c1, chromosome 6 for miR-30a/c2, and chromosome 8 for miR-30d/b) [14]. Each miRNA duplex consists of two mature complementary miRNA strands: the guide strand 5p and the passenger strand 3p. If guide strands of the miR-30 family share the same SEED (mRNA-targeting) sequence (5′-GUAAACA-3′), passenger strands have two different SEED sequences: 5′-UUUCAGU-3′ for miR-30a/d/e and 5′-UGGGAG-3′ for miR-30b/c. Within this family, miR-30a and miR-30e have been described as important anti-oncomiR (or tumor suppressor miRNAs) [12,13,15,16]. Although both miRNAs have been reported to be consistently downregulated in HNSCC compared to adjacent normal tissue [12,13,17–20], no data are available on the impact and consequences of variability in their expression on LA-HNSCC tumor behavior and progression. Moreover, functional studies have focused mainly on the 5p guide strand and less on the 3p strand, which was thought to be only passenger and always eliminated. We know now that both strands are functional and may or may not have similar functions. Because miR-30-5p is downregulated in HNSCC compared to adjacent normal tissue and act as a tumor suppressor [13], the role of its passenger strand miR-30-3p was explored. How levels of the 3p strands of miR-30a and miR-30e affect tumor behavior and their functional role in LA-HNSCC using both HNSCC cell lines and patient-derived tumoroids (PDT) were determined. The use of PDTs known to recapitulate tumor microenvironment signaling by permitting cell–cell contacts, extracellular matrix interactions, and cell signaling further strengthens our data, showing the ability of miR-30a/e-3p to stimulate PDT immune infiltration. We determine here that reduced miR-30a/e-3p levels in primary tumors are responsible for poor prognoses. We show for the first time that while the disappearance of miR-30a-3p is associated with locoregional relapse, the disappearance of miR-30e-3p is associated with metastatic relapse. Tumor-suppressive activity is characterized by a reduction in cell proliferation and motility and an induction of apoptosis in cell lines, as

well as in patient-derived tumoroids. This is linked to the ability of miR-30a/e-p to inhibit two never-before-described targets, TGFβR1 and BMPR2, in tumor cells. We also describe here for the first time a modification of the peritumoral secretome linked to miR-30a/e-3p expression that promotes macrophage phagocytic activity. Overall, these new data provide a better understanding of how miR-30a/e-3p exert their antitumor activity in HNSCC.

2. Results

2.1. Expression of miR-30-3p in HNSCC Tumors Is Correlated with Good Prognosis and Is Associated with Increased Overall Survival

To explore the role of miR-30a-3p and miR-30e-3p in HNSCC, a cohort of 110 patients with stage III-IV HPV-negative primary HNSCC (mean age 60 ± 10, range 36–84 year) was enrolled in this study. miR-30a-3p and miR-30e-3p are expressed at similar levels in LA-HNSCC (116.6 ± 5.8 and 111.5 ± 4.8, respectively, Figure 1a) and are significantly positively correlated with each other (R2 = 0.90, $p < 0.001$, Figure 1b). Patients were stratified according to miR-30a-3p and miR-30e-3p expression. The threshold between high ($n = 82$) and low ($n = 28$) expression was set at the level of the first quartile for miR-30a-3p. The threshold between high ($n = 46$) and low ($n = 64$) expression was set at the average (111.5) of miR-30e-3p. Kaplan–Meier analysis of locoregional relapse-free survival (LRFS), metastasis-free survival (MFS), and overall survival (OS) was performed. Primary endpoints were metastatic disease and locoregional recurrence free survival at 3 years after surgery. miR-30a-3p and miR-30e-3p expression could statistically discriminate two subgroups of patients. Both miRNAs were found to have a prognosis value since low miR-30a-3p and low miR-30e-3p expressions correlated with adverse prognosis (Figure 1c,d left) and poorer overall survival (Figure 1c,d right). In addition, low expression of miR-30a-3p was associated with a shorter time until locoregional relapse (Figure 1c left), and low expression of miR-30e-3p was associated with a shorter time until metastasis (Figure 1d left). Altogether, these data suggest that loss of miR-30a-3p and miR-30e-3p expression is correlated with tumor recurrence and poor prognosis.

2.2. Expression of miR-30-3p in HNSCC Cells Reduces Survival and Slows down Evasion

miR-30a-3p and miR-30e-3p were heterogeneously expressed among eight HNSCC cell lines studied (Figure 2a). As reported for LA-HNSCC, the expressions of both miRNAs are positively correlated (R2 = 0.9369, $p < 0.001$, Figure 2a). To determine underlying mechanisms that could explain relapses and decreased overall survival, miR-30a-3p and miR-30e-3p were overexpressed (Figure 2b) in three cell lines, showing high (CAL27), intermediate (CAL33), and low (SCC9) levels of each miRNA. Overexpression of both miRNAs only mildly affects the growth of cells (see Supplementary Data S1) but significantly reduces clonogenic survival of CAL27 and CAL33 without affecting SCC9 (Figure 2c). Cleavage of PARP and caspase-7 was detected in CAL27 and CAL33 cells, suggesting that reduced survival observed in both cell lines but not in SCC9 cells was most likely due to an induction of apoptosis (Figure 2d). The overexpression of both miRNAs reduces tumor cell evasion of CAL33 and SCC9 without affecting CAL27 (Figure 2c). Altogether, the data show that miR-30a-3p and miR-3e-3p alter survival and/or evasion of tumor cells without altering their growth capacity.

2.3. TGFBR1 and BMPR2 Are the Main Effector Targets of miR-30-3p in HNSCC

To identify the network of miR-30a-3p and miR-30e-3p mRNA targets, we explored whether reduced expression of both miRNAs was anticorrelated with mRNAs of potential biological importance in cancer. Linear regression analysis was performed between both miRNAs and genome-wide mRNA expression levels obtained from RNA-seq tumor specimens in the TCGA dataset (TCGA-HNSC project of the databank cBio Cancer Genomic Portal). Ten mRNAs were negatively correlated with both miRNAs: DPYSL3, TGFBR1, TGFB1, CRLF1, SPTBN1, BNC1, LTBP2, BMPR2, ACVR1, and GADD45A. Six of them interact with each other and belong to or are closely related to the TGFβ signaling pathway

as shown in STRING analysis: ACVR1, TGFBR1, TGFB1, SPTBN1, LTBP2, and BMPR2 (Figure 3a). Although most of the genes are indeed downregulated in HNSCC cells expressing miR-30a-3p or miR-30e-3p, as confirmed by RT-qPCR, some of them are overexpressed in either cell lines or in response to either miRNA (such as GADD45, ACVR1, LTBP2, BNC1, SPTBN1, and DPYSL3 in SCC9, Figure 3b). As TGFBR1 and BMPR2 are both downregulated at the RNA level in all cell lines by both miRNAs (Figure 3b), we focused the rest of the study on the common targets of miR-30a-3p and miR-30e-3p. Downregulation was confirmed at the protein level by Western blot and immunofluorescence analysis for TGFBR1 in CAL27, CAL33, and SCC9 and for BMPR2 in CAL27 and SCC9 but not in CAL33 (Figure 3c,d). Using TargetScan, we predicted SEED sequences pairing of miRNAs with TGFBR1 and BMPR2 (Figure 3e). TGFBR1 and BMPR2 signaling pathways were inhibited using A8301 and Noggin, respectively, to confirm their involvement in the in vitro relapse features of miR-30a-3p and miR-30e-3p. A8301 is a kinase inhibitor of TGFBR1 that blocks Smad2 phosphorylation and inhibits TGFb signaling. Noggin is an antagonist of BMPs that prevents them from activating the BMP pathway. A8301 significantly reduces both evasive capacity and clonogenic survival in all cell lines investigated (Figure 3f,g). Similar results were obtained for Noggin in CAL27 and SCC9 but not CAL33, which is consistent with the fact that BMPR2 was not affected by miR-30-3p in those cells (Figure 3c,d). Combining both drugs in CAL27, but not in SCC9, resulted in a significantly greater reduction in evasion and survival than each drug alone (Figure 3f,g). Growth was only mildly affected by both drugs. Altogether, the data show that pharmacological inhibition of the TGFBR1 and BMPR2 signaling pathways phenocopies the overexpression of miR-30a-3p and miR-30e-3p.

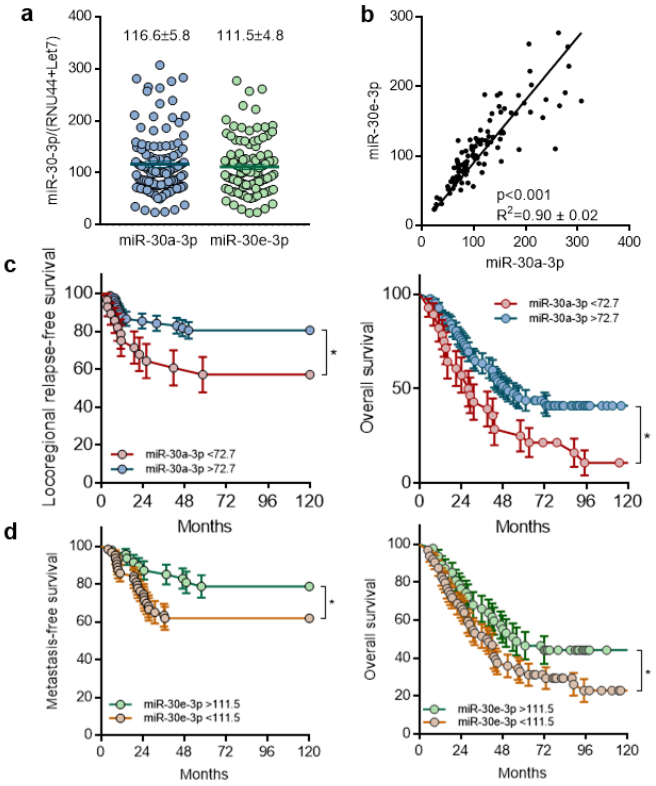

Figure 1. Expression of miR-30-3p in HNSCC tumors is correlated with good prognosis and is associated with increased overall survival. (**a**) miR-30a-3p and miR-30e-3p expression was determined by RT-qPCR in HNSCC tumor samples (n = 110). The line within the bar represents the mean value and "•" represents individual data point. (**b**) Correlation of miR-30a-3p and miR-30e-3p expression in HNSCC tumor samples (n = 110). (**c**) Kaplan–Meier analysis of miR-30a-3p expression in HNSCC tumor samples correlated to locoregional relapse-free survival and overall survival (n = 110; * $p < 0.05$). (**d**) Kaplan–Meier analysis of miR-30e-3p expression in HNSCC tumor samples correlated to metastasis-free survival and overall survival (n = 110; * $p < 0.05$).

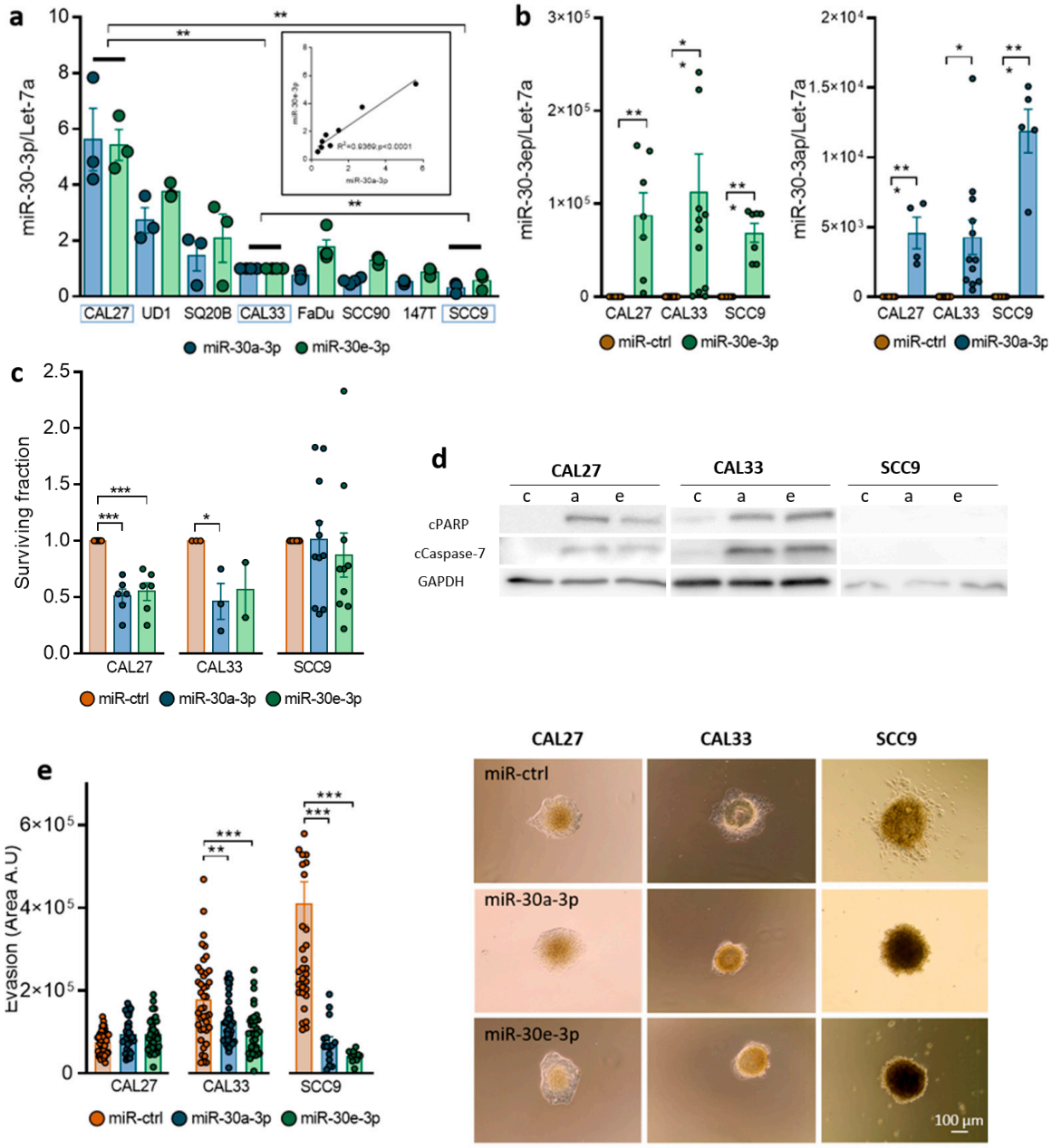

Figure 2. Expression of miR-30-3p in HNSCC cells reduces survival and slows down evasion. (**a**) miR-30a-3p and miR-30e-3p expression was determined by RT-qPCR in 8 HNSCC cell lines ($n = 3$, ** $p < 0.01$). (**b**) miR-30a-3p and miR-30e-3p expression was determined by RT-qPCR in transfected CAL27, CAL33, and SCC9 cell lines ($n = 5$–12, * $p < 0.05$ and ** $p < 0.01$). (**c**) Survival fraction of CAL27, CAL33, and SCC9 cell lines overexpressing miR-30a-3p or miR-30e-3p ($n = 3$–11, * $p < 0.05$ and *** $p < 0.001$). (**d**) Western blot analysis of CAL27, CAL33 and SCC9 cell lines overexpressing miR-30a-3p or miR-30e-3p (c for miR-ctrl, a for miR-30a-3p and e for miR-30e-3p, $n = 3$) (**e**) Evasion of CAL27, CAL33, and SCC9 cell lines overexpressing miR-30a-3p or miR-30e-3p ($n = 15$–49 spheroids, ** $p < 0.01$ and *** $p < 0.001$).

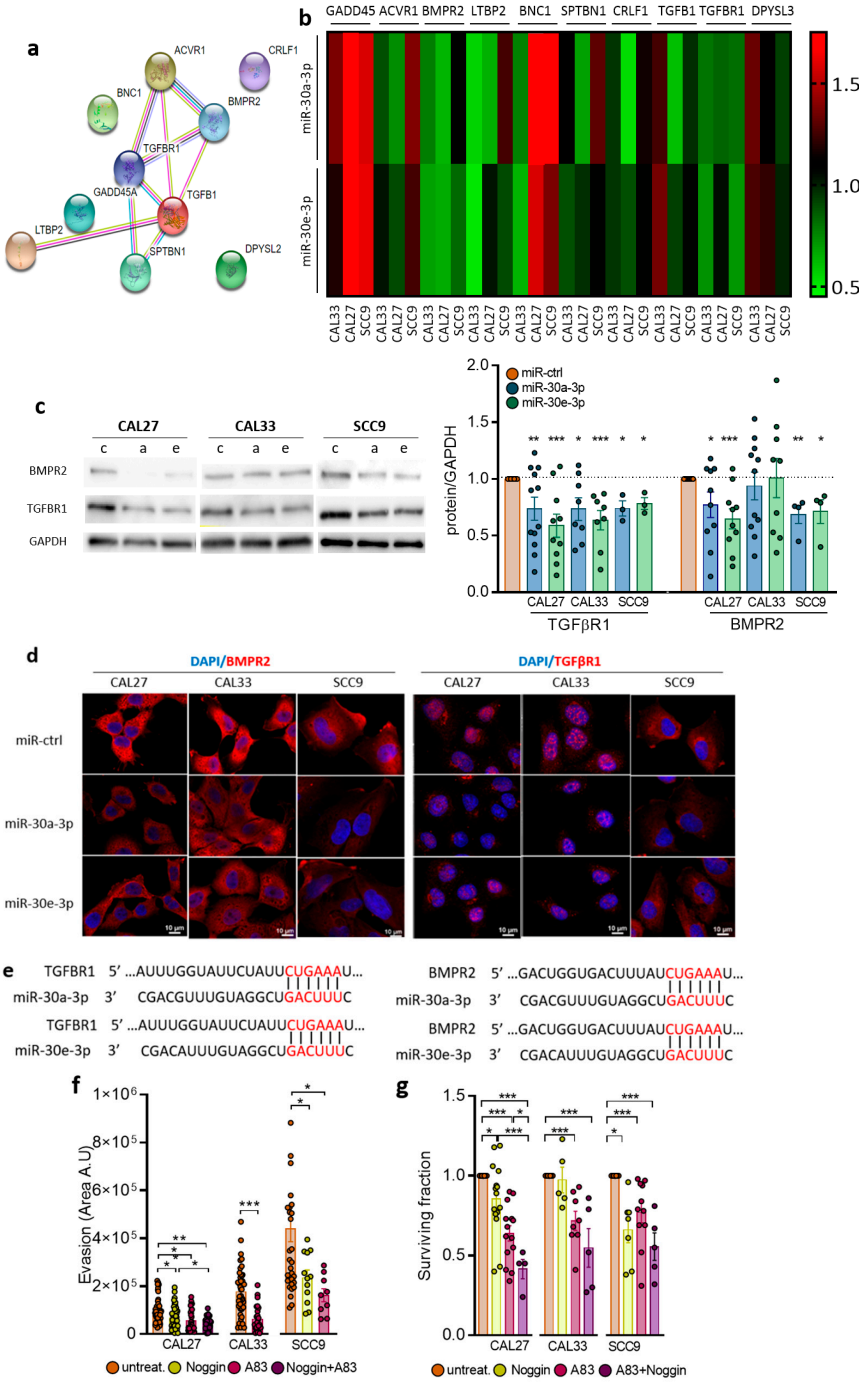

Figure 3. TGFBR1 and BMPR2 are the main effector targets of miR-30-3p in HNSCC. (**a**) Predicted interaction between target proteins was analyzed using STRING database. (**b**) Heatmap representing predicted target gene expression was determined by RT-qPCR in HNSCC cell lines (n = 4–7). (**c**) Western blot analysis of CAL27, CAL33, and SCC9 cell lines overexpressing miR-30a-3p or miR-30e-3p (c for miR-ctrl, a for miR-30a-3p and e for miR-30e-3p, n = 3–12, * $p < 0.05$, ** $p < 0.01$ and *** $p < 0.001$). (**d**) Immunofluorescence analysis by confocal microscopy of HNSCC cell lines overexpressing miR-30a-3p or miR-30e-3p (n = 3–4). (**e**) Predicted pairing region between miR-30a-3p or miR-30e-3p and TGFBR1 (position 812–818) and BMPR2 (position 1411–1417). (**f**) Evasion of CAL27, CAL33, and SCC9 cell lines with TGF-β or BMP inhibitors (n = 16–49 spheroids, * $p < 0.05$, ** $p < 0.01$ and *** $p < 0.001$). (**g**) Survival fraction of CAL27, CAL33, and SCC9 cell lines with TGF-β or BMP inhibitors (n = 9–12, * $p < 0.05$ and *** $p < 0.001$).

2.4. Overexpression of miR-30-3p Slows down HNSCC Patient-Derived Tumoroid Growth and Development

Patient-derived tumoroids are a novel relevant model to study the mechanisms of cancer progression and resistance as they maintain key features of the tumors from which they originate. Tumoroids were derived from a 68-year-old man with HPV-negative squamous cell carcinoma of the anterior oral floor, histologically described as T3N0M0. Histological examination of the primary tumor and corresponding tumoroids showed that tumoroids recapitulate cell architecture, differentiation, and heterogeneity of the primary tumors (Figure 4a). p40 (Delta Np63), p63, Keratin34BE12 (Figure 4a), and Ker 5/6 expressions were similar in the primary tumor and the tumoroid, confirming the epithelial and squamous cell carcinoma origin. Analysis of miR-30a-3p and miR-30e-3p showed that they are expressed at low levels when compared to the CAL33 cell line (Figure 4b) and maintained low expression throughout the culture. Overexpression of miR-30a-3p and miR-30e-3p (Figure 4c) decreased the number of tumoroids (Figure 4d), as well as their volume (Figure 4e), when compared to the control, confirming the tumor-suppressive role of miR-30-3p. As observed in vitro, both BMPR2 and TGFBR1 are inhibited at the mRNA level in tumoroids when miR-30e-3p is overexpressed (Figure 4f). Immunofluorescence staining followed by confocal analysis showed that BMPR2 was localized to the plasma membrane of cells forming tumoroids under miR-ctrl conditions. Expression of miR-30a/e-3p was associated with the loss of the membrane distribution of BMPR2, as well as the decrease in the intensity of BMPR2 staining (Figure 4g). Similar data could be obtained with TGFBR1 and in tumoroids from other patients. All these data suggest that miR-30a-3p and miR-30e-3p expression by tumor cells prevent prevents tumoroid growth and development.

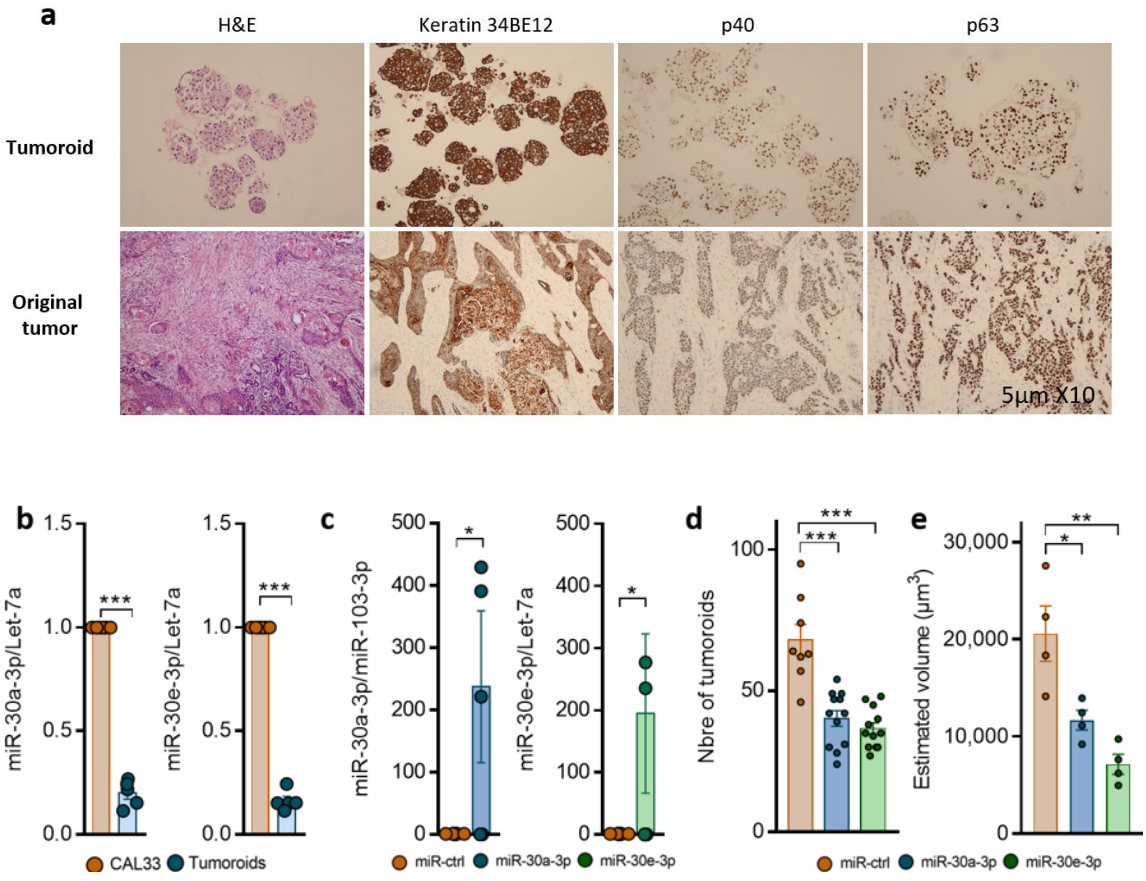

Figure 4. *Cont.*

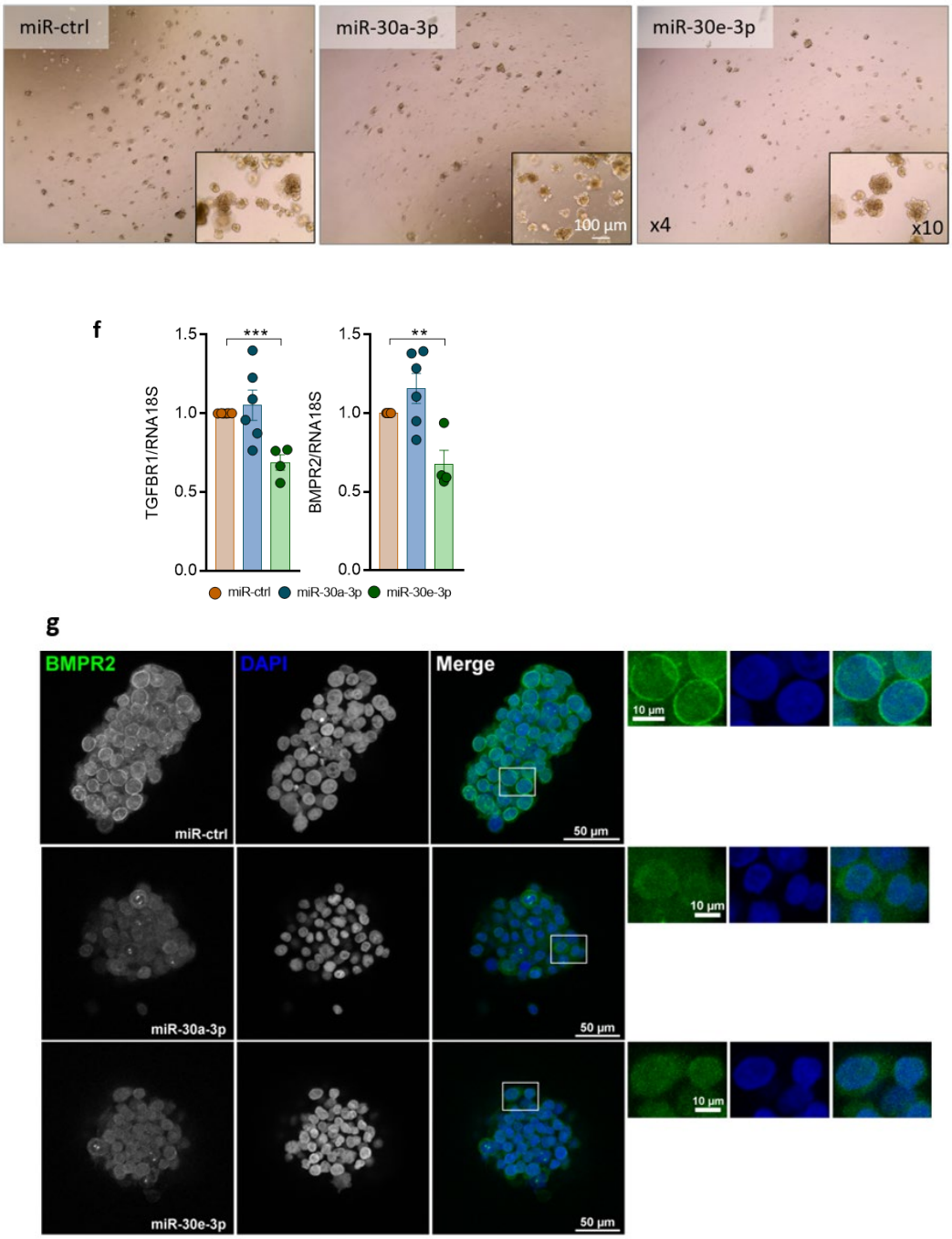

Figure 4. Overexpression of miR-30-3p slows down HNSCC patient-derived tumoroid growth and development. (**a**) Immunohistochemical staining of Keratin 34BE12, p40, p63, and hematoxylin and eosin staining in tumoroid versus the original tumor. (**b**) miR-30a-3p and miR-30e-3p expression was determined by RT-qPCR in tumoroids ($n = 5$, *** $p < 0.001$). (**c**) miR-30a-3p and miR-30e-3p expression was determined by RT-qPCR in tumoroids post-transfection ($n = 4$–5, * $p < 0.05$) (**d**) Number of tumoroids remaining at day 6 post-transfection with mir-30a-3p or miR-30e-3p ($n = 10$–20 tumoroids, *** $p < 0.001$). (**e**) Volume of tumoroids at day 6 transfected with miR-30a-3p or miR-30e-3p. Estimated volume = $(4/3) \times \pi$ (d1/2 × d2/2 × d3/3) ($n = 10$–20 tumoroids, * $p < 0.05$ and ** $p < 0.01$). (**f**) TGFBR1 and BMPR2 expressions were determined by RT-qPCR in tumoroids ($n = 4$–6, ** $p < 0.01$ and *** $p < 0.001$). (**g**) BMPR2 expressions were determined by immunostaining in tumoroids ($n = 3$).

2.5. miR-30a-3p and miR-30e-3p Influence Macrophages' Immune Response to HNSCC Cells

TGFβ signaling has key roles in cancer progression. Studies including the TCGA database show a positive correlation between high TGFβ1 expression and/or TGFβR1 signaling and macrophages (mainly M2-like) infiltrate in HNSCC [21]. M2-like macrophages are endowed with a repertoire of tumor-promoting capabilities, among which immunosuppression is known to support tumor progression. Since macrophages were reported to be the most abundant immune cell type in the tumor microenvironment of OSCC, we investigated how they might be affected by secretomes of miR-30a-3p or miR-30e-3p-transfected tumor cells. M0 macrophages polarize into CD86+ M1-like macrophages (Figure 5a,b) when exposed to a conditioned medium (CM). Incubation with the CM inhibited TGFBR1 expression in macrophages, which likely skewed macrophages to the M1 end (Figure 5c). Expression of CD163+, a marker of M2-like macrophages, was detected in miR-30a-3p and miR-30e-3p-transfected CAL27 and the miR-30e-3p-transfected CAL33 CM. BMPR2 expression remained unaffected in macrophages incubated in the CM from miR-30-3p-transfected-CAL27 and -SCC9 and increased in the CM from miR-30-3p-transfected CAL33 (Supplementary Data S2a). It is worth noting that miR-30a-3p and miR-30e-3p levels were upregulated in M0 macrophages exposed to miR-30a/e-3p-transfected CAL27, CAL33, and SCC9 CM (Supplementary Data S2b,c). However, the levels achieved are far lower than those obtained by direct transfection (see Figure 2b). We then co-cultured macrophages (green staining) with tumor cells (red staining). We found increased phagocytic activities of macrophages towards tumor cells expressing high levels of miR-30a-3p or miR-30e-3p compared to control conditions (Figure 5e,f). HNSCC and OSCC often overexpress the "don't eat me" signal CD47/SIRPα [22]. In vitro phagocytosis of tumor cells expressing miR-30a-3p or miR-30e-3p by macrophages was significantly enhanced after CD47/SIRPα blockade (Figure 5g). Altogether, the data suggest that miR-30a-3p and miR-30e-3p expression by tumor cells generate an immune-permissive microenvironment favoring M1-like macrophage polarization and tumor cell phagocytosis.

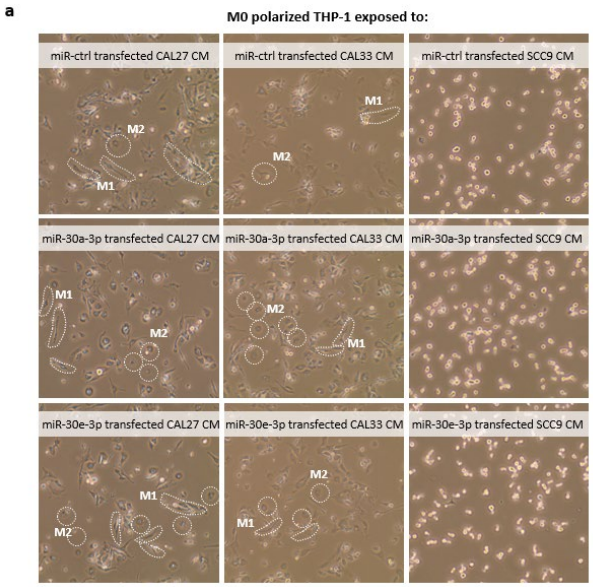

Figure 5. *Cont.*

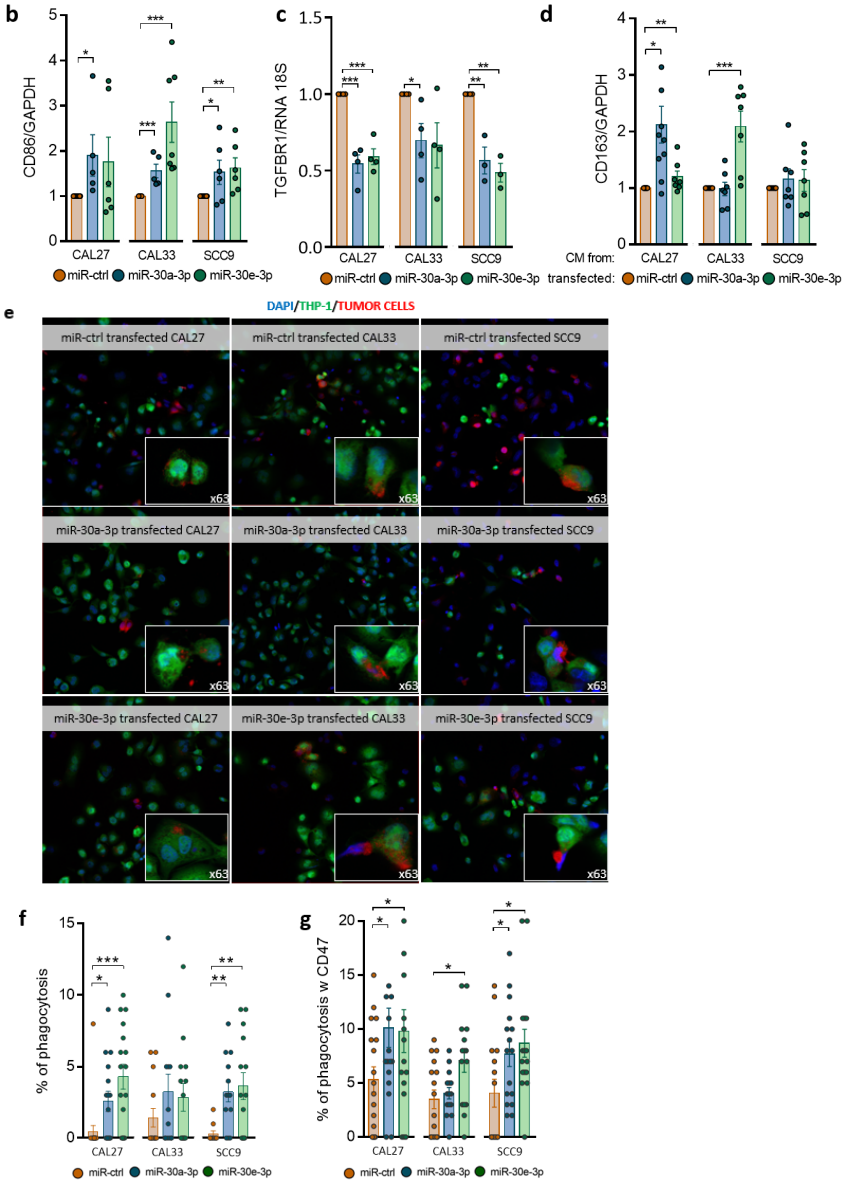

Figure 5. miR-30a-3p and miR-30e-3p influence macrophages' immune response to HNSCC cells. (**a**) Images of M0-polarized THP-1 exposed to CAL27, CAL33, SCC9 overexpressing miR-30a-3p and miR-30e-3p conditioned media in phase-contrast microscopy (×10). (**b**) Western blot analysis of CD86 in M0-polarized THP-1 exposed to CAL27, CAL33, and SCC9 overexpressing miR-30a-3p and miR-30e-3p conditioned media (n = 7–10, * $p < 0.05$, ** $p < 0.01$, *** $p < 0.001$). (**c**) TGFBR1 expression was determined by RT-qPCR in M0-polarized THP-1 exposed to CAL27, CAL33, SCC9 overexpressing miR-30a-3p and miR-30e-3p conditioned media (n = 3–4, * $p < 0.05$, ** $p < 0.01$, *** $p < 0.001$). (**d**) Western blot analysis of CD163 in M0-polarized THP-1 exposed to CAL27, CAL33, and SCC9 overexpressing miR-30a-3p and miR-30e-3p conditioned media (n = 8–10, * $p < 0.05$, ** $p < 0.01$, *** $p < 0.001$). (**e**) Images of MO-polarized THP-1 cells (green) phagocytosing miR-30a-3p or miR-30e-3p-transfected HNSCC cells (red) in confocal microscopy 20× and 63×. (**f**) Percentage of phagocytosis, calculated as the number of M0-polarized THP-1 cells phagocytosing transfected HNSCC cells/total number of M0-polarized THP-1 × 100 (n = 3–4, * $p < 0.05$, ** $p < 0.01$, *** $p < 0.001$). (**g**) Percentage of phagocytosis with antibody antiCD47, calculated as the number of M0-polarized THP-1 cells phagocytosing transfected HNSCC cells/total number of M0-polarized THP-1 × 100 (n = 10–18, * $p < 0.05$).

3. Discussion

Until very recently, the miR-30 family was not extensively studied in HNSCC in contrast to other cancers. This changed with the comprehensive meta-analysis conducted by Zeljic and colleagues in 2018 [23]. By comparing seven published miRNA expression profiling [17,20,24,25], the authors showed that both 5p and 3p strands of miR-30a were consistently downregulated in oral cancers when compared to matched noncancerous tissue [23]. In the search for miRNA of potential importance in HNSCC, Saleh and colleagues identified miR-30(a,b,d,e)-5p as tumor suppressors and potential therapeutic targets [13]. However, the passenger strands of miR-30a and miR-30e still remain poorly studied in HNSCC. Using TCGA-HNSC data, Minemura and colleagues confirmed that miR-30a-3p and miR-30e-3p were downregulated in HNSCC [12]. Patients with low expression of miR-30e-3p had significantly poorer prognosis compared to those with a high expression [26]. In accordance, we show here that low expression of both miR-30a-3p and miR-30e-3p was associated with reduced overall survival. However, we went further by showing that miR-30a-3p and miR-30e-3p could discriminate between patients progressing to locoregional relapse or metastatic recurrence. Whereas loss of miR-30a-3p seems to be associated with locoregional recurrence, metastatic prone tumors show rather low miR-30e-3p levels. Our results reinforce data showing the potential of miR-30a/e-3p to become diagnostic and prognostic biomarkers and highlight for the first time their ability to predict local or systemic recurrence of HNSCC.

Less studied than their 5p homologues, the functional characteristics of these two miRNAs are poorly characterized and remain to be discovered. Expression of miR-30a/e-3p significantly attenuates the survival and motility of HNSCC cell lines without impacting their ability to proliferate, confirming their tumor-suppressive capacity. The expression of miR-30e-3p attenuates migration and invasive abilities in SAS and Sa3 HNSCC cell lines but also significantly affects their proliferation [26]. Such differences could be related to the genes targeted by these miRNAs that might differ depending on the cell context or tumor type. One single miRNA can regulate hundreds of mRNAs and thus govern an entire expression network. Without being exhaustive, targets of the 5p guide strands of miR-30a/e identified so far are involved in the regulation of cell-cycle progression/proliferation/growth (p21, p27 [27], cyclin D [10], K-Ras [16], EGFR [28], MET [13], IGF1R [13], IRS1 [13,29], MYBL2 [30], MTDH/AEG1 [31]), DNA methylation (DNMT3 [15,19,32] and DNMT1 [33]), survival (BIRC6 [34], AVEN [34], Bcl-2 [35], BCL-xL, MDM2, p53 [28]), autophagy [36] and chemoresistance (HIF [37,38], MDR1, [39] ATG5 [40], Beclin-1 [40,41]), EMT (SNAIL [29,42], SLUG, ZEB2 [43,44]) migration/invasion (α2 [45], α5 [46], α6 [13] β3 [46,47], ADAM19, PAI-1 [13,48]), or radioresistance [49]. Because SEED sequences differ between the 5p guide strand and the 3p passenger strand, we searched for novel targets of miR-30a/e-3p. Performing linear regression analysis between both miRNAs and genome-wide mRNA from the TCGA datasets, we showed that most genes identified as potential targets belong to/or are closely related to the TGF-β signaling pathway. This pathway is found to be the most enriched signaling pathway among the 24 KEGG pathways identified in the oral cancer miRNA meta-signature conducted by Zeljic and colleagues [23].

TGFBR1 (TGF-βRI) and BMPR2 are two never-before-described targets of miR-30a/e-3p. Inhibition of both pathways significantly attenuates survival and evasive potential of cells and phenocopies miR-30a/e-3p. TGFBR1 and BMPR2 have been previously described as important players in the carcinogenesis and tumorigenesis of several cancers, including HNSCC [50–53]. TGF-βRI is mutated in 19% of HNSCC patients with metastasis [54]. TGF-β has also been reported to silence miR-30a-5p through the STAT3/MALAT1 pathway in HNSCC favoring tumor growth [55]. Although less studied in HNSCC, BMP signaling or high expressions of BMPR1A and BMPR2 have been observed in metastatic lower-lip SCC [52] and result in resistance to cetuximab [56] or confer proliferation and survival capabilities to OSCC [57]. Besides its effect on tumor cells, TGF-β signaling promotes inflammation and immune suppression in the tumor microenvironment (TME). Tumor-associated macrophages (TAMs) being the major component of the TME of HNSCC [58], we

evaluated how the secretomes of miR-30a/e-3p-expressing tumor cells might affect TAM. Secretomes (containing the miR-30a/e-3p themselves) polarize macrophages mainly into M1-like TAMs most likely through the inhibition of TGF-β signaling. M1-like TAMs are potent effector cells in the killing of tumor cells, which is consistent with our observation of an increase in phagocytic activity of macrophages exposed to miR-30a/e-3p secretomes towards tumor cells. Thus, restoring M1-like TAM phagocytic activities towards tumor cells may contribute to improved disease-free survival and progression-free survival observed in tumors with high levels of miR-30a/e-3p. To date, only a low number of CD163+ M2-like macrophages was correlated to better DFS and PFS [59]. Our work shows that therapy that restores miR-30a/e-3p levels in tumor cells could attenuate tumor progression by acting on both the tumor and its immune microenvironment.

A wealth of preclinical findings has demonstrated that targeting TGF-β signaling is a promising means of exerting antitumor activity, and several classes of TGF-β inhibitors have been developed and tested in clinical trials [60,61]. None of them are currently approved for cancer therapy, mainly because inhibition of TGF-β signaling does not lead to clinical meaningful tumor regression, precluding their use in single therapy. The focus is now on anti-TGF-β combined with other chemotherapy or on bifunctional fusion proteins targeting TGF-β and PD-L1, for example, Bintrafusp alpha (M7824, recently discontinued prematurely by GSK-Merck) or SHR 1701 [62]. We propose here a new option in the targeting of TGF-β signaling based on the restoration of the expression of miR-30a/e-3p. The multi-targeting capacity of miR-30a/e-3p makes them particularly effective as antitumor agents as validated in our preclinical study using tumoroids. Tumoroids have emerged recently as robust preclinical models because they are derived from patients and recapitulate the original tumor heterogeneity, as well as its resistance to therapy [63,64]. miR-30a-3p and miR-30e-3p overexpression attenuates both TGBR1 and BMPR2 levels and decreases tumoroid number and volume. Together, data validate the tumoroid as a reliable preclinical model that is suitable for screening new therapies. Further studies using immunocompetent tumoroids are needed to validate the influence of the miR-30a/e-3p secretome on the tumor immune landscape and the relevance of targeting miR-30a/e-3p coupled with ICIs or anti-CD47s, such as magrolimab.

4. Materials and Methods

4.1. Human Tissue Samples

All tumor specimens (N = 110) were collected during the initial surgery, stored, and used with the patients' informed consent. Patients from the north-east region of France underwent initial surgical resection of their localized head and neck squamous cell carcinoma (HNSCC) between 2003 and 2013 at the St Barbe Clinic (Strasbourg, France), followed by post-operative radiotherapy or chemoradiotherapy at the Paul Strauss Cancer Center (Strasbourg, France) or the Civil Hospitals of Colmar or Mulhouse. All of the tumors were squamous cell carcinomas (SCCs). The inclusion criteria were tumor localization (hypopharynx, oropharynx or oral cavity, HPV-negative) $\geq$T3 and/or $\geq$N2a with no clinical or radiographic evidence of distant metastases. Primary endpoints were metastatic disease and loco-regional recurrence free survival at 3 years after surgery. Secondary endpoints included overall survival (OS), defined as the time from surgery to the date of death or last follow-up. Recorded variables included age, Eastern Cooperative Oncology Group (ECOG) and Karnofsky Performance Score (KPS), comorbidities (Charlson Comorbidity Index), tumor stage, chemotherapy regimen, smoking and alcohol consumption, and follow-up data (survival data, biological parameters, and nutritional characteristics). For detailed patient demographics, see Supplementary Table S1 [65].

4.2. Cell Culture, Transfection, and Drugs

CAL27, CAL33, SCC9, and THP-1 cell lines were purchased from ATCC® and DSMZ (authenticated by STR profiling). All cell lines tested negative for mycoplasma contamination. CAL27 and CAL33 were grown in DMEM (PAN Biotech, Dutscher SAS, Brumath,

France), supplemented with 0.5 mM sodium pyruvate and 10% heat-inactivated FBS (Gibco, Dutscher SAS, Brumath, France). SCC9 was grown in DMEM-F12 (PAN Biotech), supplemented with 2.5 mM ultra-glutamine, 15 mM HEPES, 400 ng/mL hydrocortisone (Sigma-Aldrich, St Quentin Fallavier, France), and 10% FBS (Gibco). THP-1 cells were grown in RPMI-1640 (Sigma-Aldrich) supplemented with 10% heat-inactivated FBS (Gibco). To overexpress miR-30a-3p and miR-30e-3p, cells were transfected for 72 h either by 10 nM miR-30a-3p (Qiagen, Hilden, Germany) or miR-30e-3p (Qiagen) using HiPerFect (Qiagen) transfection reagent according to the manufacturer's instructions. A 10 nM AllStars negative control (miR-ctrl, Qiagen) was used. Efficient miR-30a-3p and miR-30e-3p expression was determined by RT-qPCR (Qiagen) using the StepOne Plus real-time PCR system (Applied Biosystems, Waltham, MA, USA). When indicated, cells were treated with 4% [v/v] Noggin (U-Protein Express B.V., Utrecht, The Netherlands) or 10 µM A8301 (Sigma-Aldrich). THP-1 monocytes were treated with 50 nM Phorbol 12-myristate 13-acetate (PMA) (PeproTech, Rocky Hill, NJ, USA) to differentiate monocytes into M0 macrophages.

4.3. Patient-Derived Tumoroid Culture and Transfection

The study was approved by the Scientific Committee of the tumor bank and the Department of Pathology at the CHU Strasbourg-Hautepierre (Strasbourg, France). Patients signed their informed consent. Tumor extractions were carried out in the Department of Cervicofacial Surgery at the CHU Strasbourg-Hautepierre (France). The resected pieces were histologically diagnosed in the Department of Pathology of the CHU Strasbourg-Hautepierre (France). Tumoroids were extracted from resected tumors following the protocol developed by Driehus et al. [64] and cultured in advanced DMEM/F12 supplemented with GlutaMax, Penicillin/streptomycin, 10mM HEPES, 10 µM Y-27632 (Euromedex, Mundolsheim, France), 0.5 µg/mL Capsofungin (Sigma), 1× B27 supplement (Thermo Fisher Scientific, Waltham, MA, USA), 1.25 mM N-acetyl-L-cysteine (Sigma-Aldrich), 10 mM Nicotinamide (Sigma-Aldrich), 500 nM A8301 (Sigma-Aldrich), 0.3 µM CHIR99021 (Sigma-Aldrich), 50 ng/mL human EGF (PeproTech), 10 ng/mL human FGF10 (PeproTech), 5 ng/mL human FGF2 (PeproTech), 1 µM Prostaglandin E2 (Bio-techne, Minneapolis, MN, USA) and 1 µM Forskolin (Bio-techne), 4% [v/v] RSPO3-Fc fusion protein conditioned medium (ImmunoPrecise, Utrecht, The Netherlands), and 4% [v/v] Noggin-Fc fusion protein conditioned medium (ImmunoPrecise). Quality control of tumoroids was performed by histological analysis. Tumoroids were plated at 2500 cells/10 µL of 70% Cultrex UltiMatrix reduced growth factor basement membrane extract (Bio-Techne, Rennes, France) in 24-well plates.

Tumoroids are transfected according to a protocol adapted from Lian et al. [21]. Briefly, cells were plated at a density of 10,000 cells/200 µL/well in 96-well prime surface 3D U plates (SBio, Neuss, Germany) and transfected for 6 h with 100 nM miR-30a-3p, 100 nM miR-30e-3p, or 100 nM miR-ctrl using HiPerFect transfection reagent (Qiagen). After 6 h, cells were collected, centrifuged at 430g for 10 min, and plated at 10,000/40 µL drops composed of 70% Cultrex UltiMatrix reduced growth factor basement membrane extract (Bio-Techne) in 24-well plates. Efficient miR-30a-3p and miR-30e-3p expression was determined by RT-qPCR (Qiagen) using the StepOne Plus real-time PCR system (Applied Biosystems, ThermoFisher Scientific, Illkirch, France). The number of tumoroids and their size was monitored by imaging at 4× and 20× magnification via an Evos XI Core microscope (ThermoFisher Scientific).

4.4. Real-Time Quantitative PCR of miRNA on Human Samples

miRNAs were extracted from frozen tumor tissues using miRNeasy kit (Qiagen), according to the manufacturer's instructions. The integrity of the extracted RNA was verified on an Agilent 2100 Bioanalyser (Agilent Technologies, Palo Alto, CA, USA). RNA concentrations were measured using a ND-1000 NanoDrop spectrophotometer (Labtech, Palaiseau, France). A total of 1 µg of extracted RNA was used for cDNA synthesis using miScript II RT kit (Qiagen), according to the manufacturer's instructions. A total of 2.5 µL of diluted

cDNA corresponding to 50 ng of reverse-transcribed RNA was analyzed with QuantiTect SybrGreen PCR Master Mix (Qiagen), in duplicate, using the LightCycler 480 real-time PCR system (Roche, Meylan, France). qRT-PCR data were analyzed using LightCycler 480 software (Roche, version 1.5). Ct levels were normalized to the geometric mean of the Ct values of 2 internal controls (housekeeping genes): Let7a (5′-TGAGGTAGTAGGTTGTATAGTT-3′, Invitrogen) and RNU44 (5′TGCTGACTGAACATGAAGGTCT-3′, Invitrogen, ThermoFisher Scientific). Primers for miR-30a-3p (HS_miR-30a-3p miScript primer assay, MIMAT0000088; 5′CUUUCAGUCGGAUGUUUGCAGC) and miR-30e-3p (HS_miR-30e-3p miScript primer assay, MIMAT0000693; 5′CUUUCAGUCGGAUGUUUACAGC) were purchased from Qiagen.

4.5. Real-Time Quantitative PCR of miRNA and mRNA on Cell Lines and Tumoroids

RNA and miRNAs were extracted from cells or tumoroids using miRNeasy Mini Kit (Qiagen) according to the manufacturer's instructions. RNA concentrations were measured using an ND-1000 NanoDrop spectrophotometer (Labtech, Palaiseau, France). A total of 1 µg of extracted miRNA/RNA was used for cDNA synthesis using miScript II RT kit (Qiagen, for miRNAs) or iScript Reverse Transcription SuperMix (BioRad, Hercules, CA, USA, for mRNA), respectively. cDNA was analyzed with miScript® SYBR® Green PCR kit (Qiagen) or Fast SYBR™ Green (Applied Biosystem, Thermo Fisher Scientific, Waltham, MA, USA) in duplicate, using the StepOne real-time PCR system (Applied Biosystem). qRT-PCR data were analyzed using StepOne Plus software (Applied Biosystems, version 2.3). The relative expression of each target was calculated using the relative quantification method (2-ΔΔCT) with RNU44, Let7, or miR-103-3p for miRNA experiments or RNA18S (Invitrogen) for mRNA experiments as internal controls. The following primer pairs were obtained from Qiagen: GADD45, ACVR1, BMPR2, LTBP2, BNC1, STBN1, CRLF1, TGFB1, TGFBR1, DPYSL3 (see Supplementary Table S2).

4.6. Western Blot on Cell Lines and Tumoroids

Cells were lysed (1% Triton-X100, NaF 100 mmol/L, NaPPi 10 mmol/L, Na_3VO_4 1 mmol/L in PBS, supplemented with Complete anti-protease cocktail; Roche) for 20 min at 4 °C and sonicated. A total of 20 µg of protein was separated by SDS-PAGE (4–20% TGX-denaturing gels, BioRad) and transferred to PVDF membranes (Amersham, Sigma-Aldrich, St Quentin Fallavier, France). Blots were probed with TGFBR1 (Abcam, Cambridge, UK ab235178, 1/1000), cleaved PARP (#9541, 1/1000, Cell Signaling, Danvers, MA, USA), cleaved caspase-7 (#9491, 1/1000, Cell Signaling), BMPR2 (ab130206, 1/1000, Abcam), and GAPDH (MAB374, EMD Millipore, Burlington, MA, USA). Proteins were visualized with enhanced chemiluminescence using the LAS4000 microscopy imaging system, and densitometry analysis was performed using ImageJ Software (National Institutes of Health, Bethesda, MD, USA, https://imagej.nih.gov, 1.53t).

4.7. Spheres Evasion Assay

After treatment or transfection, 500,000 cells were suspended in 1ml of regular culture medium supplemented with 20% methylcellulose. Spheroids were formed using the hanging-drop culture method. Briefly, drops of 20 µL cell suspension were placed onto the lids of 60 mm dishes, which were inverted over the dishes. Dishes were cultured in humidified chambers (containing PBS) for 48 h to allow the formation of round aggregates. Spheroids were seeded in 24-well plates (4 spheres/well) for 24 h to allow the evasion of cells from attached spheres. When indicated, 4% Noggin [v/v] or 10 µM A8301 were added to the culture medium. Pictures were taken using the Evos XI Core microscope (AMG, Thermo Fischer Scientific) with 10× magnification. The evasion area (total area − (minus) sphere area) was calculated using ImageJ software, and the results are expressed in arbitrary units of pixels.

4.8. Clonogenic Survival Assay

After transfection or treatments, cells were seeded (500 cells/2 mL/well for CAL27 and SCC9 and 1000 cells/2 mL/well for CAL33) in 6-well plates and allowed to grow for 10 days. Cells were stained with crystal violet at 0.1% (Sigma-Aldrich, St Quentin Fallavier, France). Colonies were counted to determine the plating efficiency (PE) and the surviving fraction (SF). PE = number of surviving cells/number of cells plated. SF = PE of the experimental group/PE of the control group.

4.9. Immunohistochemistry on Tumoroids

Expression of Keratin 34BE12, p40, and p63 was evaluated by immunohistochemical (IHC) analysis using a Ventana Autostainer Automat (Ventana Medical Systems, Roche Tissue Diagnostics) at the Department of Pathology (Strasbourg University Hospital). Slides were prepared from formalin-fixed paraffin-embedded tumor specimens and corresponding tumoroids. Slides were stained for Keratin 34BE12 (M0630, clone 34BE12, 1/50, DAKO Agilent), p40 (RP 136-05, 1/200, Diagnostic Biosystems Pleasanton, Pleasanton, CA, USA), and p63 (790-4509, Ventana, Roche) according to the manufacturers' instructions. Signals were revealed with the ultraView Universal DAB Detection Kit (Ventana Medical Systems, Roche Tissue Diagnostics, Oro Valley, AZ, USA), according to the manufacturer's instructions. All images were acquired with an Olympus BX60 with 20× or 40× objectives. Contrasts were uniformly adjusted on all images with Photoshop (Adobe) software (CS2, version 9).

4.10. Immunofluorescence of Cells

After transfection or treatments, cells were seeded in a Nunc Lab-Tek II CC2 8-well Chamber Slide System at a density of 10,000/well and cultured for 2 days. Cells were fixed with 4% paraformaldehyde or with ice-cold methanol for 15 min. Samples were blocked in PBS/5% BSA/0.3% Triton X-100 for 1 h and incubated overnight at 4 °C with TGFBR1 (ab235178, 1/100, Abcam) or BMPR2 (ab130206, 1/100, Abcam). After washing in PBS, cells were incubated with Alexa Fluor™ 568 goat anti-mouse or anti-rabbit secondary antibodies (1/500, Life Technologies, Thermo Fisher Scientific). Slides were mounted using Fluoromount-G medium (#00-4958-02; Thermo Fischer Scientific). Images were acquired using a LEICA DMI 4000B confocal microscope (Leica Microsystems SA, Nanterre, France) with a 63× magnification oil-immersion objective. The intensity of fluorescence was measured using ImageJ software.

4.11. Immunofluorescence on Tumoroids

Following recovery, tumoroids were fixed in PFA 4% for 20 min and washed in PBS. After a 15 min permeabilization step in PBS/0.1% Tween-20 and a 60 min blocking step in PBS/0.1% Triton X-100/2% BSA/5% NGS, tumoroids were incubated overnight at 4 °C with BMPR2 primary antibody. After washing in PBS/0.1% Triton X-100/0.2% BSA, cells were incubated for 3 h at room temperature with appropriate secondary antibodies (Life Technologies; dilution 1/500) and DAPI (#D9542; Sigma-Aldrich, St Quentin Fallavier Cedex, France; 1 µg/mL). After washing twice in PBS/0.1% Triton X-100/0.2% BSA and twice in PBS, the slides were mounted using FUnGI medium (50% [v/v] glycerol, 9.4% [v/v] dH_2O, 10.6 mM Tris base, 1.1 mM EDTA, 2.5 M fructose and 2.5 M urea). Images were acquired using a LEICA TCS SPE II confocal microscope (Leica Microsystems SA), with a 20× magnification objective, and analyzed with ImageJ software or Imaris software (Imaris ×64 9.3.1—22 May 2019).

4.12. Phagocytosis Assay

CAL27, CAL33, or SCC9 was transfected with miR-30a-3p or miR-30e-3p. A total of 72 h after transfection, particles from the supernatant were removed by centrifugation, and this medium was either frozen or used immediately. We called this medium the conditioned medium. THP-1 cells were seeded at a density of 100,000 cells/well on a Nunc Lab-Tek II

CC2 8-well Chamber Slide System and differentiated into M0 macrophages with 50 nM of PMA. After 24 h, CAL27, CAL33, or SCC9 conditioned medium was added to THP-1 cells (70% conditioned medium and 30% RPMI medium). A total of 24 h later, 1 µM of CytoTrace™ Green CMFDA (CliniSciences, Nanterre, France) was added to THP-1 and 1 µM of CellTracker™ Deep Red Dye (Invitrogen, Thermo Fisher) was added on transfected CAL27, CAL33, or SCC9 for 30 min at 37 °C. Tumor cells were then added on THP-1 cells at a 1:1 ratio for 4 h. When mentioned, 10 µg/mL of CD47 antibody (B6H12, Thermo Fisher Scientifics) was added to the co-culture as well. Cells were fixed with PFA 4% for 10 min and washed 3 times with PBS. Slides were mounted using Fluoromount-G medium (#00-4958-02; Thermo Fischer Scientific) and then observed using a LEICA DMI 4000B confocal microscope (Leica Microsystems SA) with a 20× or 63× magnification oil-immersion objective. The percentage of phagocytosis was calculated as the number of THP-1 phagocytosing HNSCC cells/total number of THP-1 × 100.

4.13. Bioinformatics Analyses of Target Genes

Expression data of miR-30a-3p (MIMAT0000088) and miR-30e-3p (MIMAT0000693) were selected from a cohort of 211 patients from the TCGA-HNSC project of the databank cBio Cancer Genomics Portal of TCGA (https://portal.gdc.cancer.gov/). Patients were sorted according to the localization of their tumors (oropharynx, hypopharynx, and oral cavity) and the availability of follow-up. Patients who died before 50 days of the follow-up and patients who were HPV+ were discarded from the analysis. All the statistics were performed using R software (R version 4.0.3). The distribution of miRNAs expression was divided into two populations of low and high expression based on the median or the third quartile. Correlation was determined between the expression of 442 genes and miRNAs, and the threshold was fixed to the absolute value of 0.2. Matching sequence between miR-30a-3p or miR-30e-3p and their target genes were performed using TargetScan release version 8.0 (https://www.targetscan.org/). The interaction between target proteins was analyzed using STRING program (Search Tool for the Retrieval of Interacting Genes/Proteins) version 11.5 (https://string-db.org/).

4.14. Statistical Analysis

Data are expressed as mean ± SEM and analyzed using GraphPad Prism version 5 (GraphPad Software, San Diego, CA, USA). Differences between groups were analyzed using a non-paired *t*-test, and $p < 0.05$ was considered statistically significant.

Survival analyses: Overall survival (OS), locoregional relapse-free survival, and metastasis-free survival were estimated using the method of Kaplan–Meier. Inferential analysis of qualitative variables was performed using a log-rank test, and comparison of quantitative variables was performed using the Cox model. Multivariate analyses were performed using all variables that were statistically significant in univariate analyses or according to clinical importance. Stepwise regression was performed with backward selection to identify variables of potential prognostic relevance. $p < 0.05$ was considered significant. All analyses were performed using R 3.1.0 software and the survival package. Cut-off values were set as the average ± SEM.

miR-30a-3p and miR-30e-3p cut-off thresholds: The thresholds were based on ROC analysis for defining high and low miR-30e-3p and were determined empirically to differentiate most significantly between miR-30a-3p high and low groups based on survival data. The threshold was fixed as the first quartile for miR-30a-3p.

5. Conclusions

In conclusion, our study showed that miR-30a-3p and miR-30e-3p act as tumor suppressors in HNSCC cells and patient-derived tumoroids. They identify subgroups of LA-HNSCC patients with different prognoses, making them good candidates to become tissue and/or circulating biomarkers predictive of survival and relapse. By targeting mem-

bers of the TGF-β family, they may emerge as an alternative to anti-TGF-β signaling drugs to use alone or in combination with immune or macrophage checkpoint inhibitors.

Supplementary Materials: The following supporting information can be downloaded at: https://www.mdpi.com/article/10.3390/ijms241311178/s1.

Author Contributions: Participated in research design: S.M., A.C.J. and O.C. Conducted experiments: O.C., J.M., A.J., C.M., M.-A.O. and S.F. Performed data analysis: O.C., S.M. and S.F. Wrote or contributed to the writing of the manuscript: O.C., S.M., M.B. and M.D. Provided and processed samples: M.B., P.S., M.-P.C., S.L., T.D., S.G., A.D. and C.T. Data analysis: O.C., S.M., S.F. and R.V. Bioinformatics: A.T. All authors have read and agreed to the published version of the manuscript.

Funding: This work was supported by the Interdisciplinary Thematic Institute program of the University of Strasbourg (France, ANR-10-IDEX-0002 and ANR-20-SFRI-0012) in the frame of the InnoVec Institute. This research was funded by Ligue Contre le Cancer, Conférence de coordination interrégionale du Grand Est program-inter region (France, No S19R417B), the URPS Chirurgiens Dentistes Grand Est (France, No21R3DDT) and the Roratary-Jetons Cancer (France, No O20RMODO).

Institutional Review Board Statement: The study protocol conformed to the ethical guidelines of the 1975 Declaration of Helsinki and was approved by the Ethics Committee of Heidelberg University (S-519/2019). Approval of the research protocol: the study was approved by the Scientific Committee of the tumor bank and the Department of Pathology at the CHU Strasbourg-Hautepierre (France). Informed consent: patients signed their informed consent. Registry and the Registration No. of the study/trial: not applicable. Animal Studies: not applicable.

Informed Consent Statement: Written informed consent was obtained from the patient(s) to publish this paper.

Data Availability Statement: Not applicable.

Acknowledgments: We acknowledge also the PIQ-Quest imaging platform.

Conflicts of Interest: The funders had no role in the design of the study; in the collection, analyses, or interpretation of data; in the writing of the manuscript; or in the decision to publish the results.

References

1. Bray, F.; Ferlay, J.; Soerjomataram, I.; Siegel, R.L.; Torre, L.A.; Jemal, A. Global cancer statistics 2018: GLOBOCAN estimates of incidence and mortality worldwide for 36 cancers in 185 countries. *CA Cancer J. Clin.* **2018**, *68*, 394–424. [CrossRef]
2. Muzio, L.L.; Ballini, A.; Cantore, S.; Bottalico, L.; Charitos, I.A.; Ambrosino, M.; Nocini, R.; Malcangi, A.; Dioguardi, M.; Cazzolla, A.P.; et al. Overview of Candida albicans and Human Papillomavirus (HPV) Infection Agents and their Biomolecular Mechanisms in Promoting Oral Cancer in Pediatric Patients. *BioMed Res. Int.* **2021**, *2021*, 7312611. [CrossRef]
3. Anonymous. Cetuximab approved by FDA for treatment of head and neck squamous cell cancer. *Cancer Biol. Ther.* **2006**, *5*, 340–342.
4. Colevas, A.D.; Yom, S.S.; Pfister, D.G.; Spencer, S.; Adelstein, D.; Adkins, D.; Brizel, D.M.; Burtness, B.; Busse, P.M.; Caudell, J.J.; et al. NCCN Guidelines Insights: Head and Neck Cancers, Version 1.2018. *J. Natl. Compr. Cancer Netw.* **2018**, *16*, 479–490. [CrossRef]
5. Vermorken, J.B.; Mesia, R.; Rivera, F.; Remenar, E.; Kawecki, A.; Rottey, S.; Erfan, J.; Zabolotnyy, D.; Kienzer, H.R.; Cupissol, D.; et al. Platinum-based chemotherapy plus cetuximab in head and neck cancer. *N. Engl. J. Med.* **2008**, *359*, 1116–1127. [CrossRef]
6. Lacas, B.; Carmel, A.; Landais, C.; Wong, S.J.; Licitra, L.; Tobias, J.S.; Burtness, B.; Ghi, M.G.; Cohen, E.E.W.; Grau, C.; et al. Meta-analysis of chemotherapy in head and neck cancer (MACH-NC): An update on 107 randomized trials and 19,805 patients, on behalf of MACH-NC Group. *Radiother. Oncol.* **2021**, *156*, 281–293. [CrossRef] [PubMed]
7. Anfossi, S.; Babayan, A.; Pantel, K.; Calin, G.A. Clinical utility of circulating non-coding RNAs—An update. *Nat. Rev. Clin. Oncol.* **2018**, *15*, 541–563. [CrossRef] [PubMed]
8. Betel, D.; Wilson, M.; Gabow, A.; Marks, D.S.; Sander, C. The microRNA.org resource: Targets and expression. *Nucleic Acids Res.* **2008**, *36*, D149–D153. [CrossRef]
9. Ha, M.; Kim, V.N. Regulation of microRNA biogenesis. *Nat. Rev. Mol. Cell Biol.* **2014**, *15*, 509–524. [CrossRef]
10. Drusco, A.; Croce, C.M. MicroRNAs and Cancer: A Long Story for Short RNAs. *Adv. Cancer Res.* **2017**, *135*, 1–24. [CrossRef] [PubMed]
11. Rupaimoole, R.; Slack, F.J. MicroRNA therapeutics: Towards a new era for the management of cancer and other diseases. *Nat. Rev. Drug Discov.* **2017**, *16*, 203–222. [CrossRef]

12. Minemura, C.; Asai, S.; Koma, A.; Kikkawa, N.; Kato, M.; Kasamatsu, A.; Uzawa, K.; Hanazawa, T.; Seki, N. Identification of Antitumor miR-30e-5p Controlled Genes; Diagnostic and Prognostic Biomarkers for Head and Neck Squamous Cell Carcinoma. *Genes* **2022**, *13*, 1225. [CrossRef]
13. Saleh, A.D.; Cheng, H.; Martin, S.E.; Si, H.; Ormanoglu, P.; Carlson, S.; Clavijo, P.E.; Yang, X.; Das, R.; Cornelius, S.; et al. Integrated Genomic and Functional microRNA Analysis Identifies miR-30-5p as a Tumor Suppressor and Potential Therapeutic Nanomedicine in Head and Neck Cancer. *Clin. Cancer Res. Off. J. Am. Assoc. Cancer Res.* **2019**, *25*, 2860–2873. [CrossRef] [PubMed]
14. Mao, L.; Liu, S.; Hu, L.; Jia, L.; Wang, H.; Guo, M.; Chen, C.; Liu, Y.; Xu, L. miR-30 Family: A Promising Regulator in Development and Disease. *BioMed Res. Int.* **2018**, *2018*, 9623412. [CrossRef]
15. Wei, D.; Yu, G.; Zhao, Y. MicroRNA-30a-3p inhibits the progression of lung cancer via the PI3K/AKT by targeting DNA methyltransferase 3a. *OncoTargets Ther.* **2019**, *12*, 7015–7024. [CrossRef] [PubMed]
16. Zhou, K.; Luo, X.; Wang, Y.; Cao, D.; Sun, G. MicroRNA-30a suppresses tumor progression by blocking Ras/Raf/MEK/ERK signaling pathway in hepatocellular carcinoma. *Biomed. Pharmacother.* **2017**, *93*, 1025–1032. [CrossRef]
17. Fukumoto, I.; Hanazawa, T.; Kinoshita, T.; Kikkawa, N.; Koshizuka, K.; Goto, Y.; Nishikawa, R.; Chiyomaru, T.; Enokida, H.; Nakagawa, M.; et al. MicroRNA expression signature of oral squamous cell carcinoma: Functional role of microRNA-26a/b in the modulation of novel cancer pathways. *Br. J. Cancer* **2015**, *112*, 891–900. [CrossRef]
18. Ganci, F.; Sacconi, A.; Manciocco, V.; Sperduti, I.; Battaglia, P.; Covello, R.; Muti, P.; Strano, S.; Spriano, G.; Fontemaggi, G.; et al. MicroRNA expression as predictor of local recurrence risk in oral squamous cell carcinoma. *Head Neck* **2016**, *38* (Suppl. S1), E189–E197. [CrossRef] [PubMed]
19. Shiah, S.G.; Hsiao, J.R.; Chang, H.J.; Hsu, Y.M.; Wu, G.H.; Peng, H.Y.; Chou, S.T.; Kuo, C.C.; Chang, J.Y. MiR-30a and miR-379 modulate retinoic acid pathway by targeting DNA methyltransferase 3B in oral cancer. *J. Biomed. Sci.* **2020**, *27*, 46. [CrossRef]
20. Soga, D.; Yoshiba, S.; Shiogama, S.; Miyazaki, H.; Kondo, S.; Shintani, S. microRNA expression profiles in oral squamous cell carcinoma. *Oncol. Rep.* **2013**, *30*, 579–583. [CrossRef]
21. Maldonado, L.A.G.; Nascimento, C.R.; Rodrigues Fernandes, N.A.; Silva, A.L.P.; D'Silva, N.J.; Rossa, C., Jr. Influence of tumor cell-derived TGF-beta on macrophage phenotype and macrophage-mediated tumor cell invasion. *Int. J. Biochem. Cell Biol.* **2022**, *153*, 106330. [CrossRef]
22. Ye, X.J.; Yang, J.G.; Tan, Y.Q.; Chen, X.J.; Zhou, G. Targeting CD47 Inhibits Tumor Development and Increases Phagocytosis in Oral Squamous Cell Carcinoma. *Anticancer Agents Med. Chem.* **2021**, *21*, 766–774. [CrossRef] [PubMed]
23. Zeljic, K.; Jovanovic, I.; Jovanovic, J.; Magic, Z.; Stankovic, A.; Supic, G. MicroRNA meta-signature of oral cancer: Evidence from a meta-analysis. *Upsala J. Med. Sci.* **2018**, *123*, 43–49. [CrossRef] [PubMed]
24. Manikandan, M.; Deva Magendhra Rao, A.K.; Arunkumar, G.; Manickavasagam, M.; Rajkumar, K.S.; Rajaraman, R.; Munirajan, A.K. Oral squamous cell carcinoma: microRNA expression profiling and integrative analyses for elucidation of tumourigenesis mechanism. *Mol. Cancer* **2016**, *15*, 28. [CrossRef]
25. Shi, W.; Yang, J.; Li, S.; Shan, X.; Liu, X.; Hua, H.; Zhao, C.; Feng, Z.; Cai, Z.; Zhang, L.; et al. Potential involvement of miR-375 in the premalignant progression of oral squamous cell carcinoma mediated via transcription factor KLF5. *Oncotarget* **2015**, *6*, 40172–40185. [CrossRef] [PubMed]
26. Minemura, C.; Asai, S.; Koma, A.; Kase-Kato, I.; Tanaka, N.; Kikkawa, N.; Kasamatsu, A.; Yokoe, H.; Hanazawa, T.; Uzawa, K.; et al. Identification of Tumor-Suppressive miR-30e-3p Targets: Involvement of SERPINE1 in the Molecular Pathogenesis of Head and Neck Squamous Cell Carcinoma. *Int. J. Mol. Sci.* **2022**, *23*, 3808. [CrossRef]
27. Kim, C.; Jeong, D.E.; Heo, S.; Ji, E.; Rho, J.G.; Jung, M.; Ahn, S.; Kim, Y.J.; Kim, Y.S.; Nam, S.W.; et al. Reduced expression of the RNA-binding protein HuD in pancreatic neuroendocrine tumors correlates with low p27(Kip1) levels and poor prognosis. *J. Pathol.* **2018**, *246*, 231–243. [CrossRef] [PubMed]
28. Song, F.; Xuan, Z.; Yang, X.; Ye, X.; Pan, Z.; Fang, Q. Identification of key microRNAs and hub genes in non-small-cell lung cancer using integrative bioinformatics and functional analyses. *J. Cell. Biochem.* **2020**, *121*, 2690–2703. [CrossRef]
29. Wang, T.; Chen, G.; Ma, X.; Yang, Y.; Chen, Y.; Peng, Y.; Bai, Z.; Zhang, Z.; Pei, H.; Guo, W. MiR-30a regulates cancer cell response to chemotherapy through SNAI1/IRS1/AKT pathway. *Cell Death Dis.* **2019**, *10*, 153. [CrossRef] [PubMed]
30. Li, X.; Jiao, M.; Hu, J.; Qi, M.; Zhang, J.; Zhao, M.; Liu, H.; Xiong, X.; Dong, X.; Han, B. miR-30a inhibits androgen-independent growth of prostate cancer via targeting MYBL2, FOXD1, and SOX4. *Prostate* **2020**, *80*, 674–686. [CrossRef] [PubMed]
31. Chen, F.; Wang, S.; Wei, Y.; Wu, J.; Huang, G.; Chen, J.; Shi, J.; Xia, J. Norcantharidin modulates the miR-30a/Metadherin/AKT signaling axis to suppress proliferation and metastasis of stromal tumor cells in giant cell tumor of bone. *Biomed. Pharmacother.* **2018**, *103*, 1092–1100. [CrossRef] [PubMed]
32. Chen, Q.; Gao, Y.; Yu, Q.; Tang, F.; Zhao, P.W.; Luo, S.K.; Lin, J.S.; Mei, H. miR-30a-3p inhibits the proliferation of liver cancer cells by targeting DNMT3a through the PI3K/AKT signaling pathway. *Oncol. Lett.* **2020**, *19*, 606–614. [CrossRef] [PubMed]
33. Han, X.; Zhen, S.; Ye, Z.; Lu, J.; Wang, L.; Li, P.; Li, J.; Zheng, X.; Li, H.; Chen, W.; et al. A Feedback Loop Between miR-30a/c-5p and DNMT1 Mediates Cisplatin Resistance in Ovarian Cancer Cells. *Cell. Physiol. Biochem.* **2017**, *41*, 973–986. [CrossRef] [PubMed]
34. Chakrabarti, M.; Klionsky, D.J.; Ray, S.K. miR-30e Blocks Autophagy and Acts Synergistically with Proanthocyanidin for Inhibition of AVEN and BIRC6 to Increase Apoptosis in Glioblastoma Stem Cells and Glioblastoma SNB19 Cells. *PLoS ONE* **2016**, *11*, e0158537. [CrossRef] [PubMed]

35. Xu, X.; Jin, S.; Ma, Y.; Fan, Z.; Yan, Z.; Li, W.; Song, Q.; You, W.; Lyu, Z.; Song, Y.; et al. miR-30a-5p enhances paclitaxel sensitivity in non-small cell lung cancer through targeting BCL-2 expression. *J. Mol. Med.* **2017**, *95*, 861–871. [CrossRef]
36. Du, X.; Liu, B.; Luan, X.; Cui, Q.; Li, L. miR-30 decreases multidrug resistance in human gastric cancer cells by modulating cell autophagy. *Exp. Ther. Med.* **2018**, *15*, 599–605. [CrossRef]
37. Mathew, L.K.; Lee, S.S.; Skuli, N.; Rao, S.; Keith, B.; Nathanson, K.L.; Lal, P.; Simon, M.C. Restricted expression of miR-30c-2-3p and miR-30a-3p in clear cell renal cell carcinomas enhances HIF2alpha activity. *Cancer Discov.* **2014**, *4*, 53–60. [CrossRef]
38. Moch, H.; Lukamowicz-Rajska, M. miR-30c-2-3p and miR-30a-3p: New pieces of the jigsaw puzzle in HIF2alpha regulation. *Cancer Discov.* **2014**, *4*, 22–24. [CrossRef] [PubMed]
39. Li, C.; Zou, J.; Zheng, G.; Chu, J. MiR-30a Decreases Multidrug Resistance (MDR) of Gastric Cancer Cells. *Med. Sci. Monit. Int. Med. J. Exp. Clin. Res.* **2016**, *22*, 4509–4515. [CrossRef]
40. Zheng, B.; Zhu, H.; Gu, D.; Pan, X.; Qian, L.; Xue, B.; Yang, D.; Zhou, J.; Shan, Y. MiRNA-30a-mediated autophagy inhibition sensitizes renal cell carcinoma cells to sorafenib. *Biochem. Biophys. Res. Commun.* **2015**, *459*, 234–239. [CrossRef]
41. Chen, W.; Li, Z.; Liu, H.; Jiang, S.; Wang, G.; Sun, L.; Li, J.; Wang, X.; Yu, S.; Huang, J.; et al. MicroRNA-30a targets BECLIN-1 to inactivate autophagy and sensitizes gastrointestinal stromal tumor cells to imatinib. *Cell Death Dis.* **2020**, *11*, 198. [CrossRef] [PubMed]
42. Zhang, Q.; Mao, Z.; Sun, J. NF-kappaB inhibitor, BAY11-7082, suppresses M2 tumor-associated macrophage induced EMT potential via miR-30a/NF-kappaB/Snail signaling in bladder cancer cells. *Gene* **2019**, *710*, 91–97. [CrossRef] [PubMed]
43. Di Gennaro, A.; Damiano, V.; Brisotto, G.; Armellin, M.; Perin, T.; Zucchetto, A.; Guardascione, M.; Spaink, H.P.; Doglioni, C.; Snaar-Jagalska, B.E.; et al. A p53/miR-30a/ZEB2 axis controls triple negative breast cancer aggressiveness. *Cell Death Differ.* **2018**, *25*, 2165–2180. [CrossRef] [PubMed]
44. Noori, J.; Sharifi, M.; Haghjooy Javanmard, S. miR-30a Inhibits Melanoma Tumor Metastasis by Targeting the E-cadherin and Zinc Finger E-box Binding Homeobox 2. *Adv. Biomed. Res.* **2018**, *7*, 143. [CrossRef] [PubMed]
45. Min, J.; Han, T.S.; Sohn, Y.; Shimizu, T.; Choi, B.; Bae, S.W.; Hur, K.; Kong, S.H.; Suh, Y.S.; Lee, H.J.; et al. microRNA-30a arbitrates intestinal-type early gastric carcinogenesis by directly targeting ITGA2. *Gastric Cancer* **2020**, *23*, 600–613. [CrossRef] [PubMed]
46. Croset, M.; Pantano, F.; Kan, C.W.S.; Bonnelye, E.; Descotes, F.; Alix-Panabieres, C.; Lecellier, C.H.; Bachelier, R.; Allioli, N.; Hong, S.S.; et al. miRNA-30 Family Members Inhibit Breast Cancer Invasion, Osteomimicry, and Bone Destruction by Directly Targeting Multiple Bone Metastasis-Associated Genes. *Cancer Res.* **2018**, *78*, 5259–5273. [CrossRef] [PubMed]
47. Dong, L.; Qian, J.; Chen, F.; Fan, Y.; Long, J. LINC00461 promotes cell migration and invasion in breast cancer through miR-30a-5p/integrin beta3 axis. *J. Cell. Biochem.* **2019**, *120*, 4851–4862. [CrossRef]
48. Park, I.; Son, H.K.; Che, Z.M.; Kim, J. A novel gain-of-function mutation of TGF-beta receptor II promotes cancer progression via delayed receptor internalization in oral squamous cell carcinoma. *Cancer Lett.* **2012**, *315*, 161–169. [CrossRef]
49. Guo, Y.; Sun, W.; Gong, T.; Chai, Y.; Wang, J.; Hui, B.; Li, Y.; Song, L.; Gao, Y. miR-30a radiosensitizes non-small cell lung cancer by targeting ATF1 that is involved in the phosphorylation of ATM. *Oncol. Rep.* **2017**, *37*, 1980–1988. [CrossRef]
50. Bach, D.H.; Park, H.J.; Lee, S.K. The Dual Role of Bone Morphogenetic Proteins in Cancer. *Mol. Ther. Oncolytics* **2018**, *8*, 1–13. [CrossRef]
51. Bian, Y.; Terse, A.; Du, J.; Hall, B.; Molinolo, A.; Zhang, P.; Chen, W.; Flanders, K.C.; Gutkind, J.S.; Wakefield, L.M.; et al. Progressive tumor formation in mice with conditional deletion of TGF-beta signaling in head and neck epithelia is associated with activation of the PI3K/Akt pathway. *Cancer Res.* **2009**, *69*, 5918–5926. [CrossRef] [PubMed]
52. De Carvalho, C.H.; Nonaka, C.F.; de Araujo, C.R.; de Souza, L.B.; Pinto, L.P. Immunoexpression of bone morphogenetic protein-2 (BMP-2), BMP receptor type IA, and BMP receptor type II in metastatic and non-metastatic lower lip squamous cell carcinoma. *J. Oral Pathol. Med. Off. Publ. Int. Assoc. Oral Pathol. Am. Acad. Oral Pathol.* **2011**, *40*, 181–186. [CrossRef] [PubMed]
53. Huang, T.; Huang, W.; Lu, H.; Zhang, B.Y.; Ma, J.; Zhao, D.; Wang, Y.J.; Yu, D.H.; He, X. Identification and validation a TGF-beta-associated long non-coding RNA of head and neck squamous cell carcinoma by bioinformatics method. *J. Transl. Med.* **2018**, *16*, 46. [CrossRef]
54. Chen, T.; Yan, W.; Wells, R.G.; Rimm, D.L.; McNiff, J.; Leffell, D.; Reiss, M. Novel inactivating mutations of transforming growth factor-beta type I receptor gene in head-and-neck cancer metastases. *Int. J. Cancer* **2001**, *93*, 653–661. [CrossRef] [PubMed]
55. Wang, Y.; Wu, C.; Zhang, C.; Li, Z.; Zhu, T.; Chen, J.; Ren, Y.; Wang, X.; Zhang, L.; Zhou, X. TGF-beta-induced STAT3 overexpression promotes human head and neck squamous cell carcinoma invasion and metastasis through malat1/miR-30a interactions. *Cancer Lett.* **2018**, *436*, 52–62. [CrossRef] [PubMed]
56. Yin, J.; Jung, J.E.; Choi, S.I.; Kim, S.S.; Oh, Y.T.; Kim, T.H.; Choi, E.; Lee, S.J.; Kim, H.; Kim, E.O.; et al. Inhibition of BMP signaling overcomes acquired resistance to cetuximab in oral squamous cell carcinomas. *Cancer Lett.* **2018**, *414*, 181–189. [CrossRef] [PubMed]
57. Fu, S.; Lv, H.B.; Liu, Y.; Zhao, Y.; He, L.S.; Jin, Y. Transfection of truncated bone morphogenetic protein receptor-II into oral squamous cell carcinoma cell line Tca8113 and inhibitory effect on proliferation and inductive effect on apoptosis. *J. Oral Pathol. Med.* **2011**, *40*, 490–496. [CrossRef]
58. Wang, G.; Zhang, M.; Cheng, M.; Wang, X.; Li, K.; Chen, J.; Chen, Z.; Chen, S.; Chen, J.; Xiong, G.; et al. Tumor microenvironment in head and neck squamous cell carcinoma: Functions and regulatory mechanisms. *Cancer Lett.* **2021**, *507*, 55–69. [CrossRef] [PubMed]

59. Bisheshar, S.K.; van der Kamp, M.F.; de Ruiter, E.J.; Ruiter, L.N.; van der Vegt, B.; Breimer, G.E.; Willems, S.M. The prognostic role of tumor associated macrophages in squamous cell carcinoma of the head and neck: A systematic review and meta-analysis. *Oral Oncol.* **2022**, *135*, 106227. [CrossRef]
60. Cho, B.C.; Daste, A.; Ravaud, A.; Salas, S.; Isambert, N.; McClay, E.F.; Awada, A.; Borel, C.; Helwig, C.; Rolfe, P.A.; et al. Long-term follow-up of bintrafusp alfa, a bifunctional fusion protein targeting TGF-β and PD-L1, in advanced squamous cell carcinoma of the head and neck (SCCHN). *J. Clin. Oncol.* **2021**, *39*, 6020. [CrossRef]
61. Hanna, G.J.; Kaczmar, J.M.; Zandberg, D.P.; Wong, D.J.; Yilmaz, E.; Sherman, E.J.; Hernando-Calvo, A.; Sacco, A.G.; Chung, C.H.; Bohr, D.; et al. Dose expansion results of the bifunctional EGFR/TGFβ inhibitor BCA101 with pembrolizumab in patients with recurrent, metastatic head and neck squamous cell carcinoma. *J. Clin. Oncol.* **2023**, *41*, 6005. [CrossRef]
62. Feng, J.; Tang, D.; Wang, J.; Zhou, Q.; Peng, J.; Lou, H.; Sun, Y.; Cai, Y.; Chen, H.; Yang, J.; et al. SHR-1701, a Bifunctional Fusion Protein Targeting PD-L1 and TGFbeta, for Recurrent or Metastatic Cervical Cancer: A Clinical Expansion Cohort of a Phase I Study. *Clin. Cancer Res.* **2022**, *28*, 5297–5305. [CrossRef] [PubMed]
63. Driehuis, E.; Kolders, S.; Spelier, S.; Lohmussaar, K.; Willems, S.M.; Devriese, L.A.; de Bree, R.; de Ruiter, E.J.; Korving, J.; Begthel, H.; et al. Oral Mucosal Organoids as a Potential Platform for Personalized Cancer Therapy. *Cancer Discov.* **2019**, *9*, 852–871. [CrossRef] [PubMed]
64. Driehuis, E.; Kretzschmar, K.; Clevers, H. Establishment of patient-derived cancer organoids for drug-screening applications. *Nat. Protoc.* **2020**, *15*, 3380–3409. [CrossRef]
65. Burgy, M.; Jehl, A.; Conrad, O.; Foppolo, S.; Bruban, V.; Etienne-Selloum, N.; Jung, A.C.; Masson, M.; Macabre, C.; Ledrappier, S.; et al. Cav1/EREG/YAP Axis in the Treatment Resistance of Cav1-Expressing Head and Neck Squamous Cell Carcinoma. *Cancers* **2021**, *13*, 3038. [CrossRef] [PubMed]

The EXTREME Regimen Associating Cetuximab and Cisplatin Favors Head and Neck Cancer Cell Death and Immunogenicity with the Induction of an Anti-Cancer Immune Response

Justine De Azevedo [1], **Jana Mourtada** [1], Cyril Bour [1,2], Véronique Devignot [1] , Philippe Schultz [1,3], Christian Borel [1,4], Erwan Pencreach [1,5], Georg Mellitzer [1] , Christian Gaiddon [1,*] and Alain C. Jung [1,2,*]

Au moment de la révision de cet article publié par De Azevedo et al., j'ai réalisé des qPCR et des Western blot présentés dans les figures 5 et 6D.

Résumé : (1) Contexte : La première ligne de traitement du carcinome à cellules squameuses de la tête et du cou (HNSCC) récurrent ou métastatique a récemment évolué avec l'approbation d'immunothérapies ciblant le point de contrôle immunitaire anti-PD-1. Toutefois, seuls 20 % des patients environ présentent une réponse tumorale objective durable. La modulation de l'immunogénicité des cellules cancéreuses par le biais d'une mort cellulaire immunogène induite par le traitement est proposée pour améliorer le taux de patients qui répondent aux immunothérapies bloquant les points de contrôle immunitaires. (2) Méthodes : En utilisant des modèles de lignées cellulaires humaines HNSCC et un modèle syngénique de cancer oral chez la souris, nous avons analysé la capacité du régime EX- TREME (thérapie combinée utilisant l'anticorps anti-EGFR cetuximab et une chimiothérapie à base de platine) à modifier l'immunogénicité des cellules HNSCC. (3) Résultats :Nous avons montré que l'association de cetuximab et de cisplatine réduit la croissance cellulaire par l'inhibition du cycle cellulaire et l'induction de la mort cellulaire apoptotique, indépendamment de p53.En outre, différents composants du traitement EXTREME induisent, dans une mesure variable et en fonction des cellules, l'émission de médiateurs de la mort cellulaire immunogène, notamment la calréticuline, le HMGB1 et les chimiokines répondant à l'interféron de type I.Il est intéressant de noter que le cetuximab seul ou associé à la dose IC50 de cisplatine peut induire une réponse immunitaire antitumorale in vivo, mais pas lorsqu'il est associé à une forte dose de cisplatine.(4) Conclusions :Nos observations suggèrent que le protocole EXTREME ou le cetuximab seul sont capables, dans des conditions d'induction modérée de l'apoptose, de susciter la mobilisation du système immunitaire et une réponse immunitaire antitumorale dans le HNSCC.

cells

MDPI

Article

The EXTREME Regimen Associating Cetuximab and Cisplatin Favors Head and Neck Cancer Cell Death and Immunogenicity with the Induction of an Anti-Cancer Immune Response

Justine De Azevedo [1], Jana Mourtada [1], Cyril Bour [1,2], Véronique Devignot [1], Philippe Schultz [1,3], Christian Borel [1,4], Erwan Pencreach [1,5], Georg Mellitzer [1], Christian Gaiddon [1,*] and Alain C. Jung [1,2,*]

1 Laboratory Streinth, Université de Strasbourg-Inserm, UMR_S 1113 IRFAC, 67200 Strasbourg, France
2 Laboratoire de Biologie Tumorale, Institut de Cancérologie Strasbourg Europe, 67200 Strasbourg, France
3 Department of Otorhinolaryngology and Head and Neck Surgery, Hôpitaux Universitaires de Strasbourg, 67200 Strasbourg, France
4 Department of Medical Oncology, Institut de Cancérologie Strasbourg Europe, 67200 Strasbourg, France
5 Laboratoire de Biochimie et Biologie Moléculaire, Hôpitaux Universitaires de Strasbourg, 67200 Strasbourg, France
* Correspondence: gaiddon@unistra.fr (C.G.); a.jung@icans.eu (A.C.J.)

Abstract: (1) Background: The first line of treatment for recurrent/metastatic Head and Neck Squamous Cell Carcinoma (HNSCC) has recently evolved with the approval of immunotherapies that target the anti-PD-1 immune checkpoint. However, only about 20% of the patients display a long-lasting objective tumor response. The modulation of cancer cell immunogenicity via a treatment-induced immunogenic cell death is proposed to potentially be able to improve the rate of patients who respond to immune checkpoint blocking immunotherapies. (2) Methods: Using human HNSCC cell line models and a mouse oral cancer syngeneic model, we have analyzed the ability of the EXTREME regimen (combination therapy using the anti-EGFR cetuximab antibody and platinum-based chemotherapy) to modify the immunogenicity of HNSCC cells. (3) Results: We showed that the combination of cetuximab and cisplatin reduces cell growth through both cell cycle inhibition and the induction of apoptotic cell death independently of p53. In addition, different components of the EXTREME regimen were found to induce, to a variable extent, and in a cell-dependent manner, the emission of mediators of immunogenic cell death, including calreticulin, HMGB1, and type I Interferon-responsive chemokines. Interestingly, cetuximab alone or combined with the IC_{50} dose of cisplatin can induce an antitumor immune response in vivo, but not when combined with a high dose of cisplatin. (4) Conclusions: Our observations suggest that the EXTREME protocol or cetuximab alone are capable, under conditions of moderate apoptosis induction, of eliciting the mobilization of the immune system and an anti-tumor immune response in HNSCC.

Keywords: head and neck squamous cell carcinoma; cetuximab; cisplatin; apoptosis; immunogenic cell death

Citation: De Azevedo, J.; Mourtada, J.; Bour, C.; Devignot, V.; Schultz, P.; Borel, C.; Pencreach, E.; Mellitzer, G.; Gaiddon, C.; Jung, A.C. The EXTREME Regimen Associating Cetuximab and Cisplatin Favors Head and Neck Cancer Cell Death and Immunogenicity with the Induction of an Anti-Cancer Immune Response. *Cells* **2022**, *11*, 2866. https://doi.org/10.3390/cells11182866

Academic Editors: Guido Kroemer and Oliver Kepp

Received: 3 August 2022
Accepted: 12 September 2022
Published: 14 September 2022

1. Introduction

Head and neck cancer squamous cell carcinoma (HNSCC) are cancers that arise from the mucosal epithelium of the oral cavity, larynx, and pharynx [1]. The principal risk factors for HNSCC are alcohol and tobacco consumption on the one hand, and Human Papillomavirus (HPV) infection on the other hand. They are the sixth most frequent malignancies with ~700,000 new cases being diagnosed worldwide each year [2]. Due to the fact that most tumors are diagnosed at locally-advanced stages [1], as well as to treatment failure despite recent medical progressions [3], the five-year overall survival of patients with HNSCC is poor (<40–50%) [4]. The management of the majority of patients with HNSCC relies on a multimodal approach that involves surgery (in amenable patients), followed by

adjuvant radiotherapy or platinum-based (e.g., cisplatin or carboplatin, and 5-fluorouracil) chemoradiotherapy [1]. Cetuximab was FDA-approved in 2006 as a targeted therapy for the management of locally advanced recurrent/metastatic (R/M) HNSCC. The rationale of this therapy relies on the overexpression of the Epidermal Growth Factor Receptor (EGFR) in >90% of HNSCC tumors. The EXTREME phase III clinical trial evaluated the efficacy of the combination of cetuximab and platinum-based chemotherapy (using cisplatin or carboplatin,) as a first-line treatment in patients with R/M HNSCC. This clinical trial showed that the combination in the EXTREME protocol of cetuximab with platinum-based chemotherapy improves both disease-free and overall survival [5–7]. Based on this positive outcome, the EXTREME regimen was FDA-approved and became a therapeutic option for the management of patients with R/M HSNCC. The efficiency of the EXTREME protocol could be rationalized by the fact that cells from various molecular subtypes of HNSCC have shown a different degree of response to EGFR blockade [8,9], and that EGFR overexpression has been shown to reduce the cytotoxicity of metal-based drugs [10].

More recently, several immune check-point blocking immunotherapies, which aim to reactivate an anti-tumor immune response, have been approved [11]. Unfortunately, resistance mechanisms to cisplatin and cetuximab are common. They include the overexpression of factors involved in DNA repair or the constitutive, ligand-independent activation of the EGFR pathway, which reduce the benefits of treatments [12]. Furthermore, only a small proportion of patients (<20%) show a tumor response to immune checkpoint-blocking immunotherapies used as monotherapies [13,14]. The immune landscape of the microenvironment (i.e., the nature of immune cells in the microenvironment and their respective proportions) has been proposed to play a role in the tumor response to immune checkpoint inhibiting immunotherapies [15]. Understanding and detecting the variations in the immune cell landscape that can account for a response to immunotherapy is a major goal to improve patient care [16].

The evolution of the cancer immune landscape during tumor progression was previously described by the three Es (Elimination; Equilibrium; Escape) of the cancer immunoediting model [17]. During the "Elimination" phase (when tumor cells are eliminated by the immune cells), tumor-associated antigens (or neoantigens) are up-taken by antigen presenting cells (APCs) like dendritic cells or macrophages phagocyte, which are further cross-presented to cytotoxic CD8+ T lymphocyte (TL) [18,19]. Cytotoxic TLs are the main actors of the anti-cancer immune response: they infiltrate tumors and trigger targeted cell death via the expression perforin and granzymes. Therefore, an "inflamed" or "immuno-suppressive" tumor microenvironment with high infiltration by cytotoxic CD8+ LT is associated with a better patient outcome [20]. Yet, several mechanisms are known to dampen this anti-tumor cytotoxicity and are responsible for the transition from the "Elimination" to the "Equilibrium" and eventually "Escape" phases (during which cancer cells are progressively maintained and escape the immune system). One of these mechanisms relies on the enrichment of the tumor microenvironment with immunosuppressive immune cells (e.g., regulatory T cells (Treg) [21]; pro-tumoral M2 macrophages [22]; myeloid-derived suppressor cells [23]). The microenvironment of HNSCC is known to be frequently "immuno-tolerant" (presence of pro-tumoral M2 macrophages and/or Treg cells) and associated with a poor outcome [11,24]. In addition, cancer cells highjack immune checkpoints to induce cytotoxic LT anergy: for example, the expression of Programmed Death-Ligand 1 (PD-L1) by cancer cells inhibits TLs' cytotoxic activity upon binding with the Programmed Death-1 (PD-1) receptor and allow immune evasion [17]. Increasing tumor immunogenicity and favorizing an immune-suppressive microenvironment to restore anti-tumor activity is therefore proposed to be an interesting option to improve the efficiency of immunotherapies.

One attractive possibility to achieve this could be to trigger an immunogenic cell death (ICD), which is known to induce an immune response [25]. This particular death cell is characterized by the emission of danger-associated molecular patterns (DAMPs) by dying cells, the activation of APCs upon binding of DAMPs to specific receptors as well as tumor

neoantigens uptake, the subsequent activation of a CD8+ TL-based immune response, and the establishment of an immune memory, which eliminates tumor cells [25]. DAMPs are danger signals that are either expressed on the cell surface and act as "eat me" signals for APCs, like the calreticulin (CRT) chaperone protein, or factors that are released in the extracellular space and act as pro-inflammatory chemoattractant signals, like the histone group mobility box (HMGB1) protein [26]. In addition, the secretion of type I interferons also acts as a DAMP and results in the production of the CXCL10 chemokine which is a chemoattractant for cytotoxic TL [27]. It has been shown that several anticancer treatments can induce ICD, such as specific chemotherapies (i.e., oxaliplatin) [28], radiotherapy [28], or even photodynamic therapy [28,29]. In the clinic, inducing ICD in patients could activate an anti-tumor immune response, provoke tumor elimination and provide protection against relapse through an immune memory. Interestingly, cetuximab was shown to induce ICD in colon cancer cells [30].

While cisplatin used alone was previously proposed to modestly induce ICD in HNSCC cell lines [31], the ICD-inducing ability of cetuximab, used either alone or in combination with cisplatin in head and neck cancers, remains to be determined. Therefore, while the protocol EXTREME is used in clinical routine to treat HNSCC patients, its precise impact on the modulation of immunogenicity of HNSCC cells has never been investigated. Based on previous findings showing that cetuximab can elicit ICD in colon cancer [30], we hypothesized that it has similar effects in HNSCC. In addition, we wanted to investigate the precise impact of the EXTREME protocol (i.e., the combination of cetuximab and cisplatin) on cell proliferation and apoptotic cell death, and how this correlates with the induction of ICD. Hence, we first analyzed the biological impact of cetuximab and cisplatin cotreatment on HNSCC cell line models through the analysis of cell cycle and apoptotic cell death. Secondly, we demonstrated the capacity of cetuximab (alone or combined with cisplatin) to induce DAMPs emission. Finally, using prophylactic vaccination of HNSCC syngeneic mouse models, we show that the treatment with cetuximab provides animals with anti-tumor immune protection.

2. Materials and Methods

2.1. Cell Lines and Reagents

The SQ20B cells originate from a laryngeal tumor, express mutated *TP53*, and are a kind gift from Dr. Pierre Bischoff. The CAL27 cell line originates from a carcinoma of the tongue, expresses mutated *TP53*, and is a kind gift from Dr. Sophie Pinel. SQ20B and CAL27 cells were maintained at 37 °C with 5% CO_2 and 90% humidity in Dulbecco's modified Eagle's medium (DMEM; PAN Biotech, Aidenbach, Germany) supplemented with 10% fetal calf serum (FCS; Gibco, Thermofisher, Waltham, MA, USA). The human monocytic leukemia THP-1 cell line was a kind gift of Elisabeth Martin (UMR1113, Strasbourg), and was maintained at 37 °C with 5% CO_2 and 90% humidity in Roswell Park Memorial Institute (RPMI) medium supplemented with 10% fetal bovine serum (Gibco, Waltham, MA, USA). The murine oral carcinoma MOC2 cell line was purchased from Kerafast, Inc, (Boston, MA, USA), and was maintained at 37 °C with 5% CO_2 and 90% humidity in Dulbecco's modified Eagle's medium (DMEM; PAN Biotech, Aidenbach, Germany) supplemented with 10% fetal calf serum (FCS; Gibco, Waltham, MA, USA).

2.2. In Vitro Cell Survival Analysis

A total of 1×10^4 cells were seeded per well in 96–well microplates (Falcon Multiwell, Thermofisher, Waltham, MA, USA), and different concentrations of cisplatin (Mylan: 0; 0.1; 0.5; 1; 2.5; 7.5; 15; 30; 100 µM), cetuximab (Merck; 5 mg/mL) or PRIMA MET were applied for 48 h in 100 µL of fresh medium. For co-treatments, 2.5 µg/mL of cetuximab and/or 50 µM of prima were added to the different concentrations of cisplatin. MTT assay was performed as previously described by replacing the cisplatin solution with fresh medium supplemented with 5 mg/L MTT (Sigma, Saint-Louis, MO, USA) for 1 h [32]. Cells were lysed in DMSO 100% (100 µL/well). Absorbance measurements were performed at 550 nm

with the LB942 Tristar2 Multimode Reader (Berthold Technologies, Bad Wildbad, Germany). The calculation of the IC_{50}, IC_{75}, and IC_{90} was performed with the GraphpadPrism V5.02 software (Graphpad, Software, San Diego, CA, USA) using non-linear regression.

2.3. Annexin V and PI Flow Cytometry

Cell apoptosis analysis was carried out using FITC-Annexin V and propidium iodide (apoptosis detection kit, BD Biosciences, Franklin Lake, WI, USA) according to the manufacturer's instructions. Briefly, cells were seeded in 10 cm Petri dishes and treated with cetuximab +/- cisplatin for 24 h or 48 h. Cells were harvested and counted, diluted in annexin buffer (BD Biosciences, Franklin Lake, WI, USA) at a concentration of 1×10^6 cells per 100 µL, and stained with 10 µL of propidium iodide and 5 µL of FITC-Annexin V. After 15 min of incubation, cells were analyzed in flow cytometer on a BD LSRFortessa™ (BD Biosciences, Franklin Lake, WI, USA) after satisfying QC using CST beads. Acquisition and data analyses have been performed using the BD FACSDiva™ Software.

2.4. Gene Expression Assays

Gene expression assays on cultured cells were performed by extracting total RNA from pelleted cells using a standard TRIZol procedure (TRI Reagent®: TR 118 Molecular Research Center, Cincinnati, OH, USA), according to the manufacturer's instructions. RNA was retro-transcribed using the High-Capacity cDNA reverse transcription system (Applied Biosystems™, Thermofisher, Waltham, MA, USA), and real-time quantitative PCR was performed using the QuantStudio 3 Real-Time PCR system (Applied Biosystems™, Thermofisher, Waltham, MA, USA). *DDB2*, *FDRX2*, *RPS27L*, and *ZMAT3* expression was measured with pairs of specific primers (see Table S1), and *CXCL9* and *CXCL10* expression was measured with TaqMan probes (see Table S2). The expression of genes of interest was normalized to the expression of *TBP*, used as a reference gene, with the $2^{-\Delta\Delta Ct}$ method.

2.5. SDS-PAGE and Western Blot Analysis

Total protein extraction was carried out by homogenizing 1×10^6 cells in 100 µL of 1X Laemmli lysis buffer 6.25 mM Tris (pH 6.8), 1%SDS, 1%DTT, protease, and phosphatase inhibitors, Sigma. A total of 20 or 30 µg of proteins were resolved by 6%–15% SDS-PAGE (depending on protein molecular weight) according to standard methods. For the analysis of HMGB1 release in the extracellular medium, 40 µL of cells culture supernatant, diluted in SDS-PAGE sample buffer (2X Laemmli lysis buffer, 2X DTT), were resolved by 10% SDS-PAGE. Proteins were detected with primary antibodies raised against cleaved Caspase-3, Calreticulin, EGFR, HMGB1, p63, p53, and p73 (see Table S3 for clones, providers, and concentrations). Depending on the host species, blots were probed with secondary antibodies (1/10,000 anti-mouse IgG-HRP linked antibody, Cell Signaling 7076S; 1/10,000 anti-rabbit IgG-HRP linked antibody, Cell Signaling 7074S) Proteins were visualized with enhanced chemiluminescence using the Clarity™ ECL Western blotting Substrate Bio-Rad reagent, according to the manufacturer instructions. Protein-related signals were acquired on a Pxi Imager (Syngene®, Cambridge, United Kingdom). Protein expression (e.g., cleaved Caspase-3, CRT, and HMGB1) was quantified by measuring the SDS-PAGE gel bands using the ImageJ software. In short, and according to the manufacturer's recommendations, a box was drawn in lanes around gel-band signals using the rectangle tool, making sure to include some of the empty gel between lanes and white space outside of the band. The same box was used for all gel-bands on the same blot. Signal acquisition of pixels was converted into peaks by the ImageJ software, and the area of each peak (which correlates with the gel-band signal intensity) was recovered. Each recovered value was normalized to their respective loading control in the same lane (cell "housekeeping" proteins (actin or GADPH) in the case of cleaved caspase-3 or intracellular HMGB1; cell-culture medium Bovine Serum Albumin (BSA) in the case of extracellular expression of released HMGB1). Finally, the protein of interest to loading control ratios were further normalized by setting the value of this ratio to 1 in the negative control

(e.g., non-treated cells). Enrichment of CRT in the membrane protein fraction was evaluated by normalizing the quantification value in a given condition to the quantification value from the same condition in the input.

2.6. Biotinylation and Immunoprecipitation of Cell Surface Proteins

Biotinylation and recovery of cell surface proteins were performed with a method adapted from Gottardi et al. [33], Hanwell et al., and T. Panaretakis et al. [34]. Briefly, cells were grown and treated in 10 cm Petri dishes, were washed three times with ice-cold PBS-$Ca^{2+-}Mg^{2+}$ (PBS with 0.1 mM $CaCl_2$ and 1 mM $MgCl_2$), and placed on ice. Membrane proteins were then biotinylated with 1.25 mg/mL NHS-SS-biotin (Pierce) freshly diluted in biotinylation buffer (10 mM triethanolamine, 2 mM $CaCl_2$, 150 mM NaCl, pH7.5) for 30 min incubation at 4 °C under gentle agitation. Cells were then rinsed and washed in with PBS-$Ca^{2+-}Mg^{2+}$-glycine (100 mM) buffer at 4 °C to quench unreacted biotin. Cells were further rinsed three times with PBS-$Ca^{2+-}Mg^{2+}$, scraped in cold PBS, and pelleted by centrifugation (800 rpm at 4 °C) and total protein was harvested for 45 min in 500 µL of lysis buffer (1%Triton X-100, 150 mM NaCl, 5 mM EDTA, 50 mM Tris pH7.5) containing protease inhibitors. A total of 500 µg of total proteins were incubated for 1 h at 4 °C with packed streptavidin-agarose beads to bind to biotinylated proteins. Beads were then pelleted by centrifugation and aliquots of supernatants were sampled to recover unbound, intracellular proteins. Biotinylated proteins (representing membrane proteins) were eluted from the beads by heating to 100 °C for 5 min in an SDS-PAGE sample buffer. Whole-cell proteins (input), the intracellular and membrane protein fractions were further loaded onto a 4–12% gradient gel (Mini protean TGX, Biorad, Marnes-La-Coquette, France) and analyzed by western blot (see above).

2.7. Immunofluorescence Staining

CAL27 or MOC2 cells were seeded on coverslips and fixed with PFA 4% for 10 min. In addition, MOC2 cells (but not CAL27 cells) were permeabilized with 0.1% Triton X-100 for 20 min at room temperature. For both cell lines, a saturation of aspecific sites was achieved with 5% Normal Goat Serum for 30 min at room temperature. CAL27 were incubated with anti-CRT antibody (1/400; D3E6 Cell signaling) and MOC2 were incubated with anti-EGFR (1/400; D38B1 Cell signaling) overnight at 4 °C. After 3 washes in 1X PBS, coverslips were further incubated with 1/1000 solutions of goat anti-rabbit-alexa488 (A11034 Invitrogen) secondary antibodies. After 3 washes in 1X PBS, nuclei were labeled with a DAPI (4′,6-diamidino-2-phenylindole) solution (1/20,000) for 5 min, and coverslips were mounted in Calbiochem FluorSave™ reagent (Merck Millipore, Darmstadt, Germany). Pictures were taken with a Zeiss Axio Imager M2-Apotome2 fluorescence microscope.

2.8. Generation of hEGFR-MOC2 Clones

MOC2 cells were transduced with lentiviral particles carrying the p-BABE-puro-hEGFR (gift from Dr Di Fiore Pier Paolo) or the empty vectors. Cells were selected with puromycin (8 µg/mL) and checked for ectopic human EGFR expression by western blot. The clone selection was realized by high dilution and seeding of isolated cells. Every clone was then tested by western blot and immunocytofluorecence for the expression of human EGFR.

2.9. Vaccination Assay

All animal experiments were approved by the local ethic comity and the French Ministry of Agriculture under the permit APAFiS#29181. C57BL/6 mice (Janvier labs, Le Genest-Saint-Isle, France) were housed in the certified animal facility (#H-67-482-21). Female mice (8 weeks old) were inoculated in the right flank with 5×10^5 hEGFR-MOC2-C1 cells (treated ex vivo with cisplatin, cetuximab or cotreatment cisplatin plus cetuximab) in 100 µL of DMEM. The injection of hEGFR-MOC2-C1 cells killed by three successive freeze/thaw cycles was used a non-immunogenic cell death inducer (negative control).

After 7 days, a second challenge was carried out by injecting 5×10^5 hEGFR-MOC2-C1 cells in 100 µL of DMEM in the contralateral flank of the same mice. A minimum of 11 animals in the negative control group (Freeze/thaw cycle group) and a maximum of 12 animals in all other treatment groups were used. Tumor growth was monitored over time by measuring the two dimensions with a caliper. Tumor-free survival was analyzed with Kaplan-Meier survival analysis (see below) and log-rank post-test. Tumors were dissected from mice for further investigation of marker expression by immunofluorescence (see below).

2.10. Statistical Analysis

MTT assays results were analyzed with a Mann-Whiney test. For all other data sets, the, the hypothesis of normality (d'Agostino and Pearson test; Shapiro-Wilk test) and homogeneity of variances (Levene test for equality of variances) of data sets were analyzed. If the sample did not meet at least one of these conditions, then a non-parametric test was used (Kruskal Wallis with Dunn post-test). Otherwise, parametric tests were used (Student *t*-test; Anova and Tuckey post-test). The tumor-free survival of mice challenged with a hEGFR-MOC2-C1 cell injection was evaluated with Kaplan-Meier survival analysis (see below) and log-rank post-test. Statistical tests were performed using GraphPad Prism 8. For all analyzes, statistical significance is represented in graphs using asterisks: * $p < 0.05$; ** $p < 0.001$; *** $p < 0.0001$.

3. Results

3.1. Cetuximab and Cisplatin Inhibit HNSCC Cell Cycle and Trigger Apoptotic Cell Death

In order to investigate the underlying mechanisms of the cotreatment with cetuximab and cisplatin used in the EXTREME protocol, we performed cell viability assays using CAL27 and SQ20B cell lines. Cells were exposed to increasing concentrations of cetuximab or cisplatin and the cell survival rate was measured with MTT and used to determine the drugs IC_{50}, IC_{75} and IC_{90} (i.e., concentrations that result in 50%, 75% and 90% of the maximal drug effect, respectively). Survival curves obtained upon cetuximab treatment showed a maximal drop to ~70% of surviving cells in both cell lines (Figure 1A,B). This maximum effect was reached at 2.5 µg/mL, and higher concentrations of cetuximab did not yield more biological effect. Therefore, we performed MTT assays using a co-treatment with cetuximab (2.5 µg/mL) and increasing concentrations of cisplatin. As expected, the addition of cisplatin to cetuximab was more cytotoxic than cetuximab alone (Mann-Whitney $p < 0.01$ in CAL27 cells and $p < 0.05$ in SQ20B cells). The cotreatment appeared slightly more cytotoxic on CAL27 cells compared to cisplatin alone than in SQ20B cells (IC_{50} = 2.4 µM vs. IC_{50} = 3.5 µM, respectively; Figure 1A). Interestingly, in CAL27 cells, cetuximab seems to mostly favor the activity of cisplatin at lower concentrations (Mann-Whitney $p < 0.001$), whereas no difference between cisplatin alone and the combination were observed at higher concentration (for instance, the IC_{75} was similar in both conditions (7.9 µM vs. 7.6 µM; Figure 1A). Intriguingly and in contrast to CAL27 cells, the addition of cetuximab seemed to lower the cytotoxicity of cisplatin in SQ20B cells (IC_{50} = 4.35 µM vs. IC_{50} = 2.9 µM, and IC_{75} = 10 µM vs. IC_{75} = 6.3 µM, respectively; Figure 1B). Consequently, the co-treatment was found to be more effective on CAL27 cells than on SQ20B cells (Figure 1 A,B).

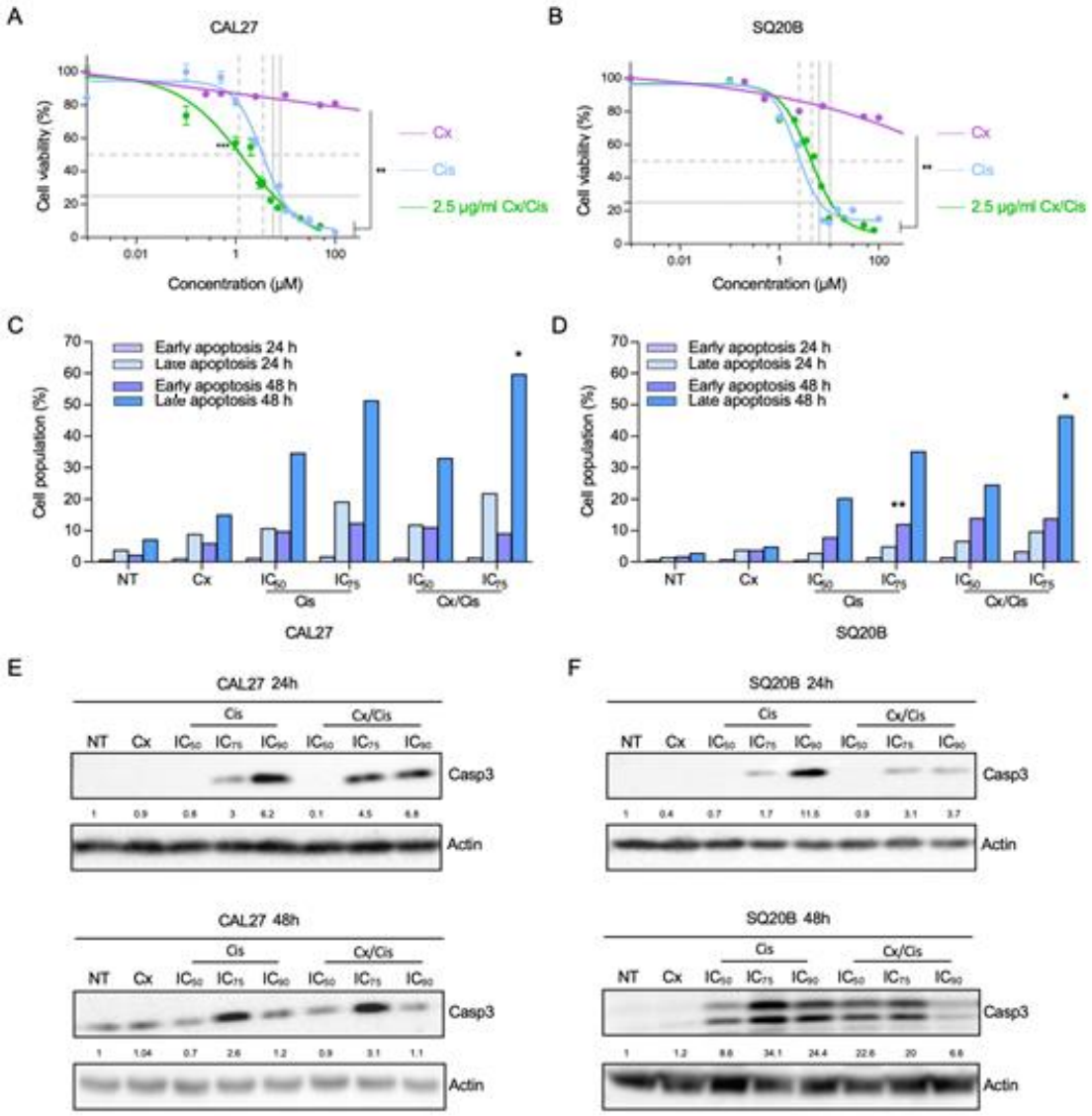

Figure 1. (**A**,**B**). Analysis of CAL27 (**A**) and SQ20B (**B**) cells survival upon treatment with increasing concentrations of cetuximab (Cx; purple line), of cisplatin (Cis; blue line) and of cisplatin +2.5 µg/mL cetuximab (green line), using a MTT-based assay. Mean values from three independent experiments are plotted as sigmoid curves and the cisplatin IC_{50} (dotted grey lines) and IC_{75} (plain grey lines) in the Cis and Cx+Cis conditions are shown. Mann-Whitney *p*-values: * $p < 0.05$; ** $p < 0.01$; *** $p < 0.001$. (**C**,**D**). Annexin V/Propidium Iodide apoptosis assay of CAL27 (**C**) and SQ20B (**D**) cells treated 24 h and 48 h with cetuximab (Cx), cisplatin (Cis) at the IC_{50} and IC_{75} and the Cx/Cis combination. The histograms show the mean number of percentages of early (annexin V-positive, Propidium Iodide-negative; purple) and late (annexin V-positive, Propidium Iodide-positive; purple) cells values from two independent experiments, after 24 h (light colors) and 48 h (dark colors) of treatment. Each treatment condition was compared to its respective non-treated control: ANOVA and Tuckey post-test *p*-values: * $p < 0.05$; ** $p < 0.01$. (**E**,**F**). Western blot analysis of cleaved caspase-3 (Casp3) expression in whole protein extracts from CAL27 (**E**) and SQ20B (**F**) cells treated with cetuximab (Cx), cisplatin (Cis) at the IC_{50}, IC_{75} and IC_{90}, and the Cx/Cis combination for 24 h (upper panels) and 48 h (lower panels). Signals were quantified respectively to the actin loading control and normalized with respect to the non-treated control (quantification results are shown). The blots shown here are representative examples of three independent experiments. Additional independent biological replicates are shown in supporting documents.

Next, we wanted to determine whether the cetuximab and/or cisplatin treatments impact CAL27 and SQ20B cell survival rates by inducing apoptosis or by inhibiting cell proliferation. To this end, cells were fixed, stained with Propidium Iodide (PI) and analyzed by flow cytometry. Upon 48 h of treatment, an increase of the proportion of cells in the G2 phase at the expanse of the G0/G1 phase was observed in both cell lines, and more particularly at the IC_{75} of cisplatin (with or without cetuximab), suggesting a cell cycle halt in G2 (Figure S1A,B). Then, to discriminate between necrosis and apoptosis, cells were stained with an Annexin V probe (AV) and Propidium Iodide (PI) and analyzed by flow cytometry. The percentage of IP− AV+ (early apoptosis) and IP+ AV+ (late apoptosis) cells was determined by flow cytometry, after 24 h and 48 h of treatment with cetuximab +/− cisplatin. Although a trend for the dose-dependent increase of the proportion of cells in early apoptosis (IP− AV+), no significant difference was detected after 24 h of treatment in both cell lines, except upon treatment of SQ20B cells with the IC_{75} of cisplatin (Figure 1C,D; $p < 0.01$). A stronger trend for a dose-dependent increased rate of cells in late apoptosis (IP+ AV+) was observed in SQ20B cells especially after 48 h (Figure 1D), and in CAL27 cells after 24 h and 48 h of treatment with cisplatin+/-cetuximab. Observed differences only reached statistical significance in CAL27 and SQ20B cells treated with cetuximab and the IC_{75} of cisplatin compared to non-treated cells. In addition, this increase was more important in CAL27 cell line (Figure 1C): for instance, the proportions of CAL27 cells in late apoptosis after 48 h of treatment with the IC_{50} and IC_{75} of cisplatin were ~35% and ~50%, respectively, whereas they reach ~20% and ~35% in SQ20B cells. The combination of cetuximab did not synergize with cisplatin, since the proportions of cells in late apoptosis were of the same order of magnitude in both cell lines.

To confirm the induction of apoptosis upon treatments, we analyzed the level of cleaved caspase-3 by western blot in whole protein extracts harvested from CAL27 and SQ20B cells 24 h and 48 h after treatment. Cleaved caspase-3 was observed in CAL27 and SQ20B cells after 24 h treatment with cisplatin at the IC_{75} and IC_{90}, used alone or in combination with cetuximab, in a dose dependent manner (Figure 1E,F, upper panels). After 48 h of treatment of CAL27 cells, the most effective caspase-3 cleavage was observed upon treatment with the IC_{75} of cisplatin +/− cetuximab (Figure 1E, lower panels). At both time points, the cleavage of caspase-3 was similar when cells were treated with cisplatin alone or combined with cetuximab (Figure 1E). In contrast, in SQ20B cells, cetuximab increased the level of cleaved caspase-3 when combined to the IC_{50} of cisplatin for 48 h, whereas it reduced caspase-3 cleavage when combined with higher cisplatin concentration (Figure 1F). In both cell lines and in all experimental conditions, cetuximab used alone did not induce the cleavage of caspase-3 (Figure 1E,F), which is consistent with the low impact of this treatment on cell growth obtained in MTT assays (Figure 1A,B). Hence, altogether, these results show that treatment of HNSCC cells with cisplatin alone or with cetuximab induces caspase-3 cleavage. However, the impact of the addition of cetuximab to cisplatin on caspase3 dependent apoptosis appears to be complex, since it differs and varies in intensity according to several parameters including drug dose, treatment time and cell line.

3.2. p53-Independent Induction of Apoptosis

The p53 family of transcription factors, and especially p53, are well documented mediators of the cytotoxicity induced by DNA damaging drugs, such as cisplatin [35]. Since CAL27 and SQ20B cells were established are from HPV-negative cancers, they both bear a mutated form of p53. CAL27 expresses the mutant H193L p53 that is a gain of function mutant able to interact with YAP [36]. SQ20B harbors a small deletion Tyr126_Lys132del whose impact on p53 activity remains to be established. To understand the contribution of p53 in the effect of the combinatory treatment in CAL27 and SQ20B cells, we first investigated the expression profile of four transcriptional targets of p53 (*FDRX2*, *DDB2*, *RPS27L* and *ZMAT3*) [37] upon treatment with cetuximab+/-cisplatin. No significant impact of the treatments on *DDB2*, *FDRX2*, *RPS27L* and *ZMAT3* gene expression was

observed in CAL27 (Figure 2A) and SQ20B cells (Figure 2B), suggesting that p53 is not activated by the treatment in those cells.

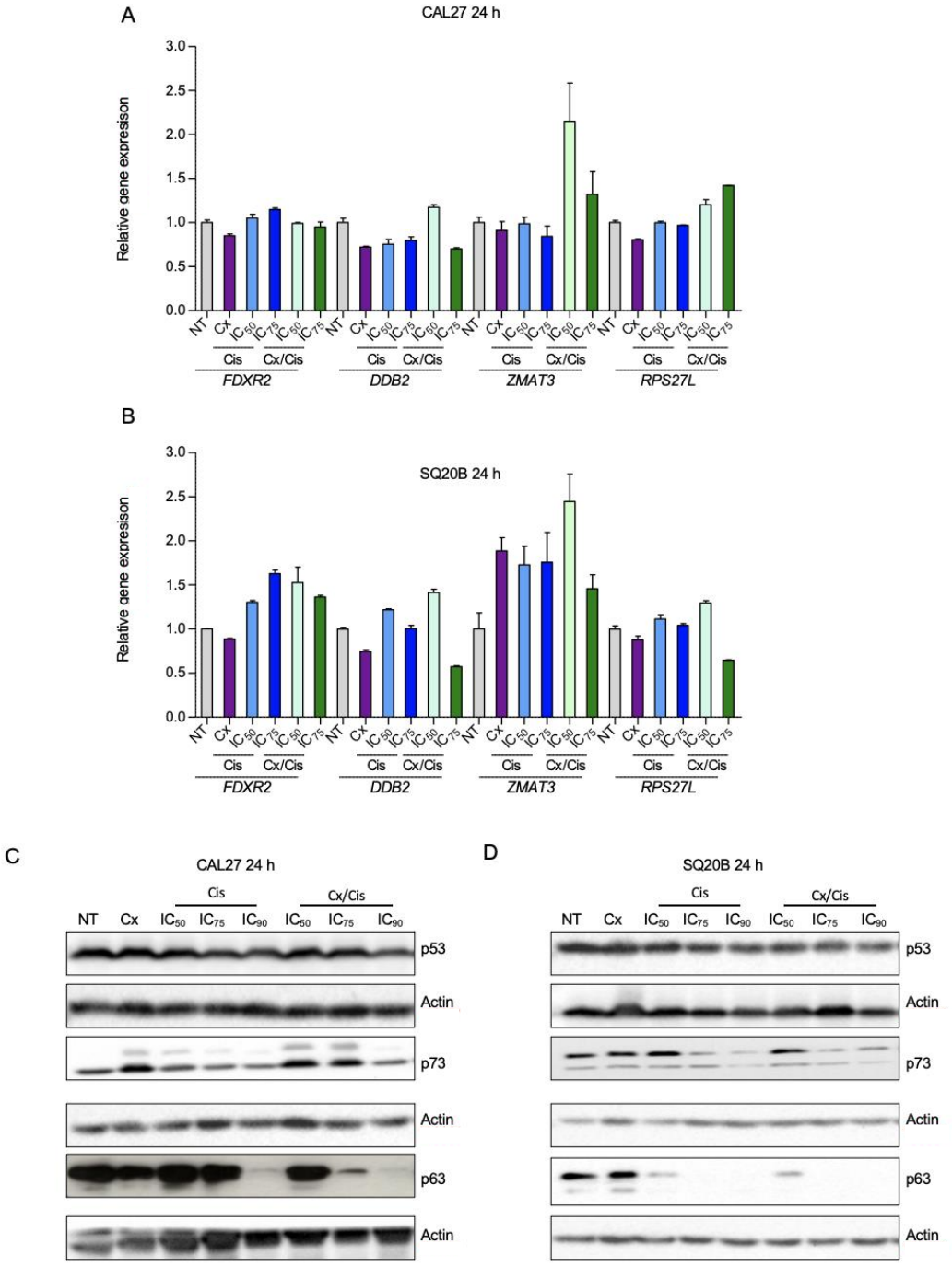

Figure 2. (**A**,**B**). Analysis of the expression of the *FDXR2*, *DDB2*, *ZMAT3* and *RPS27L* genes by RT-qPCR in CAL27 (**A**) and SQ20B (**B**) cells treated for 24 h with cetuximab (Cx), cisplatin (Cis) at the IC_{50} and IC_{75} and the Cx/Cis combination. Data is represented as mean from two independent experiments +SEM. No significant differences were observed between non-treated cells and each treated condition (Kruskal-Wallis and Dunn post-test). (**C**,**D**). Western blot analysis of p53, p73 and p63 expression in whole protein extracts from CAL27 (**C**) and SQ20B (**D**) cells treated with cetuximab (Cx), cisplatin (Cis) at the IC_{50}, IC_{75} and IC_{90}, and the Cx/Cis combination for 24 h. The blots that are shown are representative examples of three independent experiments.

We then analyzed the protein level of p53 by western blot. We found the p53 protein to be expressed at high levels in both cell lines, independently of genotoxic treatments (Figure 2C,D). The high expression level and absence of induction by chemotherapy can be explained by the mutation status of p53 in those cells [35].

p53 mutants have deleterious effects on cells and response to chemotherapy by instating new protein interactions, such as with p63 and p73. These interaction blocks p63 and p73 proapoptotic activity, including in response to chemotherapy [38]. Hence, therapeutic strategies with small molecules aiming at restoring p53 function and inhibiting those neo-interactions have been developed [39,40]. Therefore, we wanted to assess whether in CAL27 and SQ20B cells p63 and p73 were expressed and regulated by the treatment, and whether the p53 reactivator PRIMA-MET could favor the impact of the EXTREME protocol in those cells.

p63 and p73 protein levels were analyzed by western blot. Consistently with the fact that the *TP73* gene encodes multiple isoforms (including a full-length isoform with an N-terminal transactivation domain, called TAp73, and a shorter isoform lacking the N-terminal domain, called ΔNp73), two bands were observed when membranes were probed with an anti-p73 antibody [36]. In CAL27 cells, the lower band showed a stronger expression, which was further increased upon cetuximab and cetuximab/cisplatin treatment. The upper band was not detected in non-treated cells, and the expression of this isoform was induced by cetuximab and the cetuximab/cisplatin co-treatment (especially at the IC_{50} and IC_{75}), and to a lesser extend upon treatment with cisplatin alone (Figure 2C). Unlike what is observed in CAL27 cells, the most expressed p73 isoform is represented by the upper band in non-treated SQ20B cells, although the lower band was observed. Cisplatin treatments at high doses (i.e., IC_{75}; IC_{90}), alone or combined with cetuximab, decreased the expression of the upper isoform of p73. The lower isoform was not affected by the treatments (Figure 2D). We also analyzed the expression of the p63 protein, which is expressed as TA and ΔN isoforms, similarly to p73. p63 was found to be expressed in both CAL27 and SQ20B cells, and the p63-related signal appeared as two bands, the upper band being the more expressed. Strikingly, the expression of both isoforms was strongly downregulated upon treatments of CAL27 with the IC_{90} of cisplatin and the cetuximab/cisplatin (IC_{75} and IC_{90}) cotreatment (Figure 2C). Similar observations were made in SQ20B cells, where both the IC_{75} and IC_{90} of cisplatin alone or in combination with cetuximab strongly decreased the expression of the p63 protein (Figure 2D).

To analyze if p53 signaling can be reactivated, SQ20B and CAL27 cell lines were treated with PRIMA MET (50 μM), a p53 reactivator, in addition to cetuximab and/or cisplatin, and cell viability was assessed using a MTT cell survival assay. The treatments with PRIMA +/− cetuximab were found to be more cytotoxic than cetuximab used alone in both cell lines (Mann-Whitney $p < 0.001$). However, no significant increase in cytotoxicity was observed when PRIMA MET was used in combination with cisplatin and/or cetuximab (Figure 3A,B).

Altogether, these results suggest that mutated p53 has no significant impact on the cytotoxicity induced by the cotreatment. Hence, the apoptosis observed in CAL27 and SQ20B cells is independent of p53. In contrast, p63 and p73 isoforms might be involved, but additional investigations are required to precisely identified which isoforms and their respective function.

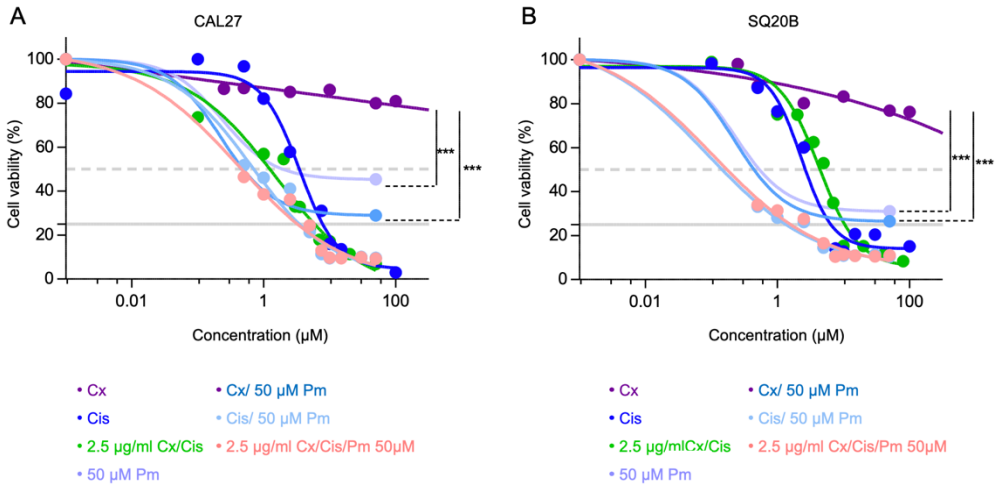

Figure 3. (**A**,**B**). Analysis of CAL27 (**A**) and SQ20B (**B**) cells survival upon treatment with growing concentrations of cetuximab (Cx) +/− 50 µM PRIMA (Pm; dark and light purple lines, respectively), growing concentrations of cisplatin (Cis) +/− 50 µM PRIMA (dark and light blue line, respectively), growing concentrations of cisplatin + 2.5 µg/mL cetuximab +/− 50 µM PRIMA (dark and light green line, respectively), and 50 µM PRIMA alone, using a MTT-based assay. Mean values from 2 independent experiments are plotted as sigmoid curves. The 50% and 25% survival thresholds are shown as a dotted red and plain green lines, respectively. Mann-Whitney *p*-values: *** $p < 0.001$.

3.3. Danger-Associated Molecular Patterns Are Emitted by HNSCC Cells upon Cetuximab and/or Cisplatin Treatment

Using colorectal cancer cell line models, Pozzi and collaborators showed that cetuximab is able to induce an ICD [30]. To explore the capacity of cetuximab to induce ICD in HNSCC, we analyzed the emission of several DAMPs by CAL27 and SQ20B cells upon treatment with cetuximab +/− cisplatin. We first assessed the plasma membrane relocalization of the Calreticulin (CRT) chaperone in CAL27 and SQ20B cells treated with cetuximab, cisplatin or the cetuximab/cisplatin co-treatment. First, based on the literature that describes CRT translocation as an early and essential event of ICD, we chose to assess its expression after 4 h of treatment using the detection of membrane proteins using a non-permeant reactive biotin. Cells were incubated with Sulfo-NHS-SS-Biotin to biotinylate plasma membrane proteins, and streptavidin beads were used to separate membrane-associated proteins from intracellular proteins. Both protein fractions were resolved with SDS-PAGE and analyzed by western blot. Membranes were probed with an anti-EGFR and an anti-GAPDH antibodies, used as positive and negative controls for the membrane fraction, respectively. Probing the blots with an anti-GAPDH antibody was also used as positive control for both the total input and intracellular fraction. Signals corresponding to the EGFR were observed in the three fractions, whereas no signal corresponding to GAPDH were observed in the membrane fraction, both in CAL27 (Figure 4A) and in SQ20B cells (Figure 4B). Membranes were also probed with a specific anti-CRT antibody, and signals corresponding to CRT in the membrane fraction were normalized to CRT signals in the input. Interestingly, the CRT was found to be ~3 and times ~5 more present in the membrane protein fraction of cells treated with cetuximab or the cetuximab/cisplatin IC_{90} combination, in CAL27 and SQ20B cells, respectively (Figure 4A,B). Considering that no changes in CRT expression are observed in the input, this suggest that CRT is translocated from the endoplasmic reticulum to the plasma membrane upon cetuximab treatment. This observation was further confirmed by an immunocytofluorescence analysis of the expression of CRT in non-permeabilized CAL27 cells (Figure 4C). Altogether, these results show that cetuximab used either alone or in combination with cisplatin induce the plasma membrane translocation of CRT in both SQ20B and CAL27 cells.

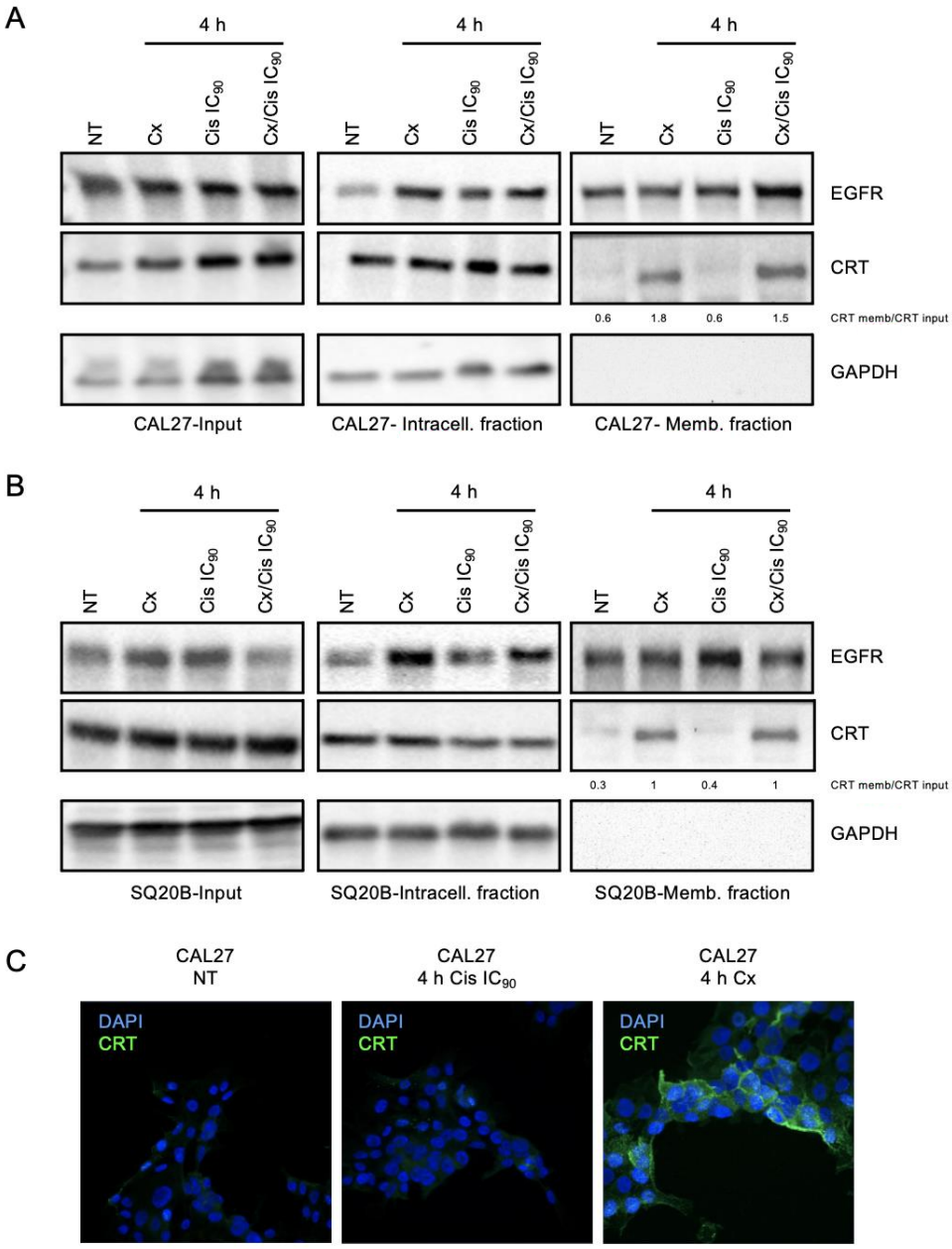

Figure 4. (**A**,**B**). Membrane protein purification and western blot analysis of EGFR, Calreticulin (CRT) and GAPDH expression in the input (left panels), intracellular (middle panels) and extracellular protein fractions of CAL27 (**A**) and SQ20B (**B**) cells treated with cetuximab (Cx), cisplatin (Cis) at the IC_{50}, IC_{75} and IC_{90}, and the Cx/Cis combination for 4 h. The enrichment of CRT in extracellular fractions is shown. The blots that are shown are representative examples of three independent experiments. Additional independent biological replicates are shown in supporting documents. (**C**). Immunocytofluorescent staining analysis of the expression of CRT in non-treated (NT) CAL27 cells (left panel), and CAL27 treated with cisplatin (Cis) at the IC_{90} (middle panel) or cetuximab (Cx; right panel). Nuclei are stained with DAPI. Magnification: X64.

We also investigated the expression of HMGB1, which is known to be released from the nucleus to the extracellular environment at later ICD stages [41]. CAL27 and SQ20B cells were treated with cetuximab +/− cisplatin, and both whole cell proteins and proteins in the cell culture medium were harvested 48 h after treatment, resolved with SDS-PAGE and analyzed by western blot. The level of BSA was used as a loading control of samples of supernatant protein and for normalization. In the CAL27 cell line, HMGB1 was present in

the supernatant upon treatment, in all conditions, with the most important signal observed after treatment with cetuximab and with cetuximab/cisplatin IC_{50}, with an induction fold compared to the untreated control of 8.5 and 8.4, respectively (Figure 5A). The induction of HMGB1 level was higher upon treatment with the IC_{50} of Cisplatin compared to the IC_{75} (Figure 5A). On the contrary, HMGB1 level in the supernatant of SQ20B cells was only triggered with treatments involving cisplatin and, in a concentration-dependent manner (i.e., cisplatin alone and the cisplatin/cetuximab with similar expression patterns; Figure 5B).

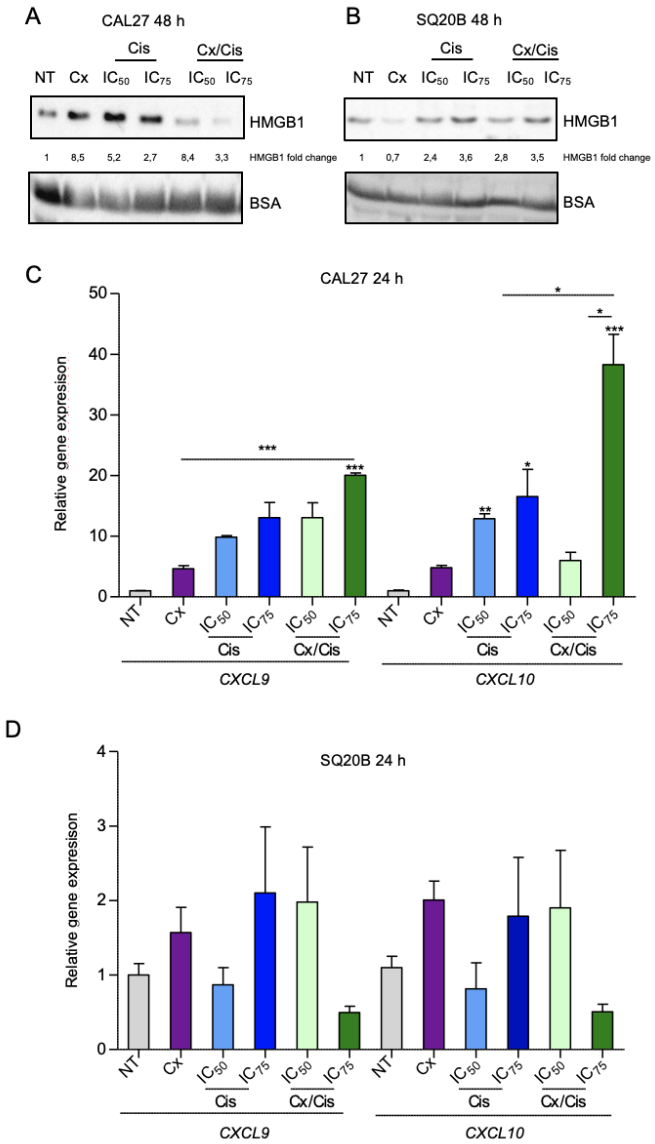

Figure 5. (**A**,**B**) Western blot analysis of the HMGB1 expression in the supernatant from CAL27 (**A**) and SQ20B (**B**) cell cultures harvested 48 h after with cetuximab (Cx), cisplatin (Cis) at the IC_{50} and IC_{75} and the Cx/Cis combination. Signals were quantified respectively to the actin loading control and normalized with respect to the non-treated control (quantification results are shown). The blots that are shown are representative examples of two independent experiments. Additional independent biological replicates are shown in supporting documents. (**C**,**D**). Analysis of the expression of the *CXCL9* and *CXCL10* by RT-qPCR in CAL27 (**C**) and SQ20B (**D**) cells treated for 24 h with cetuximab (Cx), cisplatin (Cis) at the IC_{50} and IC_{75} and the Cx/Cis combination. Data is represented as mean from two independent experiments +SEM. Kruskal-Wallis and Dunn post-test *p*-values: * $p < 0.05$; ** $p < 0.01$; *** $p < 0.001$.

Finally, we analyzed the expression of type I interferon-responsive cytokines using RT-qPCR 24 h after treatment, and namely *CXCL9* and *CXCL10*, that are known to be upregulated by type I interferons [42]. In CAL27 cells, the expression of both *CXCL9* and *CXCL10* was strongly upregulated: a significant ~10-fold induction of *CXCL10* (compared to non-treated control) was observed upon treatment with cisplatin alone. Treatment of CAL27 cells with the cetuximab/cisplatin IC_{75} combination triggered a ~20-fold and ~45-fold induction of *CXCL9* and *CXCL10*, respectively (Figure 5C). Conversely, no statistically significant impact of the treatments on *CXCL9* and *CXCL10* expression was observed in SQ20B cells (Figure 5D). However, the biological impact on treatments of these cytokine gene expression appears more complex. Indeed, a gene expression assay was also carried out 48 h after treatment, and we observed that *CXCL9* and *CXCL10* are downregulated in both cell lines upon cisplatin treatment compared to other conditions (Figure S2B).

Altogether, our observations show that treatment of HNSCC cells with cetuximab induced the emission of DAMPs in a cell-dependent manner: CAL27 cells treated with cetuximab alone or combined with cisplatin appear to be more prone to the emission of DAMPs (CRT plasma membrane translocation; HMGB1 release; induction of type I interferon response) than SQ20B cells. Interestingly, platinum-based chemotherapy alone does not trigger CRT exposure and appears to repress *CXCL9* and *CXCL10* expression 48 after treatment.

3.4. Cetuximab +/− Cisplatin Trigger DAMPs Emission in Murine Head and Neck Carcinoma Cells

To confirm that the cetuximab +/− cisplatin treatment modifies the immunogenicity of HNSCC cells, anti-cancer prophylactic immunizations of mouse syngeneic models were carried out. To this end, we used the MOC2 mouse head and neck carcinoma cell line to generate a stable murine cell line expressing the human EGFR (hEGFR). After retroviral transduction of MOC2 cells using an hEGFR expression plasmid and selection on puromycin, several clones were obtained, one of which (MOC2-phEGFR-C1) was found to express the hEGFR protein (Figure S3). An immunocytofluorescent staining of hEGFR of MOC2-phEGFR-C1 cells showed that the expression of hEGFR is homogeneous in the cell population (Figure 6A). Consistently with what was observed in CAL27 and SQ20B cells, treatment with cisplatin alone or in combination with cetuximab induced caspase-3 cleavage, 24 h (Figure 6B) and 48 h (Figure S4A) after treatment.

Interestingly, the same treatments were also found to trigger the relocalization of CRT to the plasma membrane (Figure 6C). However, unlike CAL27 and SQ20B, the cetuximab/cisplatin co-treatment was able to induce a more robust expression of CRT at the plasma membrane of MOC-2-phEGFR-C1 cells compared to treatment with cetuximab alone (Figure 6C, right panels). Finally, we observed that HMGB1 was released in the extracellular medium, 24 h, and 48 h after treatment with cisplatin alone or in combination with cetuximab, in a dose-dependent manner (Figure 6D), whereas the expression of intracellular HMBG1 was not affected by treatments (Figure S4B).

3.5. Induction of Bona Fide ICD by Cetuximab +/− IC_{50} of Cisplatin

To assess whether the treatment of MOC2-phEGFR-C1 cells by cetuximab and/or cisplatin was able to induce an anti-tumor immune response in vivo, MOC2-phEGFR-C1 cells were first treated ex vivo, and dead cells were injected in the right flank of immunocompetent C57BL/6 mice. The same mice were then challenged seven days after the first immunization, by injecting non-treated living MOC2-phEGFR-C1 cells on the left flank, and the mice progression-free survival was evaluated. An injection of MOC2-phEGFR-C1 cells killed by three consecutive freeze/thaw cycles was used as a non-immunogenic cell death control. Expectedly, tumor progression was observed within 26 days in 11/11 mice that were injected with MOC2-phEGFR-C1 cells killed by freeze/thaw cycles (Figure 7A,B). A similar observation was made for mice in the IC_{75} cisplatin (tumor growth in 10/12 mice) and cetuximab + IC_{75} cisplatin (tumor growth in 12/12 mice) treatment groups. Strikingly, the injection of cells treated with cetuximab, the IC_{50} of cisplatin, or the combination was

able to prevent tumor progression, which was observed in only 1/12, 4/12, and 2/12 mice, respectively (Figure 7A,B). Thus, these observations suggest that the injection of MOC2-phEGFR-C1 cells treated with cetuximab and/or the IC_{50} of cisplatin provides protection against a subsequent tumor challenge.

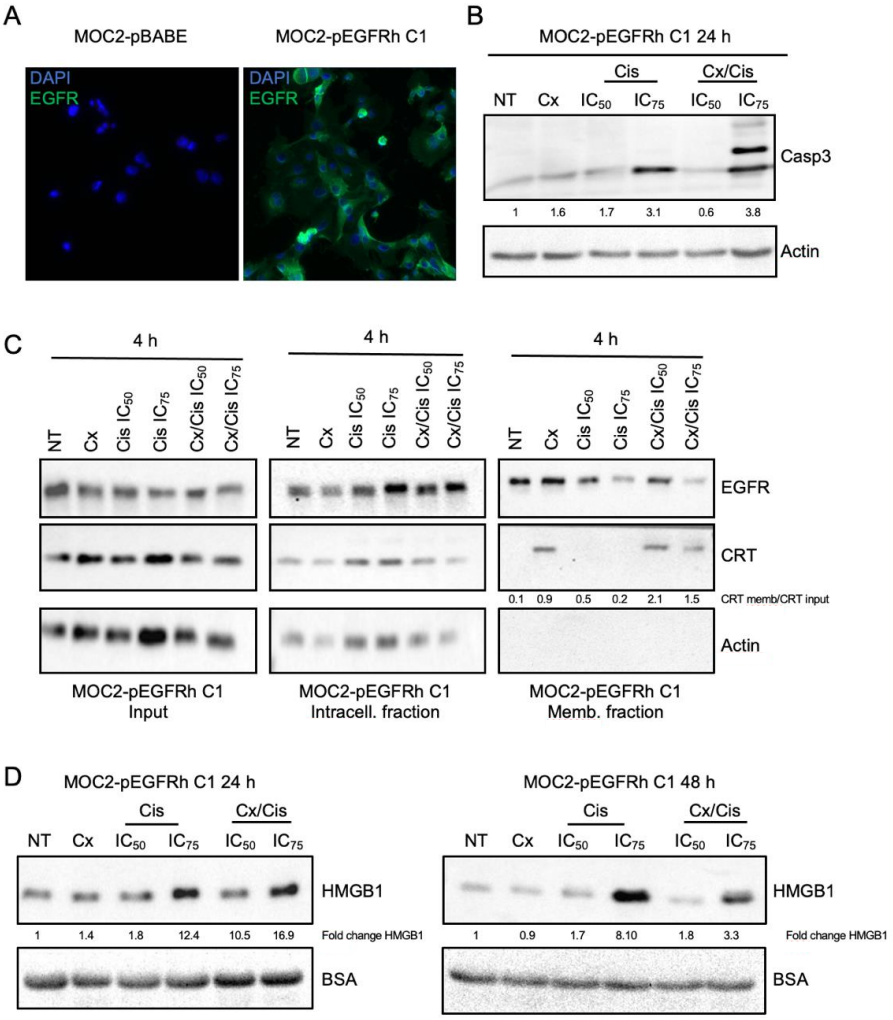

Figure 6. (**A**). Immunocytofluorescent staining analysis of the expression of EGFR in MOC2 cells that were stably transfected with the empty pBABE (left micrograph) and pBABE-hEGFR (right micrograph, MOC2-phEGFR C1 clone) expression plasmid. Nuclei are stained with DAPI. X40. (**B**). Western blot analysis of cleaved caspase-3 (Casp3) expression in whole protein extracts from MOC2-phEGFR C1 cells treated with cetuximab (Cx), cisplatin (Cis) at the IC_{50} and IC_{75}, and the Cx/Cis combination for 24 h. Signals were quantified respectively to the actin loading control and normalized with respect to the non-treated control (quantification results are shown) (**C**). Membrane protein purification and western blot analysis of EGFR, Calreticulin (CRT) and Actin expression in the input (left panels), intracellular (middle panels) and extracellular protein fractions of MOC2-phEGFR C1 cells treated with cetuximab (Cx), cisplatin (Cis) at the IC_{50} and IC_{75}, and the Cx/Cis combination for 4 h. The enrichment of CRT in extracellular fractions is shown. (**D**). Western blot analysis of the HMGB1 expression in the supernatant from MOC2-phEGFR C1 cell cultures harvested 24 h (left panels) and 48 h (right panels) after with cetuximab (Cx), cisplatin (Cis) at the IC_{50} and IC_{75} and the Cx/Cis combination. All blots shown in this figure are representative examples of three independent experiments. Additional independent biological replicates are shown in supporting documents.

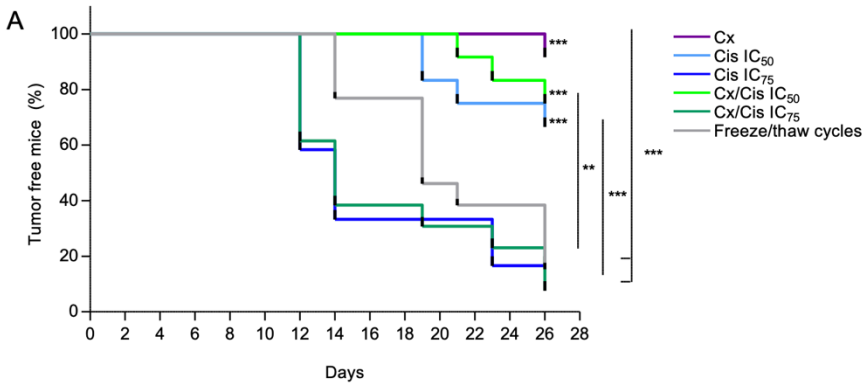

B

Ex vivo treatment	# mice with tumors
Freeze/thaw cycles	11/11 (100%)
Cx	1/12 (8.3%)
Cis IC_{50}	4/12 (33.3%)
Cis IC_{75}	10/12 (83.3%)
Cx/Cis IC_{50}	2/12 (16.7%)
Cx/Cis IC_{75}	12/12 (100%)

Figure 7. (**A**). Kaplan-Meier analysis of the tumor-free survival of MOC2-hEGFR syngeneic mice models vaccinated with ex vivo treated cells. Treatments include cetuximab (Cx), the IC_{50} and IC_{75} of cisplatin (Cis IC_{50}; Cis IC_{75}), the cetuximab and cisplatin combination (Cx/Cis IC_{50}; Cx/Cis IC_{75}) and cells killed by freeze/thaw cycles. Kaplan-Meier *p*-values: ** $p < 0.01$; *** $p < 0.001$. (**B**). Analysis of the number of tumor-free mice. The ex vivo treatment arms, number of treated mice that grew tumors/total number of mice and percentage, and the mean volume of tumors are shown.

4. Discussion

HNSCC is a particularly deadly cancer, with approximately 400,000 cancer-related deaths in 2018 [2]. Cetuximab, which targets EGFR, is the only approved targeted therapy for the management of locally advanced R/M HNSCC. However, Cetuximab is not used as a monotherapy, but is associated with either radiotherapy [1] or platinum-based chemotherapy (EXTREME regimen) [7]. To the best of our knowledge, the molecular mechanisms underlying the cytotoxicity of the EXTREME regimen have not been investigated in detail in HNSCC.

Here we showed that the cetuximab/cisplatin combined treatment displays higher toxicity than both treatments provided alone in the CAL27 cell line. These in vitro observations are consistent with clinical trials, where the EXTREME protocol results in a 3-month increase in the overall survival of patients with HNSCC compared to monotherapies [6]. In addition, similar observations were also made in nasopharyngeal cancer [43] and in colon cancer models [44]. More specifically, the cetuximab/cisplatin combination was shown to block the EGFR pathway via the inhibition of EGRF and ERK phosphorylation in the HCT116 and SW480 human colon cancer cell lines [44]. ERK is a kinase of the MAP Kinase pathway downstream of the EGFR, whose activation leads to cell proliferation. Most interestingly, ERK inhibition seems to be critical for the synergic effect of the cetuximab/cisplatin treatment, since it plays a role in the resistance to cetuximab, which can be overcome by a dual blockade of EGFR and HER3 [44,45]. However, no improved cytotoxicity of the cetuximab/cisplatin was observed in SQ20B cells. We previously have shown that the high basal and cetuximab-induced expression of the Hypoxia Inducible Factor-2α transcription factor in SQ20B cells is responsible for resistance to EGFR-blockage [8]. This could explain the lack of benefit from treatment with cetuximab. In addition, additional unidentified molecular disorders in SQ20B cells could account for the absence of synergy between cisplatin and cetuximab. Thus, the differential cytotoxicity of the cisplatin/cetuximab combination in CAL27 and SQ20B cell lines illustrates that different genetic and molecular backgrounds are likely to dictate cell response to the therapy. Key molecular differences between the

two cell lines that are likely to include the *TP53* mutational status (CAL27 and SQ20B harbor different *TP53* gene mutations, of unknown functional consequences), which might influence the induction of apoptosis upon genotoxic stress, as well as the basal and induced expression level of the Hypoxia Inducible Factor-2 (HIF-2) transcription factor (CAL27 express the lower basal level of HIF-2 that are unaffected by cetuximab treatment, whereas SQ20B expresses higher levels of HIF-2, that is upregulated upon cetuximab treatment), which is responsible for resistance to EGFR blockade in SQ20B cells [8]. These observations also highlight that the response of patients to the EXTREME protocol is likely to vary depending on tumor-specific molecular signatures.

We further analyzed the impact of the EXTREME regimen on both cell cycle deregulation and the induction of apoptotic cell death, which both contribute to cell growth, by using specific markers (iodide propidium/annexin V; cleaved caspase-3). Our observations suggest that the co-treatment induces both a cell cycle arrest in the G2 phase, as well as apoptotic cell death. More particularly, we observed that cisplatin +/− cetuximab triggered caspase-3 cleavage in both CAL27 and SQ20B cells, as well as in MOC2-phEGFR C1 cells. The induction of caspase-3 cleavage and upon cetuximab/cisplatin cotreatment was previously reported in the HCT116 and SW480 colon cancer cell lines, where both molecules seem to synergize [44]. However, the benefit of adding cetuximab to cisplatin with respect to caspase-3 cleavage and the extent of the synergy appears to depend on drug concentration, treatment timing, and treated cell line. Indeed, a mild synergy was observed in CAL27 and SQ20B after 24 h of treatment with the combination of the IC_{50} of cisplatin and cetuximab, whereas a stronger synergy was observed only in SQ20B cells after 48 h of treatment with cetuximab and cisplatin at the IC_{75}. Strikingly, the combination using high doses of cisplatin performed more poorly in SQ20B cells than drugs used alone. This suggests that SQ20B might undergo caspase-3-independent cell death upon treatment with high doses of cisplatin. This also highlights that cell response to genotoxic stress is likely to vary according to both the dose and the duration of treatment, with the induction of different signaling pathways. The level of activation of these pathways is probably dependent on the molecular and genetic background of each cell line. Further detailed analyses of these mechanisms are required to shed more light on the molecular basis of these phenomenon.

The p53 family of transcription factors is involved in DNA damage repair and apoptosis induction upon platinum-derived compound treatment [46]. Importantly, the *TP53* gene is mutated in >80% of HNSCC and plays a major role in tumor initiation and progression and resistance to platinum-based chemotherapy [47]. Interestingly, the role of p53 in the modulation of the tumor immune microenvironment and response to immunotherapy has recently emerged in the literature [48,49]. In addition, it was shown the pharmacological reactivation of p53 by Nutlin-3a induces the release of DAMPs and the activation of ICD [50]. Therefore, in order to gain further insight into the molecular mechanisms associated with the induction of apoptosis by the EXTREME protocol, and its potential correlation to the induction of ICD, we analyzed the expression of the three members of the p53 family (i.e., p53, p63, and p73). The CAL27 and SQ20B cell lines have mutated p53 and consequently, non-treated cells expressed a high level of the p53 protein. Our western blot analysis did not show any modification of the p53 protein expression level upon treatment with cetuximab and cisplatin, alone or combined, and the expression of known p53 target genes was not induced upon treatment, suggesting that p53 might not be involved in the apoptosis of CAL27 and SQ20B cells. The crosstalk between the p53 and the EGFR signaling pathway, and its consequence on therapeutic EGFR blockade has been shown in other cancer models. For instance, both wild-type and mutant p53 have been proposed to regulate *EGFR* transcription [51,52], and inhibition of p53 results in EGFR downregulation in prostate cancer cells [53]. Resistance to cetuximab has been correlated to a loss of p53 expression and an increase of p-ERK expression in H226 lung cancer cells and SCC6 HSNCC [54]. Consistently, p53 was shown to functionally impact the response of H226 cells to EGFR blockade [54], and the restoration of p53 function in p53

null prostate cancer cells stimulates EGFR and Akt phosphorylation and restores sensitivity to cetuximab [55]. We attempted to restore p53 function by treating SQ20B and CAL27 cells with the PRIMA MET reactivator but did not observe any consequences in terms of cell response to cetuximab and/or cisplatin. We cannot rule out that p53 reactivation was not achieved in our hands due to the nature of the mutations present in both cell lines, and additional functional studies about the role of p53 in the response of HNSCC cells to the EXTREME protocol are required.

The *TP73* and *TP63* genes encode two isoforms: one longer isoform called TA, which contains the N-terminal translational domain and displays pro-apoptotic function, and one shorter isoform called ΔN, which lacks the translational domain and has oncogenic activity [56]. Very scarce data is available on the expression and role of p73 in HNSCC. It has been reported to be expressed at lower levels compared to the other member of the p53 family (i.e., p53 and p63) [57]. Two bands were observed in a western blot analysis of p73 and p63 expression in whole protein extracts from CAL27 and SQ20B cells. ΔNp73, which could correspond to the lower band, seems to be the dominant p73 isoform in CAL27 cells. However, a higher band, which could correspond to TAp73, is induced by cetuximab +/− cisplatin at the IC_{50}. This might suggest a modification of the ratio of the p73 isoforms in CAL27 cells, with the induction of the expression of the pro-apoptotic TAp73 isoform (possibly the upper band) upon treatment. Interestingly, a modification of the TA/ΔNp73 (possible the upper and lower band, respectively) ratio is also observed in SQ20B cells, with a reduced expression of the TAp73 isoform upon treatment with higher doses of cisplatin (IC_{75} and IC_{90}). However, formal identification of the bands is required to confirm this hypothesis. TAp73 can induce apoptosis by indirectly regulating p53 target genes [11]. Most interestingly, EGFR signaling blockade by cetuximab has been shown to inhibit AKT and ERK, thus relieving p73 inhibition and subsequent transactivation of PUMA and the induction of mitochondrial stress-related apoptosis [58]. ΔNp63 is the dominant p63 isoform in HNSCC and is known to play a critical role in carcinogenesis and tumor cell survival [57,59]. In our hands, the expression of ΔNp63 was downregulated by high doses of cisplatin, and treatment with cetuximab increased this effect. The effect of the cisplatin +/− cetuximab treatment was found to be more important in SQ20B cells, where it resulted in total inhibition of the expression of ΔNp63. Importantly, ΔNp63 is known to inhibit p73-related apoptosis on HNSCC cells through direct physical interaction and direct binding on response elements if the promoter of *PUMA* [59,60]. Our observations are therefore consistent with the downregulation of ΔNp63 and subsequently lifted inhibition on p73 expression and/or activity upon treatment with cetuximab+/−cisplatin, which might participate in the induction of apoptotic cell death by the EXTREME protocol. Additional functional data are required to test this hypothesis.

In addition to the role that the EXTREME protocol might play in apoptosis, we also investigated whether it was able to induce ICD. Indeed, Pozzi and colleagues have shown that cetuximab is capable to trigger the emission of DAMPs as well as the activation of anti-tumor immunity in colon cancer cells [30]. Consistently with their findings, we found that cetuximab alone or in combination with cisplatin-induced the relocalization of CRT to the plasma membrane in both SQ20B and CAL27 cell lines as early as 4 h after treatment. The CRT chaperone is known to translocate from the ER to the cell surface early during ICD [61], where it is recognized by the CD91 receptor on antigen-presenting (APC) cells and acts as an "eat me" signal [27]. Consistently with the fact that cisplatin is not an ICD-inducer [62], we did not observe CRT relocalization upon treatment with cisplatin. The extracellular release of HMGB1 was triggered upon all treatments in CAL27 cells, and upon treatment with the combination only, in a dose-dependent manner, in SQ20B cells. The extracellular release of the chromatin-associated HMGB1 protein has an immunomodulatory function, including cytokine activity and pro-inflammatory activity, that depends on its oxidation state [63]. In the frame of ICD, HMGB1 is recognized by TLR4 and induces dendritic cell activation, increasing phagocytosis of tumors antigen liberated by dying cells [41]. Although, the mechanism allowing the release of HMGB1 is unknown [27], we observed a correlation

between the presence of HMGB1 in the extracellular medium and the percentage of CAL27 and SQ20B cells in late apoptosis 48 h after treatment, suggesting a potential link between the intrinsic sensitivity of HNSCC cells to the EXTREME protocol and HMGB1 emission. The production of type I interferons (IFNs) is also a feature of cells undergoing ICD. The secretion of type I IFNs activates signaling pathways through their interaction with the Interferon Alpha and Beta Receptor Subunit 1, in an autocrine and paracrine manner, which ultimately triggers the expression of T-cell chemoattractant chemokines CXC motif ligand CXCL9 and CXCL10 [27,64]. Interestingly, the expression of *CXCL9* and mainly *CXCL10* was found to be increased in the CAL27 cell line, upon treatment by cetuximab and/or cisplatin in a dose-dependent manner. This shows that the EXTREME protocol can trigger the secretion of immunomodulatory cytokines in HNSCC cells, although our observation suggests that this effect is likely to be cell-dependent. In conclusion, and consistently with what was shown by Pozzi and collaborators in colon cancer cells [30], we found that cetuximab, alone or with cisplatin, can trigger the emission of several DAMPs (including CRT, HMGB1, and type I IFN response) in HNSCC cell lines, according to different patterns and/or intensity. Further studies will be required to assess whether this heterogeneity of response is also found in human tumors, as well as the relevance it might have with response to the treatment and patient outcome.

In order to validate the immunogenic nature of the treatment of HNSCC cells by cetuximab +/− platinum-based chemotherapy, we performed a vaccination assay using immunocompetent syngeneic models, which is considered to be the gold standard to demonstrate ICD in vivo [26]. To this end, a MOC2 cell line stably expressing the human EGFR was generated. The parental MOC2 cells were derived from a tumor in the oral cavity of a C57BL/6 mouse, and generated aggressive tumors within an immunosuppressive environment [65]. Similar to what was observed in CAL27 and SQ20B cells, MOC2-phEGFR-C1 cells incubated with cisplatin and/or the cisplatin/cetuximab combination displayed apoptosis features (caspase-3 cleavage), and the plasma membrane translocation of CRT and extracellular release of HMGB1. Interestingly, ex vivo treatment of MOC2-phEGFR-C1 cells with either cetuximab, the IC_{50} of cisplatin, or their combination provided mice an anti-tumor protection against a second tumor challenge, whereas treatment with the IC_{75} of cisplatin +/− cetuximab did not. Our results suggest therefore that cetuximab can induce ICD of HNSCC cells, which is consistent with previous observations on murine lung cancer cell line [66] and on murine colon cell line expressing a human EGFR [30]. Surprisingly, we found the immunization effect provided by cisplatin treatment to be depending on drug concentration and does not correlate with the dose-dependent effect we observed in vitro on the emission of DAMPs. This could be explained by the fact that caspase-3 cleaved is induced at higher levels upon treatment with the IC_{75} of cisplatin. Indeed, the activation of caspase-3 stimulates the exposure of phosphatidylserine (PS) on the outer leaflet of cells' plasma membrane. The recognition of PS by specific PS receptors stimulates the uptake of apoptotic corpses by phagocytes of the immune system together while delivering an anti-inflammatory signal (see [67] and references therein). In addition, caspase-3 is known to stimulate the expression of prostaglandin E2, which has immunosuppressive functions [67]. Finally, caspase-3 inhibits signals known as DAMPs, including the IL-33 cytokine as well as intracellular signals that lead to the expression of type I IFNs [67]. Thus, our observations suggest that the induction of the immunogenicity of cancer cells upon cytotoxic treatment could correlate inversely with the intensity of the induction of caspase-3-related cell death, through the number of cells that undergo apoptosis and/or the level of induction of caspase-3 protein.

The lack of correlation between cisplatin concentrations and the immunogenic effect of the treatment in vivo is consistent with clinical data showing that cytotoxic anti-cancer drugs delivered at lower doses with metronomic treatment schedules rather than administrated at their maximum tolerated dose influence the infiltration of treated tumors with immune cells (for review see [68] and references therein): indeed, drugs used at their maximum tolerated dose in order to provide a high cytotoxic effect, whereas lower sub-

optimal doses have been shown to stimulate an anti-tumor effect through the stimulation of the immune system. Interestingly, the intra-tumor deliverance of nano-doses of conventional chemotherapeutic drugs has also been reported to make up the tumor immune landscape [69]. Altogether, this highlights the relative importance of the drug-related induction of apoptotic cell death vs. the emission of ICD mediators, which is more desirable to stimulate the immune system and possibly synergize with immunotherapies. Thus, there might be a subtle balance between treatment-induced stress, which could result in the improvement of cancer cell immunogenicity, and treatment-induced cell death, which potentially hinders cancer cell immunogenicity via immunomodulatory signals.

In conclusion, we have shown that cetuximab (either alone or in combination with cisplatin) is able to enhance murine and human HNSCC cells' immunogenicity through the exposure of CRT, which is known to provide a strong "eat-me" signal to phagocytes of the immune system. However, the impact of cetuximab alone on the release of HMGB1 varies in a cell-dependent manner, while cisplatin (alone or in combination with cetuximab) appears to stimulate HMGB1 release from apoptotic cells. Finally, cisplatin +/− cetuximab appears to trigger a type I IFN response that elicits the expression of CXCL9 and CXCL10 in a cell-line-dependent manner. Interestingly, only ex vivo cell treatment conditions that allow the release of DAMPs and moderate cleavage of caspase-3 (i.e., cetuximab and/or cisplatin at the IC_{50}) appear to be able to elicit an anti-tumor immune response in immunocompetent animals. Further studies are warranted to evaluate whether variations of the EXTREME protocol including the dose of cisplatin are able to trigger ICD and provide a similar effect, and to what extent this can be synergistic with immunotherapies in HNSCC patients.

Supplementary Materials: The following supporting information can be downloaded at: https://www.mdpi.com/article/10.3390/cells11182866/s1: Figure S1. Quantification of the cell cycle distribution data of CAL27 (A) and SQ20B (B) cells treated 24 h (upper histograms) and 48 h (lower histograms) with cetuximab (Cx), cisplatin (Cis) at the IC_{50} and IC_{75} and the Cx/Cis combination. The histograms show the mean number of percentages of cells in S, G2, G1/G0, and early apoptosis (EA; i.e., sub-G1); Figure S2. (A) Western blot analysis of the HMGB1 expression in the supernatant from CAL27 (left panels) and SQ20B (right panels) cell cultures harvested 68 h after with cetuximab (Cx), cisplatin (Cis) at the IC_{50} and IC_{75} and the Cx/Cis combination. Signals were quantified respectively to the actin loading control and normalized with respect to the non-treated control (quantification results are shown). The blots that are shown are re Apresentative examples of three independent experiments. Additional independent biological replicates are shown in supporting documents. (B) Analysis of the expression of *CXCL9* and *CXCL10* by RT-qPCR in CAL27 (left histographs) and SQ20B (right histographs) cells treated for 48 h with cetuximab (Cx), cisplatin (Cis) at the IC_{50} and IC_{75} and the Cx/Cis combination. Data are represented as the mean from one independent experiment +SEM; Figure S3. Western blot analysis of EGFR expression in whole-cell protein extracts from MOC-2 cells transduced with a pBABE-hEGFR expression plasmid after selection of clones on puromycin. EGFR expression is observed in the MOC2-phEGFR C1 clone. The blots that are shown are representative examples of three independent experiments; Figure S4. (A) Western blot analysis of p53 and cleaved caspase-3 (Casp3) expression in whole protein extracts from MOC2-phEGFR C1 cells treated with cetuximab (Cx), cisplatin (Cis) at the IC_{50}, $IC_{75,}$ and IC_{90}, and the Cx/Cis combination for 24 h (left panels) and 48 h (right panels). Casp3 signals were quantified respectively to the actin loading control and normalized with respect to the non-treated control (quantification results are shown). (B) Western blot analysis of the HMGB1 expression in whole protein extracts from MOC2-phEGFR C1 cell cultures treated for 24 h (left panels) and 48 h (right panels) with cetuximab (Cx), cisplatin (Cis) at the $IC_{50,}$ and IC_{75} and the Cx/Cis combination. Signals were quantified respectively to the actin loading control and normalized with respect to the non-treated control (quantification results are shown). Blots. shown are representative examples of two independent experiments. Additional independent biological replicates are shown in supporting documents; Table S1. List of oligonucleotides primers used for RT-qPCR gene expression assays: Gene names, forward and reverse primer sequences are shown; Table S2. List of TaqMan assays used for RT-qPCR gene expression assays: Gene names and TaqMan gene expression assay ID are shown; Table S3. List of antibodies used for western blot analysis; Protein names, antibody providers and used antibody dilutions are shown.

Author Contributions: Conceptualization, A.C.J. and C.G.; methodology, J.D.A. and C.B. (Cyril Bour); validation, J.D.A., J.M., C.B. (Cyril Bour), C.G. and A.C.J.; formal analysis, J.D.A., J.M., C.G. and A.C.J.; investigation, J.D.A., J.M., C.B. (Cyril Bour) and V.D.; resources, E.P.; writing—original draft preparation, J.D.A. and A.C.J.; writing—review and editing, P.S., C.B. (Christian Borel), E.P., G.M. and C.G.; visualization, J.D.A., J.M. and A.C.J.; supervision, C.G. and A.C.J.; project administration, C.G. and A.C.J.; funding acquisition, C.G. and A.C.J. All authors have read and agreed to the published version of the manuscript.

Funding: This research was financially supported by the Centre National pour la Recherche Scientifique (CNRS, France; C.G.), the Conférence de Coordination Interrégionale Grand Est-Bourgogne Franche-Comté de la Ligue Contre le Cancer and the Institut de cancérologie Strasbourg Europe. The Streinth Team is also supported by the Association pour la Recherche sur le Cancer, ITMO Cancer, European action COST Proteocure, the Interdisciplinary thematic Institute InnoVec, the IDEX Excellence grant from Unistra, and the Institut National du Cancer. J.D.A has been financially supported by a PhD fellowship awarded by the Ministère de l'Enseignement Supérieur et de la Recherche. J.M. is financially supported by a PhD fellowship awarded by the French national "Ligue Contre le Cancer".

Institutional Review Board Statement: All animal experiments were approved by the Institutional Animal Care and Use Committee (APAFIS #29181; 8 April 2021). Six weeks-old C57BL/6 female were housed in the certified animal facility (#H-67-482-21). The mice were cared for according to the Institutional Guidelines for Animal Care. Mice were acclimated for two weeks, provided with unlimited access to sterilized food and water ad libitum, and housed with 12 h day/night cycle.

Informed Consent Statement: Not applicable.

Data Availability Statement: Not applicable.

Acknowledgments: We are most grateful to Pierre Bischoff, Sophie Pinel, Elisabeth Martin and Di Fiore Pier Paolo for providing cell lines and reagents. We are grateful to Aurélie Eisenmann for her help regarding the regulatory and technical aspects of animal experimentation. We are grateful to Rob Simmons for editing the manuscript.

Conflicts of Interest: The authors declare no conflict of interest.

References

1. Johnson, D.E.; Burtness, B.; Leemans, C.R.; Lui, V.W.Y.; Bauman, J.E.; Grandis, J.R. Head and Neck Squamous Cell Carcinoma. *Nat. Rev. Dis. Primer* **2020**, *6*, 1–22. [CrossRef]
2. Bray, F.; Ferlay, J.; Soerjomataram, I.; Siegel, R.L.; Torre, L.A.; Jemal, A. Global Cancer Statistics 2018: GLOBOCAN Estimates of Incidence and Mortality Worldwide for 36 Cancers in 185 Countries. *CA. Cancer J. Clin.* **2018**, *68*, 394–424. [CrossRef] [PubMed]
3. Picon, H.; Guddati, A.K. Mechanisms of Resistance in Head and Neck Cancer. *Am. J. Cancer Res.* **2020**, *10*, 2742–2751. [PubMed]
4. Pontes, F.; Garcia, A.R.; Domingues, I.; João Sousa, M.; Felix, R.; Amorim, C.; Salgueiro, F.; Mariano, M.; Teixeira, M. Survival Predictors and Outcomes of Patients with Recurrent and/or Metastatic Head and Neck Cancer Treated with Chemotherapy plus Cetuximab as First-Line Therapy: A Real-World Retrospective Study. *Cancer Treat. Res. Commun.* **2021**, *27*, 100375. [CrossRef]
5. Vermorken, J.B.; Mesia, R.; Rivera, F.; Remenar, E.; Kawecki, A.; Rottey, S.; Erfan, J.; Zabolotnyy, D.; Kienzer, H.-R.; Cupissol, D.; et al. Platinum-Based Chemotherapy plus Cetuximab in Head and Neck Cancer. *N. Engl. J. Med.* **2008**, *359*, 1116–1127. [CrossRef]
6. Rivera, F.; García-Castaño, A.; Vega, N.; Vega-Villegas, M.E.; Gutiérrez-Sanz, L. Cetuximab in Metastatic or Recurrent Head and Neck Cancer: The EXTREME Trial. *Expert Rev. Anticancer Ther.* **2009**, *9*, 1421–1428. [CrossRef]
7. Muraro, E.; Fanetti, G.; Lupato, V.; Giacomarra, V.; Steffan, A.; Gobitti, C.; Vaccher, E.; Franchin, G. Cetuximab in Locally Advanced Head and Neck Squamous Cell Carcinoma: Biological Mechanisms Involved in Efficacy, Toxicity and Resistance. *Crit. Rev. Oncol. Hematol.* **2021**, *164*, 103424. [CrossRef]
8. Coliat, P.; Ramolu, L.; Jégu, J.; Gaiddon, C.; Jung, A.C.; Pencreach, E. Constitutive or Induced HIF-2 Addiction Is Involved in Resistance to Anti-EGFR Treatment and Radiation Therapy in HNSCC. *Cancers* **2019**, *11*, 1607. [CrossRef]
9. Job, S.; de Reyniès, A.; Heller, B.; Weiss, A.; Guérin, E.; Macabre, C.; Ledrappier, S.; Bour, C.; Wasylyk, C.; Etienne-Selloum, N.; et al. Preferential Response of Basal-Like Head and Neck Squamous Cell Carcinoma Cell Lines to EGFR-Targeted Therapy Depending on EREG-Driven Oncogenic Addiction. *Cancers* **2019**, *11*, 795. [CrossRef]
10. Licona, C.; Delhorme, J.-B.; Riegel, G.; Vidimar, V.; Cerón-Camacho, R.; Boff, B.; Venkatasamy, A.; Tomasetto, C.; da Silva Figueiredo Celestino Gomes, P.; Rognan, D.; et al. Anticancer Activity of Ruthenium and Osmium Cyclometalated Compounds: Identification of ABCB1 and EGFR as Resistance Mechanisms. *Inorg. Chem. Front.* **2020**, *7*, 678–688. [CrossRef]
11. Alsahafi, E.; Begg, K.; Amelio, I.; Raulf, N.; Lucarelli, P.; Sauter, T.; Tavassoli, M. Clinical Update on Head and Neck Cancer: Molecular Biology and Ongoing Challenges. *Cell Death Dis.* **2019**, *10*, 540. [CrossRef] [PubMed]

12. Ortiz-Cuaran, S.; Bouaoud, J.; Karabajakian, A.; Fayette, J.; Saintigny, P. Precision Medicine Approaches to Overcome Resistance to Therapy in Head and Neck Cancers. *Front. Oncol.* **2021**, *11*, 614332. [CrossRef] [PubMed]
13. Ferris, R.L.; Blumenschein, G.; Fayette, J.; Guigay, J.; Colevas, A.D.; Licitra, L.; Harrington, K.; Kasper, S.; Vokes, E.E.; Even, C.; et al. Nivolumab for Recurrent Squamous-Cell Carcinoma of the Head and Neck. *N. Engl. J. Med.* **2016**, *375*, 1856–1867. [CrossRef] [PubMed]
14. Seiwert, T.Y.; Burtness, B.; Mehra, R.; Weiss, J.; Berger, R.; Eder, J.P.; Heath, K.; McClanahan, T.; Lunceford, J.; Gause, C.; et al. Safety and Clinical Activity of Pembrolizumab for Treatment of Recurrent or Metastatic Squamous Cell Carcinoma of the Head and Neck (KEYNOTE-012): An Open-Label, Multicentre, Phase 1b Trial. *Lancet Oncol.* **2016**, *17*, 956–965. [CrossRef]
15. Bagaev, A.; Kotlov, N.; Nomie, K.; Svekolkin, V.; Gafurov, A.; Isaeva, O.; Osokin, N.; Kozlov, I.; Frenkel, F.; Gancharova, O.; et al. Conserved Pan-Cancer Microenvironment Subtypes Predict Response to Immunotherapy. *Cancer Cell* **2021**, *39*, 845–865.e7. [CrossRef]
16. Mueller, C.G.; Gaiddon, C.; Venkatasamy, A. Current Clinical and Pre-Clinical Imaging Approaches to Study the Cancer-Associated Immune System. *Front. Immunol.* **2021**, *12*, 716860. [CrossRef]
17. Dunn, G.P.; Old, L.J.; Schreiber, R.D. The Three Es of Cancer Immunoediting. *Annu. Rev. Immunol.* **2004**, *22*, 329–360. [CrossRef]
18. Munhoz, R.R.; Postow, M.A. Recent Advances in Understanding Antitumor Immunity. *F1000Research* **2016**, *5*, 2545. [CrossRef]
19. Markov, O.V.; Mironova, N.L.; Vlasov, V.V.; Zenkova, M.A. Molecular and Cellular Mechanisms of Antitumor Immune Response Activation by Dendritic Cells. *Acta Naturae* **2016**, *8*, 17–30. [CrossRef]
20. Elmusrati, A.; Wang, J.; Wang, C.-Y. Tumor Microenvironment and Immune Evasion in Head and Neck Squamous Cell Carcinoma. *Int. J. Oral Sci.* **2021**, *13*, 24. [CrossRef]
21. Wan, Y.Y. Regulatory T Cells: Immune Suppression and Beyond. *Cell. Mol. Immunol.* **2010**, *7*, 204–210. [CrossRef] [PubMed]
22. Pan, Y.; Yu, Y.; Wang, X.; Zhang, T. Tumor-Associated Macrophages in Tumor Immunity. *Front. Immunol.* **2020**, *11*, 583084. [CrossRef] [PubMed]
23. Yang, Y.; Li, C.; Liu, T.; Dai, X.; Bazhin, A.V. Myeloid-Derived Suppressor Cells in Tumors: From Mechanisms to Antigen Specificity and Microenvironmental Regulation. *Front. Immunol.* **2020**, *11*, 1371. [CrossRef] [PubMed]
24. Solomon, B.; Young, R.J.; Rischin, D. Head and Neck Squamous Cell Carcinoma: Genomics and Emerging Biomarkers for Immunomodulatory Cancer Treatments. *Semin. Cancer Biol.* **2018**, *52*, 228–240. [CrossRef] [PubMed]
25. Galluzzi, L.; Vitale, I.; Warren, S.; Adjemian, S.; Agostinis, P.; Martinez, A.B.; Chan, T.A.; Coukos, G.; Demaria, S.; Deutsch, E.; et al. Consensus Guidelines for the Definition, Detection and Interpretation of Immunogenic Cell Death. *J. Immunother. Cancer* **2020**, *8*, e000337. [CrossRef] [PubMed]
26. Kepp, O.; Senovilla, L.; Vitale, I.; Vacchelli, E.; Adjemian, S.; Agostinis, P.; Apetoh, L.; Aranda, F.; Barnaba, V.; Bloy, N.; et al. Consensus Guidelines for the Detection of Immunogenic Cell Death. *Oncoimmunology* **2014**, *3*, e955691. [CrossRef] [PubMed]
27. Galluzzi, L.; Vitale, I.; Aaronson, S.A.; Abrams, J.M.; Adam, D.; Agostinis, P.; Alnemri, E.S.; Altucci, L.; Amelio, I.; Andrews, D.W.; et al. Molecular Mechanisms of Cell Death: Recommendations of the Nomenclature Committee on Cell Death 2018. *Cell Death Differ.* **2018**, *25*, 486–541. [CrossRef]
28. Limagne, E.; Nuttin, L.; Thibaudin, M.; Jacquin, E.; Aucagne, R.; Bon, M.; Revy, S.; Barnestein, R.; Ballot, E.; Truntzer, C.; et al. MEK Inhibition Overcomes Chemoimmunotherapy Resistance by Inducing CXCL10 in Cancer Cells. *Cancer Cell* **2022**, *40*, 136–152.e12. [CrossRef]
29. Jung, A.C.; Moinard-Butot, F.; Thibaudeau, C.; Gasser, G.; Gaiddon, C. Antitumor Immune Response Triggered by Metal-Based Photosensitizers for Photodynamic Therapy: Where Are We? *Pharmaceutics* **2021**, *13*, 1788. [CrossRef]
30. Pozzi, C.; Cuomo, A.; Spadoni, I.; Magni, E.; Silvola, A.; Conte, A.; Sigismund, S.; Ravenda, P.S.; Bonaldi, T.; Zampino, M.G.; et al. The EGFR-Specific Antibody Cetuximab Combined with Chemotherapy Triggers Immunogenic Cell Death. *Nat. Med.* **2016**, *22*, 624–631. [CrossRef]
31. Park, S.-J.; Ye, W.; Xiao, R.; Silvin, C.; Padget, M.; Hodge, J.W.; van Waes, C.; Schmitt, N.C. Cisplatin and Oxaliplatin Induce Similar Immunogenic Changes in Preclinical Models of Head and Neck Cancer. *Oral Oncol.* **2019**, *95*, 127–135. [CrossRef] [PubMed]
32. Tissue-Specific Transcription Factor Pit-1/GHF-1 Binds to the c-Fos Serum Response Element and Activates c-Fos Transcription. Molecular Endocrinology. Oxford Academic. Available online: https://academic.oup.com/mend/article/13/5/742/2741697 (accessed on 27 July 2022).
33. Gottardi, C.J.; Dunbar, L.A.; Caplan, M.J. Biotinylation and Assessment of Membrane Polarity: Caveats and Methodological Concerns. *Am. J. Physiol.-Ren. Physiol.* **1995**, *268*, F285–F295. [CrossRef] [PubMed]
34. Obeid, M.; Tesniere, A.; Ghiringhelli, F.; Fimia, G.M.; Apetoh, L.; Perfettini, J.-L.; Castedo, M.; Mignot, G.; Panaretakis, T.; Casares, N.; et al. Calreticulin Exposure Dictates the Immunogenicity of Cancer Cell Death. *Nat. Med.* **2007**, *13*, 54–61. [CrossRef]
35. Blanchet, A.; Bourgmayer, A.; Kurtz, J.-E.; Mellitzer, G.; Gaiddon, C. Isoforms of the P53 Family and Gastric Cancer: A Ménage à Trois for an Unfinished Affair. *Cancers* **2021**, *13*, 916. [CrossRef] [PubMed]
36. Di Agostino, S.; Sorrentino, G.; Ingallina, E.; Valenti, F.; Ferraiuolo, M.; Bicciato, S.; Piazza, S.; Strano, S.; del Sal, G.; Blandino, G. YAP Enhances the Pro-Proliferative Transcriptional Activity of Mutant P53 Proteins. *EMBO Rep.* **2016**, *17*, 188–201. [CrossRef] [PubMed]

37. Donehower, L.A.; Soussi, T.; Korkut, A.; Liu, Y.; Schultz, A.; Cardenas, M.; Li, X.; Babur, O.; Hsu, T.-K.; Lichtarge, O.; et al. Integrated Analysis of TP53 Gene and Pathway Alterations in The Cancer Genome Atlas. *Cell Rep.* **2019**, *28*, 1370–1384.e5. [CrossRef]
38. Gaiddon, C.; Lokshin, M.; Ahn, J.; Zhang, T.; Prives, C. A Subset of Tumor-Derived Mutant Forms of P53 Down-Regulate P63 and P73 through a Direct Interaction with the P53 Core Domain. *Mol. Cell. Biol.* **2001**, *21*, 1874–1887. [CrossRef]
39. Miller, J.J.; Gaiddon, C.; Storr, T. A Balancing Act: Using Small Molecules for Therapeutic Intervention of the P53 Pathway in Cancer. *Chem. Soc. Rev.* **2020**, *49*, 6995–7014. [CrossRef]
40. Miller, J.J.; Blanchet, A.; Orvain, C.; Nouchikian, L.; Reviriot, Y.; Clarke, R.M.; Martelino, D.; Wilson, D.; Gaiddon, C.; Storr, T. Bifunctional Ligand Design for Modulating Mutant P53 Aggregation in Cancer. *Chem. Sci.* **2019**, *10*, 10802–10814. [CrossRef]
41. Apetoh, L.; Ghiringhelli, F.; Tesniere, A.; Obeid, M.; Ortiz, C.; Criollo, A.; Mignot, G.; Maiuri, M.C.; Ullrich, E.; Saulnier, P.; et al. Toll-like Receptor 4–Dependent Contribution of the Immune System to Anticancer Chemotherapy and Radiotherapy. *Nat. Med.* **2007**, *13*, 1050–1059. [CrossRef]
42. Tokunaga, R.; Zhang, W.; Naseem, M.; Puccini, A.; Berger, M.D.; Soni, S.; McSkane, M.; Baba, H.; Lenz, H.-J. CXCL9, CXCL10, CXCL11/CXCR3 Axis for Immune Activation—A Target for Novel Cancer Therapy. *Cancer Treat. Rev.* **2018**, *63*, 40–47. [CrossRef] [PubMed]
43. Sung, F.L.; Poon, T.C.W.; Hui, E.P.; Ma, B.B.Y.; Liong, E.; To, K.F. Antitumor Effect and Enhancement of Cytotoxic Drug Activity by Cetuximab in Nasopharyngeal Carcinoma Cells. *In Vivo* **2005**, *9*, 237–245.
44. Son, D.J.; Hong, J.E.; Ban, J.O.; Park, J.H.; Lee, H.L.; Gu, S.M.; Hwang, J.Y.; Jung, M.H.; Lee, D.W.; Han, S.-B.; et al. Synergistic Inhibitory Effects of Cetuximab and Cisplatin on Human Colon Cancer Cell Growth via Inhibition of the ERK-Dependent EGF Receptor Signaling Pathway. *BioMed Res. Int.* **2015**, *2015*, e397563. [CrossRef] [PubMed]
45. Jiang, N.; Wang, D.; Hu, Z.; Shin, H.; Qian, G.; Rahman, M.; Zhang, H.; Amin, A.; Nannapaneni, S.; Wang, X.; et al. Combination of Anti-HER3 Antibody MM-121/SAR256212 and Cetuximab Inhibits Tumor Growth in Preclinical Models of Head and Neck Squamous Cell Carcinoma. *Mol. Cancer Ther.* **2014**, *13*, 1826–1836. [CrossRef]
46. Hientz, K.; Mohr, A.; Bhakta-Guha, D.; Efferth, T. The Role of P53 in Cancer Drug Resistance and Targeted Chemotherapy. *Oncotarget* **2017**, *8*, 8921–8946. [CrossRef]
47. Zhou, G.; Liu, Z.; Myers, J.N. TP53 Mutations in Head and Neck Squamous Cell Carcinoma and Their Impact on Disease Progression and Treatment Response. *J. Cell. Biochem.* **2016**, *117*, 2682–2692. [CrossRef]
48. Jiang, Z.; Liu, Z.; Li, M.; Chen, C.; Wang, X. Immunogenomics Analysis Reveals That TP53 Mutations Inhibit Tumor Immunity in Gastric Cancer. *Transl. Oncol.* **2018**, *11*, 1171–1187. [CrossRef]
49. Zhang, H.; Huang, Z.; Song, Y.; Yang, Z.; Shi, Q.; Wang, K.; Zhang, Z.; Liu, Z.; Cui, X.; Li, F. The TP53-Related Signature Predicts Immune Cell Infiltration, Therapeutic Response, and Prognosis in Patients with Esophageal Carcinoma. *Front. Genet.* **2021**, *12*, 607238. [CrossRef]
50. Guo, G.; Yu, M.; Xiao, W.; Celis, E.; Cui, Y. Local Activation of P53 in the Tumor Microenvironment Overcomes Immune Suppression and Enhances Antitumor Immunity. *Cancer Res.* **2017**, *77*, 2292–2305. [CrossRef]
51. Deb, S.P.; Muñoz, R.M.; Brown, D.R.; Subler, M.A.; Deb, S. Wild-Type Human P53 Activates the Human Epidermal Growth Factor Receptor Promoter. *Oncogene* **1994**, *9*, 1341–1349.
52. Ludes-Meyers, J.H.; Subler, M.A.; Shivakumar, C.V.; Munoz, R.M.; Jiang, P.; Bigger, J.E.; Brown, D.R.; Deb, S.P.; Deb, S. Transcriptional Activation of the Human Epidermal Growth Factor Receptor Promoter by Human P53. *Mol. Cell. Biol.* **1996**, *16*, 6009–6019. [CrossRef] [PubMed]
53. Sauer, L.; Gitenay, D.; Vo, C.; Baron, V.T. Mutant P53 Initiates a Feedback Loop That Involves Egr-1/EGF Receptor/ERK in Prostate Cancer Cells. *Oncogene* **2010**, *29*, 2628–2637. [CrossRef] [PubMed]
54. Huang, S.; Benavente, S.; Armstrong, E.A.; Li, C.; Wheeler, D.L.; Harari, P.M. P53 Modulates Acquired Resistance to EGFR Inhibitors and Radiation. *Cancer Res.* **2011**, *71*, 7071–7079. [CrossRef] [PubMed]
55. Bouali, S.; Chrétien, A.-S.; Ramacci, C.; Rouyer, M.; Marchal, S.; Galenne, T.; Juin, P.; Becuwe, P.; Merlin, J.-L. P53 and PTEN Expression Contribute to the Inhibition of EGFR Downstream Signaling Pathway by Cetuximab. *Cancer Gene Ther.* **2009**, *16*, 498–507. [CrossRef]
56. Faridoni-Laurens, L.; Tourpin, S.; Alsafadi, S.; Barrois, M.; Temam, S.; Janot, F.; Koscielny, S.; Bosq, J.; Bénard, J.; Ahomadegbe, J.-C. Involvement of N-Terminally Truncated Variants of P73, DeltaTAp73, in Head and Neck Squamous Cell Cancer: A Comparison with P53 Mutations. *Cell Cycle Georget. Tex* **2008**, *7*, 1587–1596. [CrossRef]
57. Gwosdz, C.; Balz, V.; Scheckenbach, K.; Bier, H. P53, P63 and P73 Expression in Squamous Cell Carcinomas of the Head and Neck and Their Response to Cisplatin Exposure. In *Advances in Oto-Rhino-Laryngology*; Bier, H., Ed.; KARGER: Basel, Switzerland, 2004; pp. 58–71. ISBN 978-3-8055-7789-2.
58. Knickelbein, K.; Tong, J.-S.; Chen, D.; Wang, Y.-J.; Misale, S.; Bardelli, A.; Yu, J.; Zhang, L. Restoring PUMA Induction Overcomes KRAS-Mediated Resistance to Anti-EGFR Antibodies in Colorectal Cancer. *Oncogene* **2018**, *37*, 4599–4610. [CrossRef]
59. Rocco, J.W.; Leong, C.-O.; Kuperwasser, N.; DeYoung, M.P.; Ellisen, L.W. P63 Mediates Survival in Squamous Cell Carcinoma by Suppression of P73-Dependent Apoptosis. *Cancer Cell* **2006**, *9*, 45–56. [CrossRef]
60. Rocco, J.W. p63 and p73: Life and Death in Squamous Cell Carcinoma. *Cell Cycle* **2006**, *5*, 936–940. [CrossRef]

61. Panaretakis, T.; Kepp, O.; Brockmeier, U.; Tesniere, A.; Bjorklund, A.-C.; Chapman, D.C.; Durchschlag, M.; Joza, N.; Pierron, G.; van Endert, P.; et al. Mechanisms of Pre-Apoptotic Calreticulin Exposure in Immunogenic Cell Death. *EMBO J.* **2009**, *28*, 578–590. [CrossRef]
62. Martins, I.; Kepp, O.; Schlemmer, F.; Adjemian, S.; Tailler, M.; Shen, S.; Michaud, M.; Menger, L.; Gdoura, A.; Tajeddine, N.; et al. Restoration of the Immunogenicity of Cisplatin-Induced Cancer Cell Death by Endoplasmic Reticulum Stress. *Oncogene* **2011**, *30*, 1147–1158. [CrossRef]
63. Sims, G.P.; Rowe, D.C.; Rietdijk, S.T.; Herbst, R.; Coyle, A.J. HMGB1 and RAGE in Inflammation and Cancer. *Annu. Rev. Immunol.* **2010**, *28*, 367–388. [CrossRef] [PubMed]
64. Sistigu, A.; Yamazaki, T.; Vacchelli, E.; Chaba, K.; Enot, D.P.; Adam, J.; Vitale, I.; Goubar, A.; Baracco, E.E.; Remédios, C.; et al. Cancer Cell–Autonomous Contribution of Type I Interferon Signaling to the Efficacy of Chemotherapy. *Nat. Med.* **2014**, *20*, 1301–1309. [CrossRef] [PubMed]
65. Judd, N.P.; Allen, C.T.; Winkler, A.E.; Uppaluri, R. Comparative Analysis of Tumor Infiltrating Lymphocytes in a Syngeneic Mouse Model of Oral Cancer. *Octolaryngol.-Head Neck Surg.* **2012**, *147*, 493–500. [CrossRef] [PubMed]
66. Garrido, G.; Rabasa, A.; Sánchez, B.; López, M.V.; Blanco, R.; López, A.; Hernández, D.R.; Pérez, R.; Fernández, L.E. Induction of Immunogenic Apoptosis by Blockade of Epidermal Growth Factor Receptor Activation with a Specific Antibody. *J. Immunol. Baltim. Md 1950* **2011**, *187*, 4954–4966. [CrossRef]
67. Galluzzi, L.; López-Soto, A.; Kumar, S.; Kroemer, G. Caspases Connect Cell-Death Signaling to Organismal Homeostasis. *Immunity* **2016**, *44*, 221–231. [CrossRef]
68. Wu, J.; Waxman, D.J. Immunogenic Chemotherapy: Dose and Schedule Dependence and Combination with Immunotherapy. *Cancer Lett.* **2018**, *419*, 210–221. [CrossRef]
69. Tatarova, Z.; Blumberg, D.C.; Korkola, J.E.; Heiser, L.M.; Muschler, J.L.; Schedin, P.J.; Ahn, S.W.; Mills, G.B.; Coussens, L.M.; Jonas, O.; et al. A Multiplex Implantable Microdevice Assay Identifies Synergistic Combinations of Cancer Immunotherapies and Conventional Drugs. *Nat. Biotechnol.* **2022**, 1–11. [CrossRef]

Liste des publications scientifiques

Jana Mourtada[1,2], Chloé Thibaudeau[1,2] Bohdan Wasylyk[3,4,5,6] and Alain C. Jung[1,2] The Multifaceted Role of Human Dickkopf-3 (DKK-3) in Development, Immune Modulation and Cancer- *Cells MDPI. DOI: 10.3390/cells13010075*

Mourtada, J., Lony, C., Nicol, A., De Azevedo, J., Bour, C., Macabre, C., Roncarati, P., Ledrappier, S., Schultz, P., Borel, C., Burgy, M., Wasylyk, B., Mellitzer, G., Herfs, M., Gaiddon, C., Jung, A.C., 2023. A novel ΔNp63-dependent immune mechanism improves prognosis of HPV-related head and neck cancer. *Front. Immunol. 14.*

Conrad, O., Burgy, M., Foppolo, S., Jehl, A., Thiéry, A., Guihard, S., Vauchelles, R., Jung, A.C., **Mourtada, J**., Macabre, C., Ledrappier, S., Chenard, M.-P., Onea, M.-A., Danic, A., Dourlhes, T., Thibault, C., Schultz, P., Dontenwill, M., Martin, S., 2023. Tumor-Suppressive and Immunomodulating Activity of miR-30a-3p and miR-30e-3p in HNSCC Cells and Tumoroids. *Int. J. Mol. Sci. 24, 11178. https://doi.org/10.3390/ijms241311178*

De Azevedo, **J., Mourtada**, J., Bour, C., Devignot, V., Schultz, P., Borel, C., Pencreach, E., Mellitzer, G., Gaiddon, C., Jung, A.C., 2022. The EXTREME Regimen Associating Cetuximab and Cisplatin Favors Head and Neck Cancer Cell Death and Immunogenicity with the Induction of an Anti-Cancer Immune Response. *Cells 11, 2866. https://doi.org/10.3390/cells11182866*

Liste des communications orales

Titre : « Mécanismes d'activation de la réponse immunitaire par ΔNp63 dans les cancers des voies aérodigestives supérieures HPV-positifs »

Communication	Date	Lieu	Type de présentation
13ème Journée de l'AFIPP (Infections par les Papillomavirus et les Polyomavirus)	30 septembre et 1er octobre 2021	En ligne (COVID)	Présentation orale
21ème Journée Scientifique de la Ligue contre le cancer	9 novembre 2021	Ecole Supérieure de Biotechnologie de Strasbourg (ESBS)-Ilkirch-Graffenstaden	Poster
14ème Journée de l'AFIPP (Infections par les Papillomavirus et les Polyomavirus)	28-30 septembre 2022	Hôtel Le Château-fort de Sedan, Sedan, Ardennes	Présentation orale (Prix de la meilleure présentation)
22ème Journée Scientifique de la Ligue contre le cancer	14 novembre 2022	Ecole Supérieure de Biotechnologie de Strasbourg (ESBS)-Ilkirch-Graffenstaden	Poster
Journée Jeunes&chercheurs	13 avril 2023	Cité des Sciences et de l'Industrie, Paris	Poster

Liste des formations

Formation relative à l'expérimentation animale de niveau 1, Université de Strasbourg **-Le 21 Janvier 2022.**

Jana MOURTADA

Mécanismes d'activation de la réponse immunitaire par ΔNp63 dans les cancers des voies aérodigestives supérieures HPV-positifs

Résumé

Les tumeurs HPV+ de l'oropharynx sont hétérogènes d'un point de vue pronostic et moléculaire. Le pronostic des tumeurs se distinguent respectivement par la présence ou l'absence d'une signature moléculaire dépendante du facteur de transcription ΔNp63. Nous avions démontré que ΔNp63 inhibe les capacités migratoires et invasives des lignées cellulaires de cancer ORL HPV+, et augmente leur sensibilité aux chimiothérapies à base de sel de platine, suggérant son rôle dans la progression tumorale. Une analyse fonctionnelle de ΔNp63 nous a permis de montrer que son expression stimule la phagocytose de cellules cancéreuses par des macrophages *in vitro*. De manière cohérente, l'analyse du transcriptome de notre même modèle cellulaire met en évidence que ΔNp63 régule l'expression de facteurs diffusibles comme des chimiokines et des interleukines, parmi lesquels la protéine DKK3. Nos résultats montrent que la sécrétion de DKK3 par les cellules cancéreuses active la voie NF-κB dans les macrophages, et mimique les effets de ΔNp63 dans la régulation de la phagocytose. L'induction de la voie NF-κB par DKK3 dans les macrophages est réalisée par l'intermédiaire de son récepteur CKAP4. Enfin, nos analyses suggèrent que ΔNp63 régule l'expression de facteurs impliqués dans l'inflammasome, ainsi que celles d'autres cytokines comme TNFRSF11B, CCL26, CCL11, TIMP1 et TIMP2. L'ensemble de nos résultats montrent que ΔNp63 joue un rôle original dans le pronostic des patients HPV+ à travers la régulation de molécules sécrétées, impliquées dans le recrutement et l'activation de cellules immunitaires.

Mots clés : *ΔNp63, Papillomavirus humain (HPV), cancer ORL, progression tumorale, phagocytose, facteurs diffusibles, Dickkopf-3 (DKK3), activation de cellules immunitaires, pronostic.*

Abstract

HPV+ oropharyngeal tumors display both prognostic and molecular heterogeneity. Patients prognosis can be distinguished by the presence or absence of a molecular signature that depends on the ΔNp63 transcription factor. We demonstrated that ΔNp63 inhibits the migratory and invasive capabilities of HPV+ HNSCC cell lines and increases their sensitivity to platinum-based chemotherapy, implying its role in tumor progression. A functional analysis of ΔNp63 revealed its ability to stimulate the phagocytosis of cancer cells by macrophages in vitro. Consistently, a transcriptomic analysis of the same cellular model highlighted that ΔNp63 regulates the expression of secreted factors, including chemokines and interleukins, among which is the DKK3protein. Our findings indicate that DKK3 secretion by cancer cells activates the NF-κB pathway in macrophages, mimicking ΔNp63's effects on phagocytosis regulation. Induction of the NF-κB pathway by DKK3 in macrophages is mediated by its receptor CKAP4. Finally, our analyses suggest that ΔNp63 regulates the expression of factors involved in the inflammasome, as well as those of other cytokines such as TNFRSF11B, CCL26, CCL11, TIMP1 and TIMP2. Altogether, our results show that ΔNp63 plays a unique role in the prognosis of HPV+ patients by regulating secreted molecules involved in the recruitment and immune cell activation.

Keywords: *ΔNp63, Human Papillomavirus (HPV), Head and Neck Squamous Cell Carcinoma (HNSCC), tumor progression, phagocytosis, secreted factors, Dickkopf-3 (DKK3), immune cell activation, prognosis.*